Rewiring of the Adult Hippocampal Mossy Fiber System

A Thesis submitted to attain the degree of
DOCTOR OF SCIENCE AT UNIVERSITY ZURICH

Presented by

Matteo Egger

Master of Science, ETH ZURICH

Born on 18.01.1990

From Eggersriet SG

Committee Members

Prof. Dr Csaba Földy (Chair)

Prof. Dr. Martin Schwab

Prof. Dr. Benjamin Grewe

Zürich, May/June 2023

Table of Contents

Summary

The brain is a highly intricate and specialized organ which plays critical roles in regulating multitudes of functions throughout the body, perceiving and reacting the world around us, and supporting survival. Since the pioneering work of Cajal over a century ago, the central nervous system has been extensively studied to comprehend its structure and function. The progress has been extraordinary. We now own very detailed knowledge about many different aspects of the brain, including its development and ability to learn and remember, and generate movements and complex behavioral patterns. However, it is also clear that many outstanding questions still need to be answered before the brain could be "understood". Some of the greatest challenges include, for example, finding of cure for brain-related diseases and disorders. Efforts to attain this overarching goal require a detailed understanding of brain circuits and their molecular composition. Such a molecular composition includes molecules that are relevant for specifying connections between billions of brain cells, maintaining the brain's connectivity during the lifespan, and supporting neural function overall.

In this thesis, I focus on questions related to neuronal connectivity and explore wiring mechanisms in the adult brain in detail. Although evidence suggests that the adult brain retains a considerable capacity for circuit formation, adult wiring has not been broadly considered. During my thesis work, I aimed to understand at least some of the organizing principles underlying adult wiring. During developmental wiring, synaptic cell surface receptor and adhesion molecules as well as transcription factors and transcriptional regulators play fundamental roles. The key hypothesis is that proteins belonging to these molecular classes define a blueprint or a "molecular code" for the brain's intricate connectivity. Once discovered, this code could explain key features of the brain's structure and function and open exciting possibilities for the attainment of circuit therapy and repair. The role of these molecules during adult wiring is even less understood, and furthermore the question of which molecular programs can reactivate and regulate wiring in adult neurons also remains entirely open.

To address these outstanding problems, I investigated the epilepsy-associated hippocampal mossy fiber sprouting as a powerful model for adult brain wiring. My primary research aim was to characterize cellular and molecular changes that take place during further wiring.

In the first introductory chapter (Chapter 1), I provide the Reader with a historical context of my research and introduction to developmental and adult wiring, and brain areas relevant for my research. In Chapter 2, I will focus on a molecular program which can reactivate wiring in adult neurons. Specifically, I will describe our finding showing that activation of the transcriptomic regulator *Id2* can cell autonomously induce recurrent mossy fiber sprouting in adult hippocampal granule cells. This study, on which I am second author, describes the molecular program activated by *Id2* as well as the consequences of adult wiring on network operations and learning and memory, and has been published in *PNAS* (Luo *et al.*, 2021). In Chapter 3, I will focus on synaptic cell surface receptor and adhesion molecules which may be important for adult wiring. Specifically, I will describe the role of *Pcdh11x* in the target specification of mossy fiber sprouting. This study, on which I am a co-author, has been published in *Frontiers in Neurosciences* (Luo *et al.*, 2022). Then, in Chapter 4, I will describe my first author study on the rapid formation of commissural connections during adult wiring and characterization of a previously unnoted cells type, the commissural granule cells. This study has been published in *PNAS Nexus* (Egger *et al.*, 2023). Finally, in Chapters 5 and 6, I will summarize and discuss my findings in a broader context and provide a outlook on future research.

Overall, I believe that my studies make important conceptual and practical contributions to brain research. I hope that the Reader will enjoy reading this thesis and gain a fresh perspective for understanding the brain's intricate connectivity.

Riassunto

Il cervello è un organo altamente complesso e specializzato che svolge ruoli fondamentali nella regolazione di moltissime funzioni in tutto il corpo, nella percezione e reazione del mondo circostante e nel supporto alla sopravvivenza. Dal lavoro pionieristico di Cajal, oltre un secolo fa, il sistema nervoso centrale è stato ampiamente studiato per comprenderne la struttura il funzionamento. I progressi sono stati straordinari. Oggi possediamo conoscenze molto dettagliate su tanti aspetti diversi del cervello, tra cui il suo sviluppo e la sua capacità di apprendere e memorizzare, nonché di generare movimenti e modelli comportamentali complessi. Tuttavia, è chiaro, che molte domande ancora aperte devono trovare risposta prima che il cervello possa essere "compreso" nella sua totalità. Alcune delle sfide più grandi includono, ad esempio, la ricerca di una cura per le malattie e i disturbi legati al cervello. Gli sforzi per raggiungere questo obiettivo generale richiedono una comprensione dettagliata dei circuiti cerebrali e della loro composizione molecolare. Tale composizione molecolare include molecole importanti per specificare le giuste connessioni tra miliardi di cellule cerebrali, mantenere la connettività del cervello durante la vita e sostenere le funzioni neuronali in generale.

In questo lavoro di dottorato, mi concentro su questioni legate alla connettività neuronale ed esploro in dettaglio i meccanismi di cablaggio nel cervello adulto. Sebbene l'evidenza suggerisca che il cervello adulto mantenga una notevole capacità di formazione di circuiti, il cablaggio adulto non è stato ancora sufficientemente considerato. Durante il mio lavoro di tesi, ho cercato di comprendere alcuni dei principi organizzativi alla base del cablaggio in età adulta. Durante il cablaggio del cervello in fase di sviluppo, le molecole di recettori transmembrana e di adesione della superficie cellulare sinaptica, nonché i fattori di trascrizione e i regolatori trascrizionali, svolgono ruoli fondamentali. L'ipotesi chiave è che le proteine appartenenti a queste classi molecolari definiscano un modello o un "codice molecolare" per l'intricata connettività del cervello. Una volta scoperto, questo codice, potrebbe spiegare le caratteristiche chiave della struttura e del funzionamento del cervello e aprire stimolanti possibilità per lo sviluppo di terapie e riparazioni dei circuiti. Il ruolo di queste molecole durante il cablaggio in età adulta è ancora meno conosciuto, e inoltre la questione di quali programmi molecolari possano riattivare e regolare il cablaggio nei neuroni adulti rimane del tutto aperta.

Per affrontare questi problemi ancora irrisolti, ho studiato la crescita delle fibre muschiose dell'ippocampo, che sono associate all'epilessia, come importante modello di cablaggio del cervello adulto. Il mio obiettivo primario di ricerca è stato quello di caratterizzare i cambiamenti cellulari e molecolari che avvengono durante i cablaggi aggiuntivi.

Nel primo capitolo introduttivo (Capitolo 1), fornisco al lettore un contesto storico e un'introduzione al cablaggio durante lo sviluppo e nel cervello adulto e alle aree cerebrali rilevanti per la mia ricerca. Nel Capitolo 2 mi concentrerò su un programma molecolare in grado di riattivare il cablaggio nei neuroni adulti. In particolare, descriverò le nostre scoperte, che dimostrano che l'attivazione del regolatore trascrittomico *Id2* può indurre autonomamente la crescita di fibre muschiose ricorrenti nelle cellule granulari dell'ippocampo adulto. Questo studio, di cui sono il secondo autore, descrive il programma molecolare attivato da *Id2* e le conseguenze del cablaggio nel cervello adulto sulle operazioni nella rete cerebrale e sull'apprendimento e la memoria, ed è stato pubblicato su *PNAS* (Luo *et al.*, 2021). Nel Capitolo 3, mi concentrerò sulle molecole di recettori e di adesione della superficie cellulare sinaptica che possono essere importanti per il cablaggio in età adulta. In particolare, descriverò il ruolo di *Pcdh11x* nella specificazione del luogo di formazione delle sinapsi durante la crescita delle fibre muschiose. Questo studio, di cui sono coautore, è stato pubblicato su *Frontiers in Neurosciences* (Luo *et al.*, 2022). Nel Capitolo 4 descriverò il mio studio, di cui sono primo autore, sulla rapida formazione delle connessioni commissurali durante il cablaggio in età adulta e sulla caratterizzazione di un tipo di cellule finora sconosciuto, le cellule granulari commissurali. Questo studio è stato pubblicato su *PNAS Nexus* (Egger *et al.*, 2023). Infine, nei capitoli 5 e 6, riassumerò e discuterò i miei risultati in un contesto più ampio e fornirò una prospettiva sulle ricerche future.

Nel complesso, ritengo che i miei studi apportino importanti contributi concettuali e pratici alla ricerca sul cervello. Spero che il lettore apprezzi la lettura di questa tesi e acquisisca una nuova prospettiva sulla comprensione dell'intricata connettività del cervello.

Chapter 1 – General introduction

The brain is a complex and highly specialized organ responsible for controlling and coordinating diverse functions of the body. It consists of around 85 billion cells called neurons, which are responsible for processing and transmitting information through the central and peripheral nervous system. The neurons mainly communicate with each other through synapses and form complex networks which are indispensable for all brain functions. The synaptic circuits constantly change and adapt in response to new experiences and information, and perform multitudes of functions from sensation and motor control to complex cognitive processes, memory and emotions. Despite decades of research progress, the brain remains largely enigmatic. For example, it is still not understood in it is entirety how complex neural circuits are assembled and how they change and adapt throughout life, during new experiences, ageing, or injury.

Until ~1900, it was generally thought that the brain and the nervous system did not conform to cell theory. Joseph von Geerlach proposed a framework for the reticular theory, which was later most popularized by Italian biologist and pathologist Camillo Golgi. The theory suggested that the grey matter of the brain consisted of an extremely dense and intricate network of axons coming from different cells, forming a 'diffuse nervous network' (Raviola & Mazzarello, 2011). To prove this theory, Golgi developed a new staining technique, the so-called "black reaction". Although the black reaction revealed nerve cells in the cerebro-spinal axis which contrary to the theory appeared as single units, he remained focusing on the diffuse network model without fully embracing the significance of his observations (Raviola & Mazzarello, 2011).

The pathologist Santiago Ramón y Cajal learned the staining protocol of Golgi in Madrid and also realized its potential for studying the nervous system. By further developing the staining method, axons and dendrites became clearly visible and distinguishable from each other, and Ramón y Cajal was able to visualize and draw the structure of single neurons as we know them today (Ramón y Cajal, 1888a; De Carlos & Borrell, 2007). He noticed in the grey matter that axons do not form a diffuse network but contact the cell bodies and dendrites of other neurons (Ramón y Cajal, 1888b). Furthermore, he identified short processes which arise from the dendritic surface and called them *dendritic spines* (Ramón y Cajal, 1888a). Accordingly, he proposed the neural doctrine (Katz-Sidlow, 1998), a concept stating that the nervous system is

composed of discrete individual cells, conforming to the cell theory. These observations and emerging concepts proved to provide solid foundations for modern neuroscience.

The use of the black reaction represented a turning point in Ramón y Cajal's research career, as he acknowledged several times: '*And then 1888, my greatest year, arrived [...] my year of fortune*' (De Carlos & Borrell, 2007). From there, he started a systematic study of the nervous system. It applied the newly learned and improved method to study the different region of the nervous system in various animal models, and methodically and accurately drew hundreds of single neurons. During his studies on the avian retina, he realized that cells had different morphological features and axonal endings, which led to the description of two different photoreceptors cells (Ramón y Cajal, 1888a). Later, during his studies on the avian optic lobe and the organization of the circuit in the cerebellar cortex, he hypothesized the existence of a functionally-relevant directionality, from presynaptic axon terminals, to dendrites, then to cell bodies (or somata), and finally to output axons (Ramón y Cajal, 1898; Llinás, 2003). In his last article, he sometimes used the term *synapses* to refer to the complex structure forming a connection from a presynaptic axon terminal to the postsynaptic spine on the adjacent dendrites (Ramón y Cajal, 1933). With a great foresight, he claimed synapses enable neurons to receive, process, and transmit information.

Ramón y Cajal was also interested in how neurons grow their axon and contact their appropriate target cells. Whilst working on chicken embryos, he saw that the growing axon endings, or growth cones, looked like canonical protoplasm. He was able to distinguish two types of growth cones, one with divergent thin, short, thorny processes and the other with a triangular laminar shape. They are known today as filopodia and lamellipodia, respectively (Ramón y Cajal, 1890a, 1890b). In addition, he observed that the growth cones are highly dynamic and postulated that growth cones define the path for axon elongation, presumably guided by attracting and repelling forces by certain chemical substances. This led to the theory of chemotropism, in which a neuron migrates or navigates the environment in response to chemical signals (Ramón y Cajal, 1893; Tessier-Lavigne & Placzek, 1991).

In the late 1900s, Ramón y Cajal further investigated whether neurons could grow axons in adults. These studies revealed a very different picture: '*Once development was ended, the fonts of growth and regeneration of axons and dendrites dried up irrevocably. In the adult centers, the neural paths are something fixed and*

immutable: everything may die, nothing may be regenerated' (Ramón y Cajal, 1914). This became a central dogma in neuroscience until Joseph Altman showed in the 1960s that radioactive thymidine could be incorporated in the dentate gyrus of the hippocampus, suggesting the possibility of neural proliferation in the adult brain (Altman, 1962, 1963).

Ramón y Cajal was a pioneer of and to date remains a prominent figure in modern neuroscience. Through his work, he produced detailed descriptions about the structure of individual neurons, as well as the development of the nervous system and the structure of the growth cone. His work provided a fundamental framework for brain research in the decades to come. In 1906, he shared the Nobel Prize in Physiology or Medicine with Camillo Golgi.

Circuit formation during brain development

The mammalian brain starts to form in the embryo and evolves through a series of complex cellular processes until maturation, ranging from proliferation to programmed cell death of excess neurons (Stiles & Jernigan, 2010). During embryonic development, neural stem cells in the neural tube are self-renewing, and multipotent cells undergo a process of proliferation and differentiation to generate three main types of cells, which are the building blocks of the nervous system: neurons, astrocytes, and oligodendrocytes. Neurons are generated from neuronal stem cells via symmetric or asymmetric division. During asymmetric division, a neural stem cell produces two daughter cells with different features, one which is identical to the stem cell and the second one programmed to differentiate into a neuron or a glial cell (Gage, 2000). Newly generated neurons then migrate from the neurogenic zones to their final destination in the brain. The migration process is critical for the proper formation of neural circuits and for establishing functional connectivity in the nervous system. The migration from the ventricular zone is regulated by a variety of molecular signals, including growth factors and cell-surface receptor and adhesion proteins, or CAMs as I will refer to them for short (Tessier-Lavigne *et al.*, 1988; Bixby & Harris, 1991; Kuffler, 1994; Squire *et al.*, 2012).

Over the course of neuroscience, axonal tracing techniques have enabled researchers to investigate many different classes of axons in different species and their circuitry. Studies have shown that newly generated neurons, after migrating to their corrected region, must mature, elongate their primary axons, which then must reach

their target area, and form functional synapses on target cells. During development, axon growth is facilitated by an extracellular milieu composed of many different growth promoting factors, and the elongating axons are readily guided through molecularly distinct areas. Whilst growing, the axon endings encounter so-called decision points, which are locations where the axon must choose between different directions to reach its appropriate target area. This "decision" is highly regulated by specialized molecular signals and cascades. For example, such molecular signals determine if an axon remains on the same brain hemisphere or spinal side where its cell body is located or crosses the midline to form commissural projections. *Slit*, *roundabout* (*robo*) and *commissurless* (*comm*) have been shown to play a key role in midline crossing (Seeger *et al.*, 1993; Kidd *et al.*, 1999).

More broadly, molecular cues play a critical role in neural circuit formation and can be generally divided into four types: short-range ("contact") or long-range ("diffusible") cues, each of which can be either attractant ("move toward") or repellent ("move away"). To detect and respond to guidance cues in the environment the growth cone is presumed to display specific sets of surface proteins, or CAMs. Depending on the molecule they encounter, the binding between the cue and its receptor engages specific intracellular signaling cascades, which changes the cytoskeletal dynamic, whereby the growth cone moves towards or away the cue, or may collapse to end axon elongation (Mitchison & Kirschner, 1988). The combinatorial action of multiple guidance cues is thought to ensure reproducibility and high-fidelity direction selection. Molecules belonging to multiple different protein families (such as netrin-s, slit-s, semaphorin-s, and ephrin-s) have been shown to play a critical role in the guidance process (Sperry, 1963; Tessier-Lavigne & Goodman, 1996; Polleux *et al.*, 1998; Kolodkin & Tessier-Lavigne, 2011; Squire *et al.*, 2012; Kania & Klein, 2016; Stoeckli, 2018). In addition, studies on proteoglycans have indicated their involvement in the regulation of growth factor availability and axon growth promotion (Bandtlow & Zimmermann, 2000). It is important to emphasize that different axons can respond to the same set of extracellular cues in different ways depending on the availability of CAMs they display on the growth cone (Shibata *et al.*, 1998). In addition to guidance, CAM interactions can also influence axonal and dendritic branching and arborization (Schmidt & Rathjen, 2010; Gibson & Ma, 2011; Kalil & Dent, 2014; Onesto *et al.*, 2021; Moreland & Poulain, 2022).

Once the developing axon reaches its intended target area, the next step is to connect with appropriate partner neurons, which may be multiple different types of

neurons. How appropriate target neurons are recognized is not fully understood. A key hypothesis suggest that this recognition is also enabled by a matching combination of CAMs displayed on the axon ending and target cell, providing a molecular code for target recognition, similarly to a keylock mechanism. While several large and small gene families have been identified in target recognition, including members of the immunoglobulin, cadherin, teneurin, latrophilin, and leucine-rich repeat super-families (Sperry, 1963; Washbourne *et al.*, 2004; Sanes & Zipursky, 2010, 2020; Südhof, 2018, 2021), the proving of the above hypothesis is still subject to intense research (Yamagata *et al.*, 2002; Shen & Bargmann, 2003; Shen *et al.*, 2004; Kamiguchi, 2007; Pollerberg *et al.*, 2013; De Wit & Ghosh, 2015; Ribeiro *et al.*, 2018; Sanes & Zipursky, 2020; Moreland & Poulain, 2022).

After identifying the appropriate target cells, synapses appear to form "automatically" (Ziv & Garner, 2001; Yamagata *et al.*, 2003; Shen & Cowan, 2010). The physical contact between an axon terminal and a dendrite shaft is followed by controlled changes in morphology and molecular content to form mature synapses (Scheiffele *et al.*, 2000; Biederer *et al.*, 2002; Sytnyk *et al.*, 2002; Fu *et al.*, 2003). Research have shown that CAMs may also play important roles in determining synaptic size and strength (Scheiffele, 2003; Yamagata *et al.*, 2003), and are possibly responsible for the generation of structural and functional synapse diversity throughout the nervous system. During the lifespan, experience- and activity-dependent changes may constantly modify synaptic properties, including their formation, strengthening, weakening, or elimination (Missler *et al.*, 2012; De Wit & Ghosh, 2015; Qiao *et al.*, 2016; Südhof, 2017; Ribeiro *et al.*, 2018; Sanes & Zipursky, 2020).

The developing nervous system displays an extremely high capacity for axon growth, which is crucial for the proper formation of neural networks. As already mentioned, guidance cues, including growth inhibitory molecules, regulate the growth and target specification. After the vast majority of axons and synaptic connections are established, the growth promoting environment dissipates (Harel & Strittmatter, 2006; Yiu & He, 2006) and the capacity for circuit formation radically drops (Seng *et al.*, 2022). During a next stage, the elimination of exuberant axons, synaptic pruning, and activity dependency refinement shape the structure and function of the neural circuit (Purves & Lichtman, 1980; Bailey & Chen, 1989; Goodman & Shatz, 1993; Katz & Shatz, 1996; Innocenti & Price, 2005; Holtmaat & Svoboda, 2009; Squire *et al.*, 2012; Bennett *et al.*, 2018). These processes are presumed to be facilitated by a transition of the growth-

promoting environment to a growth-inhibiting environment. Growth inhibition is to play a key role in the stabilization of circuits. However, growth inhibition also poses a major limitation before the regeneration of injured axons in the adult nervous system. Multiple factors and mechanisms may contribute to growth inhibition such as a reduction of neurotrophic and growth factor levels, increased inhibitory signals, and structural/molecular changes in the extracellular matrix (Sanes, 1989; Schwab *et al.*, 1993; Horner & Gage, 2000; Lacroix & Tuszynski, 2000; Harel & Strittmatter, 2006; Yiu & He, 2006; Cohen-Cory *et al.*, 2010; Schwab, 2010; Baldwin & Giger, 2015). Understanding the molecular mechanisms of the growth promotion to inhibition switch is a focus of intense research. A comprehension of the mechanisms involved would not only help us to clarify the fundamental steps of developmental circuit formation but also how to bypass the inhibitory barriers to facilitate recovery in central nervous system after injury (Schwab, 2002; Harel & Strittmatter, 2006), and potentially enable other forms of circuit repair for neurological and neurodevelopmental disorders.

Circuit formation in the adult brain

Until the mid-20th century, it was believed that no regeneration and no cell division were possible in the nervous system. While Ramón y Cajal's research on the 'fixed' and 'immutable' adult brain critically influenced this view (Ramón y Cajal, 1928; Owji & Shoja, 2020), technological limitations also prevented further insights into this question. Studies by Altman on neurogenesis with the use of tritiated thymidine as a marker, followed by studies by Michael Kaplan and James Hinds, however, have revealed that the adult brain retains a capacity to generate new neurons, fundamentally challenging the conventional wisdom (for a historical review, see (Kaplan, 2001)). Altman demonstrated glial cell proliferation and newly generated neurons in the dentate gyrus of the hippocampus and in the cortex in adult rats and cats (Altman, 1962, 1963). In addition to adult neurogenesis, it is also become clear that under certain conditions new axons may grow in the adult brain, which were referred to as *sprouted* or *regenerated axons* (Edds & Small, 1951; Causey & Hoffman, 1955; Liu & Chambers, 1958; McCouch *et al.*, 1958). Despite the magnitude of these discoveries, the scientific community struggled to accept neurogenesis and axon growth in the adult brain, and it took another 30 years of research before other studies could partially accomplish the task of showing that neurons are continuously produced in the adult rodent brain. In the past two decades, adult neurogenesis and axon sprouting/regeneration have drawn considerable attention. As a result of this, many examples of further wiring or rewiring

in the adult brain became apparent. The growth of knowledge in this area also required terminological refinements such as referring to sprouting as further axon growth from an uninjured neuron and axon regeneration as axon growth in neurons that have experienced injury (Tuszynski & Steward, 2012).

Axon growth and circuit reorganization in the adult brain are frequently observed in human neurological disorders and after injury as well as in rodent experimental models of spinal cord and traumatic injury, stroke, and epilepsy (Noebels *et al.*, 2012; Carmichael *et al.*, 2017; Seng *et al.*, 2022). Both sprouting and regeneration have been described in many different brain regions cell types. Further, sprouting, or more broadly any wiring in the adult brain, may have different phenotypes and can be subdivided into further categories. New axons may represent short-range (or local) (Salin *et al.*, 1995; Carmichael *et al.*, 2001) or long-range projections (Liu *et al.*, 2010; Dougherty *et al.*, 2020). The new circuits can represent either feedback or feedforward motifs. Moreover, the target specificity might be so-called typical, resembling connections established during development (Salin *et al.*, 1995; Dougherty *et al.*, 2020), or atypical, creating connections that do not emerge during normal brain development (Carmichael *et al.*, 2001; Dhar *et al.*, 2016), or both (Steward, 1992; Siddiqui & Joseph, 2005). Finally, the speed of the wiring may greatly differ depending on the cell type or model investigated, from a few days to weeks or months.

Next, I will provide more background on and highlight examples of adult wiring. Given that my thesis focuses on the hippocampus, first I will focus on adult wiring phenotypes in non-hippocampal areas. Then, in the next chapter I will describe the typical hippocampal circuitry, which will help the reader to contextualize adult wiring phenotypes in the hippocampus, which I will describe and focus on afterward.

Although multiple observations in the context of neurological diseases, grafted and reprogrammed cells, adult-born neurons, and behavioral relevant rewiring (Carmichael *et al.*, 2017; Fischer *et al.*, 2020; Denoth-Lippuner & Jessberger, 2021; Seng *et al.*, 2022) evince that the brain retains a considerable capacity for axon growth and circuit formation, there are also clear examples showing that further wiring can be severely limited. Such limitations become extremely prominent during injury or stroke; for example, the connections between the cortico-spinal neurons in the sensory-motor cortex and spinal motor neurons and interneurons are frequently severed. While the injured neurons can survive the trauma and show moderate signs of regeneration, they

are unable to re-establish or rewire their connections to the original target areas and cell types. In other words, the mammalian nervous system lacks the ability to self-repair. Intensive research has revealed that the above-mentioned growth-inhibitory milieu plays a key role in this. While multiple growth inhibitory molecules exist, Nogo in particular drew much attention because of its ability to block axon regeneration (Caroni & Schwab, 1988; Chen *et al.*, 2000; Kadoya *et al.*, 2009). Research has shown that neutralizing antibodies against Nogo and/or pharmacological blockade of the Nogo-activated Rho/ROCK pathway can indeed facilitate axon regeneration, compensatory sprouting, as well as functional recovery (Bregman *et al.*, 1995; Dergham *et al.*, 2002; Schwab, 2004).

In the context of cell grafting (also referred to as cell transplantation) and programming, several examples show pronounced further wiring in adults. For example, after spinal cord injury, stem cells grafted into the injury site gave rise to neurons, which grew axons within a few days (Lu *et al.*, 2012, 2014; Sharp *et al.*, 2014; Fischer *et al.*, 2020). Some of the axons remained locally, others reached distant brain areas centimeters away. In other studies, the transplantation of embryonic or pluripotent stem cells or neurons in different cortical and subcortical areas produced striking wiring phenotypes, frequently establishing new connections with neurons in distal areas and forming functional circuits (Gaillard *et al.*, 2007, 2009; Steinbeck *et al.*, 2012, 2015; Adler *et al.*, 2019). To achieve cellular reprograming, different approaches have been developed (Gascón *et al.*, 2017), which either convert existing non-neuronal cells into neural types or directly reprogram the connectivity of adult neurons. The conversion of non-neural cell types resulted in significant axon growth phenotypes and the formation of target-specific projections to the striatum, substantia nigra, and hippocampus (Torper *et al.*, 2013; Qian *et al.*, 2020; Lentini *et al.*, 2021). The direct reprograming of wiring also revealed that axon growth or regeneration can be *cell autonomously* facilitated. Thus far, such reprograming has been achieved with the ectopic overexpression of the transcriptional regulator *Id2* in adult hippocampal and spinal neurons (Lasorella *et al.*, 2006; Yu *et al.*, 2011; Ko *et al.*, 2016; Huang *et al.*, 2019). Given that the overall regulation and maintenance of wiring during the lifespan is still poorly understood, it is feasible that the targeted activation or inactivation of other transcription factors and/or regulators can also achieve similar wiring effects. Nonetheless, these results have clearly demonstrated that the activation of cell autonomous (or cell intrinsic) wiring mechanisms have the capacity to promote robust axon growth, overcoming the limiting effects of the growth inhibitory milieu.

Finally, select types of adult neurons have been shown rewire their connectivity in response to environmental or behavioral stimuli. Such examples include the circadian clock-regulated periodic rewiring of ventral lateral neurons and in dorsal anterior clock neurons in drosophila (Petsakou *et al.*, 2015; Song *et al.*, 2021) and the estrous cycle-dependent rewiring of hypothalamic progesterone-receptor-expressing neurons in female mice (Inoue *et al.*, 2019).

The hippocampal circuitry

Beginning already with Cajal's work, the hippocampus is one brain area which has been extensively studied to understand the structure and function of neural circuits. Its unique structure, such as the organization of its cell layers, greatly facilitated this effort. The hippocampus is composed of both excitatory principal neurons and inhibitory interneurons, which can be further subdivided into several neuronal types, and proved to be critical for certain types of learning and memory processes.

Hippocampal circuitry is comprised of three major subregions, the dentate gyrus, the CA3 and CA1 areas as well as specialized cell types within each region, which define the so-called "trisynaptic hippocampal circuit". While it has become clear that the "trisynaptic" nature of the hippocampus is overly general, it still provides a framework for the general description of this brain region.

In the dentate gyrus, granule cells and mossy cells, whereas in the CA3-CA1 regions, pyramidal cells represent major glutamatergic (or principal) cell populations. Within each region, there is also many different types of GABAergic interneurons. Glutamatergic neurons greatly outnumber the GABAergic population; GABAergic interneurons are estimated to comprise about 10–15% of all neurons in the hippocampus (Pelkey *et al.*, 2017). The major input to the hippocampal neurons is from the entorhinal cortex (EC) via the perforant pathway, which can be divided into a direct and indirect path. The direct path is monosynaptic: layer III cells in the EC target CA3-CA1 neurons (Hjorth-Simonsen, 1972; Steward & Scoville, 1976; Naber *et al.*, 2001; Witter, 2007a). By contrast, the indirect path involves multiple synaptic relays and is referred to as the trisynaptic path: layer II cells in the EC target granule cells in the dentate gyrus, which target CA3 pyramidal cells, which then target CA1 pyramidal cells in a unidirectional fashion (Amaral et al., 2007; Andersen et al., 1971; Schaffer, 1892). The major output of the hippocampus is generated by the CA1 or subiculum pyramidal cells and conveyed onto layer IV and V neurons in the EC, as well as neurons in the

amygdala, nucleus accumbens, and other cortical and sub-cortical structures (Andersen *et al.*, 1971; Swanson & Cowan, 1977; Van Groen & Wyss, 1990; Cenquizca & Swanson, 2007). While CA3 pyramidal cells form extensive local collaterals to target other CA3 pyramidal cells, granule cells and CA1 pyramidal cells rarely establish synaptic contacts within the own populations (Scharfman, 1994, 2007; Witter, 2007b; Le Duigou *et al.*, 2014).

In addition to extrahippocampal projections to other areas, the two hippocampi (each located in each brain hemispheres) form extensive synaptic connections with one other. Most significant are the commissural CA3 pyramidal cell and mossy cell connections which densely innervate the contralateral hippocampus (Swanson *et al.*, 1981; Ribak *et al.*, 1985; Ishizuka *et al.*, 1990; Frotscher *et al.*, 1991; Buckmaster *et al.*, 1992; Scharfman & Myers, 2012; Shinohara *et al.*, 2012; Bui *et al.*, 2018; Botterill *et al.*, 2021). While commissural CA1 pyramidal cell connections have been also described (Van Groen & Wyss, 1990), granule cell projections have been thought to be entirely restricted to the CA3 area within each hippocampus.

In contrast to principal neurons, GABAergic interneurons establish extensive local connections within each hippocampi and hippocampal subregion, although extrahippocampal GABAergic projections have been also described (Buzsáki, 1984; Zappone & Sloviter, 2001; Maccaferri & Lacaille, 2003; Somogyi & Klausberger, 2005; Kullmann, 2011; Pelkey *et al.*, 2017; Eyre & Bartos, 2019).

As this brief overview illustrates, we have a relatively detailed knowledge base regarding the *structure* of hippocampus. With regard to the *function* of the hippocampus, and how it supports learning and memory, one of the earliest insights can be traced back to 1957. At that time, patient H. M., who suffered from pharmacologically uncontrollable medial temporal lobe epilepsy, underwent an extensive brain surgery to treat the disorder. During the surgery, a large portion of his temporal lobe was removed, including the hippocampus. The surgery was successful in the sense that it provided H.M. with a relief from seizures. However, it has quickly became apparent that H. M. lost the ability to form new declarative memories, a condition also known as anterograde amnesia. He could still recall memories from before the surgery though (Squire, 2009; Knierim *et al.*, 2014). This condition of H.M. and later that of other patient inspired an extensive research effort, which revealed the fundamental principles of how memories are formed and distributed through different

brain areas. The hippocampus in particular was found to be essential for the formation of so-called declarative memories by creating a framework which integrates distinct sensory, emotional, and cognitive elements, to allow a comprehensive encoding of experiences over time and space.

Next, I will describe the structure and function of one part of the hippocampus in greater detail, on which my research focused: the dentate gyrus.

Dentate gyrus

Anatomically, the dentate gyrus is divided into multiple layers: (1) the granule cells layer, where the densely packed cell bodies of granule cells are located, (2) the molecular layer, where the dendrites of the granule cells are located, and (3) the polymorphic layer or hilus, which is largely circumferenced by the granule cell layer and through which the output stream of granule cell axons passes toward the CA3 area. Granule cells have been largely recognized for their role in processing and integration of incoming inputs from the entorhinal cortex (Van Strien *et al.*, 2009), from the associational and commissural fibers of mossy cells which are located in the hilus (Frotscher *et al.*, 1991; Buckmaster *et al.*, 1992), as well as from several types of GABAergic interneurons (Amaral, 1978; Freund & Buzsáki, 1996).

With regard to delineating the function of the dentate gyrus, and more broadly that of the entire hippocampus, the classical works of David Marr have been extremely influential. Marr's work was motivated by the studies on patient H.M., and specifically that H.M. was unable to form new memories while still being able to recall older memories after the surgery. Marr (Marr, 1971) theorized that the hippocampus could form simple memory traces by strengthening connections between neurons. Soon after, physiological evidence for long-term potentiation of synaptic connections has been reported (Bliss & Lomo, 1973). Marr furthermore theorized that to sense the external world one needs to evaluate if daily experiences are different from or similar to those previously experienced. Such a process would require computations that support pattern separation and completion. These are two different and opposing cognitive processes which could feasibly keep similar but not identical episodes as separate entities and help to retrieve previous memories based on environmental cues. Marr hypothesized that the recurrent networks in the CA3 area could support auto-association and be involved in pattern completion. In addition to Marr's theories, others suggested that the brain could contain a "cognitive map" of the surrounding spatial

environment and underscoring such a hypothesis the so-called place cell, which only active when the animal is in a specific location in the environment, have been also discovered (Tolman, 1948; O'Keefe & Dostrovsky, 1971; Moser *et al.*, 2017). As a consequence of these influential works, multitudes of studies have focused on how the main input of CA3, the dentate gyrus could support pattern separation and completion. This large body of work, using electrophysiological, lesioning, genetic, and behavioral approaches, have revealed that the dentate gyrus and specifically the granule cells play an important role in pattern separation (McNaughton *et al.*, 1989; Leutgeb *et al.*, 2007; McHugh *et al.*, 2007; Goodrich-Hunsaker *et al.*, 2008; McTighe *et al.*, 2009; Yassa & Stark, 2011; Knierim *et al.*, 2014; GoodSmith *et al.*, 2019).

Given that the dentate gyrus is one of the two areas of the mammalian brain in which new neurons, i.e. granule cells, are generated throughout life it became an important question how newly generated a granule cells may contribute to the hippocampal function. It soon became clear that changes in the neurogenic capacity of the dentate gyrus impacts in the execution of certain hippocampal learning tasks (Kempermann *et al.*, 1997; Van Praag *et al.*, 1999; Shors *et al.*, 2001; Drapeau *et al.*, 2003; Zhang *et al.*, 2008; Jessberger *et al.*, 2009; Deng *et al.*, 2010). More specific experiments furthermore have suggested that adult-born granule cells play an important role in pattern separation (Clelland *et al.*, 2009; Sahay *et al.*, 2011; Nakashiba *et al.*, 2012a). However, other studies challenged this view (Swan *et al.*, 2014; Whoolery *et al.*, 2020), underscoring that a clear comprehension of the brain's pattern completion and separation mechanisms has not been achieved.

Nonetheless, at least in humans, pattern separation is thought to be particularly important for performing daily tasks such as recognizing faces, places, and objects and also for contextual learning and spatial navigation. Functional magnetic resonance (fMRI) studies investigating the hippocampus and in particular the dentate gyrus thus far support this hypothesis (Bakker *et al.*, 2008; Carr *et al.*, 2010; Lacy *et al.*, 2011; Azab *et al.*, 2014; Berron *et al.*, 2016; Leal & Yassa, 2018).

Circuit wiring and rewiring in the adult hippocampus

The hippocampus is also one brain regions in which multiple different adult-brain wiring phenotypes by different cell types have been extensively studied. Adult-born granule cells significantly contribute to circuit formation in the adult hippocampus. They grow their axons along the developmentally-established granule cells projections,

which are called hippocampal mossy fibers, and form synaptic connections with hilar and CA3 glutamatergic and GABAergic neurons (Stanfield & Trice, 1988; Markakis & Gage, 1999; Zhao *et al.*, 2006; Noebels *et al.*, 2012; Sun *et al.*, 2013; Drew *et al.*, 2016; Trinchero *et al.*, 2019; Briones *et al.*, 2021; Denoth-Lippuner & Jessberger, 2021). In addition, axon sprouting phenotypes have been investigated in the context of temporal lobe epilepsies. One prime example is the hippocampal mossy fiber sprouting by granule cells, whereby granule cells (or mossy fibers) sprout new axons into the inner molecular layer of the dentate gyrus creating a local feedback circuit (Laurberg & Zimmer, 1981; Tauck & Nadler, 1985; Sutula *et al.*, 1988; Wenzel *et al.*, 2000; Buckmaster, 2012; Luo *et al.*, 2021). With the exception of the ventral tip of the hippocampus, this connection does not exist and is considered to be an atypical circuit motif. Further, axonal sprouting in many different hippocampal cell types has been demonstrated, including that of CA3 and CA1 pyramidal neurons and multiple different GABAergic cell types (Perez *et al.*, 1996; Smith & Dudek, 2001; Siddiqui & Joseph, 2005; Scharfman, 2007; Zhang *et al.*, 2009; Karlócai *et al.*, 2011; Peng *et al.*, 2013; Marchionni *et al.*, 2019). Their sprouting phenotypes may greatly differ in terms of projection distance (local or long-range), typical or atypical target selectivity, and dynamics (speed) of growth. Because it will be relevant for some of my own findings, it is also important to note that CA3 pyramidal neurons and the so-called parvalbumin-expressing GABAergic interneurons have been shown to develop long-range sprouting phenotypes targeting the contralateral hippocampus (Schauwecker *et al.*, 1995; Siddiqui & Joseph, 2005; Christenson Wick *et al.*, 2017). It is feasible that other long-range sprouting phenotypes also exist, but because sprouting has been frequently studied in brain slice preparations, has not been noticed.

Brain circuit analysis: A brief methodological overview

The classification of brain regions, neurons, and connections has been a major focus of neuroscience since Golgi developed the black reaction in the late 19th century. Using the black reaction, Ramón y Cajal started to draw every neuron he was able to visualize, and classify them into different types, such as pyramidal neurons, Purkinje cells, or interneurons. His precise illustrations also highlighted the intricate nature of neuronal connections and synapses. Ever since, researchers have strived to create an all-encompassing catalogue of brain cells and create a standardized nomenclature to refer to them. Technological advances in imaging, molecular biology, and electrophysiology over the past two decades have vastly accelerated this effort, and

lead to the discovery of several previously unnoted cell types and revealed fundamental principles underlying brain function (Armstrong, 1995; Osten & Margrie, 2013; Harris *et al.*, 2014; Zeng & Sanes, 2017; Luo *et al.*, 2018; Voigt *et al.*, 2019; Navabpour *et al.*, 2020).

The anatomical characterization of neurons typically relies on the location of the cell body (or soma) as well as structural characteristics of dendrites, axons, and connections. All these properties critically determine how a neuron is integrated into a circuit, and ultimately, how it contributes to brain function. Viral tracing has proved to be a powerful method to analyze neuronal connectivity. It typically involves the injection of non-pathogenic viruses obtained from natural strains of neurotrophic viruses (Nassi *et al.*, 2015) or recombinant viral vectors (Kondratov *et al.*, 2021) containing fluorescent proteins into specific brain regions. The injected virus and/or fluorescent labeling can travel in either an anterograde (from the soma toward axon and dendrite endings) or retrograde (from axon endings toward the soma and dendrites) directions. Different viruses can be non trans-synaptic (i.e. remain in the infected neuron), trans monosynaptic or multi synaptic (i.e. the virus "jumps" one or multiple synapses, respectively), and can be used to reveal input and output cell types and connections (Xu *et al.*, 2020; Wang & Zhang, 2021; Liu *et al.*, 2022). Further, progress in circuit neuroscience has been benefiting enormously form the systematic generation of different reporters and transgenic reporter lines, by which specific cell types can be visualized and/or manipulated through controlled expression of fluorescent proteins and/or other genes, as well as the cell-specific knock-out of particular genes of interest (Roy *et al.*, 1994; Mombaerts *et al.*, 1996; Feng *et al.*, 2000; Sugino *et al.*, 2005; Madisen *et al.*, 2009; Huang & Zeng, 2013).

Functional readouts, including electrophysiology and neuronal activity imaging, have provided another dimension to cell type classification (Verkhratsky & Parpura, 2014). Similarly to anatomical properties, biophysical properties and typical activity patterns can be very specific for each cell type, helping us to acquire fundamental knowledge about their role in the circuit and its computation (Armstrong, 1995; Klausberger *et al.*, 2003; Maccaferri & Lacaille, 2003; Le Van Quyen *et al.*, 2008). Based on functional properties, passive biophysical properties (e.g. resting membrane potential, resistance, or capacitance), active features (e.g. action potential, after hyper, or after depolarization), and typical activity patterns during on-going behavior of the neurons can be characterized and classified (Connors & Gutnick, 1990; Lewicki, 1998;

Migliore & Shepherd, 2005; Le Van Quyen *et al.*, 2008; Karmažínová & Lacinová, 2010; Komendantov *et al.*, 2019).

In addition to anatomical and functional properties, transcriptomic profiling has become an extremely important and widely used approach for cell characterization. This involves the analysis of the gene expression of individual cells and the identification of genes which may be specific to a cell population (Usoskin *et al.*, 2014; Darmanis *et al.*, 2015; Hanchate *et al.*, 2015; Zeisel *et al.*, 2015). Cell types may be classified by a single or few known or unique markers, or based on their overall gene expression profiles. Next-generation single-cell sequencing now allows routine profiling of 100 to 1000s of cells simultaneously and have the advantage of specifically reporting the transcriptional profile of each cell in addition to cell type level characteristics.

The combination of the different approaches highlighted above furthermore allows simultaneous characterization of different structural, molecular, and functional features of single neurons and circuits. Such multimodal classification approaches are becoming fundamental tools in modern neuroscience (Cadwell *et al.*, 2015, 2017; Fuzik *et al.*, 2015; Poulin *et al.*, 2016; Zeng & Sanes, 2017; Que *et al.*, 2021).

In addition to classification, technological advances in gene and neuronal activity manipulations have significantly facilitated our knowledge gain about the brain. Such tools, often in combination with the above readouts, now allow the identification of single genes or molecules which are relevant to neural function in the healthy brain or contribute to pathological conditions. In this manner, the use of transgenic lines for cell type-specific molecular access; shRNA and CRISPR/Cas9 technologies for gene editing; optogenetics, chemogenetics and Tet-on or Tet-off systems for activity manipulations; tagging of immediate early genes, calcium imaging, advanced microscopy, and high density probes for activity readouts (Sheng & Greenberg, 1990; Lanahan & Worley, 1998; Földy *et al.*, 2004, 2016; Rao *et al.*, 2009; Fenno *et al.*, 2011; Yizhar *et al.*, 2011; Grienberger & Konnerth, 2012; Cadwell *et al.*, 2015; Fuzik *et al.*, 2015; Gascón *et al.*, 2017; Voigt *et al.*, 2019; Navabpour *et al.*, 2020; Ueda *et al.*, 2020; Luo *et al.*, 2021) have all became essential tools. Finally, detailed behavioral readouts can further facilitate the functional interrogation of neuronal circuits (Zhang *et al.*, 2007; Sternson, 2013; Lüthi & Lüscher, 2014; Wolff & Ölveczky, 2018; Luo *et al.*, 2021).

As the reader will see in the following Chapters, my own research has greatly benefited from several of these incredible technologies, allowing me to make the discoveries laid out in this Thesis.

Objectives of the thesis

As the general Introduction already highlights, there has been an enormous progress in neuroscience toward understanding the structure and function of the brain. However, it is also clear that the brain is not yet fully "understood", and much more work will need to be done until, for example, neurological, neurodevelopmental, and neuropsychiatric disorders and injuries will be curable. An important step toward achieving these goals is to understand the "molecular logic" of the brain's wiring, i.e. the molecular rules governing the assembly of synaptic circuits during development as well as their maintenance and function during the lifespan. In establishing this molecular logic, the combinatorial expression of CAMs is presumed to play a key role. As such, characterizing the specific expression of CAMs in different cell types and synapses is an important goal. The combination of CAMs in the synapses is thought not only to determine which cell types a neuron is connected, but also the structural and functional properties of the synaptic connections themselves (Zipursky & Sanes, 2010; Földy *et al.*, 2013, 2016; Südhof, 2018, 2021; Sanes & Zipursky, 2020). Previous work from our lab has contributed to this characterization effort (Lukacsovich *et al.*, 2019; Que *et al.*, 2019, 2021; Winterer *et al.*, 2019). In addition to revealing cell type-specific CAM expression patterns, these results illuminated an intriguing possibility that the combinatorial expression of different CAMs, potentially hundreds in a single neuron, could be attributed to a much smaller number of transcription factors controlling their expression.

The aim of my thesis was to explore this hypothesis in a greater detail. For this, we chose an experimental approach which was to study newly formed circuits in the adult brain and investigate the underlying molecular mechanisms behind their formation. The key idea behind this approach is that the formation of new circuits requires specific CAMs which define axon targeting properties. Some of these CAMs may not be endogenously expressed by the neurons before, but appear during further wiring. We hypothesized that such CAM expression changes would manifest themselves at the transcriptomic level controlled by specific transcription factors.

As described in the general Introduction, there are multiple forms of circuit formation in the adult brain, several of which are associated with neurological disorders, such as epilepsy. One key example is the hippocampal mossy fiber sprouting by granule cells, which has been associated with temporal lobe epilepsies. Mossy fiber

sprouting has been extensively studied and is reliably inducible in multiple different experimental models, such as by electrical, chemical or mechanical approaches. Despite decades of progress, the molecular mechanisms of mossy fiber sprouting as well as its contribution to seizures remain elusive (Buckmaster, 2014; Cavarsan *et al.*, 2018). We chose to focus on this paradigm of circuit formation in the adult rodent brain, and adopted the well-established intrahippocampal kainic acid microinjection model as an experimental approach. After kainic acid injection, granule cells sprout new axons and form a local recurrent excitatory circuit within the dentate gyrus. According to our hypothesis, the formation of this new recurrent circuit would require a specific set of CAMs and feasibly the activation and/or inactivation of a specific transcriptomic program, which controls CAM expression. To investigate this program, we used single-cell RNA sequencing from control and sprouting granule cells and subsequent molecular manipulations to test the involvement of presumably key "candidate" molecules.

Already the first experiments revealed that the potentials of our approach go beyond an ontological characterization of CAMs and their upstream molecular programs. Namely, we observed that activation of a single transcriptomic regulator, *Id2*, can reactivate wiring in adult neurons and drive the formation of a new mossy fiber circuit. This discovery defined my research goals.

My thesis work is composed of three conceptually interlinked and yet independent research projects. As a shared feature, I focused on the mechanisms and consequences of adult wiring in each project. As mentioned in the general introduction, wiring in the adult brain has not been broadly considered and remain overall poorly understood. In the first project (Chapter 2), I will address how we identified *Id2* as a key regulator of wiring in the kainic acid microinjection model of experimental epilepsy and characterized its wiring effect in the healthy adult brain. Key questions that I will be addressing include which transcriptomic programs are activated by *Id2*, what are the anatomical and physiological properties of the new circuits, and what is the impact of the new circuits on behavior, learning and memory. In the second project (Chapter 3), I will address the involvement of specific CAMs in mossy fiber sprouting, and more broadly, the question of how CAMs may determine target specificity during adult wiring. Finally, in the third project (Chapter 4), I will follow up on an intriguing observation we made during the previous two projects, showing the rapid onset of a so-called commissural form of adult wiring, i.e. the establishment of long axonal connections

between the two brain hemispheres. My results in this last project did not only provided insights into commissural axon growth during adult wiring but helped to reveal a previously unnoted subpopulation of hippocampal granule cells in the healthy adult brain.

Chapter 2 – Reactivation of wiring in adult hippocampal granule cells

Introduction

In contrast to developmental wiring, wiring in the adult brain has not been generally considered and its mechanisms remain poorly understood. Mossy fiber sprouting by hippocampal granule cells is one pronounced form of adult wiring, which has been extensively investigated in the context of epilepsies, for example to understand seizure mechanisms. By contrast, mossy fibers sprouting as a model of adult wiring has received much less attention. While experimental models of temporal lobe epilepsy, such as intrahippocampal kainic acid microinjection model, frequently induce both mossy fiber sprouting and seizures, most studies have been focusing on hippocampal structure and function after the onset of seizures. We took advantage of that mossy fiber sprouting typically begins to develop as early as 1 to 3 days after kainic acid injection, whereas the seizures only 3 to 4 weeks later. Thus, for a certain amount of time, circuit formation can be studied without the need of considering additional and potentially confounding consequences of the seizures. We used multimodal analyses involving electrophysiology, neuroanatomy, and single-cell transcriptomics to analyze the cellular/molecular changes in control and sprouting granule cells within this time window in order to better understand the wiring mechanisms.

I contributed to this project with research design discussions and performing different sets of experiments. Specifically, I was responsible for tissue preparation, staining, histology analysis and behavioral testing.

Recurrent rewiring of the adult hippocampal mossy fiber system by a single transcriptional regulator, Id2

Wenshu Luo[a] , Matteo Egger[a], Andor Domonkos[a] , Lin Que[a], David Lukacsovich[a], Natalia Andrea Cruz-Ochoa[a], Szilárd Szőcs[b] , Charlotte Seng[a], Antónia Arszovszki[c], Eszter Sipos[c] , Irmgard Amrein[d], Jochen Winterer[a], Tamás Lukacsovich[a] , János Szabadics[c], David P. Wolfer[d,e], Csaba Varga[b] , and Csaba Földy[a,1]

[a]Laboratory of Neural Connectivity, Brain Research Institute, Faculties of Medicine and Science, University of Zürich, Zürich, 8057, Switzerland; [b]Szentágothai Research Center, Department of Physiology, Medical School, University of Pécs, Pécs, 7624, Hungary; [c]Laboratory of Cellular Neuropharmacology, Institute of Experimental Medicine, Budapest, 1083, Hungary; [d]Institute of Anatomy, Faculty of Medicine, University of Zürich, Zürich, 8057, Switzerland; and [e]Institute of Human Movement Sciences and Sport, D-HEST, ETH Zürich, Zürich, 8057, Switzerland

Circuit formation in the central nervous system has been historically studied during development, after which cell-autonomous and non-autonomous wiring factors inactivate. In principle, balanced reactivation of such factors could enable further wiring in adults, but their relative contributions may be circuit dependent and are largely unknown. Here, we investigated hippocampal mossy fiber sprouting to gain insight into wiring mechanisms in mature circuits. We found that sole ectopic expression of Id2 in granule cells is capable of driving mossy fiber sprouting in healthy adult mouse and rat. Mice with the new mossy fiber circuit solved spatial problems equally well as controls but appeared to rely on local rather than global spatial cues. Our results demonstrate reprogrammed connectivity in mature neurons by one defined factor and an assembly of a new synaptic circuit in adult brain.

mossy fiber | single-cell RNA-seq | Id2 | circuit formation | adult brain rewiring

Connectivity is one of the most defining features of cellular identity in neurons of the brain and spinal cord. During development, cell surface receptors and neurotrophic gradients guide axon growth and formation of synaptic connections between neurons (1–3). After the developmental milieu dissipates, inhibitors of neurite growth are up-regulated (4, 5), and the axonal and dendritic structure of neurons become established. In adult brain, the lack of cell intrinsic axon growth, growth-supportive substrate, and chemoattraction hinders not only further wiring but also the attainment of therapeutic rewiring after injury (6). Currently, cell-autonomous mechanisms—including those mediated by transcription factors such as members of the CREB, HDAC, ID, KLF, SMAD, STAT, and SOX families—have been able to partially recapitulate circuit wiring (7, 8). However, it is thought that additional cell nonautonomous mechanisms are required to fully recapitulate circuit wiring (6). Nevertheless, other studies demonstrated that under mixed developmental-adult conditions, as seen after adult neurogenesis (9) and after in vivo glia/astrocyte to neuron conversion and stem cell grafting (10), long-range axonal wiring and synaptic integration can be achieved in adult circuits. This would suggest that some cell-autonomous mechanisms can overcome barriers to further circuit formation, but the nature of such permissive signals is not understood.

To explore wiring mechanisms in mature circuits of adult brain, we investigated axonal sprouting in the hippocampal mossy fiber (MF) system. Formed during normal development, naive MF axons originate from dentate gyrus granule cells (GCs) and target different cell types in hilus and CA3 (11). By contrast, during MF sprouting, which is typically studied in the context of temporal lobe epilepsies (TLE), GCs form new axons and synapses within the dentate and thereby create a new circuit on top of the developmentally established wiring scheme (12–14). MF sprouting is also inducible by different approaches, such as coarse mechanical (15, 16), electrical (17), and chemical induction (18),

or by excessive activation of the mTOR pathway in postnatally generated GCs (19). However, these manipulations coinduce multiple other alterations in the network (e.g., cell death, GC dispersion, formation of aberrant GC dendrites, and changes in cell excitability), which thus far hindered understanding their relative contributions to TLE pathology (20) and of molecular mechanisms of MF sprouting (21–23). Regardless of its relation to TLE, MF sprouting involves all key stages of circuit assembly (i.e., axon growth, target cell specification, and synapse formation) and thus also represents a comprehensive model for studying wiring mechanisms in adult brain.

Our study aimed to elucidate transcriptional mechanisms behind MF sprouting and test if, analogous to reprogramming of differentiated cells (24), the connectivity of differentiated mature GCs can be reprogrammed via cell-autonomous genetic induction. Consistent with the assembly of an entirely new circuit, we hypothesized that MF sprouting was associated with broad transcriptomic changes in GCs. To recapitulate these changes in their entirety, we focused on transcription factors and regulators, whose activation may initiate the wiring process. Using a single-cell RNA-sequencing (RNA-seq) screen, we identified Id2, an inhibitor of transcription factors, as master regulator whose sole activation in GCs drove MF sprouting and formation of functional synapses. Mechanistically, activation of Id2 led to transcriptomic up-regulation of molecules in the JAK/STAT and interferon

Significance

Neurons have an exceptional capacity to grow axons and form synaptic circuits during development but not later life. In adults, the lack of circuit formation may support retention of skilled actions and memories but also limits regeneration and repair after injuries and in disorders. Research on developing and damaged neurons has revealed many molecules that help circuit formation and regeneration, and yet factors that could induce axon growth and synapse formation in adult brain neurons remain elusive. Here, we searched for such key molecules and find one that alone can induce complete circuit formation. After engineering a new circuit in adult mice, we also looked into its function and relevance for memories.

NEUROSCIENCE

signaling pathways and controlled downstream expression of multiple wiring-related effectors. We furthermore tested if genetically induced MF sprouting generated hyperexcitability in the hippocampus, as posited by certain models of seizure generation, and investigated its consequences on learning and memory.

Results

Single-Cell Transcriptome of MF Sprouting. To begin, we used chemical induction (neuroexcitatory kainic acid [KA], microinjection into the hippocampus) in 2-mo-old mice to investigate the MF sprouting transcriptome. Using single-cell patch RNA-seq (25, 26), we sampled mature GCs 1 d (representing acute cellular response to induction) and 14 d after induction (27), by which time MF sprouting, but not epilepsy (28, 29), reliably develops (Fig. 1A). Transcriptomic analysis revealed up-regulated expression (FDR < 0.05) of several transcription regulators, including members of the ID (Id2), SMAD (Smad3), SOX (Sox11), STAT (Stat3, Stat1), HDAC (Hdac9), KLF (Klf10, Klf5), and CREB (Creb1) families (Fig. 1B and SI Appendix, Fig. S1). Of these, Id2, a developmentally active inhibitor of transcription factors, was a particular candidate of interest. Previously, Id2 was shown to have increased expression in GCs after status epilepticus (30), and separate studies have linked this gene to axon growth in cell and slice culture (31–33) and following spinal cord injury (34). Using immunostaining, we confirmed up-regulation of Id2 protein levels,

which was apparent in few GCs already 1 d after KA (SI Appendix, Fig. S1G) but present in most GCs 3 d after KA (Fig. 1C and SI Appendix, Fig. S1H). This up-regulation persisted 14 d later (Fig. 1D). At first, the Id2 signal was present in nucleus (1 d) but later (3 d and after) become enriched in cytosol. This was consistent with a model in which Id2 is either sequestered to the cytosol by other factors (35–37) or itself binds and sequesters transcription factors to the cytosol (38). Notably, our analyses also revealed the presence of Id2 protein in MF axons in CA3, which was independent of its lack (in controls) or presence (after KA) in GC soma (Fig. 1D). While this may suggest a yet unrecognized role for Id2 in MF axons, since in this study our focus was on rewiring, we followed up on the up-regulation of Id2 that corresponded to sprouting.

AAV-Id2 Induces Axon Growth in the Mature MF System. To test if Id2 played a role in MF sprouting, we cloned and ectopically expressed the Id2 gene selectively in GCs of the ventral hippocampus of adult Calb1-IRES2-Cre-D mice using Cre-dependent AAVDJ/8 virus (note that although AAV-Id2 was coinjected with AAV-EGFP to confirm the injection site by visualizing GCs, hereafter, we refer to this injection simply as AAV-Id2; for controls, only AAV-EGFP was used, in equal volume; Fig. 2A). One to three months after induction, histological analyses revealed newly formed MF axons targeting the GC and inner molecular layer (GCL and IML, respectively; Fig. 2 B and C and
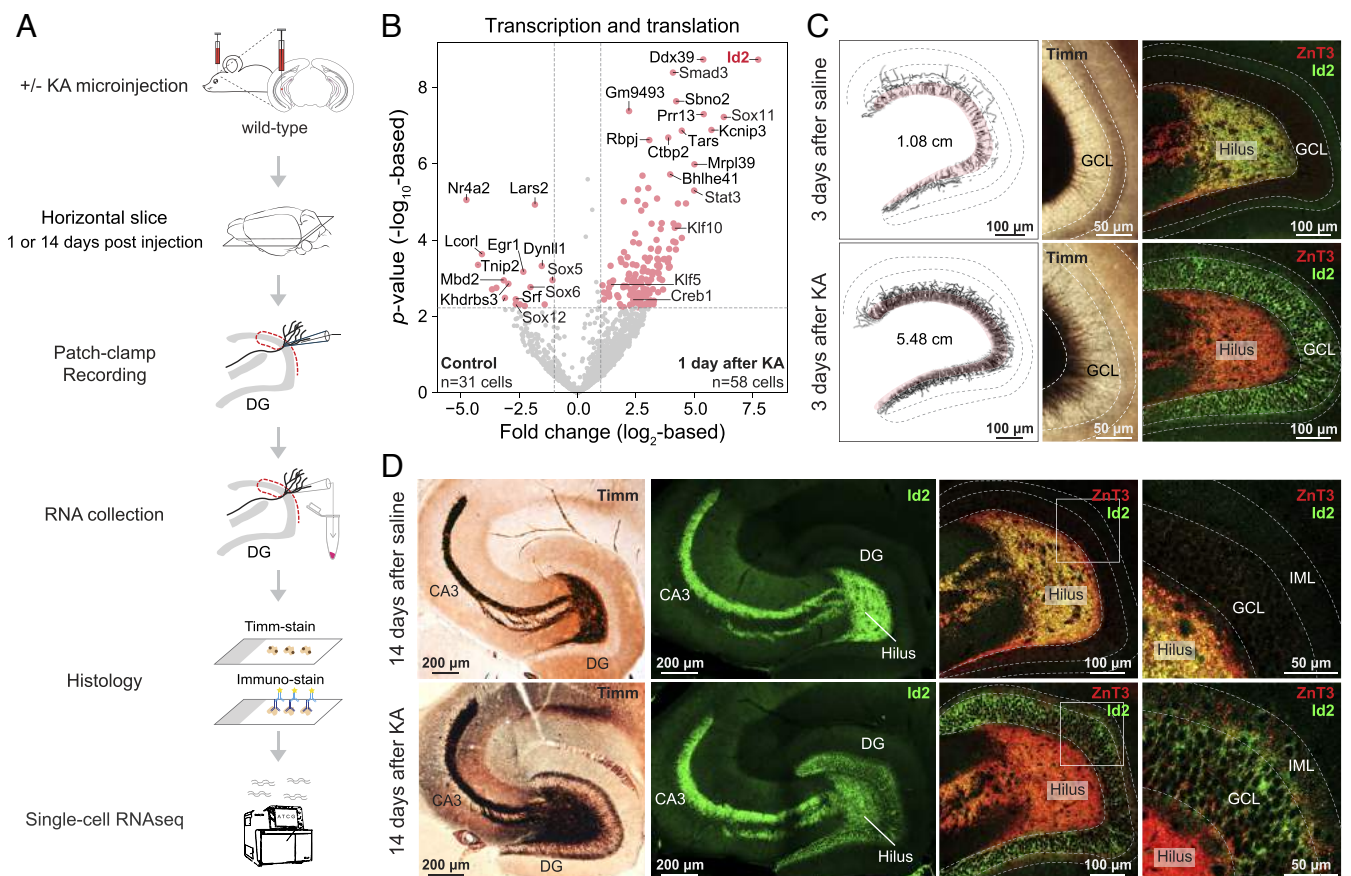

Fig. 1. Transcriptomic analysis of chemically induced MF sprouting. (A) Experimental design. (B) Volcano plot shows acute transcriptomic changes of transcription and translation-related molecules in single GCs 1 d after KA induction of MF sprouting. Red points denote differentially expressed genes (FDR < 0.05 and >2-fold change, or |$\log_2$FC| > 1 as in plot). (C) MF sprouting is already ongoing and Id2 is up-regulated in GCL 3 d after KA induction. Upper panels show saline-injected controls; lower panels show KA. From left to right: Timm's staining–based MF axon tracings reconstructed from 80-μm-thick sections; Timm's-stained brain slices at higher magnification; immunohistochemical staining of ZnT3 and Id2. (D) MF sprouting develops and Id2 remains up-regulated in GCL 14 d after KA. Upper panels show saline-injected controls; lower panels show KA. From left to right: Timm's-stained hippocampal slices displaying the whole MF system; immunostaining of Id2 in the MF system (note the presence of Id2 in naive fibers in hilus and CA3); immunostaining of ZnT3 and Id2 in dentate gyrus shown at higher magnifications.

Luo et al.
Recurrent rewiring of the adult hippocampal mossy fiber system by a single
transcriptional regulator, Id2

Quantification of axonal length and puncta further corroborated these observations. Both the measurement of MF axon length (AAV-EGFP: 1.3 ± 0.17 cm, $n = 6$ mice; AAV-Id2, 1 mo: 2.5 ± 0.34 cm, $n = 4$ mice, 2 mo: 2.8 ± 0.42 cm, $n = 3$ mice, 3 mo: 4.7 ± 0.56 cm, $n = 5$ mice; Fig. 2D) and puncta size (in GCL, AAV-EGFP: 0.82 ± 0.024 μm^2, 737 puncta/4 mice; AAV-Id2: 1 mo: 1.6 ± 0.038 μm^2, 691 puncta/3 mice, 2 mo: 1.9 ± 0.14 μm^2, 853 puncta/3 mice, 3 mo: 2.5 ± 0.25 μm^2, 712 puncta/3 mice; in IML, AAV-EGFP: 0.90 ± 0.044 μm^2, 206 puncta/4 mice; AAV-Id2, 1 mo: 1.3 ± 0.076 μm^2, 309 puncta/3 mice, 2 mo: 1.8 ± 0.22 μm^2, 534 puncta/3 mice, 3 mo: 1.8 ± 0.081 μm^2, 358 puncta/3 mice; Fig. 2E) revealed time-dependent increases after AAV-Id2 delivery. Because zinc transporter-3 (ZnT3) is a known marker of naive MFs (39), we tested its expression by immunostaining (Fig. 2F) and found both increased density (in GCL, AAV-

EGFP: $1.1 \pm 0.16 \times 10^5$ puncta/mm^3, AAV-Id2: $4.5 \pm 0.47 \times 10^5$ puncta/mm^3; in IML, control: $0.86 \pm 0.16 \times 10^5$ puncta/mm^3; AAV-Id2: $5.0 \pm 0.96 \times 10^5$ puncta/mm^3; AAV-EGFP: 11 hippocampi from 6 mice, AAV-Id2: $n = 8$ hippocampi from 6 mice; Fig. 2G) and size (in GCL, AAV-EGFP: 0.83 ± 0.15 μm^2; AAV-Id2: 1.6 ± 0.13 μm^2; in IML, AAV-EGFP: 0.83 ± 0.15 μm^2; AAV-Id2: 1.2 ± 0.17 μm^2; AAV-EGFP: $n = 5$ hippocampi from 5 mice, AAV-Id2: $n = 5$ hippocampi from 5 mice; Fig. 2H) of ZnT3+ puncta 3 mo after AAV-Id2 induction. We also confirmed that AAV-Id2 induced rewiring at the single-cell level by morphological reconstruction of individual GCs, which revealed recurrent fibers in GCL/IML after AAV-Id2 induction without apparent reorganization of the cells' developmentally established axonal and dendritic structure (Fig. 2I). In order to test if, in addition to its effect on anatomical rewiring, AAV-Id2 also
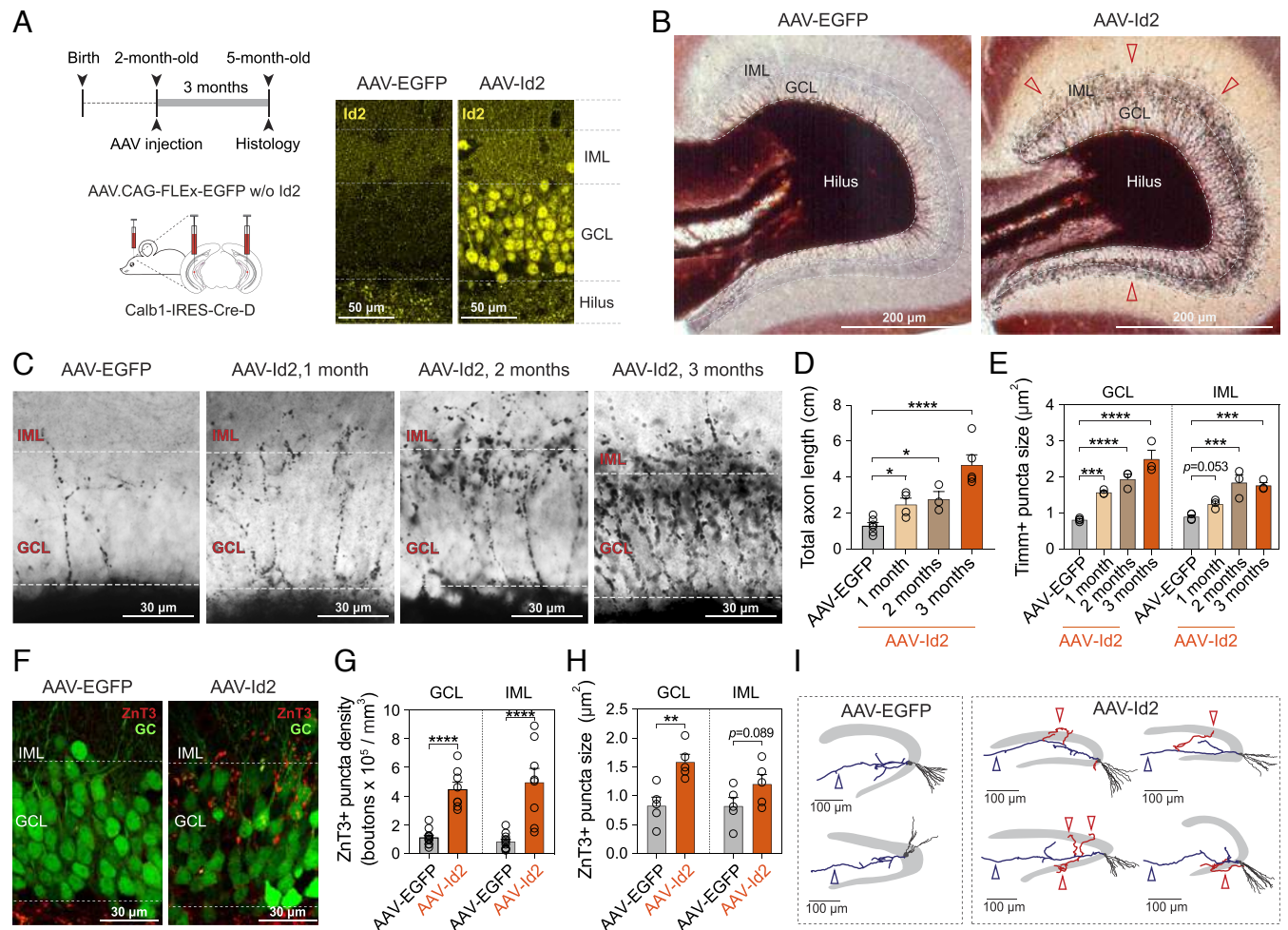

Fig. 2. AAV-delivered Id2 induces axon growth and target-specific rewiring in mature hippocampal GCs. (*A*) Experimental design. The Calb1-IRES-Cre-D transgenic line allows genetic access to dentate GCs via expression of Cre. Confocal images show confirmation of Id2 overexpression by immunostaining. (*B*) Timm's staining shows the dentate gyrus 3 mo after Cre-dependent AAV-EGFP (control) and AAV-Id2 injections. After AAV-Id2, dark ring-like precipitation around GCL represents newly formed MFs (red arrowheads). (*C*) Timm's stainings show MFs in GCL/IML 1, 2, and 3 mo after AAV-EGFP and AAV-Id2 injections. (*D*) Quantification of total axon length after AAV-EGFP and AAV-Id2 injections (one-way ANOVA, AAV-EGFP versus AAV-Id2, 1 mo, *$P = 0.043$; 2 mo, *$P = 0.023$; 3 mo, ****$P < 0.0001$). (*E*) Quantification of Timm's positive puncta size in GCL/IML after AAV-EGFP and 1, 2, and 3 mo after AAV-Id2 injections (data points represent one individual; two-way ANOVA, GCL: AAV-EGFP versus AAV-Id2, 1 mo, ***$P = 0.0003$; 2 mo, ****$P < 0.0001$; 3 mo, ****$P < 0.0001$. IML: AAV-EGFP versus AAV-Id2, 1 mo, $P = 0.053$; 2 mo, ****$P < 0.0001$; 3 mo, ****$P < 0.0001$). (*F*) EGFP labeling of GCs (green) and ZnT3 staining of MF synapses (red) in GCL/IML 3 mo after AAV-EGFP and AAV-Id2 injections (note that AAV-Id2 was coinjected with AAV-EGFP to visualize GCs). (*G*) Quantification of ZnT3-positive puncta density in GCL/IML 3 mo after AAV-EGFP and AAV-Id2 injections (two-way ANOVA, GCL: AAV-EGFP versus AAV-Id2, ****$P < 0.0001$; IML: AAV-EGFP versus AAV-Id2, ****$P < 0.0001$). (*H*) Quantification of ZnT3-positive puncta size in GCL/IML 3 mo after AAV-EGFP and AAV-Id2 (two-way ANOVA, GCL: AAV-EGFP versus AAV-Id2, **$P = 0.0022$; IML: AAV-EGFP versus AAV-Id2, $P = 0.089$). (*I*) Reconstruction of single GCs 3 mo after AAV-EGFP and AAV-Id2 injections. After AAV-Id2, newly formed axons that extend into GCL and IML are shown in red. Original MF projections to CA3 are marked with blue arrowhead. CA3 is omitted for clarity.

Luo et al.
Recurrent rewiring of the adult hippocampal mossy fiber system by a single transcriptional regulator, Id2

PNAS | 3 of 11
https://doi.org/10.1073/pnas.2108239118

changed action potential (AP) firing of GCs or their overall synaptic drive onto CA3, we performed electrophysiological characterization of these properties. These revealed that despite an increase in the cells' input resistance, AAV-Id2 did not appear to change either current-pulse–induced AP firing properties or the cells' developmentally established synaptic drive onto CA3 pyramidal cells (*SI Appendix*, Fig. S3).

Since the ventral and dorsal hippocampus support different brain functions and display distinct molecular patterns (40–42) and left-right asymmetries in hippocampal function have also been recognized (43), in a next set of experiments, we tested if AAV-Id2 induced MF rewiring in hippocampal locations other than the ventral part. For this, we expressed AAV-Id2 in dorsal and ventral GCs, both in left and right hippocampi (Fig. 3*A*), which led to development of MF rewiring throughout the entire mouse hippocampus, independent of anatomical location (Fig. 3*B* and *SI Appendix*, Fig. S2*A*).

Finally, in addition to mice, because MF sprouting has been extensively characterized in rats (12–18, 21, 22), we tested if Id2 had the ability to induce MF sprouting in this different species. For this, we injected Cre-independent AAV-Id2 into the hippocampus of wild-type rats. Similarly to observations in mouse, this manipulation revealed powerful MF rewiring (Fig. 3 *C–F*). Two to three months after injection, the relative intensity of Timm's staining was significantly higher both in GCL and IML in AAV-Id2–injected dentate gyrus compared to controls (Control, GCL: $18.4 \pm 4.3\%$, IML: $30.3 \pm 4\%$, six hippocampi from three rats; AAV-Id2, GCL: $40.4 \pm 2.8\%$, IML: $69.9 \pm 5.5\%$, seven hippocampi from five rats; percentages represent signal intensity relative to hilus in the same sections). These observations demonstrate that AAV-Id2 can uniformly activate a GC wiring program in different hippocampal segments and species.

AAV-Id2 Induces Functional MF Synapse Formation. To test if genetically induced MF sprouting by AAV-Id2 involved formation of functional synapses, we labeled MF boutons by ZnT3 immunostaining and characterized them using electron microscopy. This showed that ZnT3+ boutons were formed on GC dendrites and spines, each bouton containing one or multiple release sites and abundant supply of synaptic vesicles (Fig. 4 *A* and *B*). To probe physiological transmission, we induced MF rewiring with AAV-Id2 while also expressing channel-rhodopsin (AAV-ChR) in GCs in vivo and prepared brain slices for electrophysiology 3 mo after induction. Because large conductance ChR currents would mask the comparably smaller synaptic currents, we restricted ChR expression and rewiring to a subset of GCs by using Rbp4-Cre transgenic mice, in which only ~30% of GCs express Cre and thus Cre-dependent Id2 and ChR (Fig. 4*C*). In separate experiments in the dorsal and ventral hippocampus, we performed patch-clamp recordings from ChR nonexpressing cells. Independent of anatomical location, ChR activation by blue light evoked larger and more frequent excitatory synaptic events in slices after AAV-Id2 injection compared to controls (in dorsal hippocampus, Control: -9.9 ± 1.9 pA, AAV-Id2: -40 ± 11pA; Control, $n = 8$ out of 34 cells, from six mice; AAV-Id2, $n = 17$ out of 55 cells, from seven mice; Fig. 4*D*; in ventral hippocampus, Control: -11 ± 2.8 pA, AAV-Id2: -36 ± 9.7 pA; Control, $n = 10$ out of 36 cells, from six mice; AAV-Id2, $n = 6$ out of 39 cells, from seven mice; Fig. 4*E*). To summarize, AAV delivery of the single transcriptional regulator Id2 led to formation of a new MF circuit, including formation of functional synapses.

The transcriptomic network controlled by Id2 in mature GCs. Next, we sought to better understand the molecular mechanisms behind AAV-Id2–induced MF rewiring. Although Id2 has been extensively characterized for its role in transcriptional regulation (31, 38, 44), one previous study suggested that Id2 may directly contribute to axon growth and growth cone formation independently

of transcriptional regulation (33). This function was dependent on Akt-mediated phosphorylation of the serine 14 site in Id2 (33). To test this possibility first, we virally expressed phosphorylation-ablated mutant Id2(S14A), AAV-Id2(S14A), in the ventral hippocampus. We hypothesized that MF rewiring would not develop using this mutant form if Akt/Id2 signaling was involved. However, AAV-Id2(S14A) still induced MF rewiring (*SI Appendix*, Fig. S4), suggesting that direct growth cone formation by Id2 was unlikely.

Second, we investigated transcriptomic changes induced by Id2. By directly binding transcription factors, Id2 inhibits their DNA binding and thereby their transcriptional activity (31, 44) (Fig. 5*A*). Consequently, increased expression of Id2 would feasibly lead to both up-regulated and down-regulated expression of genes, whose identity depends on the transcription factors that were inhibited by Id2. To study transcriptomic consequences, we sequenced single GCs 1 mo after AAV-Id2 induction (Fig. 5*B*), when growing axons were already apparent (Fig. 2*C*). Consistent with a role in transcriptional regulation, this revealed broad transcriptomic changes, which were dominated by members of the JAK-STAT (Stat1, Stat3, and Irf9) (45) and interferon signaling pathways (e.g., Irf1, Irf7, Irf9 Isg15, Usp18) (46) as well as by multiple other molecules that have been associated with axonal wiring (e.g., Tle1, Nefm, Slit1, Adcy1; Fig. 5*C* and *SI Appendix*, Fig. S5; see *Discussion*).

We next asked what might be key mediators of the AAV-Id2–induced rewiring program, that is, molecules that interface Id2 and the aforementioned genes. Since Id2 inhibits the activity of transcription factors, without necessarily changing their expression, the found transcriptomic changes likely represent downstream effects and do not indicate upon which transcription factors Id2 directly acts. Therefore, we performed transcription factor-target enrichment analysis with the aim of identifying transcription factors that were either directly or indirectly inhibited or indirectly disinhibited by Id2. Using Enrichr (47, 48), we found 26 such factors whose known regulatory network matches the observed gene expression patterns and which were expressed in at least 30% of GCs (Fig. 5*D*). Together with this analysis, our results outlined a comprehensive transcriptomic model behind MF rewiring, in which Id2 exerts control over members of the wiring-related JAK-STAT, Wnt, cAMP, and Slit/Robo signaling pathways (Fig. 5*E* and *SI Appendix*, Figs. S5–S7).

Hippocampal brain dynamics after AAV-Id2–induced MF rewiring. The ability to genetically induce MF sprouting allowed us to examine the network effects of this observed rewiring event. MF sprouting is observed in human TLE and is a hallmark in experimental TLE, but the question of whether it is a cause or consequence of seizures has been debated (20, 21). Thus, by performing multichannel silicon probe recordings in the hippocampus of freely moving mice, we looked to see if signatures of pathological brain dynamics (49) have developed 3 mo after AAV-Id2–induced MF rewiring (Fig. 6 *A* and *B*). In the 1 to 400 Hz range of local field potentials, our recordings did not register pathological oscillations or seizure-like activity (Fig. 6*C*). Specifically, theta, beta, slow and fast gamma, and ripple and fast ripple range oscillations remained intact. In addition, we analyzed CA1 sharp wave-ripple (SWR) and dentate spike (DS) events because their intrinsic frequency and occurrence, respectively, both increased in TLE (50, 51). Neither of these pathologies were present in our data. The occurrence (AAV-EGFP: 0.31 ± 0.033 Hz, $n = 6$ mice; AAV-Id2: 0.27 ± 0.037 Hz, $n = 6$ mice) and intrinsic frequency (AAV-EGFP: 152 ± 7.8 Hz, $n = 6$ mice; AAV-Id2: 152 ± 2.7 Hz, $n = 6$ mice) of SWRs were not different between AAV-EGFP and AAV-Id2–injected mice (Fig. 6*D* and *SI Appendix*, Fig. S8). By contrast, the occurrence of type-1 DS (DS1) decreased (AAV-EGFP: 0.59 ± 0.12 Hz, $n = 6$ mice; AAV-Id2: 0.32 ± 0.19 Hz, $n = 6$ mice; $P = 0.06$, Mann–Whitney U test), whereas type-2 DS (DS2) were selectively lost after AAV-Id2
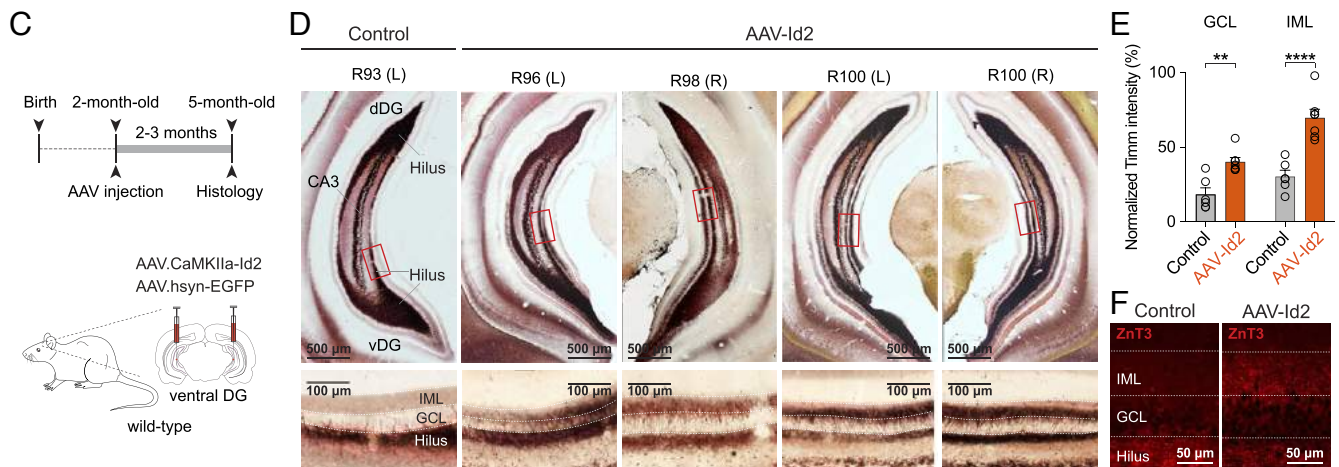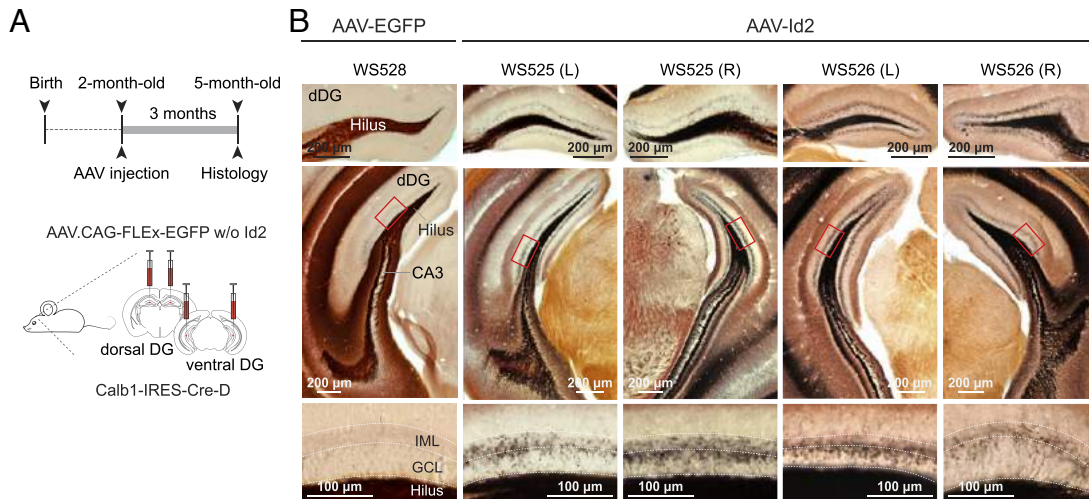
Fig. 3. AAV-delivered Id2 induces MF rewiring throughout the mouse and rat hippocampus. (*A*) Experimental design showing Id2 overexpression in mouse dorsal and ventral hippocampus. (*B*) Images show Timm's-stained sections collected from different levels of dorsal hippocampus (bregma, –2.0 mm and –3.2 mm) after AAV-EGFP (control) and AAV-Id2 injections. Higher-magnification images at bottom show sprouting in GCL and IML in AAV-Id2 mice. (*C*) Experimental design showing Id2 overexpression in rat ventral hippocampus. (*D*) Example images of Timm staining in rats after Id2 overexpression. Coronal sections of rat ventral hippocampus (bregma, –6.2 mm) were collected from regions where AAV infection was confirmed by EGFP expression. Non-AAV-infected hippocampus was used as control. (*E*) Quantification of Timm's staining intensity. Intensities were measured relative to signals in the hilus of the same sections (two-way ANOVA, GCL: Control versus AAV-Id2, **$P = 0.0017$; IML: Control versus AAV-Id2, ****$P < 0.0001$). (*F*) ZnT3 staining of MF synapses in GCL/IML 3 mo after AAV-Id2 injections.

delivery (AAV-EGFP: 0.22 ± 0.089 Hz, $n = 6$ mice; AAV-Id2: 0.021 ± 0.020 Hz, $n = 6$ mice; $P = 0.015$, Mann–Whitney U test, Fig. 6*E* and *SI Appendix,* Fig. S8). Taken together, intact oscillations and SWRs suggested that the network dynamics in AAV-Id2 mice are divergent from TLE, whereas the decrease in DS occurrence suggested that activity routing was still effectively altered in the dentate network.

Learning and memory after AAV-Id2–induced MF rewiring. DS1 and DS2 events have been suggested to be triggered by population bursts of layer II stellate cells of the lateral entorhinal cortex (LEC) and medial entorhinal cortex (MEC), respectively (52). Since the LEC and MEC are proposed to support navigation based on local ("egocentric reference framework") and global ("allocentric reference framework") landmarks, respectively (53–55), and the dentate gyrus is critically involved in certain forms of object-related and

spatial learning and memory (11, 41, 42), we hypothesized that MF sprouting-related network effects would manifest themselves during behavior. To test this hypothesis, we utilized eight different previously validated assays to phenotype mice 3 mo after bilateral, dorsal, and ventral AAV-EGFP or AAV-Id2 injections (see *Methods* for particulars of each assay).

Before the tests, the animals were subjected to light cycle inversion. To examine light cycle adaptation, locomotor activity, and freely moving behavior, we monitored each mouse in its home cage for 13 d and in a novel open-field environment for 20 min. In the home cage, mice in both groups adapted equally well to an inverted day-light cycle, and their overall activity level was not different (*SI Appendix,* Fig. S9*A*). In addition, in the open field, there was no discernible difference in total travel distance (AAV-EGFP: 66 ± 2.7 m, $n = 12$; AAV-Id2: 75 ± 4.4 m, $n = 12$) and time spent in center zone (AAV-EGFP: $29 \pm 2.2\%$,

Luo et al.
Recurrent rewiring of the adult hippocampal mossy fiber system by a single transcriptional regulator, Id2

PNAS | 5 of 11
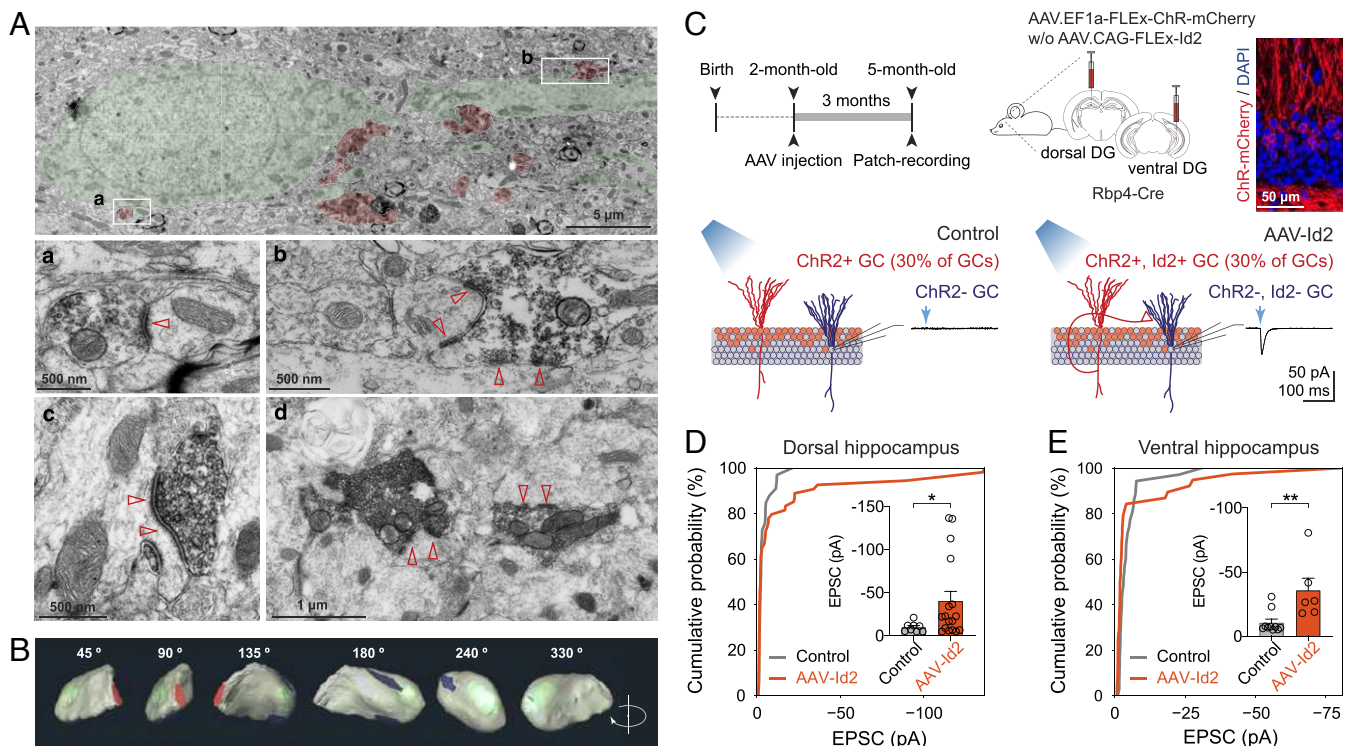https://doi.org/10.1073/pnas.2108239118

Fig. 4. AAV-delivered Id2 induces functional synapse formation. (*A*) Electron microscopy images show ZnT3-positive boutons (red) on GC dendrite and spines (green) 3 mo after AAV-Id2. *Insets* a and b are shown enlarged, whereas c and d show additional examples that are not present in panel *A*. (*B*) 3D electron-tomographic reconstruction of a ZnT3-positive MF bouton located in the GCL/IML border 3 mo after AAV-Id2. Red: axon shaft, green: mitochondria, blue: synapse formed by this bouton terminal. (*C*) Experimental design and injection schedule to test physiological transmission after MF rewiring. In acute brain slices, patch-clamp recordings were made from ChR-negative GCs, while ChR-positive GCs were activated with blue light (∼30% of total GCs population in these experiments) 3 mo after AAV-ChR (Control) and AAV-Id2 (mixed with AAV-ChR) injections. (*D*) Cumulative probability plot shows the fraction of recorded cells versus light-evoked EPSC amplitude in GCs of dorsal hippocampus (recorded in 10 μM Gabazine; Kolmogorov-Smirnov test, $P = 0.57$). *Inset* shows light-evoked EPSC amplitudes (Mann–Whitney U test, *$P = 0.048$). (*E*) Cumulative probability plot shows the fraction of recorded cells versus light-evoked EPSC amplitude in GCs of ventral hippocampus (recorded in 10 μM Gabazine; Kolmogorov-Smirnov test, *$P = 0.041$). *Inset* shows light-evoked EPSC amplitudes (Mann–Whitney U test, **$P = 0.0075$).

$n = 12$; AAV-Id2: $25 \pm 2.5\%$, $n = 12$) between the two groups (*SI Appendix*, Fig. S9B). Together, these suggest that AAV-Id2 mice did not display hyperactivity or anxiety-like behavior.

Next, we tested hippocampus-dependent long-term and short-term memory performance using novel object recognition and T-maze tests, which both take advantage of strong preference to novelty, whether object-related or environment-related, shown by rodents. The novel object recognition test showed that although both groups displayed preference to the novel object, AAV-Id2 mice did so to a lesser degree than controls (discrimination index [DI]; AAV-EGFP: $71 \pm 3.2\%$, $n = 8$; AAV-Id2: $50 \pm 8.7\%$, $n = 7$; mice with DI > 25% during training were excluded from analysis) (Fig. 7A and *SI Appendix*, Fig. S9C). In T-maze, alternation was above chance for both groups (AAV-EGFP: $71 \pm 5.6\%$, $n = 12$; AAV-Id2: $61 \pm 7.5\%$, $n = 12$) (Fig. 7B), which is also the expected outcome in untreated rodents. However, AAV-Id2 mice did not show a normally occurring increase in choice latencies across trials, and their latency to enter an arm remained significantly shorter than that of AAV-EGFP mice (at trial 6: AAV-EGFP: 35 ± 8.3 s, $n = 11$; AAV-Id2: 10 ± 2.2 s, $n = 11$) (Fig. 7B).

To test spatial information-related memory performance, we used the Morris water, Barnes, and eight-arm radial maze assays, in which goal-oriented navigation is reinforced by aversive, natural, and positive stimuli, respectively. In the Morris water maze, indicative of successful spatial learning, escape latencies (Fig. 7C) and swim path lengths (*SI Appendix*, Fig. S9D) robustly decreased in both groups during the acquisition. Moreover, both groups

displayed robust preference for the original target quadrant in the first probe trial of reversal learning, which was to test spatial retention (day 4; time in quadrant as percentage of total time, AAV-EGFP: target quadrant $36 \pm 4.8\%$, adjacent quadrants $21 \pm 2.2\%$; $n = 12$; AAV-Id2: target $39 \pm 3.0\%$, adjacent $23 \pm 1.6\%$, $n = 12$) (Fig. 7C). However, during the second probe trial of reversal learning (also on day 4), which was to test reversal learning itself, AAV-Id2, but not AAV-EGFP, mice still displayed a preference for the original target quadrant (AAV-EGFP: target quadrant $25 \pm 4.5\%$, adjacent quadrants $24 \pm 2.4\%$, $n = 12$; AAV-Id2: target $39 \pm 3.1\%$, adjacent $21 \pm 1.2\%$, $n = 12$) (Fig. 7C), suggesting spatial perseverance. Furthermore, AAV-Id2 mice reverted to a wall-oriented, nonspatial swimming strategy (Fig. 7C). Congruent with the observations in the Morris water maze, both groups learned the Barnes maze task (Fig. 7D and *SI Appendix*, Fig. S9E). However, AAV-Id2 mice made more errors in finding the escape chamber (primary errors, throughout all trials; AAV-EGFP: 7.6 ± 0.52, $n = 12$; AAV-Id2: 10 ± 0.69, $n = 12$) and did not show preference for the original target when the escape chamber was removed in the probe trial (poke ratio at original target, angle = 0°, AAV-EGFP: 3.6 ± 0.75, $n = 12$; AAV-Id2: 1.3 ± 0.28, $n = 12$). This was likely because AAV-Id2 mice more frequently adapted a serial search strategy (i.e., trying neighboring holes one after another) than AAV-EGFP mice (serial strategy, AAV-EGFP: $16 \pm 4.1\%$ of all tries, $n = 12$; AAV-Id2: $33 \pm 5.7\%$, $n = 12$). In the eight-arm radial maze, again, both groups learned equally well to decrease their memory errors, which is entry to an arm where the bait was already consumed per consumed baits of
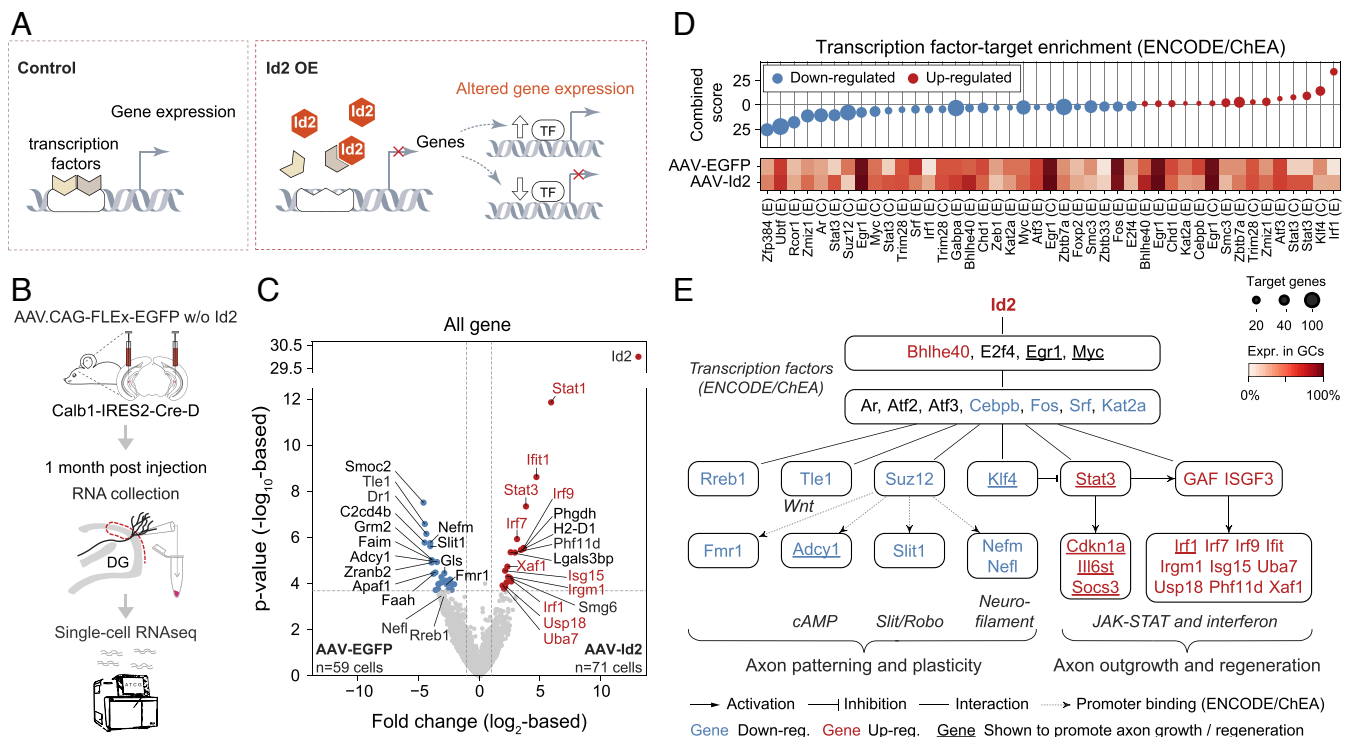
Fig. 5. Single-cell transcriptomics reveal a comprehensive rewiring program induced by AAV-delivered Id2. (*A*) Drawing depicts transcriptional function of Id2. (*B*) Experimental strategy. (*C*) Volcano plot shows gene expression differences between AAV-EGFP (*n* = 59 cells) and AAV-Id2 (*n* = 71 cells)–delivered single GCs. Horizontal and vertical dashed lines show FDR = 0.05 and 2-fold change ($|\log_2\text{FC}|>1$), respectively. Gene names highlighted in red belong to the JAK-STAT and interferon pathways. (*D*) Enrichr transcription factor-target enrichment analysis based on 285 up-regulated (red) and 848 down-regulated genes (blue) that were differentially expressed (*P* < 0.05) between the AAV-EGFP or AAV-Id2 data sets. Identified transcription factors (E: Encode, C: ChEA) and their expression rate in GCs are shown in the bottom. Circle size represents the number of target genes present in the inputted data. (*E*) The gene regulatory network activated by AAV-Id2. Nodes represent molecules from *C* and *D*; edges represent interactions. GAF and ISGF3 refer to proteomic assembly of Stat1 homodimers and Stat1, Stat2, and Irf9, respectively (45).

the total of eight baits over days (test days 9 to 10, AAV-EGFP: 0.47 ± 0.095, *n* = 12; AAV-Id2: 0.47 ± 0.13, *n* = 12) (Fig. 7*E*). However, memory errors during collection of the last two baits were higher in the AAV-Id2 mice (averaged over all test days, AAV-EGFP: 1.7 ± 0.15, *n* = 12; AAV-Id2: 2.2 ± 0.2, *n* = 12; Fig. 7*E*), suggesting a buildup of memory load in these mice. As a preferred strategy, both groups tended to enter the neighboring arm after visiting one (angle = 45°) (Fig. 7*E*). However, AVV-Id2 mice, but not AAV-EGFP, robustly increased their choices at this preferred angle over days (AAV-EGFP: days 1 to 2 = 38 ± 2.0%, days 3 to 8 = 52 ± 3.7%, days 9 to 10 = 50 ± 4.3%, *n* = 12; AAV-Id2: days 1 to 2 = 32 ± 3.5%, days 3 to 8 = 47 ± 4.1%, days 9 to 10 = 59 ± 6.7%, *n* = 12) (Fig. 7*E*).

Finally, we used a cued and contextual fear conditioning test to assay associative learning. Here, while both groups showed freezing response during context retention test, the response was smaller in AAV-Id2 mice (AAV-EGFP: 12 ± 2.1%, *n* = 12; AAV-Id2: 3.1 ± 1.7%, *n* = 12) (Fig. 7*F*). By contrast, although the response to tone retention still appeared to be lower in AAV-Id2 mice, freezing responses during tone retention and extinction tests were not significantly different between the two groups (tone retention: AAV-EGFP: 21 ± 3.1%, *n* = 12; AAV-Id2: 13 ± 3.6%, *n* = 12; extinction test: first tone: AAV-EGFP: 23 ± 4.2%, *n* = 12; AAV-Id2: 19 ± 4.6%, *n* = 12, last tone: AAV-EGFP: 11 ± 1.4%, *n* = 12; AAV-Id2: 9.1 ± 2.4%, *n* = 12) (Fig. 7*F*).

Discussion

In this study, we systematically analyzed MF sprouting with the aim of understanding transcriptomic mechanisms that can

facilitate axon growth and circuit formation in the adult brain. Our study design was motivated by the hypothesis that activation of certain cell-autonomous mechanisms may be sufficient to drive rewiring in the adult brain, where further axon growth is generally inhibited. Our results suggest three major conclusions, which have implications not only for circuit assembly in adult brain but also for TLE pathophysiology and information processing in the dentate gyrus.

Molecular Mechanisms of MF Sprouting. In the developing nervous system, Id2 enhances cell proliferation and inhibits the activity of mainly basic helix–loop–helix (31) but also other transcription factors (44). Mechanistically, developmentally regulated degradation of Id2 has been linked to up-regulation of axon growth inhibitors (31), which suggested that activation of Id2 could counteract growth inhibition and enhance axon growth, but this prediction was only tested in culture systems and after spinal cord injury (31–34). In contrast to previous studies, we identified Id2 using an unbiased single-cell RNA-seq screen and interrogated consequences of Id2 activation in mature, uninjured neurons of healthy adult mice and rats. We found that the sole activation of Id2 in mature GCs is capable of driving MF sprouting and formation of functional synapses.

During our initial analyses, we found that during chemically induced MF sprouting, both Id2 mRNA and protein became enriched in GCs (Fig. 1). This suggested that Id2 may play a role in MF sprouting, which we tested by cell-autonomous activation of Id2 in GCs. We found that AAV-Id2 had the remarkable capacity to induce MF rewiring throughout the whole hippocampus with a circuit architecture that resembled previous
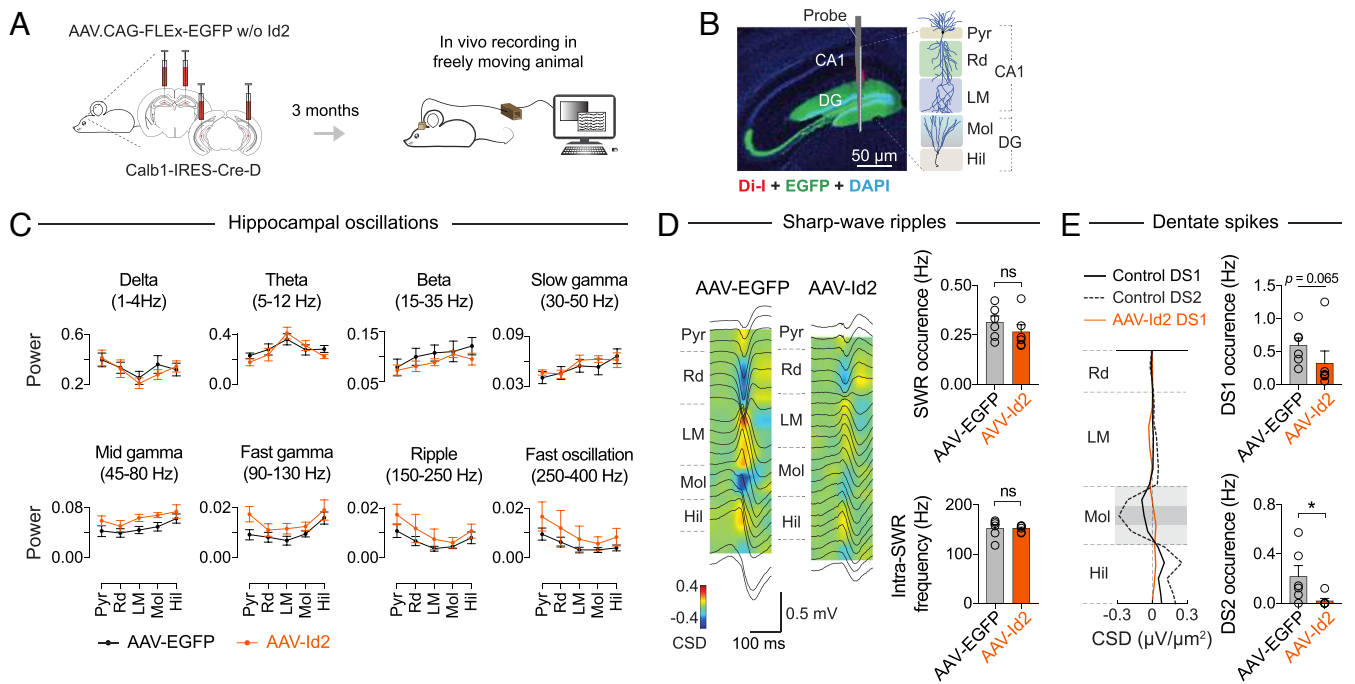
Luo et al.
Recurrent rewiring of the adult hippocampal mossy fiber system by a single transcriptional regulator, Id2

PNAS | 7 of 11
https://doi.org/10.1073/pnas.2108239118

Fig. 6. Hippocampal dynamics after AAV-Id2–induced MF rewiring. (*A*) Experimental design. After AAV-EGFP and AAV-Id2 injections, each mouse was implanted with a linear silicon probe in dorsal hippocampus. Three months after AAV delivery, recordings were made from freely moving mice. (*B*) Histological image of a silicon probe track through the hippocampus (Pyr: pyramidal layer, Rd: radiatum, LM: lacunosum-moleculare, Mol: molecular layer, Hil: hilus). (*C*) Local field potential (LFP) power of delta, theta, beta, slow gamma, midgamma, fast gamma (all during locomotion), and ripple and fast ripple (during resting) range frequencies (AAV-EGFP, $n = 7$ mice; AAV-Id2, $n = 6$ mice). Neither pair-wise comparisons between the AAV-EGFP and AAV-Id2 groups revealed statistically significant ($P < 0.05$) differences using two-way ANOVA test. (*D*) *Left*: Regional distribution of currents associated with SWRs in ripple peak-triggered CSD maps; average LFP waveforms (black traces) are shown superimposed. *Right*: Quantification of ripple occurrence (Mann–Whitney U test, $P = 0.31$) and intraripple frequency in CA1 Pyr and Rd (Mann–Whitney U test, $P = 0.45$; AAV-EGFP, $n = 6$ mice; AAV-Id2, $n = 6$ mice). (*E*) *Left*: CSD profiles of DS1 and DS2. *Right*: Quantification of DS1 (Mann–Whitney U test, $P = 0.065$) and DS2 (Mann–Whitney U test, $P = 0.015$; AAV-EGFP, $n = 6$ mice; AAV-Id2, $n = 6$) occurrence.

descriptions of MF sprouting (e.g., refs. 12–14, 21) but without signs of GC death or layer dispersion (Figs. 2–4).

As a master regulator, Id2 activated a comprehensive transcriptomic program for rewiring. Because Id2 is an inhibitor of transcription factors, MF rewiring appeared to result from suppression of persistently active transcriptional programs, and consistent with this, we found activation and silencing of molecules whose function is related to circuit-level reorganization (Fig. 5). Up-regulated JAK-Stat3 has been implicated in promoting axon growth after injury in visual and spinal systems (56–59). While previous work has separately linked Id2 and Stat3 to axon growth, our results establish a link between the two whereby activation of Id2 promotes downstream expression of Stat3. Other up-regulated genes included Phf11d, a regulator of the transcription factor Bex1 (60), which facilitates axon regeneration (61).

Down-regulated molecules were also consistent with an increased capacity for axonal organization and circuit formation and included 1) Tle1, a corepressor of the axon patterning Wnt signaling (62, 63); 2) neurofilaments Nefl and Nefm, which determine mature axon structure and caliber (64); 3) Slit1, a regulator of developmental axon guidance and patterning (65), downregulation of which may allow MF entry to the dentate gyrus; 4) Adcy1, loss of which led to developmental axon retraction arrest (66), exuberant axon branching in sensory areas (67, 68), and recovery after spinal cord injury (69); 5) Fmr1, modulator of local translation of synaptic proteins (70); and 6) Rreb1, a regulator of Wallerian axon degeneration after injury (71).

Delineating the sequential activation/inactivation and stepwise role of involved molecules will be important for understanding the MF rewiring process in detail. It remains possible that further aspects of MF rewiring could also be controlled independently of

Id2 yet still cell autonomously. For example, AAV-Id2–induced MF sprouting developed over months (Fig. 2), which is similar to other observations (21), although slower than that is achieved by non-cell-specific chemical induction (Fig. 1). Whether the factor(s) controlling the speed of circuit formation are cell autonomous and can be separately identified and how synapse targeting can be reprogrammed to other cell types instead of GCs remain outstanding questions. With regard to other pathways that have been previously implicated in axon growth, regeneration, or MF sprouting in particular, our data from single GCs did not reveal Id2-induced transcriptomic changes in the TGF-beta/BMP-Smad (axon growth) (72–74), BDNF (MF sprouting) (21, 23), PTEN-mTOR (MF sprouting in postnatally generated GCs) (19, 22), and p38/JNK (in axon regeneration) (75) pathways (*SI Appendix*, Fig. S5). Some of these may be upstream of Id2 (e.g., TGF-beta/Smad2) (72), be controlled translationally, act independently of Id2, or simply not be involved in MF sprouting by mature GCs.

MF Sprouting and Hippocampal Brain Activity. Our ability to genetically induce MF rewiring in GCs allowed us to examine consequent network effects in the context of two related but independent hypotheses. According to one hypothesis, MF sprouting may generate hyperexcitable network states. MF sprouting is observed in human TLE and is one of the hallmarks of chemically induced (which is nonspecific and broadly impacts different cell types) circuit alterations in experimental TLE (21). Whether MF sprouting is a cause or consequence of seizures has been debated (20). Thus, one particular question was whether pathological brain dynamics, such as in the epileptic brain, would appear after genetically induced MF rewiring. However, our in vivo electrophysiological recordings did not register pathological oscillations,
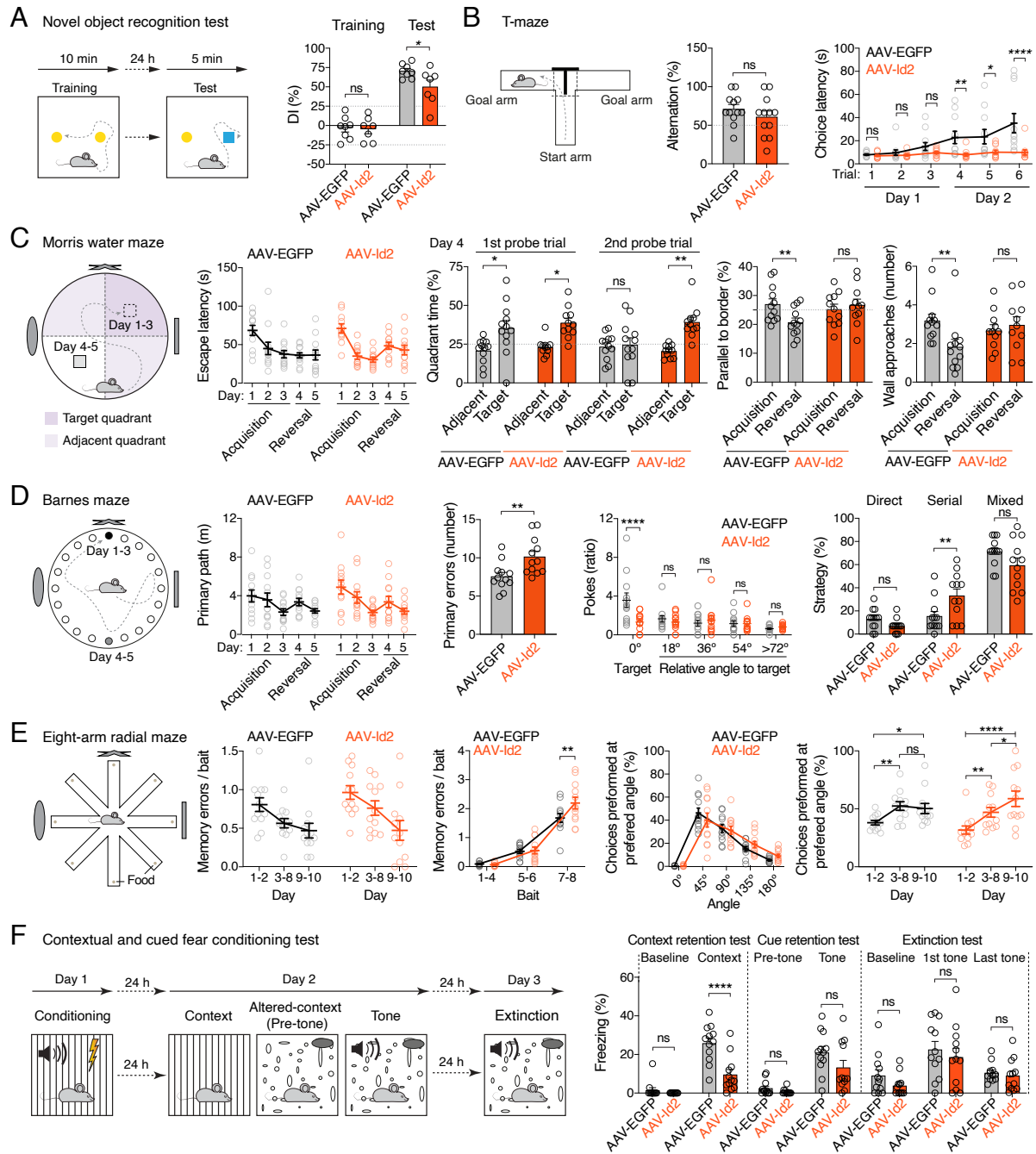
Luo et al.
Recurrent rewiring of the adult hippocampal mossy fiber system by a single
transcriptional regulator, Id2

Fig. 7. Learning and memory after AAV-Id2–induced MF rewiring. (Statistical tests are two-way ANOVA unless stated otherwise.) (*A*) Novel object recognition. Left to right: experiment design, DI (AAV-EGFP versus AAV-Id2, training $P = 0.87$, test *$P = 0.021$). (*B*) T-maze. Left to right: experiment design, alteration (Mann–Whitney U test, $P = 0.33$), and choice latency (AAV-EGFP versus AAV-Id2, trial 1, $P = 0.87$, trial 2, $P = 0.66$, trial 3, $P = 0.31$, trial 4, **$P = 0.0048$, trial 5, *$P = 0.011$, trial 6, ****$P < 0.0001$). (*C*) Morris water maze. Left to right: experiment design, escape latency [F_{Day} (4, 84) = 13, $P < 0.0001$; $F_{Treatment}$ (1, 21) = 0.056, $P = 0.82$; $F_{Treatment \times Day}$ (4, 84) = 1.4, $P = 0.23$], quadrant time (adjacent versus target, first probe trial, AAV-EGFP: *$P = 0.017$, AAV-Id2: *$P = 0.014$; second probe trial, AAV-EGFP: $P = 0.82$, AAV-Id2: **$P = 0.0026$), swim path length parallel to walls (acquisition versus reversal, AAV-EGFP: **$P = 0.0025$, AAV-Id2: $P = 0.45$), and number of wall approaches (acquisition versus reversal, AAV-EGFP: **$P = 0.0079$, AAV-Id2: $P = 0.57$). (*D*) Barnes maze. Left to right: experiment design, primary path length [F_{Day} (4, 88) = 6.6, $P = 0.0001$; $F_{Treatment}$ (1, 22) = 0.4, $P = 0.52$; $F_{Treatment \times Day}$ (4, 88) = 0.3, $P = 0.85$], primary errors (Mann–Whitney U test, **$P = 0.0038$), poke ratio in probe trial after acquisition (AAV-EGFP versus AAV-Id2, angle = 0°: ****$P < 0.0001$, angle = 18°: $P = 0.52$, angle = 36°: $P = 0.54$, angle = 54°: $P = 0.98$, angle > 72°: $P = 0.72$), and average strategy used during acquisition and reversal AAV-EGFP versus AAV-Id2: direct, $P = 0.31$, serial, **$P = 0.0047$, mixed $P = 0.059$). (*E*) Eight-arm radial maze. Left to right: experiment design, memory errors per consumed baits over days [F_{Day} (2, 44) = 9.0, $P = 0.0005$; $F_{Treatment}$ (1, 22) = 2.8, $P = 0.11$; $F_{Treatment \times Day}$ (2, 44) = 0.53, $P = 0.59$], memory errors per consumed bait (AAV-EGFP versus AAV-Id2: bait 1 to 4, $P = 0.88$, bait 5 to 6, $P = 0.86$, bait 7 to 8, **$P = 0.0029$), preferred angle [F_{Angle} (2, 44) = 16, $P < 0.0001$; $F_{Treatment}$ (1, 22) = 0.056, $P = 0.81$; $F_{Treatment \times Angle}$ (2, 44) = 2.6, $P = 0.086$], and choices performed at preferred angle (AAV-EGFP, days 1 to 2 versus 3 to 8, **$P = 0.0071$, days 1 to 2 versus 9 to 10, *$P = 0.020$, day 3 to 8 versus 9 to 10, $P = 0.68$; AAV-Id2, days 1 to 2 versus 3 to 8, **$P = 0.0049$, days 1 to 2 versus 9 to 10, ****$P < 0.0001$, days 3 to 8 versus 9 to 10, *$P = 0.026$). (*F*) Contextual and cued fear conditioning. Left to right: experiment design, freezing during context retention (AAV-EGFP versus AAV-Id2: baseline, $P = 0.60$, context, ****$P < 0.0001$), freezing during cue retention (AAV-EGFP versus AAV-Id2: pretone, $P = 0.58$, tone, $P = 0.032$, q = 0.064; does not meet FDR criterion), and freezing during extinction (AAV-EGFP versus AAV-Id2: baseline, $P = 0.24$, first tone, $P = 0.38$, last tone, $P = 0.73$).

Luo et al.
Recurrent rewiring of the adult hippocampal mossy fiber system by a single transcriptional regulator, Id2

PNAS | 9 of 11
https://doi.org/10.1073/pnas.2108239118

NEUROSCIENCE

SWRs, or seizure-like activity 3 mo after AAV-Id2 delivery (Fig. 6). By contrast, after chemically induced epilepsy, decreased theta and midgamma oscillations (49), and increased intra-SWR frequency (50) have been reported. Our results thus reveal network dynamics divergent from epilepsy and indicate that MF rewiring does not generate seizures (20).

According to another hypothesis, the dentate gyrus is presumed to process information about content (e.g., objects) and local spatial landmarks, delivered from the LEC, and about global spatial landmarks, delivered from the MEC (53–55). Our in vivo recordings in AAV-Id2 mice revealed a decrease in the occurrence of DS1 and a loss of DS2 events, which have been suggested to be triggered by population bursts in LEC and MEC, respectively (52). While circuit mechanisms behind DS events remain elusive, our data suggested that MF sprouting differentially interfered with the generation of DS1 and DS2 events. Consequently, information from LEC about content and local landmarks and from MEC about global spatial context of an experience may be differentially impacted by MF sprouting.

Learning and Memory after MF Sprouting. By employing multiple different memory assays to evaluate object and spatial-related information processing, we found a recurrent schema in the behavior of AAV-Id2 animals that had MF sprouting. With regard to objects, we found that AAV-Id2 mice displayed preference to novel objects, although the preference was less than that of controls (Fig. 7). Notably, the decreased preference to novel objects correlated with decreased occurrence of LEC-linked DS1 events in the AAV-Id2 mice. These represent further divergence from TLE, as novel object preference was not altered (76, 77) and DS occurrence was increased in epileptic mice (51) (note that DS1 and DS2 were not separately analyzed by this later study). Nonetheless, these do not contradict our findings, which suggest that DS1 events may be related to recognition of novel objects. With regard to spatial information, AAV-Id2 mice did not display deficits in primary task performance, but they appeared to solve spatial problems differently from controls. Specifically, the Morris water, Barnes, and eight-arm radial maze assays showed that AAV-Id2 mice learn and perform well, without deficits in spatial retention (Fig. 7). Note that these findings represent yet another divergence from TLE, where the same assays revealed learning and memory impairments (49, 78–80). However, AAV-Id2 mice displayed a higher level of spatial perseverance and opted to nonspatial, wall-oriented swimming strategies during reversal learning in the Morris water maze and performed more serial trials at the expense of direct and mixed trials in both the Barnes maze and eight-arm maze, together indicating that AAV-Id2 mice were prone to use local landmark-based and possibly self-referential navigation-based strategies rather than relying on global spatial cues. Since MEC (global spatial information)–linked DS2 events were specifically lost in AAV-Id2 mice, our finding suggests that DS2 events are not required for solving primary spatial tasks per se but may facilitate the processing of global spatial cues that guide navigation to enhance performance. One interpretation of these findings that should also be considered is a potential confusion in pattern separation caused by recurrent redistribution of neural activity among GCs after MF sprouting. Pattern separation is one principal function performed by dentate gyrus (11, 81) thought to be controlled by young but not mature adult-born GCs (82). Since in these experiments the Calb1-IRES2-Cre-D line was used to deliver Id2 to GCs and the onset of Calb1 expression marks a transition of adult-born GCs into more mature states (83), it is unlikely that altered pattern separation by young adult-born GCs substantially contributed to our observations. Overall, our results are consistent with the hypothesis that MEC and LEC support navigation based on global and local cues, respectively (54, 55). Finally, we also found that AAV-Id2 mice, unlike controls, did not increase their choice latencies over subsequent trials in the T-maze. This phenotype could potentially be the result of an egocentric navigation strategy that utilizes left-right sequences with high precision but could also be interpreted as an inability to habituate (although our other data did not suggest this) or faster decision making, and therefore, its relationship to MF sprouting is currently less clear.

Summary. Repair being a key objective, factors that facilitate circuit rewiring in the adult nervous system are typically studied in the context of pathology or injury. Our results provide evidence for cell-autonomous activation of axon growth and circuit formation in healthy mature neurons in the absence of developmental or injury signaling. More detailed understanding of how involved molecules contribute to this process will help to advance circuit engineering approaches that can induce axon growth and control target cell-specific circuit formation in the adult brain.

Methods

All mouse protocols and husbandry practices were approved by the Veterinary Office of Zürich Kanton. For comprehensive description of 1) animals, 2) plasmids and viruses, 3) stereotaxic injections, 4) single-cell RNA-seq and bioinformatics, 5) histology and neuroanatomy, 6) electron microscopy, 7) in vitro electrophysiology, 8) in vivo electrophysiology, 9) behavior, and 10) statistical analyses, see the *SI Appendix*.

1. M. Tessier-Lavigne, C. S. Goodman, The molecular biology of axon guidance. *Science* **274**, 1123–1133 (1996).
2. B. J. Dickson, Molecular mechanisms of axon guidance. *Science* **298**, 1959–1964 (2002).
3. J. R. Sanes, S. L. Zipursky, Synaptic specificity, recognition molecules, and assembly of neuronal circuits. *Cell* **181**, 536–556 (2020).
4. G. Yiu, Z. He, Glial inhibition of CNS axon regeneration. *Nat. Rev. Neurosci.* **7**, 617–627 (2006).
5. M. E. Schwab, Functions of Nogo proteins and their receptors in the nervous system. *Nat. Rev. Neurosci.* **11**, 799–811 (2010).
6. M. A. Anderson *et al.*, Required growth facilitators propel axon regeneration across complete spinal cord injury. *Nature* **561**, 396–400 (2018).
7. D. L. Moore, J. L. Goldberg, Multiple transcription factor families regulate axon growth and regeneration. *Dev. Neurobiol.* **71**, 1186–1211 (2011).
8. M. Mahar, V. Cavalli, Intrinsic mechanisms of neuronal axon regeneration. *Nat. Rev. Neurosci.* **19**, 323–337 (2018).
9. J. T. Gonçalves, S. T. Schafer, F. H. Gage, Adult neurogenesis in the hippocampus: From stem cells to behavior. *Cell* **167**, 897–914 (2016).
10. R. A. Barker, M. Götz, M. Parmar, New approaches for brain repair-from rescue to reprogramming. *Nature* **557**, 329–334 (2018).
11. T. Hainmueller, M. Bartos, Dentate gyrus circuits for encoding, retrieval and discrimination of episodic memories. *Nat. Rev. Neurosci.* **21**, 153–168 (2020).
12. H. J. Wenzel, C. S. Woolley, C. A. Robbins, P. A. Schwartzkroin, Kainic acid-induced mossy fiber sprouting and synapse formation in the dentate gyrus of rats. *Hippocampus* **10**, 244–260 (2000).
13. J. E. Cavazos, P. Zhang, R. Qazi, T. P. Sutula, Ultrastructural features of sprouted mossy fiber synapses in kindled and kainic acid-treated rats. *J. Comp. Neurol.* **458**, 272–292 (2003).
14. M. Frotscher, P. Jonas, R. S. Sloviter, Synapses formed by normal and abnormal hippocampal mossy fibers. *Cell Tissue Res.* **326**, 361–367 (2006).
15. S. Laurberg, J. Zimmer, Lesion-induced sprouting of hippocampal mossy fiber collaterals to the fascia dentata in developing and adult rats. *J. Comp. Neurol.* **200**, 433–459 (1981).
16. J. Zimmer, B. H. Gähwiler, Growth of hippocampal mossy fibers: A lesion and coculture study of organotypic slice cultures. *J. Comp. Neurol.* **264**, 1–13 (1987).

17. T. Sutula, X. X. He, J. Cavazos, G. Scott, Synaptic reorganization in the hippocampus induced by abnormal functional activity. *Science* **239**, 1147–1150 (1988).

18. D. L. Tauck, J. V. Nadler, Evidence of functional mossy fiber sprouting in hippocampal formation of kainic acid-treated rats. *J. Neurosci.* **5**, 1016–1022 (1985).

19. R. Y. Pun *et al.*, Excessive activation of mTOR in postnatally generated granule cells is sufficient to cause epilepsy. *Neuron* **75**, 1022–1034 (2012).

20. P. S. Buckmaster, Does mossy fiber sprouting give rise to the epileptic state? *Adv. Exp. Med. Biol.* **813**, 161–168 (2014).

21. P. S. Buckmaster, *Mossy Fiber Sprouting in the Dentate Gyrus. Jasper's Basic Mechanisms of the Epilepsies* (National Center for Biotechnology Information (US), Bethesda, MD, ed. 4, 2012).

22. C. M. Godale, S. C. Danzer, Signaling pathways and cellular mechanisms regulating mossy fiber sprouting in the development of epilepsy. *Front. Neurol.* **9**, 298 (2018).

23. R. Koyama, Y. Ikegaya, The molecular and cellular mechanisms of axon guidance in mossy fiber sprouting. *Front. Neurol.* **9**, 382 (2018).

24. K. Takahashi, S. Yamanaka, Induction of pluripotent stem cells from mouse embryonic and adult fibroblast cultures by defined factors. *Cell* **126**, 663–676 (2006).

25. C. Földy *et al.*, Single-cell RNAseq reveals cell adhesion molecule profiles in electrophysiologically defined neurons. *Proc. Natl. Acad. Sci. U.S.A.* **113**, E5222–E5231 (2016).

26. J. Winterer *et al.*, Single-cell RNA-Seq characterization of anatomically identified OLM interneurons in different transgenic mouse lines. *Eur. J. Neurosci.* **50**, 3750–3771 (2019).

27. W. Luo, D. Lukacsovich, L. Que, J. Winterer, C. Földy, Data from "Single-cell transcriptome of dentate gyrus granule cells after chemical and genetic induction." NCBI GEO. https://www.ncbi.nlm.nih.gov/geo/query/acc.cgi?acc=GSE161619. Deposited 17 November 2020.

28. Y. Ben-Ari, "Kainate and temporal lobe epilepsies: 3 decades of progress" in *Jasper's Basic Mechanisms of the Epilepsies*, J. L. Noebels, M. Avoli, M. A. Rogawski, R. W. Olsen, A. V. Delgado-Escueta, Eds. (National Center for Biotechnology Information, Bethesda, MD, ed. 4, 2012).

29. R. Jagirdar, M. Drexel, A. Bukovac, R. O. Tasan, G. Sperk, Expression of class II histone deacetylases in two mouse models of temporal lobe epilepsy. *J. Neurochem.* **136**, 717–730 (2016).

30. R. C. Elliott, S. Khademi, S. J. Pleasure, J. M. Parent, D. H. Lowenstein, Differential regulation of basic helix-loop-helix mRNAs in the dentate gyrus following status epilepticus. *Neuroscience* **106**, 79–88 (2001).

31. A. Lasorella *et al.*, Degradation of Id2 by the anaphase-promoting complex couples cell cycle exit and axonal growth. *Nature* **442**, 471–474 (2006).

32. Z. Huang *et al.*, Inhibitor of DNA binding 2 promotes axonal growth through upregulation of Neurogenin2. *Exp. Neurol.* **320**, 112966 (2019).

33. H. R. Ko *et al.*, Akt1-inhibitor of DNA binding2 is essential for growth cone formation and axon growth and promotes central nervous system axon regeneration. *eLife* **5**, e20799 10.7554/eLife.20799. (2016).

34. P. Yu *et al.*, Inhibitor of DNA binding 2 promotes sensory axonal growth after SCI. *Exp. Neurol.* **231**, 38–44 (2011).

35. X. Li *et al.*, Polycystin-1 and polycystin-2 regulate the cell cycle through the helix-loop-helix inhibitor Id2. *Nat. Cell Biol.* **7**, 1202–1212 (2005).

36. A. Lasorella, A. Iavarone, The protein ENH is a cytoplasmic sequestration factor for Id2 in normal and tumor cells from the nervous system. *Proc. Natl. Acad. Sci. U.S.A.* **103**, 4976–4981 (2006).

37. R. Haenold *et al.*, NF-κB controls axonal regeneration and degeneration through cell-specific balance of RelA and p50 in the adult CNS. *J. Cell Sci.* **127**, 3052–3065 (2014).

38. J. Samanta, J. A. Kessler, Interactions between ID and OLIG proteins mediate the inhibitory effects of BMP4 on oligodendroglial differentiation. *Development* **131**, 4131–4142 (2004).

39. H. J. Wenzel, T. B. Cole, D. E. Born, P. A. Schwartzkroin, R. D. Palmiter, Ultrastructural localization of zinc transporter-3 (ZnT-3) to synaptic vesicle membranes within mossy fiber boutons in the hippocampus of mouse and monkey. *Proc. Natl. Acad. Sci. U.S.A.* **94**, 12676–12681 (1997).

40. B. A. Strange, M. P. Witter, E. S. Lein, E. I. Moser, Functional organization of the hippocampal longitudinal axis. *Nat. Rev. Neurosci.* **15**, 655–669 (2014).

41. R. P. Kesner, An analysis of the dentate gyrus function. *Behav. Brain Res.* **254**, 1–7 (2013).

42. R. P. Kesner, An analysis of dentate gyrus function (an update). *Behav. Brain Res.* **354**, 84–91 (2018).

43. M. El-Gaby, O. A. Shipton, O. Paulsen, Synaptic plasticity and memory: New insights from hippocampal left-right asymmetries. *Neuroscientist* **21**, 490–502 (2015).

44. C. Roschger, C. Cabrele, The Id-protein family in developmental and cancer-associated pathways. *Cell Commun. Signal.* **15**, 7 (2017).

45. D. S. Aaronson, C. M. Horvath, A road map for those who don't know JAK-STAT. *Science* **296**, 1653–1655 (2002).

46. F. J. Barrat, M. K. Crow, L. B. Ivashkiv, Interferon target-gene expression and epigenomic signatures in health and disease. *Nat. Immunol.* **20**, 1574–1583 (2019).

47. E. Y. Chen *et al.*, Enrichr: Interactive and collaborative HTML5 gene list enrichment analysis tool. *BMC Bioinformatics* **14**, 128 (2013).

48. M. V. Kuleshov *et al.*, Enrichr: A comprehensive gene set enrichment analysis web server 2016 update. *Nucleic Acids Res.* **44**, W90–W97 (2016).

49. T. Shuman *et al.*, Breakdown of spatial coding and interneuron synchronization in epileptic mice. *Nat. Neurosci.* **23**, 229–238 (2020).

50. I. Marchionni, M. Oberoi, I. Soltesz, A. Alexander, Ripple-related firing of identified deep CA1 pyramidal cells in chronic temporal lobe epilepsy in mice. *Epilepsia Open* **4**, 254–263 (2019).

51. S. P. Flynn, S. Barriere, R. C. Scott, P. P. Lenck-Santini, G. L. Holmes, Status epilepticus induced spontaneous dentate gyrus spikes: In vivo current source density analysis. *PLoS One* **10**, e0132630 (2015).

52. A. Bragin, G. Jandó, Z. Nádasdy, M. van Landeghem, G. Buzsáki, Dentate EEG spikes and associated interneuronal population bursts in the hippocampal hilar region of the rat. *J. Neurophysiol.* **73**, 1691–1705 (1995).

53. J. J. Knierim, J. P. Neunuebel, S. S. Deshmukh, Functional correlates of the lateral and medial entorhinal cortex: Objects, path integration and local-global reference frames. *Philos. Trans. R. Soc. Lond. B Biol. Sci.* **369**, 20130369 (2013).

54. C. Wang *et al.*, Egocentric coding of external items in the lateral entorhinal cortex. *Science* **362**, 945–949 (2018).

55. A. Fernández-Ruiz *et al.*, Gamma rhythm communication between entorhinal cortex and dentate gyrus neuronal assemblies. *Science* **372**, eabf3119 (2021).

56. F. M. Bareyre *et al.*, In vivo imaging reveals a phase-specific role of STAT3 during central and peripheral nervous system axon regeneration. *Proc. Natl. Acad. Sci. U.S.A.* **108**, 6282–6287 (2011).

57. F. Sun *et al.*, Sustained axon regeneration induced by co-deletion of PTEN and SOCS3. *Nature* **480**, 372–375 (2011).

58. V. Pernet *et al.*, Misguidance and modulation of axonal regeneration by Stat3 and Rho/ROCK signaling in the transparent optic nerve. *Cell Death Dis.* **4**, e734 (2013).

59. X. Luo *et al.*, Enhanced transcriptional activity and mitochondrial localization of STAT3 co-induce axon regrowth in the adult central nervous system. *Cell Rep.* **15**, 398–410 (2016).

60. F. Accornero *et al.*, BEX1 is an RNA-dependent mediator of cardiomyopathy. *Nat. Commun.* **8**, 1875 (2017).

61. M. R. Khazaei *et al.*, Bex1 is involved in the regeneration of axons after injury. *J. Neurochem.* **115**, 910–920 (2010).

62. J. V. Chodaparambil *et al.*, Molecular functions of the TLE tetramerization domain in Wnt target gene repression. *EMBO J.* **33**, 719–731 (2014).

63. L. Ciani, P. C. Salinas, WNTs in the vertebrate nervous system: From patterning to neuronal connectivity. *Nat. Rev. Neurosci.* **6**, 351–362 (2005).

64. E. Fuchs, D. W. Cleveland, A structural scaffolding of intermediate filaments in health and disease. *Science* **279**, 514–519 (1998).

65. K. Brose, M. Tessier-Lavigne, Slit proteins: Key regulators of axon guidance, axonal branching, and cell migration. *Curr. Opin. Neurobiol.* **10**, 95–102 (2000).

66. X. Nicol, A. Muzerelle, J. P. Rio, C. Métin, P. Gaspar, Requirement of adenylate cyclase 1 for the ephrin-A5-dependent retraction of exuberant retinal axons. *J. Neurosci.* **26**, 862–872 (2006).

67. T. Iwasato *et al.*, Cortical adenylyl cyclase 1 is required for thalamocortical synapse maturation and aspects of layer IV barrel development. *J. Neurosci.* **28**, 5931–5943 (2008).

68. A. Ravary *et al.*, Adenylate cyclase 1 as a key actor in the refinement of retinal projection maps. *J. Neurosci.* **23**, 2228–2238 (2003).

69. H. Nait Taleb Ali *et al.*, Lack of adenylate cyclase 1 (AC1): Consequences on corticospinal tract development and on locomotor recovery after spinal cord injury. *Brain Res.* **1549**, 1–10 (2014).

70. J. C. Darnell *et al.*, FMRP stalls ribosomal translocation on mRNAs linked to synaptic function and autism. *Cell* **146**, 247–261 (2011).

71. J. E. Farley *et al.*, Transcription factor Pebbled/RREB1 regulates injury-induced axon degeneration. *Proc. Natl. Acad. Sci. U.S.A.* **115**, 1358–1363 (2018).

72. J. Stegmüller, M. A. Huynh, Z. Yuan, Y. Konishi, A. Bonni, TGFbeta-Smad2 signaling regulates the Cdh1-APC/SnoN pathway of axonal morphogenesis. *J. Neurosci.* **28**, 1961–1969 (2008).

73. J. J. Yi, A. P. Barnes, R. Hand, F. Polleux, M. D. Ehlers, TGF-beta signaling specifies axons during brain development. *Cell* **142**, 144–157 (2010).

74. J. Zhong, H. Zou, BMP signaling in axon regeneration. *Curr. Opin. Neurobiol.* **27**, 127–134 (2014).

75. P. Nix, N. Hisamoto, K. Matsumoto, M. Bastiani, Axon regeneration requires coordinate activation of p38 and JNK MAPK pathways. *Proc. Natl. Acad. Sci. U.S.A.* **108**, 10738–10743 (2011).

76. Z. Zeidler *et al.*, Targeting the mouse ventral hippocampus in the intrahippocampal kainic acid model of temporal lobe epilepsy. *eNeuro* **5**, ENEURO.0158-18.2018 (2018).

77. A. D. Bui *et al.*, Dentate gyrus mossy cells control spontaneous convulsive seizures and spatial memory. *Science* **359**, 787–790 (2018).

78. M. H. Mohajeri *et al.*, The impact of genetic background on neurodegeneration and behavior in seizured mice. *Genes Brain Behav.* **3**, 228–239 (2004).

79. I. Gröticke, K. Hoffmann, W. Löscher, Behavioral alterations in a mouse model of temporal lobe epilepsy induced by intrahippocampal injection of kainate. *Exp. Neurol.* **213**, 71–83 (2008).

80. Y. Van Den Herrewegen *et al.*, The Barnes maze task reveals specific impairment of spatial learning strategy in the intrahippocampal kainic acid model for temporal lobe epilepsy. *Neurochem. Res.* **44**, 600–608 (2019).

81. J. K. Leutgeb, S. Leutgeb, M. B. Moser, E. I. Moser, Pattern separation in the dentate gyrus and CA3 of the hippocampus. *Science* **315**, 961–966 (2007).

82. T. Nakashiba *et al.*, Young dentate granule cells mediate pattern separation, whereas old granule cells facilitate pattern completion. *Cell* **149**, 188–201 (2012).

83. M. D. Brandt *et al.*, Transient calretinin expression defines early postmitotic step of neuronal differentiation in adult hippocampal neurogenesis of mice. *Mol. Cell. Neurosci.* **24**, 603–613 (2003).

Luo et al.
Recurrent rewiring of the adult hippocampal mossy fiber system by a single transcriptional regulator, Id2

PNAS | 11 of 11
https://doi.org/10.1073/pnas.2108239118

Discussion

In this study, we performed multimodal analyses of single hippocampal granule cells in order to understand the molecular mechanisms of mossy fiber sprouting, and more broadly, that of adult wiring. A key motivation behind this study was to determine potential expression changes in CAMs as crucial controllers of the wiring process and, simultaneously, transcription factors and regulators, which may regulate the combinatorial expression of CAMs. As a result, we identified a single transcriptomic regulator, *Id2*, whose sole activation could drive the entire wiring process. In addition to the Discussion presented in our paper, here I highlight conceptually important aspects of this work that are relevant for adult brain wiring and potential next steps which can help to deepen our understanding in the regulation of neuronal wiring during the lifespan.

First, the corollary of our results and that of other studies, which showed that *Id2* can facilitate axon regeneration after injury (Yu *et al.*, 2011; Ko *et al.*, 2016), is the hypothesis that at least some bHLH transcription factors actively suppress neuronal wiring in adult neurons. This hypothesis is supported by that (1) *Id2* is an inhibitor of bHLH transcription factors (Benezra *et al.*, 1990; Norton, 2000) and (2) the activation of *Id2* reactivates wiring in adult neurons, which observations together suggest that *Id2* reveals its wiring effect by neutralizing a wiring suppressing transcriptional program. This model has important implications toward the post developmental regulation of wiring in neurons. Developing neurons display a large capacity for wiring. After development, this wiring capacity rapidly decreases, and most neurons cease further wiring. How this change of wiring capacity is regulated within the neuron ("cell autonomously") and/or in the tissue environment ("cell nonautonomously") remains elusive. A key hypothesis suggests broad upregulation of neurite growth inhibitors in the tissue environment during later stages of development, which are to significantly contribute to the cell nonautonomous inhibition of further wiring and stabilization of circuits. The cell autonomous regulation of wiring is comparably less understood. It is feasible that developmentally-relevant wiring programs in the neuron are disassembled after development. An alternative possibility is that such wiring programs are not disassembled but suppressed after development. Our results provide support for this later scenario. To further test this hypothesis, it will be important to address in future experiments if *Id2* can reactivate wiring in adult neuron types other than hippocampal

granule cells; i.e. if wiring is being actively suppressed in other adult neuronal types as well.

Second, our results provide evidence that the connectivity of adult neurons can be reprogrammed by targeted molecular manipulations. In our experiments, we cell type-specifically activated *Id2* only in hippocampal granule cells, but not in other cell types or in the tissue, which lead to further wiring. In this manner, the seen adult wiring phenotype (in this case mossy fiber sprouting) relied on molecular mechanisms within the manipulated cells, suggesting that the regulation of wiring is purely a cell autonomous process. However, as a further consideration, during mossy fiber sprouting granule cells form new connections with other granule cells, and therefore it is possible that the kainic acid injection or the *Id2* activation simultaneously primes wiring both in the pre and postsynaptic population, which are here the same. Thus, to further test the hypothesis of cell autonomous wiring regulation, it will be crucially important to identify other transcriptional factors and/or regulators, which can induce wiring in adult neurons, and ideally lead to circuit formation between different cell types. In this scenario, the two cell types could be independently manipulated in order to determine if the circuit formation indeed required molecular reconfigurations only in the presynaptic or both neuronal populations.

Finally, important questions regarding the new circuits are whether how stable they are on the long term, and what molecular mechanisms support their maintenance. I will revisit these questions in the final Discussion of this thesis.

Chapter 3 – Molecular control of target specification

Introduction

The initial goal of our previous study (Luo *et al.*, 2021) was to characterize CAM changes and their transcriptomic regulation during mossy fiber sprouting. As discussed above, we first followed up on the role of a transcriptomic regulator, *Id2*, which we found drives the entire sprouting process. In this project, we revisited our initial goal and specifically focused on CAMs. It is feasible, that at least some of the CAMs, whose expression has changed during mossy fiber sprouting play important roles in determining target specificity. Target specificity includes (1) to which brain region(s) the new axons grow, and (2) on which cell type(s) and (3) in which subcellular domain(s) the new synapses are formed. To gain insights into these questions, we further analyzed our single-cell transcriptomic data generated during the aforementioned study (Luo *et al.*, 2021), containing transcriptomic information on virtually all CAMs before and after mossy fiber sprouting. Based on these data, we identified three potential candidates – *Cntn4*, *Fat3*, and *Pcdh11x* – whose transcript expression were absent in control granule cells but significantly upregulated during sprouting. To characterize the function of these molecules, we devised a CRISPR-Cas9-based screen to introduce deleterious (or loss of function) mutations in these genes in adult granule cells *in vivo* and investigated their loss of function effects on the target specificity of mossy fiber sprouting.

I contributed to this project with experimental design, experiments, and analysis. Specifically, I was responsible for tissue preparation, staining, histological analysis, and guide RNA testing in cell culture.

Pcdh11x controls target specification of mossy fiber sprouting

Wenshu Luo, Natalia Andrea Cruz-Ochoa, Charlotte Seng,
Matteo Egger, David Lukacsovich, Tamás Lukacsovich and
Csaba Földy*

Laboratory of Neural Connectivity, Brain Research Institute, Faculties of Medicine and Science,
University of Zürich, Zurich, Switzerland

Circuit formation is a defining characteristic of the developing brain. However, multiple lines of evidence suggest that circuit formation can also take place in adults, the mechanisms of which remain poorly understood. Here, we investigated the epilepsy-associated mossy fiber (MF) sprouting in the adult hippocampus and asked which cell surface molecules define its target specificity. Using single-cell RNAseq data, we found lack and expression of *Pcdh11x* in non-sprouting and sprouting neurons respectively. Subsequently, we used CRISPR/Cas9 genome editing to disrupt the *Pcdh11x* gene and characterized its consequences on sprouting. Although MF sprouting still developed, its target specificity was altered. New synapses were frequently formed on granule cell somata in addition to dendrites. Our findings shed light onto a key molecular determinant of target specificity in MF sprouting and contribute to understanding the molecular mechanism of adult brain rewiring.

Introduction

Mossy fiber (MF) sprouting in the hippocampal dentate gyrus represents a non-developmental form of circuit formation in the adult brain (for review, see Seng et al., 2022). MF sprouting has been extensively studied in the context of temporal lobe epilepsies (Noebels et al., 2012) and is inducible by mechanical (Laurberg and Zimmer, 1981; Zimmer and Gähwiler, 1987), electrical (Sutula et al., 1988), chemical (Tauck and Nadler, 1985), and genetic approaches (Luo et al., 2021). During MF sprouting, granule cells (GCs) grow new axonal branches into the inner molecular layer (IML) of dentate gyrus and form synapses mostly on proximal dendrites of GCs (Laurberg and Zimmer, 1981; Wenzel et al., 2000; Cavazos et al., 2003; Frotscher et al., 2006; Luo et al., 2021), but potentially also on interneurons as observed in chronically epileptic rats (Frotscher et al., 2006). This new circuit is formed on top of the developmentally established

MF circuit, which extends into CA3 (Hainmueller and Bartos, 2020). As any neuronal wiring, MF sprouting is thought to require molecular programs for axon growth, target specification, and synapse formation (Godale and Danzer, 2018; Koyama and Ikegaya, 2018; Luo et al., 2021). Such processes generally involve synaptic cell-surface receptors and cell-adhesion molecules (Missaire and Hindges, 2015; de Wit and Ghosh, 2016; Sanes and Zipursky, 2020; Südhof, 2021), which hereafter we collectively refer to as CAMs, for short.

The role of different CAMs during developmental MF wiring is relatively well understood. Netrin and slit signaling control axon guidance toward CA3 (Muramatsu et al., 2010). Plexin and semaphorin signaling establish layer specificity within CA3 (Chen et al., 2000; Suto et al., 2007; Tawarayama et al., 2010). Other CAMs regulate MF target specificity and/or synapse function to CA3 pyramidal cells (NCAM, Cdh9, Gpr158) (Cremer et al., 1998; Williams et al., 2011; Basu et al., 2017; Condomitti et al., 2018), interneurons (Kirrel3, Igsf8) (Martin et al., 2015; Apóstolo et al., 2020), or possibly to both (Pcdh19) (Hoshina et al., 2021). Finally, semaphorin-neuropilin-plexin (Bagri et al., 2003) and ephrin (Xu and Henkemeyer, 2009; Liu et al., 2018) signaling control MF pruning. By contrast, CAM signaling in MF sprouting is much less understood. While abundance changes in multiple CAMs have been reported in models of temporal lobe epilepsy or directly in sprouting fibers, their involvement in sprouting remains elusive (see section "Discussion"). Recently, we studied transcriptomic mechanisms of MF sprouting and identified a transcriptomic regulator, Id2, whose sole overexpression in GCs induced MF sprouting (Luo et al., 2021). While Id2-induced MF sprouting alone was insufficient to provoke pathological network activity seen in epilepsy, further lessening its potential as a clinical target (Buckmaster, 2014), MF sprouting remains a robust model for studying circuit formation in the adult brain.

Here, we used single-cell RNA-seq data generated using the intrahippocampal kainic acid- (KA) injection model to study CAMs in MF sprouting. We used the KA, but not Id2, model because MF sprouting develops significantly faster by KA (within weeks) than by Id2 (requires months) (Luo et al., 2021). Thus, functional testing, which here we aimed for, is more attainable in the KA model. We focused on differentially expressed CAMs, and identified three candidate genes–Fat3, Cntn4 and Pcdh11x–which were upregulated after sprouting. We targeted these genes by CRISPR/Cas9 guide RNAs (gRNAs) to disrupt their genomic sequences in GCs in vivo, and confirmed mutation/deletions in Pcdh11x, likely rendering this gene null mutant in most cells. After GC-specific Pcdh11x KO, KA still induced MF sprouting, but new synapses frequently and atypically formed on GC somata.

Materials and methods

Animals

All animal protocols and husbandry practices were approved by the Veterinary Office of Zurich Kanton. The University of Zurich animal facilities comply with all appropriate standards (cages, space per animal, temperature, light, humidity, food, and water) and cages were enriched with materials that allow the animals to exert their natural behavior. The following lines were used in this study: Calb1-Cre: B6;129S-Calb1$^{TM2.1(cre)Hze}$/J, JAX:028532 and H11-LSL-Cas9: B6;129-Igs2tm1(CAG-cas9*)Mmw/J, JAX:026816. The animals used in this study were obtained by mating the homozygous Calb1-Cre mice with heterozygous H11-LSL-Cas9 mice. In each experiment, the control and non-control animals were littermates.

List of CAMs

An extended set of 421 CAMs was used for gene expression analysis. We used a previously published list of 406 CAMs (Földy et al., 2016), to which Nptxr, Sema3a, Sema3c, Sema3d, Sema3g, Sema4a, Sema4b, Sema4c, Sema4f, Sema5a, Sema5b, Sema6a, Sema6b, Sema6c, Slit1, Slit2, Slit3 were added, whereas Ptpn2 and Ptpn5 were removed as non-receptor type protein tyrosine phosphatases.

Design of guide RNAs

To design guide RNAs (gRNAs), we prioritized to (i) target early coding regions that are shared by all transcript variants of a gene in order to maximize the probability of introducing functionally disabling mutations and/or deletions, (ii) minimize the possibility of unwanted off-target effects, and (iii) maximize editing efficacy at the intended target site. For each targeted gene (i.e., Fat3, Cntn4, and Pcdh11x), two gRNAs (19 - 21 bp long) were designed targeting possible target sites on exons 1-3, followed by a 3 bp long NGG PAM sequence on the 3′ end (see **Supplementary Figure 1A** for specific sequences). Each gRNAs were evaluated by "CRISPR-Cas9 gRNA checker" (Integrated DNA technologies, Inc.), resulting in two scores: (1) "on-target score" that indicates the predicted editing performance of gRNA at the intended target site (higher value indicates better performance) and (2) "off-target score" that indicates potential off-target effects and N (number) nucleotide mismatch hits during genome screening (in a range from 0 to 100, higher value indicates lower off-target risk). Fat3-gRNA1: on-target score 66, off-target score 36 (high off-target risk), 0 mismatch only on Fat3, no potential off-target sites were identified with

1 or 2 mismatches. *Fat3-gRNA2*: on-target score 36 (low on-target performance), off-target score 82, 0 mismatch hit only on *Fat3*, no potential off-target sites with 1 mismatch, one 2 mismatch off-target site were found in a non-coding region (chr5: + 18040716). *Cntn4-gRNA1*: on-target score 40 (low on-target performance), off-target score 86, 0 mismatch hit only on *Cntn4*, no potential off-target sites with 1 mismatch, one 2 mismatch off-target site were found in a non-coding region (chr6: + 8683610). *Cntn4-gRNA2*: on-target score 8 (low on-target performance), off-target score 58, 0 mismatch hit only on *Cntn4*, no potential off-target sites with 1 or 2 mismatches. *Pcdh11x-gRNA1*: on-target score 56, off-target score 85, 0 mismatch only on *Pcdh11x*, no potential off-target sites with 1 or 2 mismatches. *Pcdh11x-gRNA2*: on-target score 53, off-target score 72, 0 mismatch hit only on *Pcdh11x*, no potential off-target sites with 1 or 2 mismatches. Note that the gRNA's on-target performance was subsequently tested and validated in cell cultures before *in vivo* experiments (see below).

Plasmids and viruses

For *in vivo* genomic targeting of CAMs, gRNAs were designed and cloned into pBSK-U6 backbone (pBSK-U6-gRNAs). The plasmids were purified and used for evaluation of knockout efficiency in cell culture. After evaluation, the same gRNAs were cloned into Cre-dependent tRFP expression vector and packaged into adeno-associated virus (AAV) serotype DJ/8. For *Fat3* targeting, a viral mixture (2.2×10^{13} vg/ml) of vWL51.AAVDJ8/2-[hU6-gRNA1(mFat3)]rev-hSyn1-dlox-TurboRFP(rev)-dlox-WPRE-hGHp(A) and vWL52.AAVDJ8/2-[hU6-gRNA2(mFat3)]rev-hSyn1-dlox-TurboRFP(rev)-dlox-WPRE-hGHp(A) were used. For *Cntn4* targeting, a viral mixture (1.7×10^{13} vg/ml) of vWL44.AAVDJ8/2-[hU6-gRNA1(mCNTN4)]rev-hSyn1-TurboRFP(rev)-WPRE-hGHp(A) and vWL45.AAVDJ8/2-[hU6-gRNA2(mCntn4)]rev-hSyn1-TurboRFP(rev)-WPRE-hGHp(A) were used. For *Pchd11x* targeting, a viral mixture (1.7×10^{13} vg/ml) of wWL46.AAVDJ8/2-[hU6-gRNA1(mPcdh11x)]rev-hSyn1-TurboRFP(rev)-WPRE-hGHp(A) and vWL47.AAVDJ8/2-[hU6-gRNA2(mPcdh11x)]rev-hSyn1-TurboRFP(rev)-WPRE-hGHp(A) were used. All viral vectors were produced by the Viral Vector Facility (VVF) of the Neuroscience Center Zurich (ZNZ).

Validation of CAM targeting guide RNAs in cell culture

The mixture of gRNA expressing vectors (0.4 µg of pBSK-U6-gRNA1 and 0.4 µg of pBSK-U6-gRNA2) were transfected into Neuro-2a cells expressing doxycycline-inducible CRISPR Cas9 nuclease from Rosa26 locus (GeneCopoeia, SL508)

using Lipofectamine 3000, according to recommendations of the manufacturer (Invitrogen). Forty-eight hours after transfection, doxycycline (1 µg/ml) was applied to induce stable Cas9 expression. To maintain Cas9 expression, the medium containing doxycycline was renewed every 48 h. Cells were harvested 7 days after transfection and prepared for Sanger sequencing.

Stereotaxic injection

Mice were deeply anesthetized and placed into a stereotactic apparatus. Microinjections were performed at a rate of 100 nl/min using a programmable syringe pump with a 35-gauge beveled NanoFil needle (World Precision Instruments, United States). For *in vivo* CAM targeting, 500 nl of the above mentioned viruses were injected into the ventral dentate gyrus (−3.4 mm anterior/posterior, 2.9 mm middle/lateral, −3.3 mm ventral/dorsal to bregma). To induce MF sprouting, 70 nl of KA (5 mM) was injected into the same position 4 weeks later or into gRNA non-injected animals.

In vitro electrophysiology

Brain slice preparation, recording solutions, whole-cell patch-clamp recording, and measurement of biophysical properties were as previously described (Luo et al., 2021). In short, neurons were visualized by infrared differential interference contrast optics in an upright microscope (Olympus; BX-51WI) using Hamamatsu Orca-Flash 4.0 CMOS camera and recorded using borosilicate glass pipettes with filament (Harvard Apparatus; GC150F-10; o.d. 1.5 mm; i.d. 0.86 mm; 10-cm length). Recordings were made using MultiClamp700B amplifier (Molecular Devices), signals were filtered at 10 kHz (Bessel filter) and digitized (50 kHz) with a Digidata1440A and pClamp10 (Molecular Devices). Spontaneous events were recorded in voltage clamp mode at -60 mV for 5 min, in presence of Gabazine (10 µM), or APV (10 µM) and NBQX (5 µM). The data analysis was performed using Python, R, Clampfit (Molecular Devices), and MiniAnalysis. For subsequent *post hoc* visualization, cells were filled with biocytin (Sigma-Aldrich, 2%) during recording. For all electrophysiological experiments, the experimenter was blind to the recording condition.

Histology

Sample preparation

Animals were deeply anesthetized and transcardially perfused first with 3 ml 0.9% saline solution followed by 3 ml 0.1% Na_2S in 0.1 M PB solution, and then by 4%

paraformaldehyde (PFA) in 0.1 M PB (1ml/1g bodyweight). Brains were immersed into 4% PFA in 0.1 M PB overnight at 4°C and then sectioned the next day using a vibratome, or further transferred into 30% sucrose in 0.1 M PB and stored at 4°C until sectioning using a frozen tissue sliding microtome. Fixed brains were cut into 50 or 80 μm thick horizontal sections.

Immunohistochemistry

Slices were first permeabilized and blocked in incubating medium (0.1 M PB containing 5% normal goat serum and 0.2% Triton) for 1 hour at room temperature, and then incubated overnight with primary antibodies at 4°C. Primary antibodies used: rabbit monoclonal anti-SLC30A3 (ZnT3; ThermoFisher, PA5-77769, 1:600), guinea pig polyclonal ZnT3 antiserum (Synaptic system, #197004, 1:500), rabbit polyclonal PCDH11X antibody (aa987-1117, LS-C673568, LifeSpan BioSciences, 1:500). Next day, slices were rinsed in 0.1 M PB and incubated with secondary antibodies overnight at 4°C. Secondary antibodies used: goat anti-rabbit IgG (H + L) cross-adsorbed, Alexa Fluor 488 (Invitrogen, A-11008, 1:500), anti-guinea pig IgG (H + L) highly cross-adsorbed secondary antibody, Alexa Fluor 568 (Invitrogen, A-11075, 1:500). Sections were rinsed in 0.1 M PB (some sections were subsequently stained with DAPI for nuclear staining) and mounted in Vectashield (Vector Laboratories) for analysis.

Timm's staining

Sections were rinsed in 0.1 M PB and post-fixed in 2.5% glutaraldehyde in 0.1 M PB solution for 10 min. Then, sections were rinsed in 0.1 M PB and immersed in Timm's reaction solutions, a 12:6:2 mixture of 20% gum arabic, hydroquinone, and citric acid trisodium citrate buffer, with 100 μl of 17% silver nitrate solution. The reaction was carried out for 20–30 min at 29°C, then slices were washed thoroughly in 0.1 M PB. After dehydration steps, the sections were mounted using DPX mounting medium and imaged using a Leica wide-field microscope.

Morphological reconstruction

Biocytin-filled cell-containing brain slices were fixed 4% PFA in 0.1 M PB overnight at 4°C. Next day, DAB staining (Vectastain ABC KIT, Vector Laboratories) was performed, and sections were dehydrated and mounted in DPX mounting medium (Electron Microscopy Science, United Kingdom). Cells were reconstructed using Neurolucida (MicroBrightField, Inc., United States).

Image analysis and quantification

Fluorescent images were acquired using Leica Stellaris 5 confocal microscope. Image analyses and quantification were performed in Fiji (version 2.0.0-rc-68/1.52h).

Quantification of PCDH11X immunostaining in wild-type animals after kainic acid injection

Tile-scan confocal images (1,024 × 1,024 pixels, zoom 0.75) were obtained using 20x immersion lens (0.75 NA). The mean gray value of PCDH11X immunostaining signals were measured in hilus, granule cell layer (GCL), inner molecular layer (IML), and middle/outer molecular layer (MML/OML). In addition, the mean gray value of PCDH11X immunostaining signal was measured in an area (that is below CA3 and outside hilus) that appeared to be PCDH11X negative in all conditions, to be used as baseline. Then, GCL, IML, and MML/OML signal intensities were normalized by subtracting this baseline signal intensity. In this manner, two images per animal were analyzed, the average values of which are shown in figure(s). As controls, normalized mean gray values from sections collected from ipsi- and contralateral hippocampus of saline injected animals (6 or 10 days after saline) and from the contralateral hippocampus of KA injected animals (6 or 10 days after KA) were averaged and used.

Quantification of PCDH11X immunostaining after *Pcdh11x*$^{Control+KA}$ and *Pcdh11x*$^{KO+KA}$

To confirm the location of injections and sufficient delivery of gRNAs into GCs, we included a turboRFP (tRFP) sequence in gRNA expression vectors. As intended, the tRFP signal broadly labeled GCs. However, we also found that the tRFP signal was strong and cross-bleed into the GFP channel to be used for detection of PCDH11X signals. This effect was most prominent in GCL where GC somata were strongly labeled with tRFP. To alleviate this problem, we exposed sections to light for several hours to bleach the tRFP signal and stained them for PCDH11X only afterward. While this treatment lowered the tRFP intensity, it did not completely eliminate the tRFP signal from the GFP channel. We then quantified PCDH11X signal intensity with and without normalization for the tRFP signal seen in the GFP channel. For quantification, tile-scan confocal images (1,024 × 1,024 pixels, zoom 0.75) were obtained using 20x immersion lens (0.75 NA). To obtain tRFP-non-normalized values, we used the same approach as described above (see *Quantification of PCDH11X immunostaining in wild-type animals after KA injection*). To obtain tRFP-normalized values, we first measured signal intensity in the GFP channel in hilus, GCL, IML, MML, and OML separately in sections from *Pcdh11x*^{Control} and *Pcdh11x*^{KO} animals. We chose to do this in KA-non-injected samples, because in these the tRFP signal in the GFP channel was similar to those in KA-injected samples, but the PCDH11X signal was expected to be the lowest. Then, these values were averaged between *Pcdh11x*^{Control} and *Pcdh11x*^{KO} in each region separately (i.e. hilus, GCL, IML, MML/OML), to be used as baselines. Subsequently, these baseline values

were subtracted from PCDH11X signal intensities measured in each area (i.e., hilus, GCL, IML, MML/OML) from KA-injected $Pcdh11x^{Control+KA}$ and $Pcdh11x^{KO+KA}$ animals. In this manner, two images per animal were analyzed, the average values of which are shown in figure(s). Independently of the approach used (i.e., tRFP-normalization or tRFP-non-normalization), PCDH11X signal intensities were significantly lower in GCL and IML of $Pcdh11x^{KO+KA}$ samples compared to $Pcdh11x^{Control+KA}$ samples.

Quantification of Timm's staining intensity

Bright-field images were acquired using a THUNDER (Leica) wide-field microscope using 40x lens (0.95 NA). Using Fiji, the mean gray value of Timm signals were measured in both GCL and IML, from which the GCL/IML ratio of gray values was calculated. The average value from 4 sections per animal was shown in the plot.

Quantification of ZnT3-positive puncta surrounding GC somata

Single panel confocal images (1,024 × 1,024 pixels) were obtained using 63× oil lens (1.4 NA). ZnT3 + signals on 95-170 GC somata from at least 2 images were quantified per animal. The percentage of GC somata surrounded by different numbers of ZnT3 + puncta was calculated based on the surrounding ZnT3 + puncta numbers per soma and total number of somata analyzed.

Immuno-electron microscopy

After fixation, brains were cut into 80 μm thick sections using a vibratome. For better penetration of the antibodies, single sections were frozen/thawed in liquid nitrogen using sucrose as cryoprotectant with the following concentration steps 10, 20, 30, 20, 10% and washed several times in 0.1 M PB. Then, the sections were treated with 0.5% $NaBH_4$ to bind free aldehyde groups for 15 min, followed by 5 min treatment with 3% H_2O_2 and 10% Methanol in 0.1 M PB to reduce endogenous peroxidase. After thoroughly washing in 0.1 M PB, the sections were blocked for 1 h at room temperature in 5% normal goat serum in 0.1 M PB and then incubated in rabbit monoclonal anti-SLC30A3 (ZnT3; ThermoFisher, PA5-77769, 1:600) at 4°C overnight. Next day, sections were incubated in biotinylated anti-rabbit solution (1:100, Vector Laboratories) at 4°C overnight. Next day, sections were developed with a standard avidin-biotin peroxidase kit (1:500; Vectastain) and postfixed in 1% OsO_4 followed by 3 × 5 min washing in 0.1 M PB. After washing, sections were dehydrated and embedded in durcupan

(Sigma-Aldrich) and re-sectioned. Finally, 60 nm ultra-thin sections were contrasted with 3% Lead citrate (Leica) and imaged using a FEI Tecnai G2 Spirit transmission electron microscope or Apreo VS (Thermo Fisher Scientific) scanning electron microscope. 3D rendering was performed with Fiji/ImageJ.
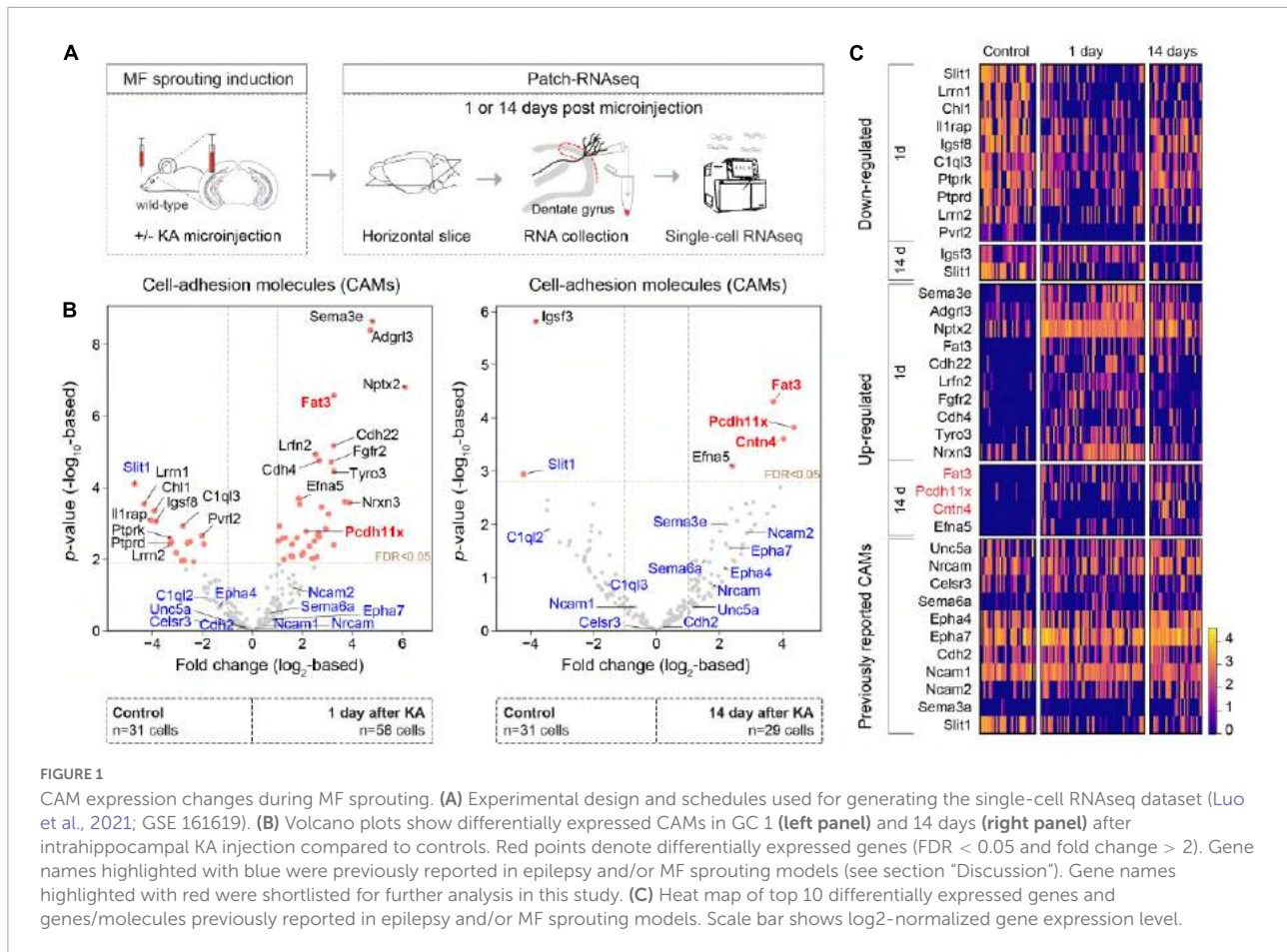
Statistical analyses

Statistical analyses were performed using Prism 9. All values represent mean ± standard error of the mean (SEM). The significance of differences was assessed using Welch's t-test, Mann–Whitney U test, one-way ANOVA, or two-way ANOVA, whichever is applicable (noted in text and/or figure legends). Data distribution normality was tested by Shapiro–Wilk Test. For normal distributions, Welch's t-test was performed. For non-normal distributions, non-parametric Mann–Whitney U test were performed. Significant main effects or interactions were followed up with *post hoc* testing using the original FDR method of Benjamini and Hochberg. The threshold for significance was $p = 0.05$ or FDR = 0.05, with a precise p value stated in each case. Non-significance is indicated with 'ns'. All tests were two-sided. Data analyses and quantifications were done blindly with respect to treatment.

Results

CAM expression changes during mossy fiber sprouting

To begin, we further analyzed our previously published single-cell transcriptomic data set consisting of control GCs as well as GCs 1 and 14 days after unilateral hippocampal KA injection (**Figure 1A**) (Luo et al., 2021; GSE 161619). Based on an extended list of 421 CAMs (see Földy et al., 2016 and section "Materials and methods"), we considered differentially expressed genes (fold change > 2 and FDR < 0.05) between the control and KA data sets (**Figure 1B**). This analysis revealed significant enrichment of *Fat3, Pcdh11x* in KA GCs, both 1 and 14 days after KA injection. *Fat3*, an atypical cadherin, has been implicated in the development of neuronal morphology (Deans et al., 2011; Krol et al., 2016). *Pcdh11x*, a delta1-type protocadherin, has been implicated in homophilic *trans* cell-cell interactions (Harrison et al., 2020; Pancho et al., 2020), dendritic branching (Wu et al., 2015), and neuronal stem cell differentiation and proliferation (Zhang et al., 2014). We shortlisted these molecules for further analysis. Although *Cntn4* was significantly enriched only in 14-day KA GCs after MF sprouting has developed, we also shortlisted this gene, because it has been linked to circuit formation

FIGURE 1

CAM expression changes during MF sprouting. **(A)** Experimental design and schedules used for generating the single-cell RNAseq dataset (Luo et al., 2021; GSE 161619). **(B)** Volcano plots show differentially expressed CAMs in GC 1 **(left panel)** and 14 days **(right panel)** after intrahippocampal KA injection compared to controls. Red points denote differentially expressed genes (FDR < 0.05 and fold change > 2). Gene names highlighted with blue were previously reported in epilepsy and/or MF sprouting models (see section "Discussion"). Gene names highlighted with red were shortlisted for further analysis in this study. **(C)** Heat map of top 10 differentially expressed genes and genes/molecules previously reported in epilepsy and/or MF sprouting models. Scale bar shows log2-normalized gene expression level.
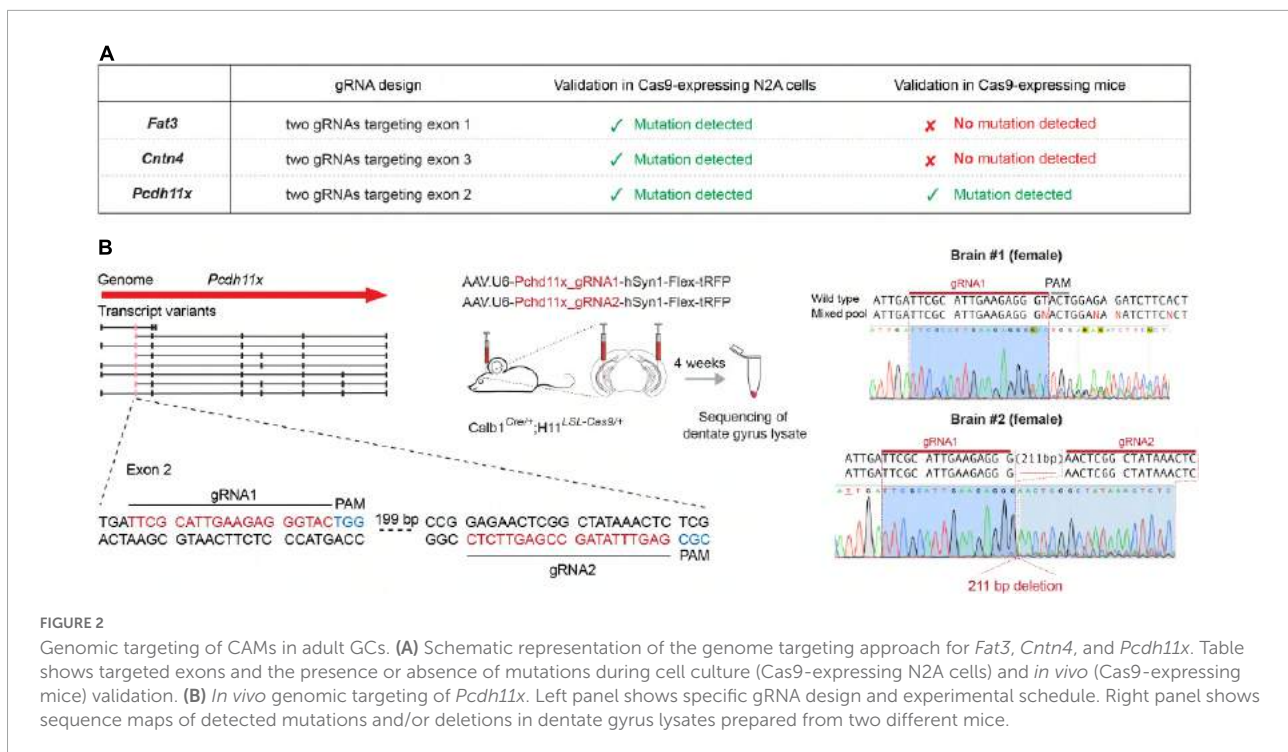
(Oguro-Ando et al., 2017), target specification (Osterhout et al., 2015), synaptic plasticity (Oguro-Ando et al., 2021), neurodevelopmental disorders (Baig et al., 2017; Oguro-Ando et al., 2017), and Alzheimer's disease (Carrasquillo et al., 2009). In addition, we looked for CAMs, whose abundance change has been reported in different temporal lobe epilepsy models or in MF sprouting (see section "Discussion," **Figure 1C**). However, with the exception of *Slit1* (previously reported to be up-regulated in hippocampal tissue, but down-regulated in KA GCs), their expression did not significantly change in our single-cell data (**Figures 1B,C**).

Genomic targeting of CAMs in adult granule cells

To study the role of *Fat3*, *Pcdh11x*, and *Cntn4* in MF sprouting, we aimed to introduce loss-of-function deletions and/or mutations in their genomic sequences. To achieve this goal, we designed two CRISPR/Cas9 guide RNAs (gRNAs) targeting each gene, to be delivered into GCs in the adult brain (**Figure 2A** and **Supplementary Figure 1A**, and section "Materials and methods"). To identify the transfected area

and neurons that expressed the gRNA, we also included a Cre-dependent turboRFP (tRFP) reporter into the gRNA-expressing AAV vectors. This *in vivo* gene editing approach minimized unwanted effects during development, ensured cell type-specificity and—since *Fat3*, *Pcdh11x*, and *Cntn4* transcripts were virtually absent from control GCs (**Figure 1C**)—that loss-of-function effects would manifest themselves only after KA injections.

First, we tested gRNAs targeting each gene in cell cultures and confirmed their efficacy in introducing genomic mutations (**Supplementary Figure 1**). Second, to achieve GC-specific gene manipulations, we separately delivered the pairs of gRNAs into the dentate gyrus of 2 months old $Calb1^{Cre/+};H11^{LSL-Cas9/+}$ mice, in which GCs expressed Cas9. Four weeks later, we confirmed broad presence of the tRFP reporter in the dentate gyrus and prepared lysates for target gene specific PCR amplification. Genomic sequence analysis revealed multiple mutations or large deletions (>200 basepair) in *Pcdh11x*, likely rendering this gene null mutant (KO) in most neurons (**Figure 2B** and **Supplementary Figure 1**). By contrast, *Fat3* and *Cntn4* sequences did not display deleterious effects. To further test these two genes, we sequenced 24 single clones from the PCR product of each. This analysis revealed insertions/deletions

FIGURE 2
Genomic targeting of CAMs in adult GCs. **(A)** Schematic representation of the genome targeting approach for *Fat3*, *Cntn4*, and *Pcdh11x*. Table shows targeted exons and the presence or absence of mutations during cell culture (Cas9-expressing N2A cells) and *in vivo* (Cas9-expressing mice) validation. **(B)** *In vivo* genomic targeting of *Pcdh11x*. Left panel shows specific gRNA design and experimental schedule. Right panel shows sequence maps of detected mutations and/or deletions in dentate gyrus lysates prepared from two different mice.

only in 1/24 of Fat3 and 2/24 of Cntn4 clones, further confirming their inefficient targeting *in vivo* (**Supplementary Figure 1**). Variations in the *in vivo* targeting efficiency of different genes were not completely unexpected, however, based on these results we could proceed further only with *Pcdh11x*.

PCDH11X protein levels in the dentate gyrus

To investigate the role of *Pcdh11x* in MF sprouting, we first aimed to establish the extent of PCDH11X protein expression (we refer to protein form with capitalized gene name) in the dentate gyrus of wild-type animals, including if cell types other than GCs expressed this protein. Using PCDH11X antibody, we immunostained sections 6–10 days after saline- and KA-injections (**Figures 3A,B** and **Supplementary Figure 2**). We presumed that *Pcdh11x* mRNA seen 1 day after KA (**Figure 1**) would be translated and detectable by this time. In addition, 6–10 days after KA likely represents a critical period for establishing MF target specificity, since most growing axons would still advance toward IML during this phase (MF sprouting starts ∼2–3 days after KA and becomes largely established ∼14 days after KA) (Luo et al., 2021).

In controls, some cells in the hilus, GCL and dentate molecular layers appeared to be PCDH11X positive and a weak punctate, possibly background signal, could be observed in all dentate layers (**Figure 3B** and **Supplementary Figure 2**). About 6–10 after KA, less hilar but more GCL cells were

PCDH11X positive, and a prominent punctate PCDH11X signal became apparent in GCL and IML (**Figures 3B,C**). In part, the emergence of this signal was due to PCDH11X located in the somato-dendritic domain of GCs (**Figure 3B**). In addition, PCDH11X appeared to localize in zinc transporter-3 (ZnT3, a frequently used MF marker) positive MF boutons in IML and GCL (**Figure 3B**, inserts in lower right panels). These results thus revealed KA-induced PCDH11X enrichment in areas relevant for MF sprouting and during a phase likely critical for target specification. However, the question whether PCDH11X enrichment originated only from GCs or possibly also from other cells expressing this protein remained open. To answer this question, we used the above described Cas9 system to evaluate if genetic *Pcdh11x* KO in GCs occluded KA-induced PCDH11X enrichment.

We injected *Pcdh11x* targeting gRNA- and tRFP-containing AAVs into the ventral dentate gyrus of $Calb1^{Cre/+}$ ($Pcdh11x^{Control}$, lacking Cas9 expression) or $Calb1^{Cre/+};H11^{LSL-Cas9/+}$ mice ($Pcdh11x^{KO}$). Four weeks later, we injected KA into the left dentate gyrus to induce *Pcdh11x* upregulation and MF sprouting, and then two weeks later, we prepared 50 µm thick horizontal sections for histological analysis (**Figure 3D**). Using the tRFP reporter, we localized the transfected area and quantified the ratio of tRFP + and DAPI + cells in GCL, which revealed > 90% transfection efficacy both conditions ($Pcdh11x^{Control+KA}$: 92.4 ± 0.97%, n = 3; $Pcdh11x^{KO+KA}$: 92.82 ± 0.49%, n = 3) showing that our manipulations broadly impacted GCs. Using immunostaining, we then examined PCDH11X protein expression 14 days
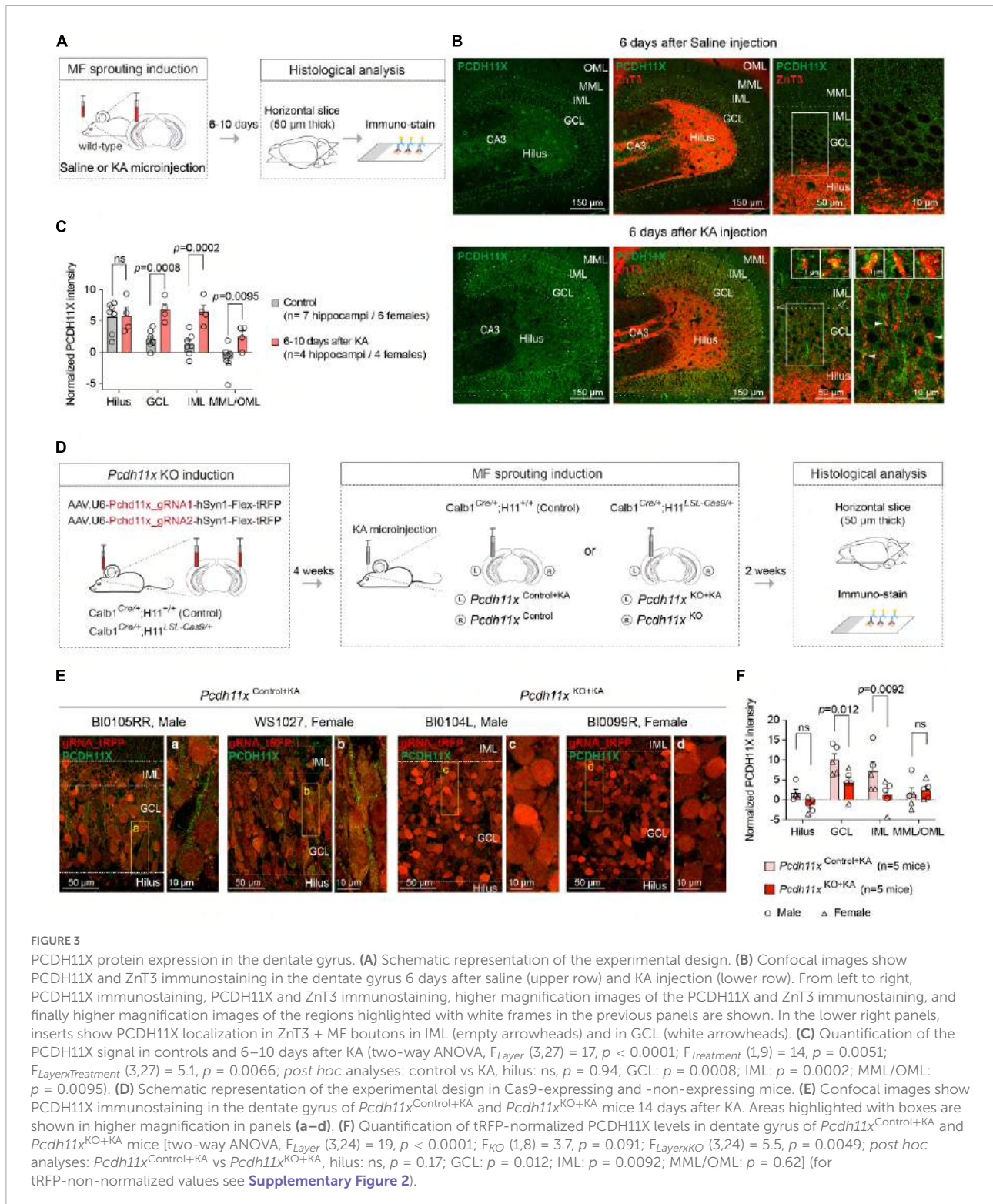
FIGURE 3

PCDH11X protein expression in the dentate gyrus. **(A)** Schematic representation of the experimental design. **(B)** Confocal images show PCDH11X and ZnT3 immunostaining in the dentate gyrus 6 days after saline (upper row) and KA injection (lower row). From left to right, PCDH11X immunostaining, PCDH11X and ZnT3 immunostaining, higher magnification images of the PCDH11X and ZnT3 immunostaining, and finally higher magnification images of the regions highlighted with white frames in the previous panels are shown. In the lower right panels, inserts show PCDH11X localization in ZnT3 + MF boutons in IML (empty arrowheads) and in GCL (white arrowheads). **(C)** Quantification of the PCDH11X signal in controls and 6–10 days after KA (two-way ANOVA, F_{Layer} (3,27) = 17, $p < 0.0001$; $F_{Treatment}$ (1,9) = 14, $p = 0.0051$; $F_{LayerxTreatment}$ (3,27) = 5.1, $p = 0.0066$; $post$ hoc analyses: control vs KA, hilus: ns, $p = 0.94$; GCL: $p = 0.0008$; IML: $p = 0.0002$; MML/OML: $p = 0.0095$). **(D)** Schematic representation of the experimental design in Cas9-expressing and -non-expressing mice. **(E)** Confocal images show PCDH11X immunostaining in the dentate gyrus of $Pcdh11x^{Control+KA}$ and $Pcdh11x^{KO+KA}$ mice 14 days after KA. Areas highlighted with boxes are shown in higher magnification in panels **(a–d)**. **(F)** Quantification of tRFP-normalized PCDH11X levels in dentate gyrus of $Pcdh11x^{Control+KA}$ and $Pcdh11x^{KO+KA}$ mice [two-way ANOVA, F_{Layer} (3,24) = 19, $p < 0.0001$; F_{KO} (1,8) = 3.7, $p = 0.091$; $F_{LayerxKO}$ (3,24) = 5.5, $p = 0.0049$; $post$ hoc analyses: $Pcdh11x^{Control+KA}$ vs $Pcdh11x^{KO+KA}$, hilus: ns, $p = 0.17$; GCL: $p = 0.012$; IML: $p = 0.0092$; MML/OML: $p = 0.62$] (for tRFP-non-normalized values see **Supplementary Figure 2**).

after KA injection. We found that the punctate and in some cells somato-dendritic PCDH11X labeling was present in $Pcdh11x^{Control+KA}$ (following the same pattern as in wild-type animals 6 days after KA), but largely absent from $Pcdh11x^{KO+KA}$

samples (**Figure 3B**). However, in both $Pcdh11x^{Control+KA}$ and $Pcdh11x^{KO+KA}$ samples, we also noticed that the tRFP signal used for cell labeling (intended to be visible only in RFP channel) was intense and visible in the GFP channel used

for PCDH11X detection. This effect was most prominent in GCL where GC somata are located. To address this issue, we quantified PCDH11X signals with and without normalization to tRFP seen in the GFP channel (see section "Materials and methods"). Independently of the normalization approach used, PCDH11X signal intensity was significantly lower in GCL and IML in $Pcdh11x^{KO+KA}$ compared to $Pcdh11x^{Control+KA}$ samples (tRFP-normalized, $Pcdh11x^{Control+KA}$: hilus: 1.7 $\pm$ 0.88, GCL: 9.97 $\pm$ 1.57, IML: 7.17 $\pm$ 2.39, MML/OML: 1.33 $\pm$ 1.68, n = 5; $Pcdh11x^{KO+KA}$: hilus: -1.28 $\pm$ 0.81, GCL: 4.30 $\pm$ 1.49, IML: 1.27 $\pm$ 1.57, MML/OML: 2.40 $\pm$ 0.98, n = 5, **Figures 3E,F**) (for tRFP-non-normalized data, see **Supplementary Figure 2B,C**).

Together, these results suggested that the KA-induced $Pcdh11x$ mRNA upregulation (**Figures 1B,C**) lead to an increased PCDH11X protein expression in the dentate gyrus, and this PCDH11X enrichment was GC-dependent. In addition, related to $Pcdh11x$ KO but irrespective of PCDH11X labeling, an increased GCL dispersion in the $Pcdh11x^{KO+KA}$ dentate gyrus become apparent (see **Figure 3E** and below).

Impact of $Pcdh11x$ KO on mossy fiber sprouting

To study the KA-induced phenotypes in $Pcdh11x$ KO, we employed the same experimental approach as described above (**Figure 3D**). First, we analyzed GCL dispersion, which is although mechanistically independent from MF sprouting (Haas et al., 2002; Heinrich et al., 2006; Duveau et al., 2011), a known phenotype of KA injections in the dentate gyrus. While KA-induced GCL dispersion developed both in $Pcdh11x^{Control+KA}$ and $Pcdh11x^{KO+KA}$, it was more pronounced in KOs (GCL width: non-injected, 66 $\pm$ 1.8 µm, $Pcdh11x^{Control+KA}$, 109 $\pm$ 6.2 µm, $Pcdh11x^{KO+KA}$, 138 $\pm$ 5.9 µm; one-way ANOVA, $Pcdh11x^{Control+KA}$ vs $Pcdh11x^{KO+KA}$, p = 0.0031; GCL area: non-injected, 0.097 $\pm$ 0.005 mm^2, $Pcdh11x^{Control+KA}$, 0.16 $\pm$ 0.013 mm^2, $Pcdh11x^{KO+KA}$, 0.21 $\pm$ 0.011 mm^2, **Figures 4A,B**).

Next, we examined the impact of $Pcdh11x$ KO on MF sprouting. To visualize MF sprouting, we utilized two MF labeling approaches: Timm's staining and ZnT3 immunostaining (**Figure 4C**) (Luo et al., 2021). Using Timm's staining, we observed dense signal in IML of $Pcdh11x^{Control+KA}$, which is the typical targeting zone of MF sprouting. By contrast, the Timm's signal became more diffuse overall but also denser in GCL of $Pcdh11x^{KO+KA}$, highlighting a pattern atypical for MF sprouting. To quantify these observations, we measured the signal intensity ratio between GCL and IML, which was significantly higher in KOs than in controls (GCL/IML signal ratio: $Pcdh11x^{KO+KA}$, 0.93 $\pm$ 0.046, n = 6 mice; $Pcdh11x^{Control+KA}$, 0.71 $\pm$ 0.04, n = 6 mice; Welch's t-test, p = 0.0054) (**Figures 4D,E**). ZnT3 immunostaining confirmed this pattern. A large number of ZnT3 + puncta were present

in the IML of both $Pcdh11x^{Control+KA}$ and $Pcdh11x^{KO+KA}$, but become significantly enriched in the GCL of $Pcdh11x^{KO+KA}$ compared to $Pcdh11x^{Control+KA}$ (**Figure 4F**), suggesting that MF sprouting target specification was altered in KOs.

To further study this phenotype, we first considered the possibility that the apparent change in target specificity appeared as a consequence of increased GCL dispersion in KOs. According to this scenario, sprouting MF axons in KOs populated the same spatial area as in controls, but the broader GC dispersion created an altered context. To test this possibility, we quantified ZnT3 + puncta density in the inner (proximal to hilus) and outer (proximal to IML) half of GCL, and in IML. We hypothesized that ZnT3 + puncta density would not change in the inner half of GCL if the effect was due to increased GCL dispersion, because the inner half of GCL in KOs remained before the GCL/IML border seen in controls. However, ZnT3 + puncta density was significantly increased both in the inner and outer half of GCL in KOs compared to controls, whereas that in IML was similar in both conditions ($Pcdh11x^{Control+KA}$: GCL inner: 1.4 $\pm$ 0.26 $\times$ 10^4 puncta/mm^2, GCL outer: 1.0 $\pm$ 0.13 $\times$ 10^4 puncta/mm^2, IML: 3.4 $\pm$ 0.58 $\times$ 10^4 puncta/mm^2, n = 5 mice; $Pcdh11x^{KO+KA}$: GCL inner: 2.6 $\pm$ 0.27 $\times$ 10^4 puncta/mm^2, GCL outer: 2.2 $\pm$ 0.21 $\times$ 10^4 puncta/mm^2, IML: 3.8 $\pm$ 0.31 $\times$ 10^4 puncta/mm^2, n = 6 mice) (**Figure 4G**), suggesting that target specificity in KOs has changed independently of GCL dispersion. Consequently, the total (as measured in the inner and outer half of GCL, and IML) ZnT3 + puncta density ($Pcdh11x^{Control+KA}$: 1.8 $\pm$ 0.25 $\times$ 10^4 puncta/mm^2, n = 5 mice; $Pcdh11x^{KO+KA}$: 2.8 $\pm$ 0.17 $\times$ 10^4 puncta/mm^2, n = 6 mice) and the GCL/IML ZnT3 + puncta density ratio increased in KOs ($Pcdh11x^{Control+KA}$: 0.39 $\pm$ 0.044, n = 5 mice; $Pcdh11x^{KO+KA}$: 0.66 $\pm$ 0.043, n = 6 mice) (**Figure 4G**).

To gain further insights into the target specification of MF sprouting, we quantified the number of ZnT3 + puncta surrounding GC somata as a proxy for potential synapses. In $Pcdh11x^{Control+KA}$, we found that ~50% of GCs somata were lacking adjacent ZnT3 + puncta. By contrast, in $Pcdh11x^{KO+KA}$, only ~20% of GCs somata were lacking adjacent ZnT3 + puncta while the rest were surrounded with more ZnT3 + puncta than those in controls (**Figure 4H**).

Electrophysiological characterization of $Pcdh11x$ KO GCs

Next, following the same injection schedule as above, we made patch-clamp recordings from $Pcdh11x^{Control+KA}$ and $Pcdh11x^{KO+KA}$ GCs. As additional controls, we also included GCs from $Pcdh11x^{Control}$ and $Pcdh11x^{KO}$ (six weeks after gRNA injection), neither of which received KA (**Figure 5A**). The resting membrane potential (RMP), input resistance (R), and capacitance (C) of cells reflected consequences of
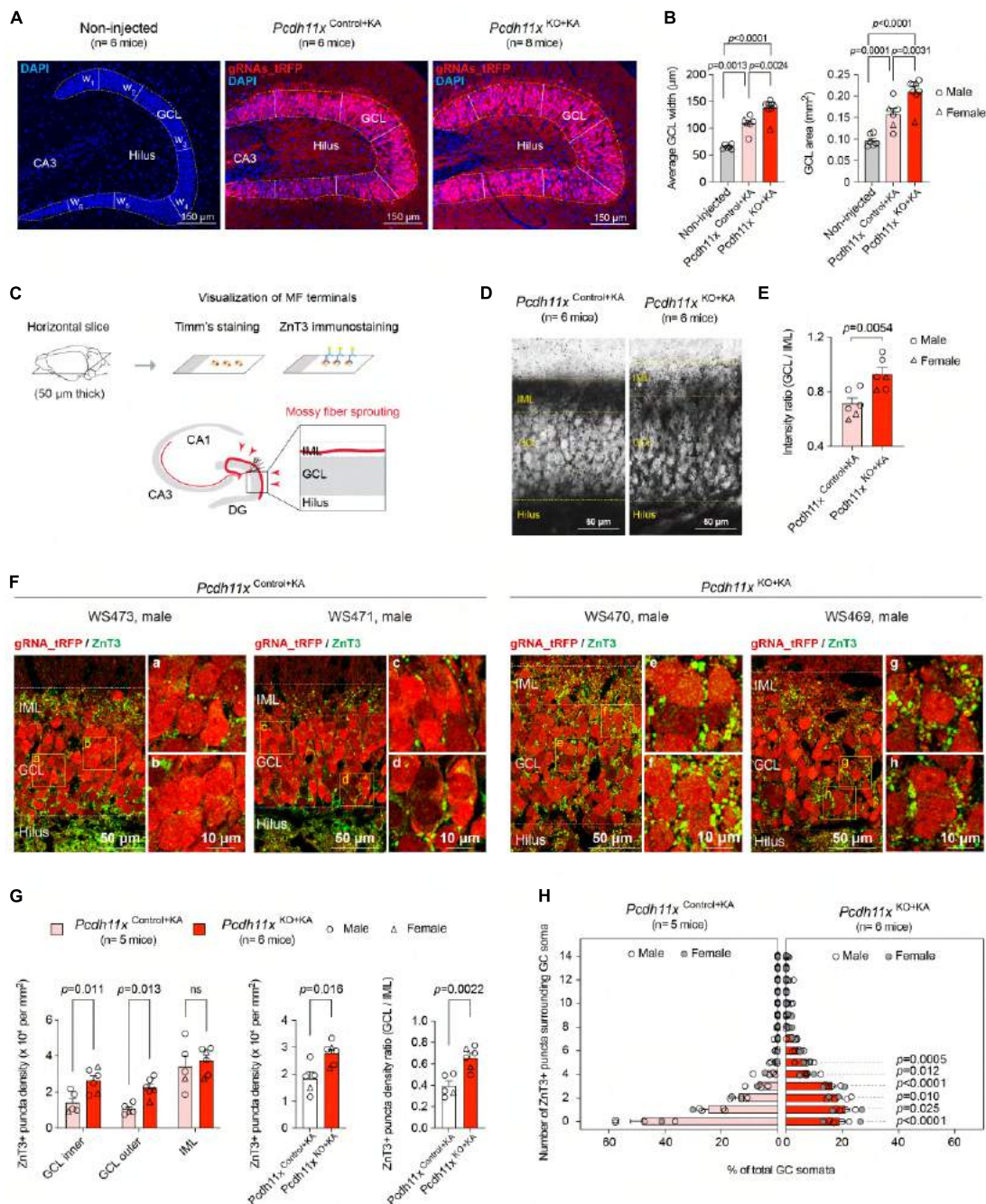
FIGURE 4

Impact of *Pcdh11x* KO on MF sprouting. **(A)** Confocal images show DAPI immunostaining and virally-delivered tRFP signal in the dentate gyrus of non-injected control, *Pcdh11x*^Control+KA^, and *Pcdh11x*^KO+KA^ mice. In each sample, the width of GCL was determined as the average of six width measurement (w_1 to w_6) based on DAPI staining. **(B)** Left plot shows quantification of average GCL width in non-injected, *Pcdh11x*^Control+KA^, and *Pcdh11x*^KO+KA^ samples. The transfected area was localized based on the tRFP signal. Right plot shows quantification of GCL area (quantified as the circumference of DAPI staining) in non-injected, *Pcdh11x*^Control+KA^, and *Pcdh11x*^KO+KA^ samples. Each data point represents one animal (one-way ANOVA tests, $F_{(2,17)} = 29$, $p < 0.0001$; p-values of the *post hoc* analyses are indicated in the figure).
(C) Experimental design for visualizing MF boutons by Timm's staining and ZnT3 immunostaining. **(D)** Timm's staining shows stratification of MF boutons in *Pcdh11x*^Control+KA^ and *Pcdh11x*^KO+KA^ mice. **(E)** Quantification of Timm's signal intensity between GCL and IML in *Pcdh11x*^Control+KA^ and *Pcdh11x*^KO+KA^ mice (Welch's *t*-test). **(F)** ZnT3 staining shows stratification of MF boutons in *Pcdh11x*^Control+KA^ and *Pcdh11x*^KO+KA^ mice. Areas highlighted with boxes are shown in higher magnification in panels **(a−h)**. **(G)** Quantification of ZnT3 + puncta density in the inner and outer half of GCL and in IML [left plot; two-way ANOVA, F_{Layer} $(2,18) = 31$, $p < 0.0001$; F_{KO} $(1,9) = 7.8$, $p = 0.021$; $F_{Layer \times KO}$ $(2,18) = 1.9$, $p = 0.18$; *post hoc* analyses: *Pcdh11x*^Control+KA^ vs *Pcdh11x*^KO+KA^, GCL inner: $p = 0.01$; GCL outer: $p = 0.013$; IML: ns, $p = 0.46$], in GCL and IML together (middle plot; Welch's *t*-test, $p = 0.016$), and the GCL/IML ratio of ZnT3 + puncta density (right plot; Welch's *t*-test, p = 0.0022). **(H)** Distribution of GC somata (in %) that are surrounded by 0, 1, 2, ..., 14 ZnT3 + boutons in *Pcdh11x*^Control+KA^ and *Pcdh11x*^KO+KA^ mice (two-way ANOVA, $F_{\# of puncta}$ $(14,126) = 141$, $p < 0.0001$; F_{KO} $(1,9) = 2.8$, $p = 0.13$; $F_{\# of puncta \times KO}$ $(14,126) = 26$, $p < 0.0001$; p-values of the *post hoc* analysis are indicated in the figure; *p*-values are > 0.05 for 6 or more puncta).
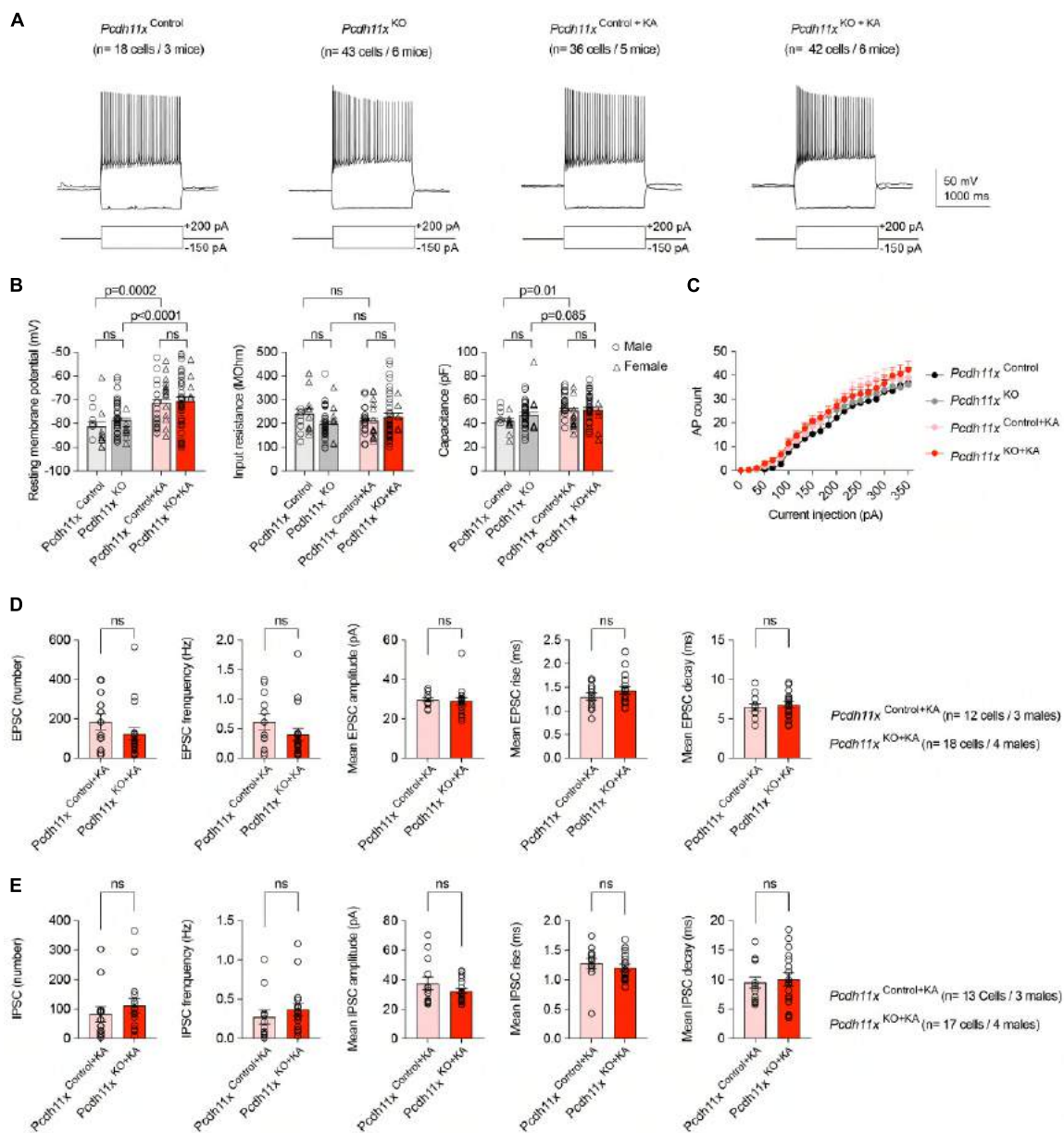
FIGURE 5

Electrophysiological characterization of $Pcdh11x^{Control+KA}$ and $Pcdh11x^{KO+KA}$ GCs. **(A)** Example electrophysiological traces show responses to 1.5 s long current pulse injections in $Pcdh11x^{Control}$, $Pcdh11x^{KO}$, $Pcdh11x^{Control+KA}$, and $Pcdh11x^{KO+KA}$ GCs. **(B)** Quantification of resting membrane potential, input resistance, and capacitance (two-way ANOVA tests; resting membrane potential: $F_{KA\ treatment}$ (1,135) = 30, $p < 0.0001$; F_{KO} (1, 135) = 1.1, $p = 0.30$; $F_{KA\ treatment\ x\ KO}$ (1,135) = 0.35, $p = 0.56$; input resistance: $F_{KA\ treatment}$ (1,135) = 0.0009, $p = 0.98$; F_{KO} (1, 135) = 0.92, $p = 0.33$; $F_{KA\ treatment\ x\ KO}$ (1,135) = 4.3, $p = 0.04$; capacitance: $F_{KA\ treatment}$ (1,135) = 9.8, $p = 0.0022$; F_{KO} (1, 135) = 1.8, $p = 0.18$; $F_{KA\ treatment\ x\ KO}$ (1,135) = 1.1, $p = 0.30$; p-values of *post hoc* analyses are indicated in the figure; data points represent single cells). **(C)** Quantification of steady-state current injection-evoked action potential (AP) counts. **(D)** Quantification of EPSC parameters recorded from $Pcdh11x^{Control+KA}$ and $Pcdh11x^{KO+KA}$ GCs (Mann–Whitney U test; data points represent single cells recorded from males). **(E)** Quantification of IPSC parameters recorded from $Pcdh11x^{Control+KA}$ and $Pcdh11x^{KO+KA}$ GCs (Mann-Whitney U test; data points represent single cells recorded from males).

KA, but not gRNA treatment (for $Pcdh11x^{Control}$, n = 18 cells/$Pcdh11x^{KO}$, n = 43 cells/$Pcdh11x^{Control+KA}$, n = 36 cells/$Pcdh11x^{KO+KA}$, n = 42 cells, respectively; RMP (mV): $-81 \pm 1.80/-79 \pm 1.0/-71 \pm 1.6/-71 \pm 1.7$; R

(MOhm): $240 \pm 20/198 \pm 10/211 \pm 11/226 \pm 14$; C (pF): $42 \pm 1.8/47 \pm 1.8/51 \pm 2.0/52 \pm 1.8$) (**Figure 5B**). In addition, we analyzed action potential firing threshold, amplitude, and attenuation, none of which showed difference between

the different conditions (not shown). Further, steady-state current injection-evoked action potential (AP) counts did not differ between the groups (**Figure 5C**). These results established that *Pcdh11x* KO had no effect on the intrinsic electrophysiological properties of GCs. Next, we analyzed spontaneous glutamatergic EPSCs (in presence of 10 μM Gabazine) and GABAergic IPSCs (in presence of 10 μM APV and 5 μM NBQX) in *Pcdh11x*[Control+KA] and *Pcdh11x*[KO+KA] GCs. We hypothesized that somatic boutons in *Pcdh11x* KOs may elicit larger and/or faster synaptic events, because they were closer to the recording pipette. However, neither the number and frequency of recorded EPSCs and IPSCs, nor their amplitudes, rise and decay times revealed significant differences between the two groups (**Figures 5D,E**). This could be because synaptic events evoked by sprouted synapses were not sufficiently represented in our recordings (e.g., they were not spontaneously activated or possibly represented silent synapses), or the recordings did not have sufficient resolution for differences, or both.

Morphological characterization of *Pcdh11x* KO GCs

To study the morphology of individual GCs, we filled cells with biocytin during the patch-clamp recordings and reconstructed them afterwards. A limitation of this approach, however, is that the recovery of axons (e.g. in CA3 or sprouted fibers in IML) is limited in brain slice preparation. First, we analyzed dendritic morphology (**Figure 6A**), because the overexpression and knockdown of *Pcdh11x* was previously reported to reduce and increase dendritic complexity in developing neurons, respectively (Wu et al., 2015). However, neither the total dendritic length, total dendritic branch count, number of primary and secondary dendrites, nor Sholl analysis showed a difference between *Pcdh11x*[Control], *Pcdh11x*[KO], *Pcdh11x*[Control+KA], and *Pcdh11x*[KO+KA] GCs (**Figures 6B,C**). Second, whenever possible, we reconstructed axons from GCs. As expected, GCs in the KA-non-injected control groups (*Pcdh11x*[Control] and *Pcdh11x*[KO] GCs) lacked axons in GCL or IML. By comparison, GCs in both KA-injected groups (*Pcdh11x*[Control+KA] and *Pcdh11x*[KO+KA] GCs) displayed MF sprouting, i.e., axons were detectable in GCL and to some extent in IML (**Figure 6D** and **Supplementary Figure 3**). While insights into target specification by this analysis were limited, it confirmed the presence of *Pcdh11x*[KO+KA] GC axons in GCL.

Immuno-electron microscopy characterization of sprouted *Pcdh11x* KO GC synapses

Thus far, our histological analyses revealed differences in target specificity between *Pcdh11x* controls and KOs after MF sprouting, but our electrophysiological and morphological analyses could not further substantiate this. Importantly, the question whether ZnT3 + and Timm + boutons in GCL formed synapses remained open. To answer this question, we prepared horizontal sections from the ventral dentate gyrus, immunostained them with ZnT3 antibody and used immuno-electron microscopy (**Figure 7** and **Supplementary Figure 4**). In *Pcdh11x*[Control+KA], we only found dendritic synapses, an expected outcome after KA treatment (**Supplementary Figure 4**). By contrast, in *Pcdh11x*[KO+KA], electron microscopy revealed an abundance of ZnT3 + synapses on GC somata (7G,F,M,N and **Supplementary Figure 4**). The synapses contained one or multiple release sites and many vesicles. In some cases, ZnT3 + boutons formed synapses both on soma and neighboring dendrites in GCL (**Figure 7H**) or only on dendrites (**Figures 7I,J** and **Supplementary Figure 4**). Such dendrites in GCL may have belonged to GCs whose soma was proximal to hilus or interneurons (Frotscher et al., 2006).

Discussion

Hippocampal MF sprouting is a striking example of circuit formation in the adult brain (Seng et al., 2022). Previously, we studied the induction mechanisms of MF sprouting (Luo et al., 2021). Here, we investigated the question of target specificity.

Associated with MF sprouting, CAM expression and/or abundance changes have been previously described in different models, such as pilocarpine (PC) or kainate (KA) induced status epilepticus and intrahippocampal electrical stimulation (IES). Arguably, the most striking phenotype was achieved by the knockdown of *Unc5a*, which prevented PC-induced recurrent MF sprouting in hippocampal slice cultures (Muramatsu et al., 2010), directly implicating this molecule in axon guidance. Others reported up-regulation of *Nrcam*, *Slit1*, *Celsr3*, *Sema6a*, *Epha4*, and *Epha7* transcripts in whole hippocampal tissue (PC model) (Hansen et al., 2014), increased protein abundance of N-cadherin (Cdh2) (PC model) (Shan et al., 2002) and NCAM (encoded by *Ncam1* or *Ncam2*) (KA model) (Niquet et al., 1993) in sprouted MF synapses, and transient down-regulation of *Sema3a* (IES model) (Holtmaat et al., 2003). In addition, C1q-like-s were characterized in MF sprouting. Typically, C1QL1 and C1QL3 are secreted from MF synapses and form a complex with presynaptic NRXN3 to facilitate trans-synaptic recruitment of kainate-sensitive glutamate receptors (KARs) in CA3 cells (Matsuda et al., 2016). While MF sprouting still developed in the double *C1ql2*/*C1ql3* knock-out mice, KARs were not recruited to sprouted synapses (PC model; Matsuda et al., 2016), showing a shared feature between naive and sprouted MF synapses.

Together, these findings illuminated a complex landscape behind MF sprouting. As a caveat, most observations were made in tissue-level samples and/or after seizures, limiting delineation of cell types in which CAM abundance has
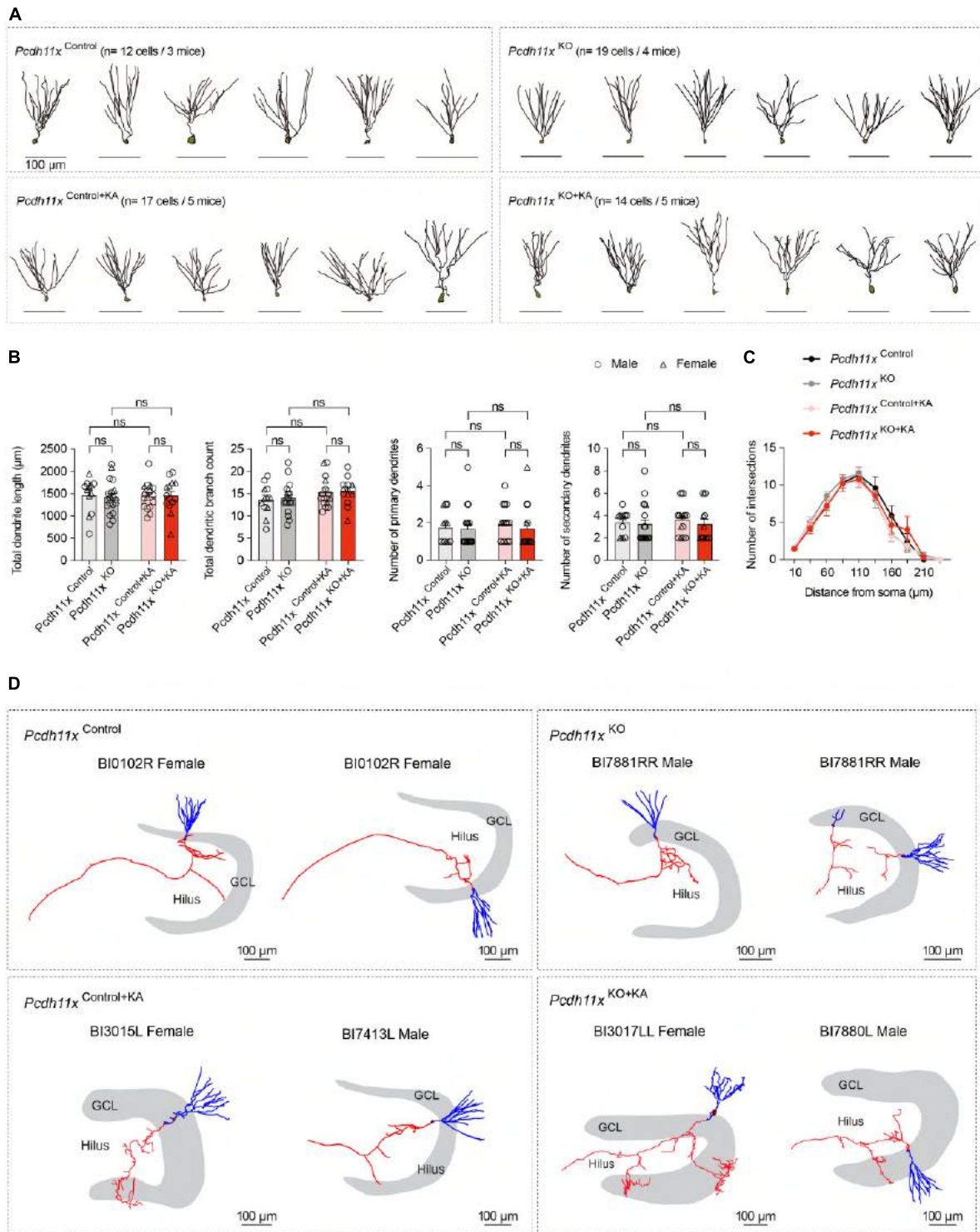
FIGURE 6

Morphological characterization of *Pcdh11x*Control+KA and *Pcdh11x*KO+KA GCs. **(A)** Morphological reconstruction of dendrites from *Pcdh11x*Control, *Pcdh11x*KO, *Pcdh11x*Control+KA, and *Pcdh11x*KO+KA GCs. **(B)** Quantification of dendritic parameters, such as total dendrite length, total dendritic branch count, number of primary dendrites, and number of secondary dendrites (two-way ANOVA test; data points represent single cells). **(C)** Sholl analysis of dendritic complexity. None of the comparisons had significance $p < 0.05$ (two-way ANOVA test). **(D)** Morphological reconstruction of axons from *Pcdh11x*Control, *Pcdh11x*KO, *Pcdh11x*Control+KA, and *Pcdh11x*KO+KA GCs. Axons and dendrites are shown in red and blue respectively. For further examples, see **Supplementary Figure 3**.
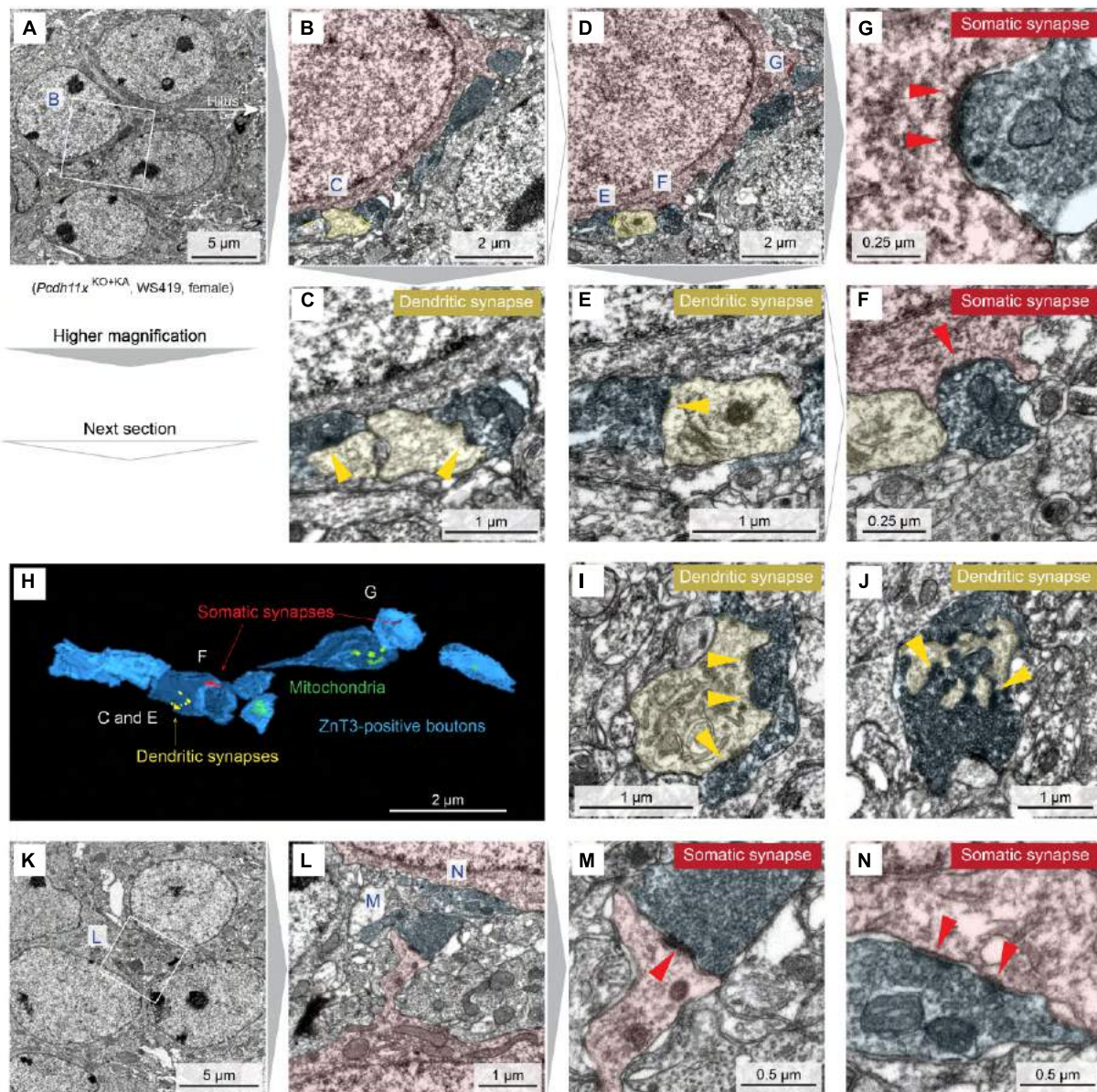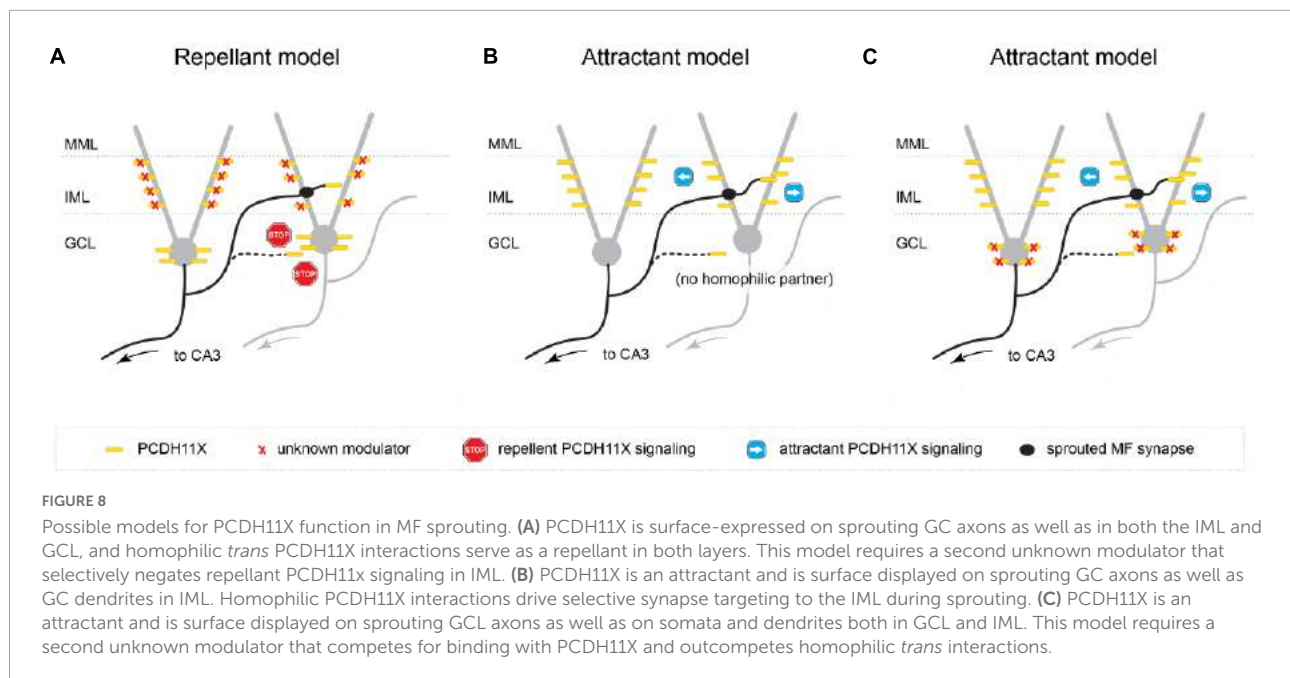
FIGURE 7

Immuno-electron microscopy characterization of *Pcdh11x*[KO+KA] GC synapses. **(A)** Transmission electron microscopy image of four GC somata in GCL. In white box, ZnT3 + boutons are visible next to GC soma. **(B)** Magnification of the white box in panel A. GC soma, dendrite, and presynaptic ZnT3 + boutons are presudo-colored in red, yellow, and blue, respectively. **(C)** Magnification of the area labeled with C in panel B shows synapses on dendrites (yellow arrowheads). **(D)** Image shows the next section of what is shown in panel **(B)**. **(E–G)** Magnification of the areas labeled with E, G, and F in panel **(D)** show somatic, somatic and dendritic, and dendritic synapses, respectively (yellow and red arrowheads). In the lower right part of panel **(F)**, a dendritic synapse is also visible. However, the presynaptic compartment is lacking ZnT3 and thus MF identity of this synapse could not be confirmed. **(H)** 3D reconstruction of ZnT3 + boutons and synapses shown in panels **(A–F)**. **(I,J)** Images show additional dendritic synapses with multiple release sites (yellow arrowheads) from the same animal. **(K)** Image show five GC somata in GCL. **(L)** Magnification of the area shown in panel **(K)**. **(M,N)** Magnification of the areas labeled with M and N in panel **(L)** show somatic synapses with one and multiple release sites, respectively (red arrowheads).

changed and causal dependencies (e.g., if CAM changes were required for sprouting or induced by seizures). We alleviated these limitations by specifically studying non-sprouting and sprouting GCs (1 and 14 days after KA), sampled before the expected onset of status epilepticus (typically 14–28 days after KA) (Tanaka et al., 1992; Ben-Ari and Cossart, 2000). Our results did not reveal significant transcriptomic changes in the above listed molecules, with the one exception of *Slit1*. However, in contrast to up-regulation at the tissue level (Hansen et al., 2014), we found down-regulation of

FIGURE 8
Possible models for PCDH11X function in MF sprouting. **(A)** PCDH11X is surface-expressed on sprouting GC axons as well as in both the IML and GCL, and homophilic *trans* PCDH11X interactions serve as a repellant in both layers. This model requires a second unknown modulator that selectively negates repellant PCDH11x signaling in IML. **(B)** PCDH11X is an attractant and is surface displayed on sprouting GC axons as well as GC dendrites in IML. Homophilic PCDH11X interactions drive selective synapse targeting to the IML during sprouting. **(C)** PCDH11X is an attractant and is surface displayed on sprouting GCL axons as well as on somata and dendrites both in GCL and IML. This model requires a second unknown modulator that competes for binding with PCDH11X and outcompetes homophilic *trans* interactions.

Slit1 in KA GCs (**Figure 1**). It is possible that (i) previously reported molecules did not change in GCs (but in other cell types), (ii) their expression changed in GCs but at other time points as in our study, (iii) they were induced by status epilepticus, (iv) they manifested themselves only at protein level (e.g., N-cadherin, NCAM), or (v) they were model specific. Thus, we focused on differentially expressed CAMs that were upregulated in our single GC data set, and shortlisted *Fat3*, *Pcdh11x*, and *Cntn4* for a CRISPR/Cas9-based *in vivo* screen. Sequence analysis revealed loss-of-function deletions in *Pcdh11x*, but not in *Fat3* or *Cntn4*, which were not considered further in this study.

With regard to *Pcdh11x*, we showed upregulation of *Pcdh11x* mRNA and enrichment of PCDH11X protein in *Pcdh11x* non-deficient control GCs during MF sprouting. Furthermore, using a CRISPR/Cas9-based strategy *in vivo*, we showed that while MF sprouting still developed in *Pcdh11x* KOs (*Pcdh11x*[KO+KA]), (i) GC dispersion was increased, (ii) sprouted synapses frequently formed on GC somata in addition to dendrites, and (iii) ∼50% more ZnT3 + puncta were detectable in GCL compared to *Pcdh11x* non-deficient controls (**Figures 1–4**, **7** and **Supplementary Figure 4**).

Pcdh11x was previously implicated in dendritic branching in developing neurons (Wu et al., 2015) and in the differentiation and proliferation of neural stem cells (Zhang et al., 2014). However, it is unlikely that these functions contributed to the phenotypes. First, dendritic branching was not different between *Pcdh11x*[Control+KA] and *Pcdh11x*[KO+KA] GCs (**Figure 6**), and second, although the adult dentate gyrus retains a neurogenic niche producing GCs, the use of *Calb1*[Cre/+] line and adeno associated virus (AAV) ensured that *Pcdh11x* mutations

occurred only in mature GCs but not in neural stem cells (Brandt et al., 2003).

Alternatively, *Pcdh11x* also has been implicated in homophilic *trans* cell-cell interactions (Harrison et al., 2020; Pancho et al., 2020). In a first potential hypothesis, PCDH11X is surface-expressed on sprouting GC axons (ZnT3 + MF boutons) as well as in both the IML and GCL, and homophilic *trans* PCDH11X interactions serve as a repellant or inhibit synapse targeting in both layers. This model is consistent with the phenotype we observed in the *Pcdh11x* KOs, where KA-induced sprouting occurs not only in the IML (as seen in controls) but in the GCL as well—presumably, according to this model, due to a release of PCDH11X-mediated inhibition of synapse targeting in the GCL. However, in order to achieve the IML-specific targeting seen in KA-treated wildtypes, this model requires that either (a) PCDH11X is exclusively expressed in GCL, which our immunostaining data shows not to be the case, or (b) a second unknown modulator selectively negates repellant PCDH11x signaling or releases inhibition of synapse targeting in the IML (**Figure 8A**).

A second, simpler model assumes that PCDH11X is a strong attractive signal and is surface displayed on sprouting GC axons as well as GC proximal dendrites in the IML; by virtue of specific expression in the IML (as opposed to the GCL), homophilic PCDH11X interactions drive selective synapse targeting to the IML during sprouting. In apparent contradiction to the model, we observed PCDH11X immunostaining in both the IML and GCL, including somatic and proximal dendritic compartments of GCs; however, the antibody we used targeted the intracellular domain of PCDH11X and could conceivably label intracellularly-retained molecules instead of

surface-displayed PCDH11X in the soma, therefore preserving the possibility of this second hypothesis. Assuming this model, we explain the targeting of sprouted MF synapses onto both GC somata and dendrites of $Pcdh11x^{KO+KA}$ as follows: in the absence of a strong attractive signal that condenses or concentrates synapse targeting to the IML, synapses will form indiscriminately, in both the GCL and IML (**Figure 8B**).

Finally, a third model posits that PCDH11X—similarly to the second model—is an attractive cue. However, unlike the second model, it assumes that PCDH11X is expressed in both the GCL and/or GC cell bodies as well as in the IML and/or GC proximal dendrites, since we cannot rule out the possibility that the antibody used in our immunostaining experiments does indeed label surface-displayed PCDH11X molecules at the soma. Instead, it invokes a modulatory or repellant signal specific to the GCL, such as an unidentified CAM that competes for binding with PCDH11X (e.g., via repellant, heterophilic interactions that outcompete homophilic *trans* interactions) (**Figure 8C**).

While not in our focus, the lack of an attractant, homophilic *trans* PCDH11X interaction may also explain the increased GCL dispersion seen in *Pcdh11x* KOs. Although both GC dispersion and MF sprouting were induced by KA, they are mechanistically independent. GC dispersion is due to impaired Reelin secretion by Cajal-Retzius cells (Haas et al., 2002; Heinrich et al., 2006; Duveau et al., 2011), whereas MF sprouting is a GC autonomous process (Luo et al., 2021). It is plausible that *trans* binding of PCDH11Xs displayed on neighboring neurons/dendrites after KA could serve as a structural break before further dispersion in controls, but not in KOs.

Together, our results revealed that PCDH11X controls synapse targeting during MF sprouting. With regard to implications for epilepsy, partial *Pcdh11x* duplication (as part of a broader Xq13-q21 duplication) was reported in one patient with recurrent seizures (Linhares et al., 2016). Based on the association of other protocadherins with epilepsy, such as *Pcdh19* (Dibbens et al., 2008; also see Hoshina et al., 2021) and *Pcdh7* (Lal et al., 2015), authors of the partial *Pcdh11x* duplication study hypothesized that the *Pcdh11x* mutation may be relevant for the seizures of this patient (Linhares et al., 2016). Our results provide additional insights showing altered connectivity in *Pcdh11x* KO. However, a more thorough testing of a link between *Pcdh11x* mutations and seizures, including conditions under which somatic synapses become activated in the brain, is beyond the scope of our study. Further, it is also clear that other CAMs may be involved in MF sprouting which our study did not cover. As such, the roles of SLIT1, FAT3, and CNTN4, if any, remain to be determined. More broadly, delineating which signals control target cell type selectivity (among GCs and different GABAergic interneuron types) as postsynaptic targets remain a major challenge. MF sprouting is a robust model to study these questions. Potentially, at least some of the mechanisms will be generalizable beyond MF sprouting, and applicable in other cell types in which to facilitate circuit repair in brain disorders and after injuries.

Data availability statement

The original contributions presented in this study are included in the article/**Supplementary material**, further inquiries can be directed to the corresponding author.

Ethics statement

The animal study was reviewed and approved by Veterinary Office of Zurich Kanton.

Author contributions

Funding

Acknowledgments

Conflict of interest

The authors declare that the research was conducted in the absence of any commercial or financial relationships that could be construed as a potential conflict of interest.

Publisher's note

All claims expressed in this article are solely those of the authors and do not necessarily represent those of their affiliated organizations, or those of the publisher, the editors and the reviewers. Any product that may be evaluated in this article, or claim that may be made by its manufacturer, is not guaranteed or endorsed by the publisher.

Supplementary material

The Supplementary Material for this article can be found online at: https://www.frontiersin.org/articles/10.3389/fnins.2022.888362/full#supplementary-material

References

Apóstolo, N., Smukowski, S. N., Vanderlinden, J., Condomitti, G., Rybakin, V., Ten Bos, J., et al. (2020). Synapse type-specific proteomic dissection identifies IgSF8 as a hippocampal CA3 microcircuit organizer. *Nat. Commun.* 11:5171. doi: 10.1038/s41467-020-18956-x

Bagri, A., Cheng, H. J., Yaron, A., Pleasure, S. J., and Tessier-Lavigne, M. (2003). Stereotyped pruning of long hippocampal axon branches triggered by retraction inducers of the semaphorin family. *Cell* 113, 285–299. doi: 10.1016/s0092-8674(03)00267-8

Baig, D. N., Yanagawa, T., and Tabuchi, K. (2017). Distortion of the normal function of synaptic cell adhesion molecules by genetic variants as a risk for autism spectrum disorders. *Brain Res. Bull.* 129, 82–90. doi: 10.1016/j.brainresbull.2016.10.006

Basu, R., Duan, X., Taylor, M. R., Martin, E. A., Muralidhar, S., Wang, Y., et al. (2017). Heterophilic Type II Cadherins Are Required for High-Magnitude Synaptic Potentiation in the Hippocampus. *Neuron* 96, 160–176.e8. doi: 10.1016/j.neuron.2017.09.009

Ben-Ari, Y., and Cossart, R. (2000). Kainate, a double agent that generates seizures: Two decades of progress. *Trends Neurosci.* 23, 580–587. doi: 10.1016/s0166-2236(00)01659-3

Brandt, M. D., Jessberger, S., Steiner, B., Kronenberg, G., Reuter, K., Bick-Sander, A., et al. (2003). Transient calretinin expression defines early postmitotic step of neuronal differentiation in adult hippocampal neurogenesis of mice. *Mol. Cell Neurosci.* 24, 603–613. doi: 10.1016/s1044-7431(03)00207-0

Buckmaster, P. S. (2014). Does mossy fiber sprouting give rise to the epileptic state? *Adv. Exp. Med. Biol.* 813, 161–168. doi: 10.1007/978-94-017-8914-1_13

Carrasquillo, M. M., Zou, F., Pankratz, V. S., Wilcox, S. L., Ma, L., Walker, L. P., et al. (2009). Genetic variation in PCDH11X is associated with susceptibility to late-onset Alzheimer's disease. *Nat. Genet.* 41, 192–198. doi: 10.1038/ng.305

Cavazos, J. E., Zhang, P., Qazi, R., and Sutula, T. P. (2003). Ultrastructural features of sprouted mossy fiber synapses in kindled and kainic acid-treated rats. *J. Comp. Neurol.* 458, 272–292. doi: 10.1002/cne.10581

Chen, H., Bagri, A., Zupicich, J. A., Zou, Y., Stoeckli, E., Pleasure, S. J., et al. (2000). Neuropilin-2 regulates the development of selective cranial and sensory nerves and hippocampal mossy fiber projections. *Neuron* 25, 43–56. doi: 10.1016/s0896-6273(00)80870-3

Condomitti, G., Wierda, K. D., Schroeder, A., Rubio, S. E., Vennekens, K. M., Orlandi, C., et al. (2018). An Input-Specific Orphan Receptor GPR158-HSPG Interaction Organizes Hippocampal Mossy Fiber-CA3 Synapses. *Neuron* 100, 201–215.e9. doi: 10.1016/j.neuron.2018.08.038

Cremer, H., Chazal, G., Carleton, A., Goridis, C., Vincent, J. D., and Lledo, P. M. (1998). Long-term but not short-term plasticity at mossy fiber synapses is impaired in neural cell adhesion molecule-deficient mice. *Proc. Natl. Acad. Sci. U. S. A.* 95, 13242–13247. doi: 10.1073/pnas.95.22.13242

de Wit, J., and Ghosh, A. (2016). Specification of synaptic connectivity by cell surface interactions. *Nat. Rev. Neurosci.* 17, 22–35. doi: 10.1038/nrn.2015.3

Deans, M. R., Krol, A., Abraira, V. E., Copley, C. O., Tucker, A. F., and Goodrich, L. V. (2011). Control of neuronal morphology by the atypical cadherin Fat3. *Neuron* 71, 820–832. doi: 10.1016/j.neuron.2011.06.026

Dibbens, L. M., Tarpey, P. S., Hynes, K., Bayly, M. A., Scheffer, I. E., Smith, R., et al. (2008). X-linked protocadherin 19 mutations cause female-limited epilepsy and cognitive impairment. *Nat. Genet.* 40, 776–781. doi: 10.1038/ng.149

Duveau, V., Madhusudan, A., Caleo, M., Knuesel, I., and Fritschy, J. M. (2011). Impaired reelin processing and secretion by Cajal-Retzius cells contributes to granule cell dispersion in a mouse model of temporal lobe epilepsy. *Hippocampus* 21, 935–944. doi: 10.1002/hipo.20793

Földy, C., Darmanis, S., Aoto, J., Malenka, R. C., Quake, S. R., and Südhof, T. C. (2016). Single-cell RNAseq reveals cell adhesion molecule profiles in electrophysiologically defined neurons. *Proc. Natl. Acad. Sci. U. S. A.* 113, E5222–E5231. doi: 10.1073/pnas.1610155113

Frotscher, M., Jonas, P., and Sloviter, R. S. (2006). Synapses formed by normal and abnormal hippocampal mossy fibers. *Cell Tissue Res.* 326, 361–367.

Godale, C. M., and Danzer, S. C. (2018). Signaling pathways and cellular mechanisms regulating mossy fiber sprouting in the development of epilepsy. *Front. Neurol.* 9:298. doi: 10.3389/fneur.2018.00298

Haas, C. A., Dudeck, O., Kirsch, M., Huszka, C., Kann, G., Pollak, S., et al. (2002). Role for reelin in the development of granule cell dispersion in temporal lobe epilepsy. *J. Neurosci.* 22, 5797–5802. doi: 10.1523/JNEUROSCI.22-14-05797.2002

Hainmueller, T., and Bartos, M. (2020). Dentate gyrus circuits for encoding, retrieval and discrimination of episodic memories. *Nat. Rev. Neurosci.* 21, 153–168. doi: 10.1038/s41583-019-0260-z

Hansen, K. F., Sakamoto, K., Pelz, C., Impey, S., and Obrietan, K. (2014). Profiling status epilepticus-induced changes in hippocampal RNA expression using high-throughput RNA sequencing. *Sci. Rep.* 4:6930. doi: 10.1038/srep06930

Harrison, O. J., Brasch, J., Katsamba, P. S., Ahlsen, G., Noble, A. J., Dan, H., et al. (2020). Family-wide Structural and Biophysical Analysis of Binding Interactions among Non-clustered δ-Protocadherins. *Cell Rep.* 30, 2655–2671.e7. doi: 10.1016/j.celrep.2020.02.003

Heinrich, C., Nitta, N., Flubacher, A., Müller, M., Fahrner, A., Kirsch, M., et al. (2006). Reelin deficiency and displacement of mature neurons, but not neurogenesis, underlie the formation of granule cell dispersion in the epileptic hippocampus. *J. Neurosci.* 26, 4701–4713. doi: 10.1523/JNEUROSCI.5516-05.2006

Holtmaat, A. J., Gorter, J. A., de Wit, J., Tolner, E. A., Spijker, S., Giger, R. J., et al. (2003). Transient downregulation of Sema3A mRNA in a rat model for temporal lobe epilepsy. A novel molecular event potentially contributing to mossy fiber sprouting. *Exp. Neurol.* 182, 142–150. doi: 10.1016/s0014-4886(03)00035-9

Hoshina, N., Johnson-Venkatesh, E. M., Hoshina, M., and Umemori, H. (2021). Female-specific synaptic dysfunction and cognitive impairment in a mouse model of PCDH19 disorder. *Science* 372:eaaz3893. doi: 10.1126/science.aaz3893

Koyama, R., and Ikegaya, Y. (2018). The Molecular and cellular mechanisms of axon guidance in mossy fiber sprouting. *Front. Neurol.* 9:382. doi: 10.3389/fneur.2018.00382

Krol, A., Henle, S. J., and Goodrich, L. V. (2016). Fat3 and Ena/VASP proteins influence the emergence of asymmetric cell morphology in the developing retina. *Development* 143, 2172–2182. doi: 10.1242/dev.133678

Lal, D., Ruppert, A. K., Trucks, H., Schulz, H., de Kovel, C. G., Kasteleijn-Nolst Trenité, D., et al. (2015). Burden analysis of rare microdeletions suggests a strong

impact of neurodevelopmental genes in genetic generalised epilepsies. *PLoS Genet.* 11:e1005226. doi: 10.1371/journal.pgen.1005226

Laurberg, S., and Zimmer, J. (1981). Lesion-induced sprouting of hippocampal mossy fiber collaterals to the fascia dentata in developing and adult rats. *J. Comp. Neurol.* 200, 433–459. doi: 10.1002/cne.902000310

Linhares, N. D., Valadares, E. R., da Costa, S. S., Arantes, R. R., de Oliveira, L. R., Rosenberg, C., et al. (2016). Inherited Xq13.2-q21.31 duplication in a boy with recurrent seizures and pubertal gynecomastia: Clinical, chromosomal and aCGH characterization. *Meta Gene* 9, 185–190. doi: 10.1016/j.mgene.2016.07.004

Liu, X. D., Zhu, X. N., Halford, M. M., Xu, T. L., Henkemeyer, M., and Xu, N. J. (2018). Retrograde regulation of mossy fiber axon targeting and terminal maturation via postsynaptic Lnx1. *J. Cell Biol.* 217, 4007–4024. doi: 10.1083/jcb.201803105

Luo, W., Egger, M., Domonkos, A., Que, L., Lukacsovich, D., Cruz-Ochoa, N. A., et al. (2021). Recurrent rewiring of the adult hippocampal mossy fiber system by a single transcriptional regulator. Id2. *Proc. Natl. Acad. Sci. U. S. A.* 118:e2108239118. doi: 10.1073/pnas.2108239118

Martin, E. A., Muralidhar, S., Wang, Z., Cervantes, D. C., Basu, R., Taylor, M. R., et al. (2015). The intellectual disability gene Kirrel3 regulates target-specific mossy fiber synapse development in the hippocampus. *Elife* 4:e09395. doi: 10.7554/eLife.09395

Matsuda, K., Budisantoso, T., Mitakidis, N., Sugaya, Y., Miura, E., Kakegawa, W., et al. (2016). Transsynaptic Modulation of Kainate Receptor Functions by C1q-like Proteins. *Neuron* 90, 752–767. doi: 10.1016/j.neuron.2016.04.001

Missaire, M., and Hindges, R. (2015). The role of cell adhesion molecules in visual circuit formation: From neurite outgrowth to maps and synaptic specificity. *Dev. Neurobiol.* 75, 569–583. doi: 10.1002/dneu.22267

Muramatsu, R., Nakahara, S., Ichikawa, J., Watanabe, K., Matsuki, N., and Koyama, R. (2010). The ratio of 'deleted in colorectal cancer' to 'uncoordinated-5A' netrin-1 receptors on the growth cone regulates mossy fibre directionality. *Brain* 133, 60–75. doi: 10.1093/brain/awp266

Niquet, J., Jorquera, I., Ben-Ari, Y., and Represa, A. (1993). NCAM immunoreactivity on mossy fibers and reactive astrocytes in the hippocampus of epileptic rats. *Brain Res.* 626, 106–116. doi: 10.1016/0006-8993(93)90569-9

Noebels, J. L., Avoli, M., Rogawski, M. A., Olsen, R. W., and Delgado-Escueta, A. V. (eds) (2012). *Jasper's Basic Mechanisms of the Epilepsies*, (4th Edn). Bethesda, MD: National Center for Biotechnology Information.

Oguro-Ando, A., Bamford, R. A., Sital, W., Sprengers, J. J., Zuko, A., Matser, J. M., et al. (2021). Cntn4, a risk gene for neuropsychiatric disorders, modulates hippocampal synaptic plasticity and behavior. *Transl. Psychiatry* 11:106. doi: 10.1038/s41398-021-01223-y

Oguro-Ando, A., Zuko, A., Kleijer, K. T. E., and Burbach, J. P. H. (2017). A current view on contactin-4, -5, and -6: Implications in neurodevelopmental disorders. *Mol. Cell Neurosci.* 81, 72–83. doi: 10.1016/j.mcn.2016.12.004

Osterhout, J. A., Stafford, B. K., Nguyen, P. L., Yoshihara, Y., and Huberman, A. D. (2015). Contactin-4 mediates axon-target specificity and functional development of the accessory optic system. *Neuron* 86, 985–999. doi: 10.1016/j.neuron.2015.04.005

Pancho, A., Aerts, T., Mitsogiannis, M. D., and Seuntjens, E. (2020). Protocadherins at the Crossroad of Signaling Pathways. *Front. Mol. Neurosci.* 13:117. doi: 10.3389/fnmol.2020.00117

Sanes, J. R., and Zipursky, S. L. (2020). Synaptic specificity, recognition molecules, and assembly of neural circuits. *Cell* 181, 536–556. doi: 10.1016/j.cell.2020.04.008

Seng, C., Luo, W., and Földy, C. (2022). Circuit formation in the adult brain. *Eur. J. Neurosci.* 56, 4187–4213. doi: 10.1111/ejn.15742

Shan, W., Yoshida, M., Wu, X. R., Huntley, G. W., and Colman, D. R. (2002). Neural (N-) cadherin, a synaptic adhesion molecule, is induced in hippocampal mossy fiber axonal sprouts by seizure. *J. Neurosci. Res.* 69, 292–304. doi: 10.1002/jnr.10305

Südhof, T. C. (2021). The cell biology of synapse formation. *J. Cell Biol.* 220:e202103052. doi: 10.1083/jcb.202103052

Suto, F., Tsuboi, M., Kamiya, H., Mizuno, H., Kiyama, Y., Komai, S., et al. (2007). Interactions between plexin-A2, plexin-A4, and semaphorin 6A control lamina-restricted projection of hippocampal mossy fibers. *Neuron* 53, 535–547. doi: 10.1016/j.neuron.2007.01.028

Sutula, T., He, X. X., Cavazos, J., and Scott, G. (1988). Synaptic reorganization in the hippocampus induced by abnormal functional activity. *Science* 239, 1147–1150. doi: 10.1126/science.2449733

Tanaka, T., Tanaka, S., Fujita, T., Takano, K., Fukuda, H., Sako, K., et al. (1992). Experimental complex partial seizures induced by a microinjection of kainic acid into limbic structures. *Prog. Neurobiol.* 38, 317–334. doi: 10.1016/0301-0082(92)90023-8

Tauck, D. L., and Nadler, J. V. (1985). Evidence of functional mossy fiber sprouting in hippocampal formation of kainic acid-treated rats. *J. Neurosci.* 5, 1016–1022. doi: 10.1523/JNEUROSCI.05-04-01016.1985

Tawarayama, H., Yoshida, Y., Suto, F., Mitchell, K. J., and Fujisawa, H. (2010). Roles of semaphorin-6B and plexin-A2 in lamina-restricted projection of hippocampal mossy fibers. *J. Neurosci.* 30, 7049–7060. doi: 10.1523/JNEUROSCI.0073-10.2010

Wenzel, H. J., Woolley, C. S., Robbins, C. A., and Schwartzkroin, P. A. (2000). Kainic acid-induced mossy fiber sprouting and synapse formation in the dentate gyrus of rats. *Hippocampus* 10, 244–260. doi: 10.1002/1098-1063(2000)10:3<244::AID-HIPO5>3.0.CO;2-7

Williams, M. E., Wilke, S. A., Daggett, A., Davis, E., Otto, S., Ravi, D., et al. (2011). Cadherin-9 regulates synapse-specific differentiation in the developing hippocampus. *Neuron* 71, 640–655. doi: 10.1016/j.neuron.2011.06.019

Wu, C., Niu, L., Yan, Z., Wang, C., Liu, N., Dai, Y., et al. (2015). Pcdh11x Negatively Regulates Dendritic Branching. *J. Mol. Neurosci.* 56, 822–828. doi: 10.1007/s12031-015-0515-8

Xu, N. J., and Henkemeyer, M. (2009). Ephrin-B3 reverse signaling through Grb4 and cytoskeletal regulators mediates axon pruning. *Nat. Neurosci.* 12, 268–276. doi: 10.1038/nn.2254

Zhang, P., Wu, C., Liu, N., Niu, L., Yan, Z., Feng, Y., et al. (2014). Protocadherin 11 x regulates differentiation and proliferation of neural stem cell in vitro and in vivo. *J. Mol. Neurosci.* 54, 199–210. doi: 10.1007/s12031-014-0275-x

Zimmer, J., and Gähwiler, B. H. (1987). Growth of hippocampal mossy fibers: A lesion and coculture study of organotypic slice cultures. *J. Comp. Neurol.* 264, 1–13. doi: 10.1002/cne.902640102

Discussion

In this study, we investigated the role of CAMs in the target specificity of mossy fiber sprouting. The key hypothesis is that CAMs are important for determining the regional, cellular, and subcellar specification of synapses. As described in our paper (Luo *et al.*, 2022), we employed a CRISPR-Cas9-based screen in the adult brain *in vivo*, in which we were able to confirm deleterious genetic mutations only in one of the candidate genes, *Pcdh11x*. In addition to the Discussion presented in our paper, here I discuss further, conceptually relevant points.

Importantly, our results revealed that *Pcdh11x* is important for the subcellular, as opposed to regional or cellular, targeting of mossy fiber sprouting. We found that sprouting granule cells lacking functional *Pcdh11x* establish synapses on both on the soma and proximal dendrites of other granule cells, instead of only on dendrites as typically seen in mossy fiber sprouting. In this manner, our study clarified one of the multiple features of mossy fiber target specification, suggesting the involvement of other CAMs. While the question remains, which CAMs control the regional and cellular targeting of mossy fiber sprouting, our results clearly indicate that different CAMs may combinatorically contribute to wiring in the adult brain, similarly to developmental wiring.

It is clear that technological improvements and/or emerging technologies will be required to uncover a broader set of CAMs in adult wiring. First, our study demonstrates the potential of CRISPR-Cas9-based screens to identify CAMs involved in adult wiring. However, our study also revealed a limitation of this approach. The *in vivo* gene editing was inefficient for several genes (targeting of only 1 out of 3 target genes, that is *Pcdh11x*, was successful) despite the same gRNAs displayed high editing efficacy *in vitro* (3 out of 3 genes; i.e. *Pcdh11x*, *Cntn4*, *Fat3*). The reason for this discrepancy is currently unknown. It is possible that the efficiency of the gene editing may depend on the characteristic chromatin state and nucleosomes of the cell type (Horlbeck *et al.*, 2016; Isaac *et al.*, 2016; Verkuijl & Rots, 2019), in this case that of granule cells. It is feasible that our intended editing sites in *Cntn4* and *Fat3* were inaccessible before the induction of wiring, i.e. at the time when we employed gene editing, or in controls. Given the rapid onset of these gene's expression during wiring, these editing sites most likely became accessible after induction. However, this scenario leaves only a very narrow timeframe for effective gene manipulations before the onset of wiring. How quickly deleterious mutations could be inferred in the genome (while the not yet manipulated

genes start to express the endogenous isoforms) to influence wiring is both unpredictable and difficult to control. In any case, I envision this limitation to overcome by technological advances in gene editing, such as the use of modified versions designed to increase editing specificity while preserving effectiveness or avoid the need of protospacer adjacent motifs near the target location (Tycko *et al.*, 2017; Uddin *et al.*, 2020). The use of short-hairpin RNAs (shRNAs) would represent an alternative approach (Rao *et al.*, 2009; Huang & Zeng, 2010). The shRNA technology is based on targeting the already transcribed mRNA, whose translation is to be prevented by the binding of matching shRNAs. An advantage of this approach is that the mRNA of virtually any gene could be reasonable targeted. A disadvantage, however, is the potentially broad off target effects, which are also harder to control than that of gRNAs. To alleviate potential off target effects, multiple rounds (even up to 5-10) of shRNA designs may be used to target a single gene in independent experiments. If the results of these manipulations are similar, then the influence of potential off target effects becomes less likely.

Finally, it will be clearly important to gain insights into wiring mechanisms at the proteomic level. I envision that the use of multiplexed or iterative immunofluorescence staining will likely make significant impact in this regard. Using iterative immunostaining, it is possible to gain insights into the localization and/or abundance of potentially dozens of proteins in the same samples (Gut *et al.*, 2018; Cole *et al.*, 2022). Using this approach, future experiments could include the simultaneous monitoring broad sets of CAMs during adult wiring, from which to systematically deduce their combinatorial or complementary role in the target specific of adult wiring.

In the next chapter, I will present another study which provided us with further insights into the target specificity of mossy fiber sprouting. However, as the Reader of this thesis will notice, this discovery was facilitated by fair amount of serendipity in addition to my diligent efforts.

Chapter 4 – Commissural mossy fiber sprouting

Introduction

The previous two Chapters (Luo *et al.*, 2021, 2022) were motivated by the hypothesis that generation of the epilepsy-associated mossy fiber requires the activation and/or inactivation of a specific set of transcription factors/regulators and CAMs. These studies highlighted the power of single-cell transcriptomics in understanding the molecular bases of adult wiring and the potentials of harnessing such mechanisms for circuit therapy and repair. To briefly recapitulate, in Chapter 2, I described the role of a single transcription regulator, *Id2*, in inducing the canonical steps of circuit formation (i.e. axon growth, target specification, and synapse formation) in the adult brain, and recapitulating mossy fiber sprouting (Luo *et al.*, 2021). Then, in Chapter 3, I described a study on investigating the role of CAMs specifically in the target specification of mossy fiber sprouting (Luo *et al.*, 2022).

Importantly, as already mentioned in the Introduction, the epilepsy-associated mossy fiber sprouting has been described as a so-called local form of sprouting, meaning that growing axons remain and form new connections within each dentate gyrus. In addition to mossy fiber sprouting, local sprouting or further wiring has been observed in other adult brain regions and experimental models (Seng *et al.*, 2022). In contrast to local wiring, however, multiple studies also demonstrated long-range wiring phenotypes in the adult brain (Seng *et al.*, 2022). During long-range wiring, new axons leave the brain region where the cell body is located and extend into other areas, which can be even centimeters away.

In this final Chapter, I will describe the discovery of a previously unnoticed form of mossy fiber sprouting, whereby in addition to local sprouting, adult granule cells grow new axons into the contralateral hippocampus located in the other brain hemisphere. In addition to the extensive characterization of this wiring phenotype in the intrahippocampal kainic acid microinjection model of experimental epilepsy (the same model we used in the above studies), my results revealed that contralateral hippocampus-projecting granule cells (or "commissural granule cells" as I will hereafter refer to these neurons) exist in the unperturbed or healthy adult brain.

In this manner, my results do not only reveal a new inter-hemispheric form of adult, but also include the description of a new neuronal cell type. Similarly to our

previous studies, we employed a multimodal approach involving electrophysiology, neuroanatomy, single-cell transcriptomics, and circuit tracing to examine the wiring of this unique cell type.

I contributed to this project with experimental design, performing most of the experiments and analyses, and data interpretation.

Commissural dentate granule cell projections and their rapid formation in the adult brain

Matteo Egger[a,b,1], Wenshu Luo[a,1], Natalia Cruz-Ochoa[a,b], David Lukacsovich[a], Csaba Varga[a], Lin Que[a], Gyula Maloveczky[a], Jochen Winterer[a], Rashmit Kaur[a], Tamás Lukacsovich[a] and Csaba Földy[a,b,*]

[a]Laboratory of Neural Connectivity, Brain Research Institute, Faculties of Medicine and Science, University of Zürich, Zürich 8057, Switzerland
[b]Adaptive Brain Circuits in Development and Learning (AdaBD), University Research Priority Program (URPP), University of Zürich, Zürich 8057, Switzerland
*To whom correspondence should be addressed: Email: foldy@hifo.uzh.ch
[1]M.E. and W.L. contributed equally to this study.
Edited By: Eric Klann

Abstract

Dentate granule cells (GCs) have been characterized as unilaterally projecting neurons within each hippocampus. Here, we describe a unique class, the commissural GCs, which atypically project to the contralateral hippocampus in mice. Although commissural GCs are rare in the healthy brain, their number and contralateral axon density rapidly increase in a rodent model of temporal lobe epilepsies. In this model, commissural GC axon growth appears together with the well-studied hippocampal mossy fiber sprouting and may be important for the pathomechanisms of epilepsy. Our results augment the current view on hippocampal GC diversity and demonstrate powerful activation of a commissural wiring program in the adult brain.

Keywords: hippocampal granule cell, contralateral projection, commissural axon, sprouting, circuit formation, adult brain

---

Significance Statement

Neuronal connections between the two hippocampi are composed mainly of axons of mossy cells and CA3 pyramidal cells and to lesser degree axons of CA1 pyramidal cells and different interneurons. Here, we show that dentate granule cells also project to the contralateral hippocampus and that the density of commissural granule cell axons rapidly increases in a rodent model of temporal lobe epilepsy. Our results reveal a striking capacity for commissural axon growth in the adult brain and open up multiple questions for future research regarding possible mechanisms of adult-brain circuit formation and epilepsy.

Introduction

In contrast to during brain development, circuit formation in the adult brain is generally thought to be absent. However, research on neurological disorders, adult-born, grafted, and reprogrammed neurons, and innate behaviors has shown that the adult brain retains a considerable capacity for axon growth and circuit formation (1). Understanding the underlying mechanisms or identifying new forms of circuit formation in adults would facilitate insights into the organization of brain circuits in health and diseases.

The hippocampal dentate gyrus is one brain region where circuit formation in adults can be routinely observed, either as circuit integration of adult-born immature granule cells (GCs) (2) or epilepsy-associated local mossy fiber sprouting by mature GCs (3). The circuit formed by adult-born GCs is virtually identical to that formed by GCs during development: GCs project their axons, the mossy fibers, through the hilus to ipsilateral CA3 area, and form synapses on different glutamatergic and GABAergic cell types. By contrast, during mossy fiber sprouting, new GC axons mostly grow into the molecular layer of dentate gyrus and create a local feedback circuit. Thus, target specification is different between adult-born and sprouting adult mossy fibers. Adult-born GCs likely utilize similar cues to those during development, whereas target specification during sprouting remains comparably less understood (4).

In this study, we followed up on an observation we made while studying mossy fibers in the intrahippocampal kainic acid (KA) injection model of temporal lobe epilepsy (4, 5). Specifically, signatures of sprouting became apparent in the associational/commissural pathway. Such a locale would be unexpected for sprouted (as well as for developmentally established and adult-born) GC axons and represent a previously undisclosed axon targeting. Meanwhile, it remained possible that these axons originated from cell types other than GCs. Using the Rbp4-Cre transgenic mouse line with a genetic access restricted to GCs in the hippocampus, we tested the hypothesis that sprouting axons in

the associational/commissural pathway originated from GCs. We show that some GCs atypically project to the contralateral hippocampus in the healthy mouse brain and that the number of such commissural GCs as well as their contralateral axon density rapidly increases in a rodent model of temporal lobe epilepsy.

Results

Commissural GC projections in saline- and KA-injected mouse brain

To study control and sprouting mossy fibers, we performed unilateral intrahippocampal saline and KA (known to induce mossy fiber sprouting within 1–2 weeks) microinjections, respectively, in mice. Hereafter, we refer to these specific procedures as saline or KA, for short (note that although bilateral hippocampal or intraperitoneal KA injections can be also used to induce mossy fiber sprouting, as shown by many studies, the term KA should be unambiguous in this current study). To enable GC-specific labeling, we used the Rbp4-Cre transgenic mouse line. In published reports, this line appeared to selectively express Cre in the dentate gyrus, as opposed to other hippocampal areas (6, Fig.2; 7, Fig.S7E). To verify this, we crossed Rbp4-Cre with the Ai14 reporter line and saw that Cre expression was highly specific to GCs, with ∼30% of GCs expressing Cre (Fig. S1). To begin, we coinjected AAV.cDIO-EGFP (EGFP is to be expressed in GCs in a Cre-dependent manner) and KA (70 nl, 5 mM) or saline (equal volume to KA; used as control) into the left ventral dentate gyrus (ipsilateral side). Two weeks later, we prepared 50-μm-thick whole-brain serial sections and looked for EGFP+ axons in the ipsilateral (left) and contralateral (right) hemispheres.

We made two observations. First, we found EGFP+ axons entering the ipsilateral associational/commissural pathway and appearing on the contralateral side after both saline and KA (Fig. 1A). In the contralateral side, the axons appeared to terminate in the hippocampal CA1-CA3 and subiculum areas (Fig. 1B). These findings were unexpected because contralateral GC projections have not been described before in naïve or epileptic brain. Second, we found visibly more EGFP+ commissural axons after KA. To quantify this, we reconstructed all EGFP+ axons on the contralateral side starting from the midline, which revealed significantly more EGFP+ axons after KA (total axon length, saline: 2.74 ± 0.45 cm, $n = 5$ mice; KA: 11.78 ± 2.36 cm, $n = 5$ mice; data represent mean $\pm$ SEM; $P = 0.007$, Mann–Whitney test) (Fig. 1C). The increased axon length after KA suggested robust growth of new commissural GC fibers within 2 weeks after injection. To further investigate this phenotype, we also considered an alternative scenario whereby a potentially increased EGFP transfection efficacy after KA (e.g. due to cellular changes) labeled more GCs, including already existing commissural GCs. For this, we calculated the ratio of EGFP+ versus DAPI+ labeled cells in the transfected area of the ipsilateral GC layer after saline and KA; however, rather than increased, EGFP transfection efficacy was decreased after KA (EGFP+/DAPI+ cells, saline: $34 \pm 0.48\%$, $n = 5$ mice and KA: $20 \pm 2.3\%$, $n = 5$ mice), suggesting that the increased contralateral axon length after KA appeared despite less ipsilateral neurons was labeled.

Retrograde labeling identifies commissural GCs

Next, we aimed to identify GCs that project to the contralateral side. The previous experiment did not allow separate visualization of such cells, because the somato-dendritic domain of all Cre-expressing GCs was EGFP labeled independent of their axonal

targeting (see ipsilateral side in Fig. 1A). Thus, to specifically label contralaterally projecting cells, we injected retroAAV.EGFP into the right (contralateral) ventral hippocampus and saline or KA together with AAV.cDIO-mCherry (mCherry is to be expressed in GCs in a Cre-dependent manner to visualize the injection site) into the left (ipsilateral) hippocampus with symmetrical injection coordinates (Fig. 2A).

Two weeks later, we prepared serial sections from the left (ipsilateral) hippocampus and looked for retrogradely labeled EGFP+ cells. A caveat of this approach is that other contralaterally projecting neurons, such as mossy and CA3 pyramidal cells, were also retrogradely labeled; nonetheless, we could alleviate this issue by restricting our analysis into the GC layer. Again, we made two observations. First, we found EGFP+ cells after both saline and KA (Fig. 2B), whose localization and dendritic morphology resembled typical GCs (Fig. 2C and D). Second, consistent with the increased length of commissural projections after KA, we detected significantly more retrogradely labeled GC cells after KA (120.8 ± 26.2 cells, $n = 9$ mice), approximately five to six times more, than after saline (22.1 ± 6.1 cells, $n = 8$ mice) ($P = 0.0001$, Mann–Whitney test) (Fig. 2E). As expected from a KA-induced effect, most EGFP+ GCs appeared around the injection site (Fig. 2F). However, unexpectedly, a similar pattern was apparent after saline injection as well, raising the possibility that the injection procedure itself contributed to the detection of commissural GCs. Thus, as a control experiment, we injected retroAAV.EGFP contralaterally without any ipsilateral injection in wild-type mice, in which EGFP+ GCs were still visible in similar number and distribution as after ipsilateral saline injection (Fig. S2). Note that meanwhile these experiments identified commissural GCs projecting from the left to the right hippocampus, commissural GCs projecting from the right to the left hippocampus were also detectable in similar number and distribution (Fig. S3).

Together, these results provided support for the notion that some GCs atypically project to the contralateral hippocampus in naïve mice and established that the number of such commissural GCs significantly increases after KA. In addition, the distribution of commissural GCs in ipsilateral saline- and noninjected mice suggested that the contralateral axons of commissural GCs are organized in a laminar fashion; i.e. they projected to the same septo-temporal level where their somata were located.

Finally, in addition to the KA model, we looked for retrogradely labeled GCs in the Id2 overexpression (OE) model of local (ipsilateral) mossy fiber sprouting (5). If in addition to local GC sprouting Id2 OE induced commissural GC growth, then the number of retrogradely labeled GCs should increase, similar to the KA model; however, the number of retrogradely labeled GCs did not increase in the Id2 OE model (3.2 ± 2.6 cells, $n = 4$ mice) compared to saline-injected controls (12.5 ± 0.5 cells, $n = 2$ mice), suggesting that Id2 OE alone does not have the capacity to induce commissural GC axon growth.

Anterograde labeling identifies contralateral targets of commissural GCs

To identify neurons targeted by commissural GCs, we used a two-component *trans*-synaptic labeling approach. The first component, AAV.cDIO-WGA_Flpe, was injected into the left (ipsilateral) dentate gyrus (WGA_Flpe is to be expressed in GCs in a Cre-dependent manner and transported to target cells *trans*-synaptically). The second component, AAV.fDIO-mRuby, was injected into the right (contralateral) hippocampus (mRuby is to be expressed in a WGA_Flpe-dependent manner). In theory, only
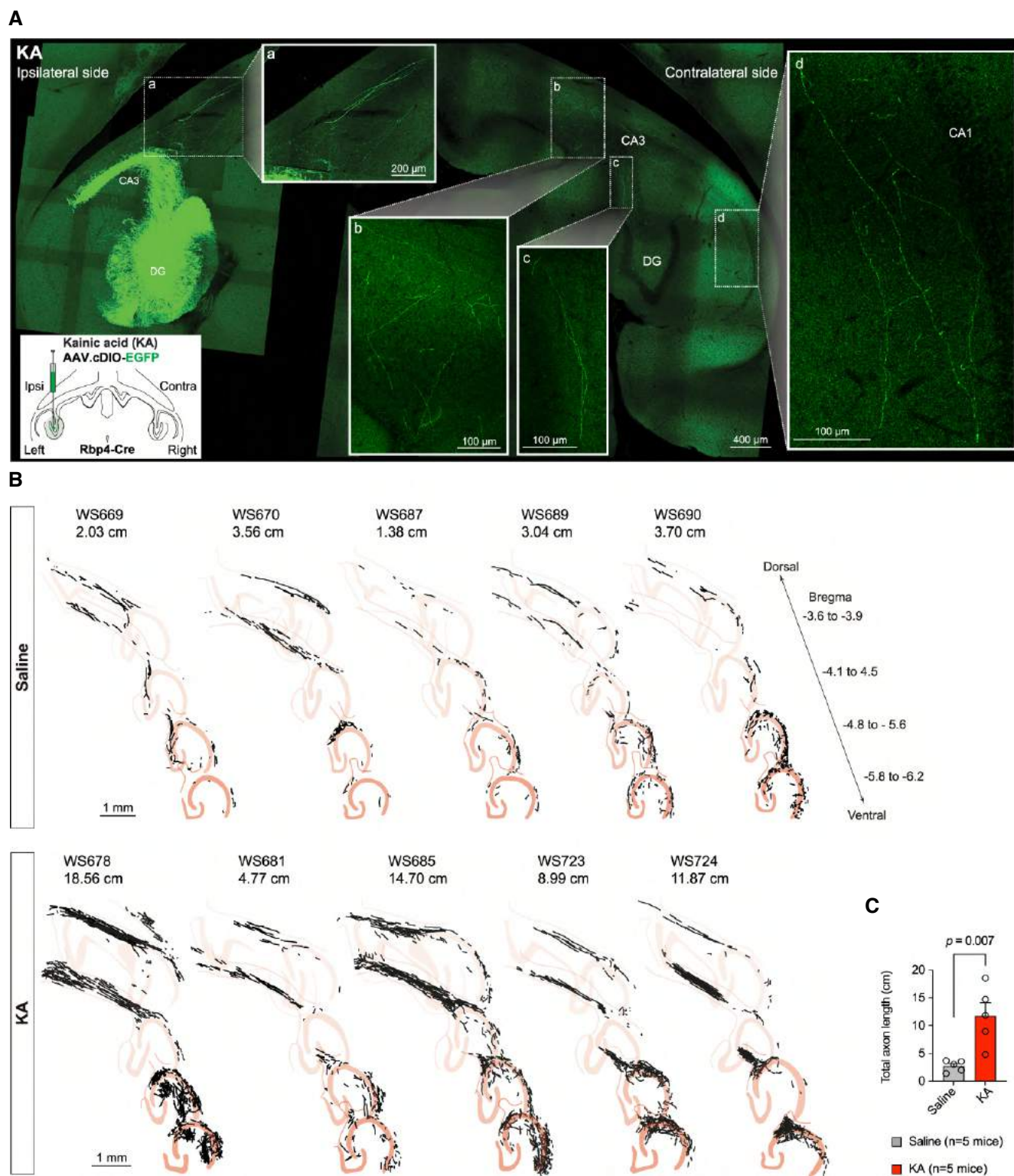
Fig. 1. Commissural GC projections in the contralateral hippocampus. A) Tiled confocal image shows EGFP+ GCs at the ipsilateral injection site (left hippocampus), as well as EGFP+ axons entering the commissural/associational pathway (a), before entering the contralateral hippocampus (b), and in the contralateral hippocampal CA3 (c) and CA1 (d) areas. The bottom left inset shows the experimental design (also see main text). DG, dentate gyrus. B) Reconstruction of contralateral EGFP+ axons from saline- and KA-injected mice. Each image shows axons reconstructed from 20 to 26 consecutive, 50-μm-thick sections from one animal, labeled with sample ID and total axon length. C) Quantification of total contralateral EGFP+ axon length. Each data point represents the total axon length traced from one animal, as in B). Data represent mean ± SEM (Mann–Whitney test).

those cells should express mRuby in the right hippocampus, which received WGA_Flpe from commissural GCs in the left hippocampus. As a limitation of this approach, multicomponent

expression systems may display unwanted transcription in the first, second, or both components, resulting in false-positive labeling. To mitigate this issue, we first tested our system in wild-type
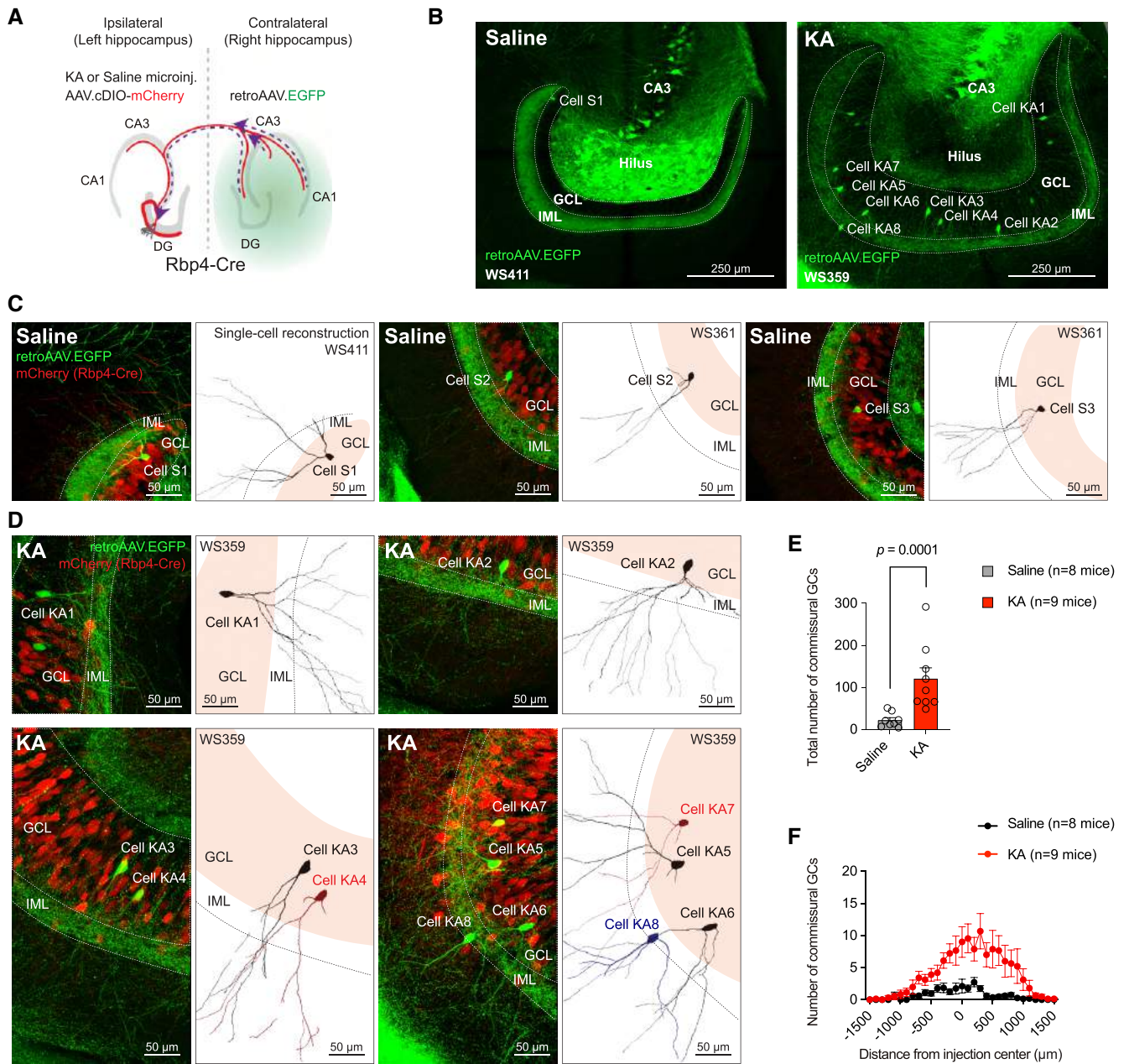
Fig. 2. Retrograde labeling identifies commissural GCs. A) Experimental design (also see main text). B) Confocal images show retrogradely labeled, EGFP+ cells in GC layer (GCL) in the left hippocampus after ipsilateral saline or KA injection. Note the (i) presence of retrogradely labeled mossy cells (which also project to the contralateral hippocampus) and their axons in the inner molecular layer after saline injection and (ii) lack of mossy cells and axons and GCL dispersion (these are known effects of KA) after KA injection; retrogradely labeled CA3 pyramidal cells (which also project to the contralateral hippocampus) are visible in both images. C and D) Confocal image and morphological reconstruction of retrogradely labeled commissural GCs after saline (cell S1 is also shown in B, left) and KA injection (cell KA1–8 are also shown in B, right), respectively. E) Plot shows the number of retrogradely labeled commissural GCs in the ipsilateral (with respect to saline or KA injection) left hippocampus. Each data point represents the total number of commissural GCs detected in one animal. Data represent mean ± SEM (Mann–Whitney test). F) Plot shows the septo-temporal distribution of retrogradely labeled commissural GCs after ipsilateral saline and KA injection. For averaging, individual distributions were aligned to the ipsilateral (saline and KA) injection sites.

animals, lacking Cre. In the contralateral dentate, CA3-CA2, and CA1-subiculum areas, we found an average of 92 ± 6.2, 55 ± 2.9, and 58 ± 2.5 mRuby+ cells, respectively, in 50-μm-thick sections ($n = 5$ mice), which we then considered as baselines (Fig. S4).

Next, we performed the same experiment but now in Rbp4-Cre mice and together with ipsilateral saline or KA injection (Fig. 3A). In both conditions, this experiment revealed *trans*-synaptically labeled mRuby+ cells in the contralateral CA3-CA1 and subiculum areas (Fig. 3B), where most commissural GC axons terminated (Fig. 1B).

For the accurate estimation of mRuby+ cell numbers, we subtracted the above-derived baselines from the cell counts (for nonnormalized data, see Fig. S4). The number of mRuby+ cells was significantly increased after KA, most prominently in CA1 and subiculum (saline vs. KA, $n = 5$ and 5 mice; dentate: 1.5 ± 3.4 vs. 16 ± 4.8 cells, CA3-CA2: 26 ± 4.9 vs. 44 ± 5.2 cells, CA1-subiculum: 18 ± 3.5 vs. 81 ± 6.5 cells, per 50-μm-thick sections) (Fig. 3C). Because mRuby+ cells resided in the principal cell layers, glutamatergic cells likely represented the major targets of commissural GCs. To examine this
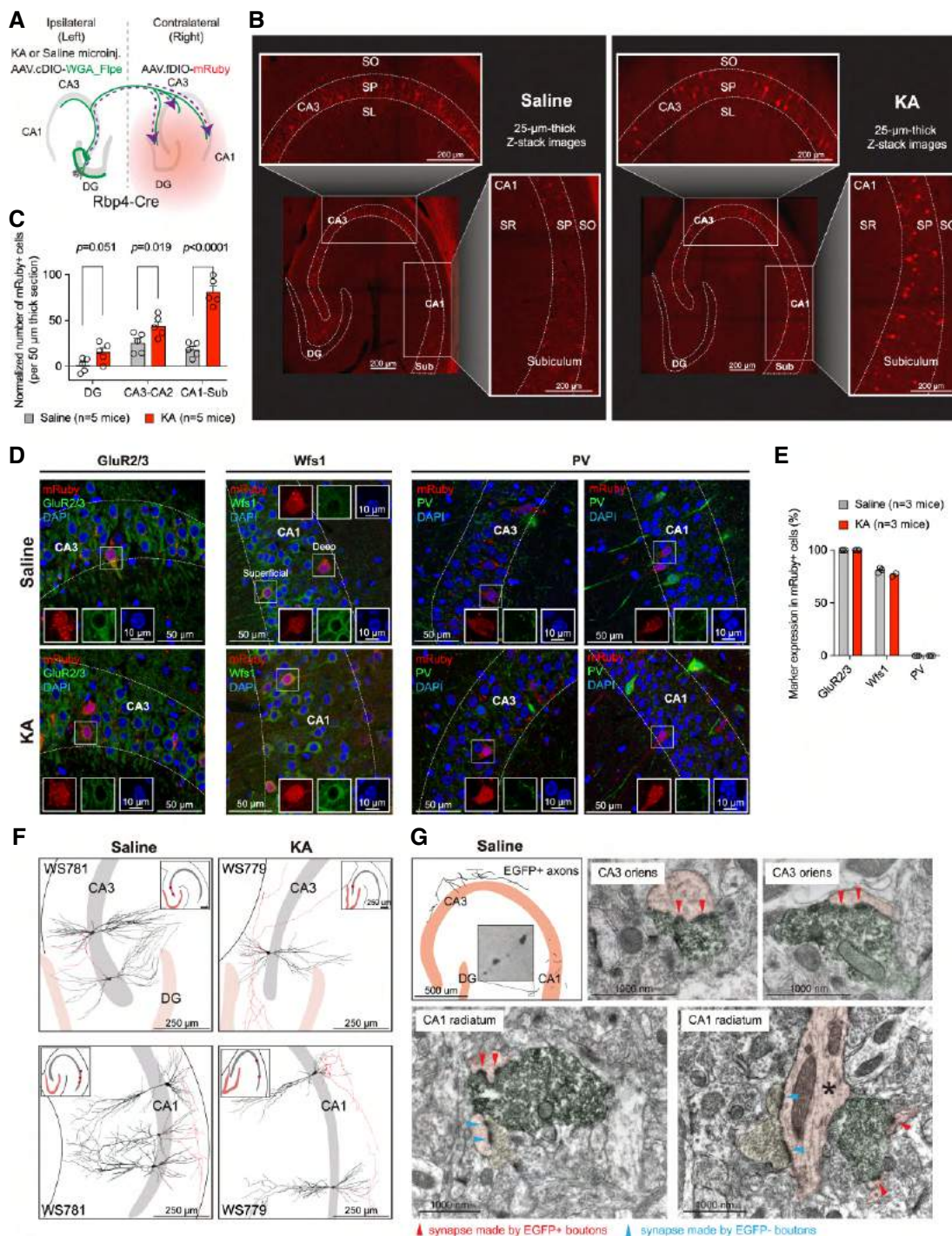
Fig. 3. *Trans*-synaptic labeling identifies postsynaptic targets of commissural GCs. A) Experimental design (also see main text). B) Confocal images show mRuby+ cells in the contralateral hippocampus after ipsilateral saline or KA injection. The CA3 and CA1 areas are shown in higher magnification in both panels. SO, stratum oriens; SP, stratum pyramidale; SL, stratum lucidum; SR, stratum radiatum. C) Quantification of mRuby+ cells in contralateral hippocampal DG, CA3-CA2, and CA1-subiculum areas after ipsilateral saline or KA injection. Each point represents data from one animal. Data were normalized by subtracting mRuby+ cell counts obtained from wild-type animals [see main text; for nonnormalized data, see Fig. S4; two-way ANOVA, $F_{area}(2, 16) = 56$, $P < 0.0001$; $F_{treatment}(1, 8) = 38$, $P = 0.0003$; $F_{area \times treatment}(2, 16) = 24$, $P < 0.0001$; adjusted P-values (FDR) of post hoc analyses are indicated in the figure]. D) Confocal images show immunostaining for mRuby and DAPI as well as immunostaining for either GluR2/3 (left, in contralateral CA3), Wfs1 (middle, in contralateral CA1; note that Wfs1 immuno-positivity was mostly apparent in the superficial, but not deep, CA1 pyramidal cells), or PV (right, in contralateral CA3 and CA1) in 50-μm-thick sections after saline (top row) and KA injections (bottom row). Insets show magnification of the highlighted areas (the three staining methods are shown separately). E) Bar plots show the coexpression of mRuby with GluR2/3 (in CA3), or Wfs1 (in CA1), or PV (in CA3 and CA1). F) Reconstruction of *trans*-synaptically labeled mRuby+ neurons after saline and KA injections reveals pyramidal cell morphology. Dendrites and axons are shown in black and red or magenta, respectively. G) The upper left image shows reconstruction of anterogradely labeled EGFP+ axons in the contralateral hippocampus in a 50-μm-thick section after ipsilateral saline injection. The electron microscopy images show EGFP+ synapses (green and red arrowheads) in the CA3 (stratum oriens) and CA1 (stratum radium) area, as well as EGFP nonlabeled synapses (yellow and blue arrowheads), for comparison. In the lower right image, the asterisk labels a putative interneuron dendrite; synapses between interneuron dendrites and adjacent EGFP+ processes were not present.

possibility, we immunostained sections with AMPA-type glutamate receptor subunit 2/3 (GluR2/3), Wfs1, and parvalbumin (PV) antibodies and tested the colocalization of these markers with *trans*-synaptically activated mRuby in CA3 pyramidal neurons (note, however, that GluR2/3 is also expressed by some GABAergic interneuron types) [8, 9], CA1 pyramidal neurons [7], and GABAergic PV interneurons [10], respectively, after KA (Fig. 3D). We found that most mRuby+ cells expressed GluR2/3+ in CA3 (saline: 269/269 cells, 3 mice, 100%; KA: 226/226 cells, 3 mice, 100%) and Wfs1 in CA1 (saline: 237/294 cells, 3 mice, 81 ± 1.4%; KA: 156/204 cells, 2 mice, 77 ± 1.4%), but not PV (saline: 0/370 cells, 3 mice, 0%; KA, 1/367 cells, 3 mice, 0.27%; intriguingly, this also suggested that PV neurons were not prone to nonspecific mRuby expression) (Fig. 3E). To further investigate the identity of targeted neurons, we filled mRuby+ cells with biocytin during electrophysiological recordings and reconstructed them afterwards. In agreement with the immunostaining, these mRuby+ cells displayed pyramidal cell morphology (Fig. 3F).

Finally, we used electron microscopy to visualize synaptic contacts made by anterogradely labeled (from the left, ipsilateral dentate gyrus) EGFP+ axons in the contralateral hippocampal CA1 and CA3 areas after ipsilateral saline injection. This analysis revealed structurally intact synapses abundantly filled with synaptic vesicles and multiple release sites juxtaposing postsynaptic densities in dendritic spines (Fig. 3G), but not on interneuron dendrites, suggesting that commissural GCs established functional synapses with postsynaptic target cells. In addition, we found that EGFP+ synapses in the CA1 area were comparably larger (1–3 μm in diameter) than surrounding EGFP nonlabeled, presumed Schaffer collateral synapses ($\sim \leq 1\,\mu$m) (Figs. 3G and S5). Together, these results showed that commissural GCs targeted glutamatergic cells in the contralateral hippocampus.

Electrophysiological and morphological characterization of commissural GCs

Thus far, we made multiple observations showing more commissural GCs, contralaterally projecting GC axons, and *trans*-synaptically labeled contralateral hippocampal cells after KA. Consistent with one other, these observations suggested that commissural GCs represent a unique GC class. To test if additional distinctions could be recognized in the biophysical, morphological, and transcriptomic domains, we employed a multimodal cell characterization approach [5, 10–12] after retroAAV.EGFP labeling (Fig. 4A).

Two weeks after injections, we prepared 300-μm-thick brain slices and performed electrophysiological patch-clamp recordings from EGFP+ commissural and neighboring EGFP– noncommissural GCs after saline or KA; from a subset of cells, we also collected the mRNA after recordings for subsequent single-cell sequencing. We refer to the four groups as saline–noncommissural ($n = 103$ cells/6 mice), saline–commissural ($n = 8$ cells/6 mice), KA–noncommissural ($n = 49$ cells/12 mice), and KA–commissural ($n = 33$ cells/12 mice) GCs (Fig. 4B). Limited by their overall number (Fig. 2E and F) ($\sim$3–5 cells in 300-μm-thick slices, but not all accessible with the patch pipette), the number of saline–commissural GCs remained relatively low compared to other groups.

With regard to electrophysiological properties, GCs from KA-injected mice had more depolarized resting membrane potential and higher capacitance and lower input resistance; however, independently of the treatment, there was no difference between commissural and noncommissural GCs (resting membrane potential, saline–noncommissural: −80 ± 0.8 mV; saline–commissural: −78 ± 2.4 mV; KA–noncommissural: −66 ± 0.95 mV; KA–commissural: −64 ± 1.4 mV; capacitance, saline–noncommissural: 46 ± 1.2 pF;

saline–commissural: 47 ± 3.9 pF; KA–noncommissural: 59 ± 2.1 pF; KA–commissural: 61 ± 2.6 pF; input resistance, saline–noncommissural: 188 ± 6.9 MOhm; saline–commissural: 196 ± 29 MOhm; KA–noncommissural: 140 ± 5.8 MOhm; KA–commissural: 125 ± 10 MOhm) (Fig. 4C). In addition, current injection-evoked action potential firing was enhanced in GCs after KA, but not different between commissural and noncommissural GCs (Fig. 4D). Thus, while the biophysical and AP firing properties reflected KA effects, e.g. [4, 5, 13, 14], they did not reveal commissural GC-specific features.

We also analyzed the local axonal morphology of commissural GCs, which could not be visualized in our previous experiment (see Fig. 2C and D). Because KA also induces ipsilateral mossy fiber sprouting in GCs, one key question was whether commissural GCs sprouted new ipsilateral axons in addition to the contralateral ones. To answer this question, we reconstructed biocytin-filled commissural GCs after the recordings (Fig. 4E). Due to severance of long axons in brain slices, the recovery of GC axons beyond the hilus was limited. However, in four out of seven commissural GCs, we confirmed the presence of ipsilateral mossy fiber sprouting, suggesting that contralateral and ipsilateral sprouting phenotypes were not distinctive markers for the commissural and noncommissural GC populations.

Transcriptomic characterization of commissural GCs

Next, we analyzed single-cell RNAseq data from 27 saline–noncommissural, 5 saline–commissural, 36 KA–noncommissural, and 27 KA–commissural GCs 2 weeks after injections. An advantage of this time point is the insights into potentially lasting transcriptomic changes in commissural GCs whose contralateral axons have been already established (a prerequisite for retrograde labeling). However, insights into the potentially transient induction phase (most likely within 1–2 days after KA, when contralateral axons are not yet established) and molecular programs that control commissural axon growth would be limited (see Discussion).

First, we examined the expression of known GC markers (Fig. 5A). Independently of commissural projections or KA treatment, cells expressed mature GC markers Calb1 and Prox1 [15, 16] but lacked immature GC markers Dcx or Calb2 [17, 18]. In addition, cells expressed Gad1 (glutamate decarboxylase 1) [19], Slc17a7 (vesicular glutamate transporter 1) [20], and Slc30a3 (zinc transporter 3, ZnT-3) [21]. Congruent with our previous observation (Figs. 2C and D and S1), only $\sim$30% of the cells expressed Rbp4, further indicating that commissural GCs are not restricted to the Rbp4-expressing GC population. Furthermore, we analyzed genes with known lasting expression changes after KA. Following previously described patterns, Npy [22] and Pnoc [23, 24] were up-regulated, whereas Cck was down-regulated [22], both in KA–commissural and KA–noncommissural GCs. Other interneuronal markers (e.g. Reln, Ndnf, Pvalb, Vip, and Sst) were not or infrequently detected (Fig. 5A). Thus, commissural and noncommissural GCs did not differ by known markers.

To analyze transcriptomic profiles more broadly, we performed differential gene expression analysis between KA–commissural and KA–noncommissural GCs (although the low number of commissural GCs hindered such a comparison after saline, we presumed that unique properties of the commissural GCs should be similar both after saline and KA). This comparison revealed differentially regulated genes between the two groups (Figs. 5B and S6). Although the expression of several genes were significantly different by single comparison ($P < 0.05$), none of them were by multiple comparisons (false discovery rate or FDR < 0.05 and fold-change > 2 or $|\log_2 FC| > 1$). In addition, top ranking genes did not display a
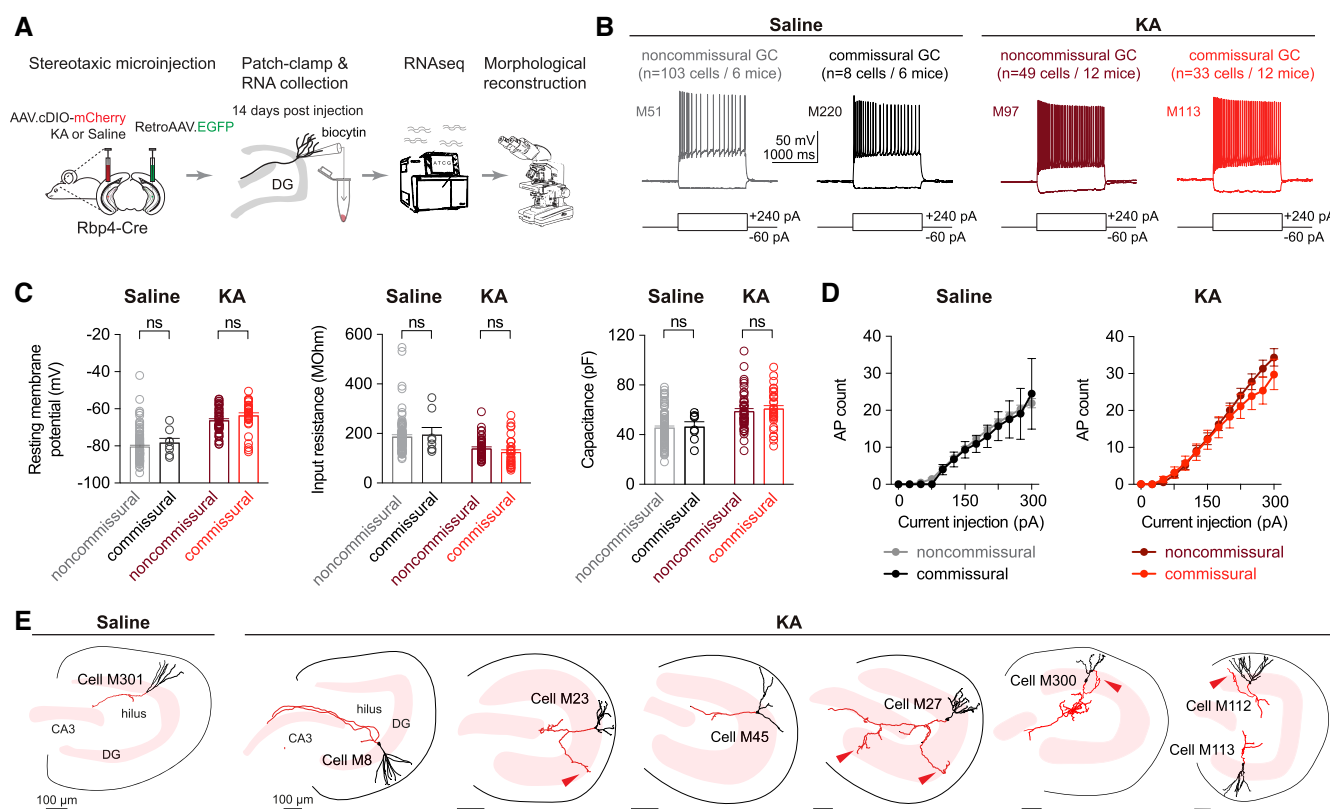
Fig. 4. Electrophysiological and morphological characterization of commissural GCs. A) Experimental design (also see main text). B) Example electrophysiological traces in response to 1.5-s-long depolarizing and hyperpolarizing current injections recorded from GCs after saline or KA. C) Quantification of resting membrane potential, input resistance, and capacitance of saline–noncommissural, saline–commissural, KA–noncommissural, and KA–commissural GCs [two-way ANOVA, resting membrane potential: $F_{treatment}(1, 189) = 75$, $P < 0.0001$; $F_{commissural}(1, 189) = 2.1$, $P = 0.15$; $F_{treatment \times commissural}(1, 189) = 0.017$, $P = 0.90$; input resistance: $F_{treatment}(1, 189) = 19$, $P < 0.0001$; $F_{commissural}(1, 189) = 0.081$, $P = 0.78$; $F_{treatment \times commissural}(1, 189) = 0.71$, $P = 0.40$; capacitance: $F_{treatment}(1, 189) = 23$, $P < 0.0001$; $F_{commissural}(1, 189) = 0.25$, $P = 0.62$; $F_{treatment \times commissural}(1, 189) = 0.039$, $P = 0.84$; post hoc analyses: for all noncommissural vs. commissural comparisons, the P-values were >0.05, indicated as nonsignificant or "ns" in figure; for all noncommissural vs. noncommissural and commissural vs. commissural comparisons between saline and KA, the P-values were <0.01; each circle represents a single cell; data represent mean ± SEM]. D) Quantification of action potential firing (AP count) in response to depolarizing current injections recorded from GCs after ipsilateral saline [left panel, two-way ANOVA, $F_{treatment}(1, 109) = 0.077$, $P = 0.78$; $F_{current}(11, 1,177) = 65$, $P < 0.0001$; $F_{treatment \times current}(11, 1,177) = 0.29$, $P = 0.99$] or KA injection [right panel, $F_{treatment}(1, 79) = 0.38$, $P = 0.54$; $F_{current}(11, 854) = 180$, $P < 0.0001$; $F_{treatment \times current}(11, 854) = 1.7$, $P = 0.073$]. E) Morphological reconstruction of retrogradely labeled EGFP+ commissural GCs, which were filled with biocytin during electrophysiological recordings. Arrowheads indicate ispilaterally sprouting axons.

clear distinguishing pattern, suggesting that commissural GCs cannot be identified by specific marker expression (Fig. 5C).

To further examine the transcriptomic profile of commissural GCs, we performed gene ontology (GO) enrichment analysis based on genes, whose expression level was >2-fold higher or lower than in noncommissural GCs. Using Enrichr (25), we found significant enrichment of multiple translation and protein transport-related biological pathways in commissural GCs (Fig. 5D). These pathways shared several genes which encoded ribosomal proteins (such as ribosomal protein large subunit, RPL, and ribosomal protein small subunit, RPS) (Fig. S7). As an independent approach, using STRING, we analyzed protein interactions based on the top 150 up- and down-regulated genes. Consistent with the Enrichr results, this analysis also revealed a significantly enriched cluster of ribosome proteins in commissural GCs (Figs. 5E and S8). While both Enrichr and STRING revealed significant enrichments, neither approach suggested de-regulation of molecular pathways (Figs. S7 and S9).

Discussion

In the present study, we systematically characterized GCs targeting the contralateral hippocampus. Our current results suggest three conclusions that have implications not only for GC diversity

and circuit formation in the adult brain but potentially also for the pathophysiology of epilepsy.

First, we described a rare type of hippocampal GCs that atypically project to the contralateral hippocampus in naïve mice. Previously, GCs had been extensively characterized as unilaterally projecting neurons within each hippocampus, critically involved in certain forms of learning and memory (26–28). While most GCs are located in the dentate GC layer and relatively homogenous, other atypical GC types have been also described, such as semilunar GCs in the inner molecular layer (29–34) and GCs in CA3 (35). Unlike these other types, commissural GCs are embedded in the GC layer. Using retrograde tracing, we identified ~20 commissural GCs in each dentate gyrus. As a caveat, this cell count was based on retrograde tracer injections at a single level of the septo-temporal axis of the hippocampus and therefore does not account for all commissural GCs in the entire hippocampus; in addition, imperfect axonal uptake, retrograde transport, and/or expression of the tracer may limit the efficacy of retrograde labeling. Thus, the actual number of commissural GCs is likely higher, possibly a few hundred or thousand in each dentate gyrus. In the contralateral hippocampus, commissural GC axons mostly innervated the CA3-CA1 and subiculum areas, and using *trans*-synaptic labeling, we showed that the major postsynaptic
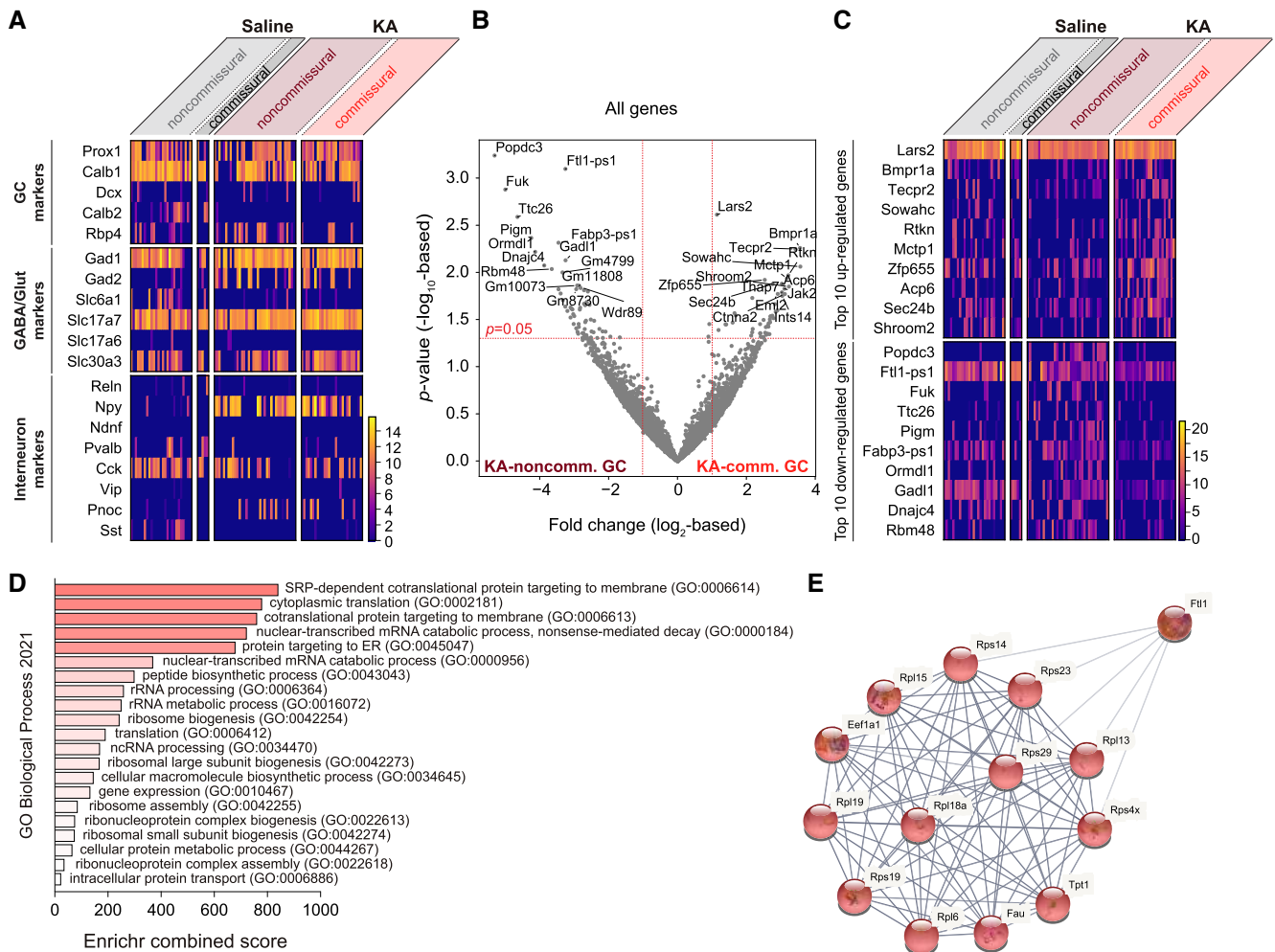
Fig. 5. Transcriptomic characterization of commissural GCs. A) Heat map shows expression GC, GABAergic versus glutamatergic, and interneuron marker genes. Scale shows log10-based gene expression level. B) Volcano plot shows differential gene expression between KA–noncommissural and KA–commissural GCs. C) Heat map shows expression of the top 10 up- and down-regulated genes in KA–commissural GCs compared to KA–noncommissural GCs. D) GO enrichment analysis based on genes, whose expression level was >2-fold higher in KA–commissural GCs compared to noncommissural GCs. Enriched biological processes (FDR < 0.005 for all; also see Fig. S7) are ranked by decreasing Enrichr combined score from bottom to top. The analysis of genes whose expression level was >2-fold lower in KA–commissural GCs compared to noncommissural GCs did not reveal significantly enriched biological processes (see Fig. S7). E) Plot shows the only enriched protein cluster identifiable by STRING cluster analysis based on the top 150 up-regulated genes in KA–commissural GCs compared to KA–noncommissural GCs (also see Fig. S8). Proteins in this cluster are related to ribosome function. STRING analysis of the 150 down-regulated genes did not reveal identifiable clusters (see Fig. S9).

targets are pyramidal neurons. As an additional caveat, the anterograde axon and *trans*-synaptic cell tracing experiments were based on the ~30% of GCs that express Cre in the Rbp4-Cre transgenic line, although we also showed that commissural GCs are not restricted to Rbp4-expressing GC population. Thus, the total length of commissural GC axons and the number of innervated neurons are also likely higher. Irrespectively, our results indicate that commissural GCs are uniquely positioned to mediate interhemispheric information transfer within the hippocampal GC population.

To gain further insights into the identity of these cells, we used multimodal electrophysiological, morphological, and transcriptomic analyses, which revealed that commissural GCs are principally very similar to other mature GCs. Apart from their commissural axons, our analyses did not reveal unique features that could be used as biomarker for this atypical GC population. Nonetheless, we detected several differentially regulated genes and, based on these, significant enrichment of ribosome- and translation-related biological processes in commissural GCs, feasibly reflecting an increased cellular load to support the biogenesis and/or maintenance of long commissural axons.

Second, in contrast with a prevalent hypothesis that posits broad axon growth inhibition in the adult central nervous system (36, 37), our results revealed robust growth of contralateral projections after KA treatment. Specifically, we found that the number of retrogradely labeled commissural GCs, length of anterogradely labeled contralateral GC axons, and the number of *trans*-synaptically labeled contralateral hippocampal neurons increased by ~5–6-, 4.3-, and 2- to 10-fold, respectively. With regard to previous reports on inter-hippocampal projections, contralateral sprouting of commissurally projecting hippocampal PV (38) and CA3 pyramidal neurons (39) and of an unidentified cell type (40) was observed in epilepsy models. Independently of epilepsy, human embryonic stem cells grafted into the mouse and rat dentate gyrus grew new commissural axons into the contralateral hippocampus (41). Thus, our finding together with other evidence indicates that the adult brain retains a capacity for inter-hippocampal axon growth and/or sprouting and that such processes are exempt from growth inhibition.

Given that most GCs activate a unilateral wiring program for local mossy fiber sprouting after KA, the commissural growth of

axons may be controlled by additional wiring mechanisms (e.g. for midline crossing and for contralateral target specification), the identification of which remains an important goal. Similarly to local mossy fiber sprouting (5), commissural axon growth feasibly starts within 1–2 days after KA injection. Induction mechanisms may be active only transiently, constrained by KA availability and/or neuronal sensitivity to KA. For example, we previously identified Id2 as a key regulator of local mossy fiber sprouting based on its exceptionally strong up-regulation 1 day after KA (5); however, 2 weeks later, its expression was decreased to the level of a much less likely candidate. Thus, assuming that commissural fiber growth is controlled transcriptionally, it is possible that our transcriptomic data (2 weeks after KA) reflected molecular states associated with maintenance rather than induction. Currently, the major limitation of exploring the molecular mechanisms of induction in greater detail is the inability to access commissural GCs shortly after KA: retrograde labeling does not solve this problem, because commissural axons are not yet established in the contralateral hippocampus.

Third, commissural GC projections may contribute to epilepsy. In the unilateral intrahippocampal KA microinjection model, spontaneous behavioral seizures may develop several weeks after injections (42–44). Approximately 60% of the seizures start in the KA-injected (ipsilateral) hippocampus, whereas the remainder starts in the noninjected (contralateral) hippocampus, bilaterally, or elsewhere (42). Independently of the locus of seizure onset, closed-loop (seizure-triggered) activation of local inhibitory PV interneurons in the hippocampus contralateral to KA microinjection effectively reduced seizure duration and/or completely stopped seizures (45), suggesting that contralateral excitatory neurons (major targets of PV neurons) and their commissural connections are important for seizure activity. Consistent with this, corpus callosum bisection may lead to seizure reduction and/or freedom in pharmacologically intractable seizures (46). Here, we showed that commissural GCs contribute to an inter-hippocampal excitatory-to-excitatory circuit. By directly targeting pyramidal cells in the contralateral hippocampus, commissural GCs bypass several feedback and feedforward inhibitory microcircuits which could control seizures (47), suggesting that excessive activation of this cell type may facilitate the generation and/or generalization of seizures (48).

Conclusion

In this study, we characterized commissural GCs that atypically project to the contralateral hippocampus. Multiple questions arise regarding this cell population, for example, how commissural GCs contribute to information processing in the healthy brain and if they play a role in epilepsy. Although we showed that commissural GC form synapses on contralateral pyramidal cells, the physiological properties of these synapses as well as the conditions under which they are activated remain to be elucidated. Furthermore, deciphering molecular mechanisms that control contralateral axon growth in the adult brain will likely have important implications for understanding the molecular logic of adult brain circuits. A critical next step to addressing these problems is to gain more specific access to commissural GCs, allowing higher throughput molecular and activity readouts as well as activity manipulations. The anterograde and retrograde approaches employed in our study have had limited capacity to achieve these goals. Finally, the question whether commissural GCs are present in species other than mice remains open.

Materials and methods

All mouse protocols and husbandry practices were approved by the Veterinary Office of Zürich Kanton. For comprehensive description of (i) mouse breeding and husbandry, (ii) stereotactic injection, (iii) histology and neuroanatomy, (iv) image analysis, (v) in vitro electrophysiology, (vi) single-cell RNA sequencing and bioinformatics, and (vii) statistical analysis, see Appendix S1.

Acknowledgments

Supplementary material

Supplementary material is available at *PNAS Nexus* online.

Funding

Author contributions

W.L., M.E., and C.F. designed research; M.E., W.L., N.A.C.-O., D.L., C.V., L.Q., G.M., J.W., R.K., and T.L. performed research and analyzed data; W.L. and C.F. wrote the paper.

Data availability

The RNA sequencing data have been deposited to National Center for Biotechnology Information Gene Expression Omnibus (NCBI GEO, GSE214905).

References

1 Seng C, Luo W, Földy C. 2022. Circuit formation in the adult brain. *Eur J Neurosci*. 56(3):4187–4213.

2 Denoth-Lippuner A, Jessberger S. 2021. Formation and integration of new neurons in the adult hippocampus. *Nat Rev Neurosci*. 22(4):223–236.

3 2012. *Jasper's basic mechanisms of the epilepsies [internet]*. 4th edition. Bethesda (MD): National Center for Biotechnology Information (US).

4 Luo W, *et al*. 2022. *Pcdh11x* controls target specification of mossy fiber sprouting. *Front Neurosci*. 16:888362.

5 Luo W, *et al*. 2021. Recurrent rewiring of the adult hippocampal mossy fiber system by a single transcriptional regulator, Id2. *Proc Natl Acad Sci U S A*. 118(40):e2108239118.

6 Gerfen CR, Paletzki R, Heintz N. 2013. GENSAT BAC Cre-recombinase driver lines to study the functional organization of cerebral cortical and basal ganglia circuits. *Neuron* 80(6):1368–1383.

7 Cembrowski MS, *et al*. 2016. Spatial gene-expression gradients underlie prominent heterogeneity of CA1 pyramidal neurons. *Neuron* 89(2):351–368.

8 He Y, Janssen WG, Vissavajjhala P, Morrison JH. 1998. Synaptic distribution of GluR2 in hippocampal GABAergic interneurons

and pyramidal cells: a double-label immunogold analysis. *Exp Neurol*. 150(1):1–13.

9   Cox DJ, Racca C. 2013. Differential dendritic targeting of AMPA receptor subunit mRNAs in adult rat hippocampal principal neurons and interneurons. *J Comp Neurol*. 521(9):1954–2007.

10 Que L, Lukacsovich D, Luo W, Földy C. 2021. Transcriptional and morphological profiling of parvalbumin interneuron subpopulations in the mouse hippocampus. *Nat Commun*. 12(1):108.

11 Földy C, et al. 2016. Single-cell RNAseq reveals cell adhesion molecule profiles in electrophysiologically defined neurons. *Proc Natl Acad Sci U S A*. 113(35):E5222–E5231.

12 Winterer J, et al. 2019. Single-cell RNA-Seq characterization of anatomically identified OLM interneurons in different transgenic mouse lines. *Eur J Neurosci*. 50(11):3750–3771.

13 Young CC, et al. 2009. Upregulation of inward rectifier K+ (Kir2) channels in dentate gyrus granule cells in temporal lobe epilepsy. *J Physiol*. 587(Pt 17):4213–4233.

14 Janz P, et al. 2017. Synaptic remodeling of entorhinal input contributes to an aberrant hippocampal network in temporal lobe epilepsy. *Cereb Cortex*. 27(3):2348–2364.

15 Celio MR. 1990. Calbindin D-28k and parvalbumin in the rat nervous system. *Neuroscience* 35(2):375–475.

16 Iwano T, Masuda A, Kiyonari H, Enomoto H, Matsuzaki F. 2012. Prox1 postmitotically defines dentate gyrus cells by specifying granule cell identity over CA3 pyramidal cell fate in the hippocampus. *Development* 139(16):3051–3062.

17 Brandt MD, et al. 2003. Transient calretinin expression defines early postmitotic step of neuronal differentiation in adult hippocampal neurogenesis of mice. *Mol Cell Neurosci*. 24(3):603–613.

18 von Bohlen Und Halbach O. 2007. Immunohistological markers for staging neurogenesis in adult hippocampus. *Cell Tissue Res*. 329(3):409–420.

19 Sloviter RS, et al. 1996. Basal expression and induction of glutamate decarboxylase and GABA in excitatory granule cells of the rat and monkey hippocampal dentate gyrus. *J Comp Neurol*. 373(4):593–618.

20 Gómez-Lira G, Lamas M, Romo-Parra H, Gutiérrez R. 2005. Programmed and induced phenotype of the hippocampal granule cells. *J Neurosci*. 25(30):6939–6946.

21 Wenzel HJ, Cole TB, Born DE, Schwartzkroin PA, Palmiter RD. 1997. Ultrastructural localization of zinc transporter-3 (ZnT-3) to synaptic vesicle membranes within mossy fiber boutons in the hippocampus of mouse and monkey. *Proc Natl Acad Sci U S A*. 94(23):12676–12681.

22 Gall C, Lauterborn J, Isackson P, White J. 1990. Seizures, neuropeptide regulation, and mRNA expression in the hippocampus. *Prog Brain Res*. 83:371–390.

23 Hunsberger JG, Bennett AH, Selvanayagam E, Duman RS, Newton SS. 2005. Gene profiling the response to kainic acid induced seizures. *Brain Res Mol Brain Res*. 141(1):95–112.

24 Armagan G, et al. 2012. Kainic acid-induced changes in the opioid/nociceptin system and the stress/toxicity pathways in the rat hippocampus. *Neurochem Int*. 60(6):555–564.

25 Xie Z, et al. 2021. Gene set knowledge discovery with Enrichr. *Curr Protoc*. 1(3):e90.

26 Blaabjerg M, Zimmer J. 2007. The dentate mossy fibers: structural organization, development and plasticity. *Prog Brain Res*. 163:85–107.

27 Josselyn SA, Tonegawa S. 2020. Memory engrams: recalling the past and imagining the future. *Science* 367(6473):eaaw4325.

28 Hainmueller T, Bartos M. 2020. Dentate gyrus circuits for encoding, retrieval and discrimination of episodic memories. *Nat Rev Neurosci*. 21(3):153–168.

29 Williams PA, Larimer P, Gao Y, Strowbridge BW. 2007. Semilunar granule cells: glutamatergic neurons in the rat dentate gyrus with axon collaterals in the inner molecular layer. *J Neurosci*. 27(50):13756–13761.

30 Larimer P, Strowbridge BW. 2010. Representing information in cell assemblies: persistent activity mediated by semilunar granule cells. *Nat Neurosci*. 13(2):213–222.

31 Rovira-Esteban L, et al. 2020. Semilunar granule cells are the primary source of the perisomatic excitatory innervation onto parvalbumin-expressing interneurons in the dentate gyrus. *eNeuro* 7(4):ENEURO.0323-19.2020.

32 Erwin SR, et al. 2020. A sparse, spatially biased subtype of mature granule cell dominates recruitment in hippocampal-associated behaviors. *Cell Rep*. 31(4):107551.

33 Gupta A, et al. 2020. Dendritic morphology and inhibitory regulation distinguish dentate semilunar granule cells from granule cells through distinct stages of postnatal development. *Brain Struct Funct*. 225(9):2841–2855.

34 Afrasiabi M, Gupta A, Xu H, Swietek B, Santhakumar V. 2022. Differential activity-dependent increase in synaptic inhibition and parvalbumin interneuron recruitment in dentate granule cells and semilunar granule cells. *J Neurosci*. 42(6):1090–1103.

35 Szabadics J, Varga C, Brunner J, Chen K, Soltesz I. 2010. Granule cells in the CA3 area. *J Neurosci*. 30(24):8296–8307.

36 Yiu G, He Z. 2006. Glial inhibition of CNS axon regeneration. *Nat Rev Neurosci*. 7(8):617–627.

37 Schwab ME. 2010. Functions of Nogo proteins and their receptors in the nervous system. *Nat Rev Neurosci*. 11(12):799–811.

38 Christenson Wick Z, Leintz CH, Xamonthiene C, Huang BH, Krook-Magnuson E. 2017. Axonal sprouting in commissurally projecting parvalbumin-expressing interneurons. *J Neurosci Res*. 95(12):2336–2344.

39 Siddiqui AH, Joseph SA. 2005. CA3 Axonal sprouting in kainate-induced chronic epilepsy. *Brain Res*. 1066(1–2):129–146.

40 Davenport CJ, Brown WJ, Babb TL. 1990. Sprouting of GABAergic and mossy fiber axons in dentate gyrus following intrahippocampal kainate in the rat. *Exp Neurol*. 109(2):180–190.

41 Steinbeck JA, Koch P, Derouiche A, Brüstle O. 2012. Human embryonic stem cell-derived neurons establish region-specific, long-range projections in the adult brain. *Cell Mol Life Sci*. 69(3):461–470.

42 Bragin A, Engel J Jr, Wilson CL, Vizentin E, Mathern GW. 1999. Electrophysiologic analysis of a chronic seizure model after unilateral hippocampal KA injection. *Epilepsia* 40(9):1210–1221.

43 Ben-Ari Y. 2002. Kainate and temporal lobe epilepsies: 3 decades of progress. In: Noebels JL. Avoli M. Rogawski MA. Olsen RW, Delgado-Escueta AV, editors. *Jasper's basic mechanisms of the epilepsies [internet]*. 4th ed. Bethesda (MD): National Center for Biotechnology Information (US). p. 501–526.

44 Jagirdar R, Drexel M, Bukovac A, Tasan RO, Sperk G. 2016. Expression of class II histone deacetylases in two mouse models of temporal lobe epilepsy. *J Neurochem*. 136(4):717–730.

45 Krook-Magnuson E, Armstrong C, Oijala M, Soltesz I. 2013. On-demand optogenetic control of spontaneous seizures in temporal lobe epilepsy. *Nat Commun*. 4:1376.

46 Wada JA. 2005. Callosal bisection and transcallosal secondary antiepileptogenesis. *Epilepsia*. 46(Suppl 1):2–6.

47 Paz JT, Huguenard JR. 2015. Microcircuits and their interactions in epilepsy: is the focus out of focus? *Nat Neurosci*. 18(3):351–359.

48 Fei F, et al. 2022. Discrete subicular circuits control generalization of hippocampal seizures. *Nat Commun*. 13(1):5010.

Discussion

In this study, I characterized a long-range or commissural form of wiring in the adult brain and a new cell type, the commissural granule cells (Egger *et al.*, 2023). My findings open multiple questions for future research, some of which are already discussed in the Discussion of our paper.

First, it will be critically important to investigate the function of commissural granule cells in health and disease. Our work characterized these cells in the anatomical, biophysical, and transcriptomic domains; however, what these cells "really do" remains an outstanding question. Additional anatomical and physiological characterization (e.g. synapse number counts, further characterization of target cells in the ipsilateral and contralateral hippocampus, the electrophysiological recording of synaptic responses elicited by commissural GCs, and addressing the question if commissural granule cell axons are myelinated) could provide further insights. For example, mossy fibers and sprouted mossy fibers associated with medial temporal lobe epilepsy have been previously described as thin, non-myelinated axons (Frotscher *et al.*, 2006; Andersen *et al.*, 2010; Squire *et al.*, 2012), suggesting a potentially slower conduction velocity compared to myelinated axons (Waxman & Bennett, 1972). Therefore, future studies that use electron microscopy to visualize the myelin ensheathment (Sherman & Brophy, 2005) of commissural axons could clarify at least the basic dynamics of signal propagation enabled by commissural granule cells between the two hippocampi. Further, the targeted activation and/or inactivation (or silencing) of commissural granule cells would represent a more direct approach to understand their function. However, as mentioned in the paper, these efforts currently remain limited by our inability to molecularly access commissural granule cells and deliver the necessary viral constructs for activity manipulations.

Second, it will be important to further investigate the molecular mechanisms underlying commissural sprouting. Why do many, if not all, granule cells sprout new axons ipsilaterally, but only comparably fewer contralaterally? How do contralaterally sprouting granule cells reach and find their targets in the contralateral hippocampus? Our molecular analysis thus far indicated a potentially increased protein translation rate in commissural granule cells, but thus far did not reveal insights into answering the above questions. As discussed in our study, I hypothesize that the transcriptomic results, obtained 2 weeks after wiring induction (i.e. kainic acid microinjection), may

reflect the transcriptomic states of wiring maintenance rather than formation. In order to gain insights into mechanisms that are active during the wiring phase, it will be necessary to sample and sequence the transcriptomic content of commissural granule cells 1-3 days after induction. It is possible that in addition to wiring, potentially distinct marker expression seen in this time window would allow the much sought after molecular access to commissural granule cells. However, during 1-3 days after induction, growing axons do not reach the contralateral hippocampus yet, and as a consequence, commissural granule cells cannot be retrogradely labeled from the contralateral hippocampus. Currently, this is the only way we can identify these cells. To circumvent this limitation, I recently performed additional experiments, in which I intended to label the elongating cells by injecting the retrograde AAV markers into commissural fiber tracks rather than the contralateral hippocampus. However, conclusive results from this experiment were limited by nearly unavoidable virus spread into the ventricles and ipsilateral hippocampus. In addition, the success of this experiment is also contingent on that the virus can be taken up by elongating axon endings (rather than by synapses), for which we currently do not have solid evidence. In this manner, molecular access to commissural granule cells as well as insights into the wiring mechanisms will clearly require the establishment of a more refined technological approaches.

Third, our results have also revealed an intriguing pattern of commissural granule cell axons in the contralateral hippocampus. Specifically, we found a high density of axons in the contralateral CA1 and subiculum areas. Granule cell axons, or mossy fibers, have been extensively studied before and their extensive innervation of the ipsilateral CA3 area and inability to enter the ipsilateral CA1 area in most rodent and primate species are one of their hallmark features (Andersen *et al.*, 2010). Intriguingly, however, there are also select species, such as in the siamese cat, water shrew and European Hedgehogs (Laurberg & Zimmer, 1980; Gaarskjaer *et al.*, 1982; West *et al.*, 1984; Blaabjerg & Zimmer, 2007) in which mossy fibers reach deep into CA1 and appear to be essential part of the CA1 circuit; the functional relevance of this projection is entirely unknown. The desire to understand the reasons behind the general lack of mossy fibers in CA1 has motived multiple research studies. These studies employed various techniques such as mechanical damage or neurotoxic destruction of CA3 (Cook & Crutcher, 1985), grafting of cells (Zimmer *et al.*, 1985), or co-culturing of dentate gyrus slice posed in proximity to CA1 slices (Zimmer *et al.*, 1985) to find potential signatures of mossy fiber sprouting into the ipsilateral CA1; however,

such signatures could not be detected (see also Blaabjerg & Zimmer, 2007). These observations are consistent with the overall hypothesis that a single or a combination of few CAMs and/or guidance cues may repel mossy fibers from entering the ipsilateral CA1. Although my results do not provide further mechanistic insights into this problem, they highlight conceptual possibilities.

It is possible that commissural granule cells employ a different combination of CAMs compared to noncommissural granule cells, feasibly allowing their axons to (1) enter the commissural/associational pathway in the ipsilateral hippocampus, (2) cross the midline and enter the contralateral hippocampus, and (3) enter CA1 and subiculum in the contralateral hippocampus. However, this hypothesis would not explain why commissural granule cells do not already enter the spatially much closer ipsilateral CA1. Further, it is possible that commissural and noncommissural granule cells utilize the same set of CAMs, but molecular asymmetries between the left and right hippocampus play a role in allowing commissural granule cell axons to enter the contralateral CA1. This scenario would not be completely unexpected as functionally relevant left-right asymmetries between the two hippocampi have been previously observed (Shinohara *et al.*, 2008; Kohl *et al.*, 2011; Shipton *et al.*, 2014; El-Gaby *et al.*, 2015). However, this scenario assumes that the repelling mechanisms have evolved differently in each hippocampus, which although is not impossible, I consider unlikely. In addition, this hypothesis would not explain why only commissural, but not noncommissural, granule cells enter the commissural/associational pathway. To resolve these conceptual inconsistencies, I hypothesize that both CAM differences between commissural and noncommissural granule cells and left-right asymmetries may combinatorically contribute to this effect. However, it is clear that any experimental validation of this hypothesis will require a significant and technically nontrivial effort, and again contingent on molecular readouts from commissural granule cells shortly after wiring induction.

Overall, the identification of commissural granule cells and their rapid circuit formation in the adult brain has raised several questions for future experiments, in which understanding the molecular mechanisms will be crucial not only for generating further insights into adult brain wiring but to systematically analyze the function of new circuits.

Chapter 5 – Discussion and perspectives

Summary of key findings

In the three studies I presented, my colleagues and I systematically analyzed the epilepsy-associated hippocampal mossy fiber sprouting by granule cells using the well-established intrahippocampal kainic acid microinjection model as an experimental approach. The overarching goal of my thesis work aimed at understanding the molecular mechanisms of mossy fiber sprouting, and more broadly, of adult wiring. Although mossy fiber sprouting has been extensively researched, previous studies mostly focused on its relevance for epilepsies. In our projects, we took advantage of the fact that the circuit rewiring takes place before the seizures, and thus for a certain time window we were able to study wiring mechanisms with the need of considering the potentially confounding consequences of seizures. My research outcomes have not only established solid bases for future investigations on adult wiring and circuit assembly in the adult brain, but also revealed important insights into the cellular composition of dentate gyrus and the pathophysiology of temporal lobe epilepsies.

The thesis design was motivated by the hypothesis that the combinatorial expression of CAMs determines wiring specificity (or the "molecular code") of brain circuits, and this code could be understood through a potentially much smaller group of transcription factors and regulators controlling the combinatorial expression of CAMs. To explore this hypothesis, my research employed single-cell RNA transcriptomic profiling of control and sprouting granule cells, and subsequent molecular, electrophysiological, neuroanatomical and behavioral experiments.

First, in Chapter 2, I presented a study showing how systematic transcriptional profiling can be used to identify wiring mechanisms in adult neurons. Previous research results on regenerating axons (Bareyre *et al.*, 2011; Sun *et al.*, 2011; Pernet *et al.*, 2013) have indicated that regeneration, and by extension further wiring in the adult nervous system requires the simultaneous deployment of several cell autonomous and cell nonautonomous factors. In contrast with this hypothesis, we found that the cell autonomous activation of a single transcriptomic regulator, *Id2*, can induce axon growth, target specification, and synapse formation (Luo *et al.*, 2021). Given that *Id2* is an inhibitor of bHLH transcription factors, this finding suggested that – at least in adult granule cells – the capacity of wiring is transcriptionally suppressed rather than deregulated. Further, this finding shed new light on how to approach the systematic

analysis of adult wiring mechanisms and potentially the development of new circuit engineering technologies. Finally, results from this study have also provided valuable insights into the pathophysiology of temporal lobe epilepsies, which I will discuss further below.

Second, in Chapter 3, I described a study aiming to identify which specific CAMs contribute to the target specification of mossy fiber sprouting. By employing a single cell transcriptomic- and CRISPR-Cas9 technology-based screen, we identified a role for *Pcdh11x* in the subcellular targeting of mossy fiber sprouting (Luo *et al.*, 2022). This finding has directly implicated CAMs in adult wiring, and because our *Pcdh11x* manipulations only explained one component of target specification, suggested a role for further CAMs in mossy fiber sprouting. Although technological limitations hindered our efforts to uncover the roles of other CAMs, our results highlight a potentially capable approach for the future investigation of CAMs in adult wiring.

Finally, in Chapter 4, I presented my first author work on the rapid development on commissural projections in the adult brain and characterization of a previously unnoted granule cell subpopulation (Egger *et al.*, 2023). The results of this work represent a fundamental set of observations, rather than mechanistic insights, regarding adult wiring. These observations also open far reaching possibilities which I believe have the potential to facilitate our understanding of adult wiring as well as the pathomechanisms of epilepsy.

Formation and stability of the new circuits

Clearly important questions regarding adult wiring include what rules shape formation of the new circuits and how stable they are in the long term. Currently, we have limited evidence providing answers to these questions.

A key difference between developmental and adult wiring is that further adult wiring takes place on top of already established and functional circuits. During development, synaptic competition is thought to play a central role in determining precisely which connections will be stabilized for the long term (Purves & Lichtman, 1980; Bailey & Chen, 1989; Goodman & Shatz, 1993; Katz & Shatz, 1996; Lin & Koleske, 2010; Stiles & Jernigan, 2010). Whether synaptic competition plays a role in adult wiring is an entirely open question. It is possible that the formation of new synapses inevitably leads to elimination of some of the established synapses. Such

synapse elimination may take place "directly", i.e. at the time of synapse formation, or "indirectly", i.e. later, when synaptic weights in the network may adjust to accommodate information transfer through the new circuits. I envision that knowledge gain in this domain will be facilitated by cutting-edge technologies, such as direct imaging of the growing axons during adult wiring. In such an experiment, it would be possible to directly analyze the postsynaptic environment, such as dendrites, where new synapses are formed, and determine structural dynamics (growth or elimination) of neighboring synapses. Not least, such an experiment would provide direct insight into the synaptic contact formation during adult wiring. While technically challenging, similar experiments have demonstrated the feasibility of this approach (Niell *et al.*, 2004; Meyer & Smith, 2006; Holtmaat & Svoboda, 2009; Dhar *et al.*, 2016).

With regard to the long-term stability of circuits, the most concrete insights are from studies on the circuit integration of adult-born granule cells and behaviorally-relevant periodic rewiring. Surviving adult born neurons integrate into existing circuit in subsequent maturation steps, after which they become essentially undisguisable from other adult granule cells (Carlén *et al.*, 2002; Zhao *et al.*, 2006; Toni *et al.*, 2007; Sierra *et al.*, 2010; Pilz *et al.*, 2018; Denoth-Lippuner & Jessberger, 2021). This suggests that the circuits formed by adult-born neurons are stable. By contrast, the circuits formed by periodic rewiring (Fernández *et al.*, 2008; Gorostiza *et al.*, 2014; Inoue *et al.*, 2019; Song *et al.*, 2021) are inherently disassembled after a certain time, most likely governed by specific molecular signals. In contrast to these types of adult wiring, the long-term stability of circuits formed after cell grafting or reprogramming has not been systematically assessed. These studies, including ours, have thus far focused on the molecular mechanisms or other technical considerations underlying circuit formation, rather than on maintenance, and typically analyzed the circuits up to 3-6 months after induction. Given that the grafting and reprograming technologies have clear therapeutic potentials, it will be important to evaluate the long-term stability of these circuits, possibly over years.

This question also directly precipitated itself in my own research, highlighting another important question. As described in Chapter 2, we found that *Id2* activation in adult granule cells induces the formation of a recurrent mossy fiber circuit. To achieve this, we employed AAV-mediated overexpression of the *Id2* gene together with fluorescent reporters, which we mainly used to identify the site of injection. Although we do not have direct evidence showing how long the AAV expression vectors would

actively support transcription of the exogenous *Id2*, based on the sustained presence of the fluorescent reporter signal, it is likely to be at least several months. Therefore, an important question that will need to be addressed in future experiments is whether *Id2* is only required for the induction or also for the maintenance of the new circuit. Answering this question will require precise temporal control over *Id2* activation and, subsequently, inactivation. In principle, such temporal control could be achieved with a newly engineered transgenic mouse line in which expression of the endogenous *Id2* gene is to be controlled, for example, by a tetracycline-inducible or a Cre-loxP system (Kühn & Torres, 2002; Sun *et al.*, 2007). However, the generation of such transgenic mouse line will also require careful considerations to ensure cell type specificity for the activation/inactivation of *Id2*. I envision that this and other similar experiments would provide fundamental insights into the mechanisms of induction and maintenance, and the relationship between the two.

Functional considerations regarding the new circuits

Although the results from the projects presented in this thesis as well as those from others have provided insights into the function of new circuits, addressing this overall question will be clearly an important challenge for all future research on adult wiring.

Previously, others have shown that periodic brain rewiring plays a key role in the behavioral response to light in drosophila (circadian rewiring) (Fernández *et al.*, 2008; Gorostiza *et al.*, 2014; Petsakou *et al.*, 2015) and the sexual behavior of female mice (estrous cycle-dependent rewiring) (Inoue *et al.*, 2019). In addition, research on adult-born granule cells have shown the relevance of new circuits for pattern separation (Clelland *et al.*, 2009; Sahay *et al.*, 2011; Nakashiba *et al.*, 2012b), whereas studies focusing on brain repair have shown that new circuits can replace injured pathways and promote functional recovery after brain injury (Gaillard *et al.*, 2007, 2009; Thompson *et al.*, 2009; Benowitz & Carmichael, 2010; Lu *et al.*, 2012; Tornero *et al.*, 2013, 2017; Filli & Schwab, 2015; Steinbeck *et al.*, 2015; Besusso *et al.*, 2020). In these examples, the functional assessment was facilitated by detailed investigation of a specific cell type (such as adult-born granule cells), a circuit rewiring phenotype (such as circadian rewiring in drosophila), a behavior for which the found circuit rewiring proved to be important (such as sexual behavior in female mice), or known functions which were impaired by injury.

My research focused on the epilepsy-associated mossy fiber sprouting, in which the new circuits may do not have a physiological function in the above sense. Instead, they may contribute to pathomechanisms, such as the generation of seizures. The rationale for this hypothesis is that the new circuits, such as the recurrent and commissural mossy fiber circuits described in Chapters 2 to 4, may represent network motifs capable of amplifying excitatory signals and promoting seizure prone network states. We specifically addressed this possibility in the study on *Id2*-induced recurrent mossy fiber sprouting, described in Chapter 2. We performed *in vivo* electrophysiological recordings from freely-moving mice after *Id2*-induced rewiring to uncover potential signatures of neuronal hyperexcitability, pathological oscillations, or electrographic and behavioral seizures (Luo et al., 2021). However, contrary to the above hypothesis, we did not find such signatures, suggesting that the recurrent mossy fiber sprouting is not epileptogenic per se. However, it is important to note, as discussed in our paper (Luo et al., 2021), that recurrent mossy fiber spouting is only one of the pathologies associated with temporal lobe epilepsies. Therefore, it is possible that other pathologies, such as cell dispersion and death, play more important roles in epileptogenesis, or that recurrent mossy fiber sprouting would only manifests its relevance only on the background of other pathologies. Related to this issue, an important question, which our study did not directly address is whether *Id2* is essentially required for the development of recurrent mossy fiber sprouting in the unilateral hippocampal kainic acid injection model, which also induces epilepsy on the long term. As outlined in Chapter 3, we now should have the technological means (e.g. CRIPSP-Cas9 editing- or shRNA-based technologies) to investigate if the blockade of kainic acid-induced *Id2* upregulation would occlude recurrent mossy fiber sprouting. Finding this to be the case would help us to better understand the molecular mechanisms underlying mossy fiber sprouting, and importantly, enable more detailed investigations into the question if seizures occur in the absence of recurrent mossy fiber sprouting.

Although we did not find signatures of hyperexcitability in the *Id2* model, our results revealed significant alterations in specific network events, such as the drastic decrease in the occurrence of dentate spikes. Dentate spikes have been linked to information transfer from the entorhinal cortex to the hippocampus and may play a role in spatial information processing (Penttonen *et al.*, 1997; Knierim *et al.*, 2014; Wang *et al.*, 2018; Fernández-Ruiz *et al.*, 2021). Congruent with this hypothesis, we found that mice with the *Id2*-induced circuits appeared to rely on local rather than global spatial cues when solving spatial problems (Luo et al., 2021).

Functional insights in the two further studies discussed in Chapter 3 and 4 remain possibly more elusive. In Chapter 3, I described a new recurrent mossy fiber circuit in which the target specificity was altered, whereas in Chapter 4, I described the formation of a new commissural circuit. In principle, both could significantly contribute to the generation of epileptic seizures, the investigation of which will be an important goal for future research. Finally, in Chapter 4, I also described a subpopulation of granule cells in the healthy brain, the commissural granule cells, which although are relatively infrequent, establish a direct excitatory connection between the two hippocampi. Also here, our ability to explain the physiological function of commissural granule cells remains speculative as most. As discussed in Chapter 4, attempts to uncover the role of commissural granule cells in health and disease would greatly benefit from a specific molecular access to this cell population.

Further considerations and outlook

As the above chapters and sections highlight, understanding the molecular mechanisms and harnessing the potentials of adult wiring is an outstanding challenge. Many insights presented in this thesis have been enabled by the transformative power of cutting-edge technologies, such as next-generation single cell sequencing and gene editing, which provide unprecedented access and control to the transcriptomic states and mechanisms of single neurons. Overall, the corollary of my findings is the hypothesis that there are specific molecular programs which can control wiring in adult neurons. However, such programs may be only in part transcriptional. It is likely that future research will delineate additional translational and post translational mechanisms and/or effectors that support adult wiring (Seng et al., 2022). Their identification may be enabled by future proteomic studies that can specifically assay the cell types undergoing further wiring. For known or presumed molecules involved, immunostaining may already provide a viable approach. However, a broader investigation of proteomic mechanisms and/or consequences of adult wiring will require more unbiased approaches. In the near future, this could be feasibly achieved by mass-spectroscopy analysis of dissected brain tissue containing the relevant cellular processes for further wiring, such as cell bodies and axons. Such a readout would not have the single cell resolution as for example single cell transcriptomics has, but could reliably report on differentially enriched proteins before and after wiring. In the future, these efforts may be significantly facilitated by eventual technological breakthroughs toward achieving single cell proteomics.

Chapter 6 - Concluding remarks

Over the last century, an incredible progress has been made toward understanding the structure and function of brain circuits. This progress was accelerated by several technological advances, starting from Golgi's black staining to next generation single cell sequencing and editing technologies, and beyond. However, it is also clear that the human endeavor "to understand the brain" – and ultimately ourselves – is still ongoing.

In my thesis, I aimed to provide the Reader with detailed insights into one area of brain research, which I find particularly exciting and to which I contributed the most: to understand wiring mechanisms in the adult brain. In contrast to developmental wiring, adult wiring has not been broadly considered and remain comparably less understood. I provided the Reader with several examples, including those from my own research, demonstrating different adult wiring phenotypes (Seng et al., 2021), already representing an extensive list. I envision that more detailed insights into structure and function of specific brain circuits will add many more examples to this list.

I foresee that the studying of adult brain wiring will make significant impact in two major domains. First, it provides us with a unique window through which to understand how brain circuits are regulated and maintained during the lifespan. These mechanisms are poorly understood at any stage of life, and feasibly altered by aging. Second, the knowledge of how specific circuits could be induced or circuit maintenance could be facilitated has the potential to significantly facilitate the development of new circuit therapy approaches for neurodevelopmental, neurological, neuropsychiatric disorders and repair after injury. Achieving either aims will require a significant effort and rigorous experimentation, similarly to the path leading to the knowledge we have today.

It fills me with an immense amount of gratitude that at least to the extent of the work I presented in this thesis I could contribute to the endeavor of understanding the brain. I hope that my results will prove to be a considerable step toward achieving the above goals and provide a solid foundation for future investigations following up on the mechanism, consequences, and potentials of adult brain wiring.

References

Adler, A.F., Cardoso, T., Nolbrant, S., Mattsson, B., Hoban, D.B., Jarl, U., Wahlestedt, J.N., Grealish, S., Björklund, A., & Parmar, M. (2019) hESC-Derived Dopaminergic Transplants Integrate into Basal Ganglia Circuitry in a Preclinical Model of Parkinson's Disease. *Cell Rep*, **28**, 3462-3473.e5.

Altman, J. (1962) Are new neurons formed in the brains of adult mammals? *Science (1979)*, **135**, 1127–1128.

Altman, J. (1963) Autoradiographic investigation of cell proliferation in the brains of rats and cats. *Anat Rec*, **145**, 573–591.

Amaral, D. (1978) A Golgi study of cell types in the hilar region of the hippocampus in the rat. *Wiley Online Library*, **182**, 851–914.

Amaral, D.G., Scharfman, H.E., & Lavenex, P. (2007) The dentate gyrus: fundamental neuroanatomical organization (dentate gyrus for dummies). *Prog Brain Res*, **163**.

Andersen, P., Bliss, T.V.P., & Skrede, K.K. (1971) Lamellar organization of hippocampal excitatory pathways. *Exp Brain Res*, **13**, 222–238.

Andersen, P., Morris, R., Amaral, D., Bliss, T., & O'Keefe, J. (2010) *The Hippocampus Book*, Oxford University Press.

Armstrong, W.E. (1995) Morphological and electrophysiological classification of hypothalamic supraoptic neurons. *Prog Neurobiol*, **47**, 291–339.

Azab, M., Stark, S.M., & Stark, C.E.L. (2014) Contributions of human hippocampal subfields to spatial and temporal pattern separation. *Hippocampus*, **24**, 293–302.

Bailey, C.H. & Chen, M. (1989) Structural plasticity at identified synapses during long-term memory in Aplysia. *J Neurobiol*, **20**, 356–372.

Bakker, A., Kirwan, C.B., Miller, M., & Stark, C.E.L. (2008) Pattern separation in the human hippocampal CA3 and dentate gyrus. *Science (1979)*, **319**, 1640–1642.

Baldwin, K.T. & Giger, R.J. (2015) Insights into the physiological role of CNS regeneration inhibitors. *Front Mol Neurosci*, **8**, 23.

Bandtlow, C.E. & Zimmermann, D.R. (2000) Proteoglycans in the developing brain: New conceptual insights for old proteins. *Physiol Rev*, **80**, 1267–1290.

Bareyre, F.M., Garzorz, N., Lang, C., Misgeld, T., Büning, H., & Kerschensteiner, M. (2011) In vivo imaging reveals a phase-Specific role of stat3 during central and peripheral nervous system axon regeneration. *Proc Natl Acad Sci U S A*, **108**, 6282–6287.

Benezra, R., Davis, R.L., Lockshon, D., Turner, D.L., & Weintraub, H. (1990) The protein Id: A negative regulator of helix-loop-helix DNA binding proteins. *Cell*, **61**, 49–59.

Bennett, S.H., Kirby, A.J., & Finnerty, G.T. (2018) Rewiring the connectome: Evidence and effects. *Neurosci Biobehav Rev*, **88**, 51–62.

Benowitz, L.I. & Carmichael, S.T. (2010) Promoting axonal rewiring to improve outcome after stroke. *Neurobiol Dis*, **37**, 259–266.

Berron, D., Schütze, H., Maass, A., Cardenas-Blanco, A., Kuijf, H.J., Kumaran, D., & Düzel, E. (2016) Strong Evidence for Pattern Separation in Human Dentate Gyrus. *Journal of Neuroscience*, **36**, 7569–7579.

Besusso, D., Schellino, R., Boido, M., Belloli, S., Parolisi, R., Conforti, P., Faedo, A., Cernigoj, M., Campus, I., Laporta, A., Bocchi, V.D., Murtaj, V., Parmar, M., Spaiardi, P., Talpo, F., Maniezzi, C., Toselli, M.G., Biella, G., Moresco, R.M., Vercelli, A., Buffo, A., & Cattaneo, E. (2020) Stem Cell-Derived Human Striatal Progenitors Innervate Striatal Targets and Alleviate Sensorimotor Deficit in a Rat Model of Huntington Disease. *Stem Cell Reports*, **14**, 876–891.

Biederer, T., Sara, Y., Mozhayeva, M., Atasoy, D., Liu, X., Kavalali, E.T., & Südhof, T.C. (2002) SynCAM, a synaptic adhesion molecule that drives synapse assembly. *Science (1979)*, **297**, 1525–1531.

Bixby, J.L. & Harris, W.A. (1991) Molecular mechanisms of axon growth and guidance. *Annu. Rev. Cell Bioi*, **7**, 1–7.

Blaabjerg, M. & Zimmer, J. (2007) The dentate mossy fibers: structural organization, development and plasticity. *Prog Brain Res*, **163**.

Bliss, T. V. & Lomo, T. (1973) Long-lasting potentiation of synaptic transmission in the dentate area of the anaesthetized rabbit following stimulation of the perforant path. *Wiley Online Library*, **232**, 331–356.

Botterill, J.J., Gerencer, K.J., Vinod, K.Y., Alcantara-Gonzalez, D., & Scharfman, H.E. (2021) Dorsal and ventral mossy cells differ in their axonal projections throughout the dentate gyrus of the mouse hippocampus. *Hippocampus*, **31**, 522–539.

Bregman, B.S., Kunkel-Bagden, E., Schnell, L., Dai, H.N., Gao, D., & Schwab, M.E. (1995) Recovery from spinal cord injury mediated by antibodies to neurite growth inhibitors. *Nature*, **378**, 498–501.

Briones, B.A., Pisano, T.J., Pitcher, M.N., Haye, A.E., Diethorn, E.J., Engel, E.A., Cameron, H.A., & Gould, E. (2021) Adult-born granule cell mossy fibers preferentially target parvalbumin-positive interneurons surrounded by perineuronal nets. *Hippocampus*, **31**, 375–388.

Buckmaster, P.S. (2012) Mossy Fiber Sprouting in the Dentate Gyrus. *Epilepsia*, **51**, 39.

Buckmaster, P.S. (2014) Does Mossy Fiber Sprouting Give Rise to the Epileptic State? *Adv. Exp. Med. Biol.*, **813**, 161–168.

Buckmaster, P.S., Strowbridge, B.W., Kunkel, D.D., Schmiege, D.L., & Schwartzkroin, P.A. (1992) Mossy cell axonal projections to the dentate gyrus molecular layer in the rat hippocampal slice. *Hippocampus*, **2**, 349–362.

Bui, A.D., Nguyen, T.M., Limouse, C., Kim, H.K., Szabo, G.G., Felong, S., Maroso, M., & Soltesz, I. (2018) Dentate gyrus mossy cells control spontaneous convulsive seizures and spatial memory. *Science (1979)*, **359**, 787–790.

Buzsáki, G. (1984) Feed-forward inhibition in the hippocampal formation. *Prog Neurobiol*, **22**, 131–153.

Cadwell, C.R., Palasantza, A., Jiang, X., Berens, P., Deng, Q., Yilmaz, M., Reimer, J., Shen, S., Bethge, M., Tolias, K.F., Sandberg, R., & Tolias, A.S. (2015) Electrophysiological, transcriptomic and morphologic profiling of single neurons using Patch-seq. *Nat Biotechnol*, **34**, 199–203.

Cadwell, C.R., Scala, F., Li, S., Livrizzi, G., Shen, S., Sandberg, R., Jiang, X., & Tolias, A.S. (2017) Multimodal profiling of single-cell morphology, electrophysiology, and gene expression using Patch-seq. *Nat Protoc*, **12**, 2531–2553.

Carlén, M., Cassidy, R.M., Brismar, H., Smith, G.A., Enquist, L.W., & Frisén, J. (2002) Functional Integration of Adult-Born Neurons. *Current Biology*, **12**, 606–608.

Carmichael, S., Wei, L., Rovainen, C.M., & Woolsey, T.A. (2001) New patterns of intracortical projections after focal cortical stroke. *Neurobiol Dis*, **8**, 910–922.

Carmichael, S.T., Kathirvelu, B., Schweppe, C.A., & Nie, E.H. (2017) Molecular, cellular and functional events in axonal sprouting after stroke. *Exp Neurol*, **287**, 384–394.

Caroni, P. & Schwab, M.E. (1988) Two membrane protein fractions from rat central myelin with inhibitory properties for neurite growth and fibroblast spreading. *Journal of Cell Biology*, **106**, 1281–1288.

Carr, V.A., Rissman, J., & Wagner, A.D. (2010) Imaging the Human Medial Temporal Lobe with High-Resolution fMRI. *Neuron*, **65**, 298–308.

Causey, G. & Hoffman, H. (1955) Axon sprouting partially deneurotized nerves. *Brain*, **78**, 661–668.

Cavarsan, C.F., Malheiros, J., Hamani, C., Najm, I., & Covolan, L. (2018) Is mossy fiber sprouting a potential therapeutic target for epilepsy? *Front Neurol*, **9**, 1–13.

Cenquizca, L.A. & Swanson, L.W. (2007) Spatial organization of direct hippocampal field CA1 axonal projections to the rest of the cerebral cortex. *Brain Res Rev*, **56**, 1–26.

Chen, M.S., Huber, a B., van der Haar, M.E., Frank, M., Schnell, L., Spillmann, a a, Christ, F., & Schwab, M.E. (2000) Nogo-A is a myelin-associated neurite outgrowth inhibitor and an antigen for monoclonal antibody IN-1. *Nature*, **403**, 434–439.

Christenson Wick, Z., Leintz, C.H., Xamonthiene, C., Huang, B.H., & Krook-Magnuson, E. (2017) Axonal sprouting in commissurally projecting parvalbumin-expressing interneurons. *J Neurosci Res*, **95**, 2336–2344.

Clelland, C.D., Choi, M., Romberg, C., Clemenson, G.D., Fragniere, A., Tyers, P., Jessberger, S., Saksida, L.M., Barker, R.A., Gage, F.H., & Bussey, T.J. (2009) A functional role for adult hippocampal neurogenesis in spatial pattern separation. *Science (1979)*, **325**, 210–213.

Cohen-Cory, S., Kidane, A.H., Shirkey, N.J., & Marshak, S. (2010) Brain-derived neurotrophic factor and the development of structural neuronal connectivity. *Dev Neurobiol*, **70**, 271–288.

Cole, J.D., Del Castillo, J.S., Gut, G., Gonzalez-Bohorquez, D., Pelkmans, L., & Jessberger, S. (2022) Characterization of the neurogenic niche in the aging dentate gyrus using iterative immunofluorescence imaging. *Elife*, **11**.

Connors, B.W. & Gutnick, M.J. (1990) Intrinsic firing patterns of diverse neocortical neurons. *Trends Neurosci*, **13**, 99–104.

Cook, T.M. & Crutcher, K.A. (1985) Extensive target cell loss during development results in mossy fibers in the regio superior (CA1) of the rat hippocampal formation. *Brain Res*, **353**, 19–30.

Darmanis, S., Sloan, S.A., Zhang, Y., Enge, M., Caneda, C., Shuer, L.M., Gephart, M.G.H., Barres, B.A., & Quake, S.R. (2015) A survey of human brain transcriptome diversity at the single cell level. *Proc Natl Acad Sci U S A*, **112**, 7285–7290.

De Carlos, J.A. & Borrell, J. (2007) A historical reflection of the contributions of Cajal and Golgi to the foundations of neuroscience. *Brain Res Rev*, **55**, 8–16.

De Wit, J. & Ghosh, A. (2015) Specification of synaptic connectivity by cell surface interactions. *Nat Rev Neurosci*, **17**, 4–4.

Deng, W., Aimone, J.B., & Gage, F.H. (2010) New neurons and new memories: how does adult hippocampal neurogenesis affect learning and memory? *Nat Rev Neurosci*, **11**, 339–350.

Denoth-Lippuner, A. & Jessberger, S. (2021) Formation and integration of new neurons in the adult hippocampus. *Nat Rev Neurosci*, **22**, 223–236.

Dergham, P., Ellezam, B., Essagian, C., Avedissian, H., Lubell, W.D., & McKerracher, L. (2002) Rho Signaling Pathway Targeted to Promote Spinal Cord Repair. *Journal of Neuroscience*, **22**, 6570–6577.

Dhar, M., Brenner, J.M., Sakimura, K., Kano, M., & Nishiyama, H. (2016) Spatiotemporal dynamics of lesion-induced axonal sprouting and its relation to functional architecture of the cerebellum. *Nat Commun*, **7**.

Dougherty, S.E., Kajstura, T.J., Jin, Y., Chan-Cortés, M.H., Kota, A., & Linden, D.J. (2020) Catecholaminergic axons in the neocortex of adult mice regrow following brain injury. *Exp Neurol*, **323**.

Drapeau, E., Mayo, W., Aurousseau, C., Le Moal, M., Piazza, P.V., & Abrous, D.N. (2003) Spatial memory performances of aged rats in the water maze predict levels of hippocampal neurogenesis. *Proceedings of the National Academy of Sciences*, **100**, 14385–14390.

Drew, L.J., Kheirbek, M.A., Luna, V.M., Denny, C.A., Cloidt, M.A., Wu, M. V., Jain, S., Scharfman, H.E., & Hen, R. (2016) Activation of local inhibitory circuits in the dentate gyrus by adult-born neurons. *Hippocampus*, **26**, 763–778.

Edds, M. V. & Small, W.T. (1951) The behavior of residual axons in partially denervated muscles of the monkey. *Journal of Experimental Medicine*, **93**, 207–215.

Egger, M., Luo, W., Cruz-Ochoa, N., Lukacsovich, D., Varga, C., Que, L., Maloveczky, G., Winterer, J., Kaur, R., Lukacsovich, T., & Földy, C. (2023) Commissural dentate granule cell projections and their rapid formation in the adult brain. *PNAS Nexus*, **2**.

El-Gaby, M., Shipton, O.A., & Paulsen, O. (2015) Synaptic Plasticity and Memory: Insights from Hippocampal LeftRight Asymmetries. *Neuroscientist*, **21**, 490–502.

Eyre, M.D. & Bartos, M. (2019) Somatostatin-Expressing Interneurons Form Axonal Projections to the Contralateral Hippocampus. *Front Neural Circuits*, **13**, 56.

Feng, G., Mellor, R.H., Bernstein, M., Keller-Peck, C., Nguyen, Q.T., Wallace, M., Nerbonne, J.M., Lichtman, J.W., & Sanes, J.R. (2000) Imaging Neuronal Subsets in Transgenic Mice Expressing Multiple Spectral Variants of GFP. *Neuron*, **28**, 41–51.

Fenno, L., Yizhar, O., & Deisseroth, K. (2011) The Development and Application of Optogenetics. *Annu Rev Neurosci*, **34**, 389–412.

Fernández, M.P., Berni, J., & Ceriani, M.F. (2008) Circadian remodeling of neuronal circuits involved in rhythmic behavior. *PLoS Biol*, **6**, 0518–0524.

Fernández-Ruiz, A., Oliva, A., Soula, M., Rocha-Almeida, F., Nagy, G.A., Martin-Vazquez, G., & Buzsáki, G. (2021) Gamma rhythm communication between entorhinal cortex and dentate gyrus neuronal assemblies. *Science (1979)*, **372**.

Filli, L. & Schwab, M.E. (2015) Structural and functional reorganization of propriospinal connections promotes functional recovery after spinal cord injury. *Neural Regen Res*, **10**, 509.

Fischer, I., Dulin, J.N., & Lane, M.A. (2020) Transplanting neural progenitor cells to restore connectivity after spinal cord injury. *Nat Rev Neurosci*, **21**, 366–383.

Földy, C., Aradi, I., Howard, A., & Soltesz, I. (2004) Diversity beyond variance: modulation of firing rates and network coherence by GABAergic subpopulations. *European Journal of Neuroscience*, **19**, 119–130.

Földy, C., Darmanis, S., Aoto, J., Malenka, R.C., Quake, S.R., & Südhof, T.C. (2016) Single-cell RNAseq reveals cell adhesion molecule profiles in

electrophysiologically defined neurons. *Proc Natl Acad Sci U S A*, **113**, E5222–E5231.

Földy, C., Malenka, R.C., & Südhof, T.C. (2013) Autism-associated neuroligin-3 mutations commonly disrupt tonic endocannabinoid signaling. *Neuron*, **78**, 498–509.

Freund, T.F. & Buzsáki, G. (1996) Interneurons of the Hippocampus. *Hippocampus*, **6**, 347–470.

Frotscher, M., Jonas, P., & Sloviter, R.S. (2006) Synapses formed by normal and abnormal hippocampal mossy fibers. *Cell Tissue Res*, **326**, 361–367.

Frotscher, M., Seress, L., Schwerdtfeger, W.K., & Buhl, E. (1991) The mossy cells of the fascia dentata: A comparative study of their fine structure and synaptic connections in rodents and primates. *Journal of Comparative Neurology*, **312**, 145–163.

Fu, Z., Washbourne, P., Ortinski, P., & Vicini, S. (2003) Functional excitatory synapses in HEK293 cells expressing neuroligin and glutamate receptors. *J Neurophysiol*, **90**, 3950–3957.

Fuzik, J., Zeisel, A., Mate, Z., Calvigioni, D., Yanagawa, Y., Szabo, G., Linnarsson, S., & Harkany, T. (2015) Integration of electrophysiological recordings with single-cell RNA-seq data identifies neuronal subtypes. *Nat Biotechnol*, **34**, 175–183.

Gaarskjaer, F.B., Danscher, G., & West, M.J. (1982) Hippocampal mossy fibers in the regio superior of the European hedgehog. *Brain Res*, **237**, 79–90.

Gage, F.H. (2000) Mammalian neural stem cells. *Science (1979)*, **287**, 1433–1438.

Gaillard, A., Decressac, M., Frappé, I., Fernagut, P.O., Prestoz, L., Besnard, S., & Jaber, M. (2009) Anatomical and functional reconstruction of the nigrostriatal pathway by intranigral transplants. *Neurobiol Dis*, **35**, 477–488.

Gaillard, A., Prestoz, L., Dumartin, B., Cantereau, A., Morel, F., Roger, M., & Jaber, M. (2007) Reestablishment of damaged adult motor pathways by grafted embryonic cortical neurons. *Nat Neurosci*, **10**, 1294–1299.

Gascón, S., Masserdotti, G., Russo, G.L., & Götz, M. (2017) Direct Neuronal Reprogramming: Achievements, Hurdles, and New Roads to Success. *Cell Stem Cell*, **21**, 18–34.

Gibson, D.A. & Ma, L. (2011) Developmental regulation of axon branching in the vertebrate nervous system. *Development*, **138**, 183–195.

Goodman, C.S. & Shatz, C.J. (1993) Developmental mechanisms that generate precise patterns of neuronal connectivity. *Cell*, **72**, 77–98.

Goodrich-Hunsaker, N.J., Hunsaker, M.R., & Kesner, R.P. (2008) The Interactions and Dissociations of the Dorsal Hippocampus Subregions: How the Dentate Gyrus, CA3, and CA1 Process Spatial Information. *Behavioral Neuroscience*, **122**, 16–26.

GoodSmith, D., Lee, H., Neunuebel, J.P., Song, H., & Knierim, J.J. (2019) Dentate Gyrus Mossy Cells Share a Role in Pattern Separation with Dentate Granule Cells and Proximal CA3 Pyramidal Cells. *Journal of neuroscience*, **39**, 9570–9584.

Gorostiza, E.A., Depetris-Chauvin, A., Frenkel, L., Pírez, N., & Ceriani, M.F. (2014) Circadian pacemaker neurons change synaptic contacts across the day. *Current biology*, **24**, 2161–2167.

Grienberger, C. & Konnerth, A. (2012) Imaging Calcium in Neurons. *Neuron*, **73**, 862–885.

Gut, G., Herrmann, M.D., & Pelkmans, L. (2018) Multiplexed protein maps link subcellular organization to cellular states. *Science (1979)*, **361**.

Hanchate, N.K., Kondoh, K., Lu, Z., Kuang, D., Ye, X., Qiu, X., Pachter, L., Trapnell, C., & Buck, L.B. (2015) Single-cell transcriptomics reveals receptor transformations during olfactory neurogenesis. *Science (1979)*, **350**, 1251–1255.

Harel, N.Y. & Strittmatter, S.M. (2006) Can regenerating axons recapitulate developmental guidance during recovery from spinal cord injury? *Nat Rev Neurosci*, **7**, 603–616.

Harris, J.A., Hirokawa, K.E., Sorensen, S.A., Gu, H., Mills, M., Ng, L.L., Bohn, P., Mortrud, M., Ouellette, B., Kidney, J., Smith, K.A., Dang, C., Sunkin, S., Bernard, A., Oh, S.W., Madisen, L., & Zeng, H. (2014) Anatomical characterization of Cre driver mice for neural circuit mapping and manipulation. *Front Neural Circuits*, **8**, 76.

Hjorth-Simonsen, A. (1972) Projection of the lateral part of the entorhinal area to the hippocampus and fascia dentata. *Journal of Comparative Neurology*, **146**, 219–231.

Holtmaat, A. & Svoboda, K. (2009) Experience-dependent structural synaptic plasticity in the mammalian brain. *Nat Rev Neurosci*, **10**, 647–658.

Horlbeck, M.A., Witkowsky, L.B., Guglielmi, B., Replogle, J.M., Gilbert, L.A., Villalta, J.E., Torigoe, S.E., Tjian, R., & Weissman, J.S. (2016) Nucleosomes impede cas9 access to DNA in vivo and in vitro. *Elife*, **5**.

Horner, P.J. & Gage, F.H. (2000) Regenerating the damaged central nervous system. *Nature*, **407**, 963–970.

Huang, J.Z. & Zeng, H. (2010) Short Hairpin RNA (shRNA): Design, Delivery, and Assessment of Gene Knockdown. *Methods in molecular biology*, **629**, 141.

Huang, J.Z. & Zeng, H. (2013) Genetic Approaches to Neural Circuits in the Mouse. *Annu Rev Neurosci*, **36**, 183–215.

Huang, Z., Liu, J., Jin, J., Chen, Q., Shields, L.B.E., Zhang, Y.P., Shields, C.B., Zhou, L., Zhou, B., & Yu, P. (2019) Inhibitor of DNA binding 2 promotes axonal growth through upregulation of Neurogenin2. *Exp Neurol*, **320**.

Innocenti, G.M. & Price, D.J. (2005) Exuberance in the development of cortical networks. *Nat Rev Neurosci*, **6**, 955–965.

Inoue, S., Yang, R., Tantry, A., Davis, C. ha, Yang, T., Knoedler, J.R., Wei, Y., Adams, E.L., Thombare, S., Golf, S.R., Neve, R.L., Tessier-Lavigne, M.,

Ding, J.B., & Shah, N.M. (2019) Periodic Remodeling in a Neural Circuit Governs Timing of Female Sexual Behavior. *Cell*, **179**, 1393–1408.

Isaac, R.S., Jiang, F., Doudna, J.A., Lim, W.A., Narlikar, G.J., & Almeida, R. (2016) Nucleosome breathing and remodeling constrain CRISPR-Cas9 function. *Elife*, **5**.

Ishizuka, N., Weber, J., & Amaral, D.G. (1990) Organization of intrahippocampal projections originating from CA3 pyramidal cells in the rat. *Journal of Comparative Neurology*, **295**, 580–623.

Jessberger, S., Clark, R.E., Broadbent, N.J., Clemenson, G.D., Consiglio, A., Lie, D.C., Squire, L.R., & Gage, F.H. (2009) Dentate gyrus-specific knockdown of adult neurogenesis impairs spatial and object recognition memory in adult rats. *Learning & Memory*, **16**, 147–154.

Kadoya, K., Tsukada, S., Lu, P., Coppola, G., Geschwind, D., Filbin, M.T., Blesch, A., & Tuszynski, M.H. (2009) Combined Intrinsic and Extrinsic Neuronal Mechanisms Facilitate Bridging Axonal Regeneration One Year after Spinal Cord Injury. *Neuron*, **64**, 165–172.

Kalil, K. & Dent, E.W. (2014) Branch management: mechanisms of axon branching in the developing vertebrate CNS. *Nat Rev Neurosci*, **15**, 7.

Kamiguchi, H. (2007) The role of cell adhesion molecules in axon growth and guidance. *Adv Exp Med Biol*, **621**, 95–103.

Kania, A. & Klein, R. (2016) Mechanisms of ephrin-Eph signalling in development, physiology and disease. *Nat Rev Mol Cell Biol*, **17**, 240–256.

Kaplan, M.S. (2001) Environment complexity stimulates visual cortex neurogenesis: death of a dogma and a research career. *Trends Neurosci*, **24**, 617–620.

Karlócai, M.R., Tóth, K., Watanabe, M., Ledent, C., Juhász, G., Freund, T.F., & Maglóczky, Z. (2011) Redistribution of CB1 Cannabinoid Receptors in the Acute and Chronic Phases of Pilocarpine-Induced Epilepsy. *PLoS One*, **6**, e27196.

Karmažínová, M. & Lacinová, L. (2010) Measurement of Cellular Excitability by Whole Cell Patch Clamp Technique. *Physiol. Res*, **59**, 1–7.

Katz, L.C. & Shatz, C.J. (1996) Synaptic activity and the construction of cortical circuits. *Science (1979)*, **274**, 1133–1138.

Katz-Sidlow, R.J. (1998) The Formulation of the Neuron Doctrine: The Island of Cajal. *Arch Neurol*, **55**, 237–240.

Kempermann, G., Kuhn, H.G., & Gage, F.H. (1997) More hippocampal neurons in adult mice living in an enriched environment. *Nature*, **386**, 493–495.

Kidd, T., Bland, K.S., & Goodman, C.S. (1999) Slit is the midline repellent for the Robo receptor in Drosophila. *Cell*, **96**, 785–794.

Klausberger, T., Magill, P.J., Márton, L.F., Roberts, J.D.B., Cobden, P.M., Buzsáki, G., & Somogyi, P. (2003) Brain-state- and cell-type-specific firing of hippocampal interneurons in vivo. *Nature*, **421**, 844–848.

Knierim, J.J., Neunuebel, J.P., & Deshmukh, S.S. (2014) Functional correlates of the lateral and medial entorhinal cortex: Objects, path integration and local - Global reference frames. *Phil. Trans. R. Soc. B*, **369**.

Ko, H.R., Kwon, I.S., Hwang, I., Jin, E.J., Shin, J.H., Brennan-Minnella, A.M., Swanson, R., Cho, S.W., Lee, K.H., & Ahn, J.Y. (2016) Akt1-inhibitor of DNA binding2 is essential for growth cone formation and axon growth and promotes central nervous system axon regeneration. *Elife*, **5**, 21.

Kohl, M.M., Shipton, O.A., Deacon, R.M., Rawlins, J.N.P., Deisseroth, K., & Paulsen, O. (2011) Hemisphere-specific optogenetic stimulation reveals left-right asymmetry of hippocampal plasticity. *Nat Neurosci*, **14**, 1413–1415.

Kolodkin, A.L. & Tessier-Lavigne, M. (2011) Mechanisms and molecules of neuronal wiring: a primer. *Cold Spring Harb Perspect Biol*, **3**, 1–14.

Komendantov, A.O., Venkadesh, S., Rees, C.L., Wheeler, D.W., Hamilton, D.J., & Ascoli, G.A. (2019) Quantitative firing pattern phenotyping of hippocampal neuron types. *Sci Rep*, **9**, 1–17.

Kondratov, O., Kondratova, L., Mandel, R.J., Coleman, K., Savage, M.A., Gray-Edwards, H.L., Ness, T.J., Rodriguez-Lebron, E., Bell, R.D., Rabinowitz, J., Gamlin, P.D., & Zolotukhin, S. (2021) A comprehensive study of a 29-capsid AAV library in a non-human primate central nervous system. *Molecular Therapy*, **29**, 2806–2820.

Kuffler, D.P. (1994) Promoting and directing axon outgrowth. *Mol Neurobiol*, **9**, 233–243.

Kühn, R. & Torres, R.M. (2002) Cre/loxP recombination system and gene targeting. *Methods in molecular biology*, **180**, 175–204.

Kullmann, D.M. (2011) Interneuron networks in the hippocampus. *Curr Opin Neurobiol*, **21**, 709–716.

Lacroix, S. & Tuszynski, M.H. (2000) Neurotrophic factors and gene therapy in spinal cord injury. *Neurorehabil Neural Repair*, **14**, 265–275.

Lacy, J.W., Yassa, M.A., Stark, S.M., Muftuler, L.T., & Stark, C.E.L. (2011) Distinct pattern separation related transfer functions in human CA3/dentate and CA1 revealed using high-resolution fMRI and variable mnemonic similarity. *Learning & Memory*, **18**, 15–18.

Lanahan, A. & Worley, P. (1998) Immediate-Early Genes and Synaptic Function. *Neurobiol Learn Mem*, **70**, 37–43.

Lasorella, A., Stegmüller, J., Guardavaccaro, D., Liu, G., Carro, M.S., Rothschild, G., De La Torre-Ubieta, L., Pagano, M., Bonni, A., & Iavarone, A. (2006) Degradation of Id2 by the anaphase-promoting complex couples cell cycle exit and axonal growth. *Nature*, **442**, 471–474.

Laurberg, S. & Zimmer, J. (1980) Aberrant hippocampal mossy fibers in cats. *Brain Res.*, **188**, 555–559.

Laurberg, S. & Zimmer, J. (1981) Lesion-induced sprouting of hippocampal mossy fiber collaterals to the fascia dentata in developing and adult rats. *Journal of Comparative Neurology*, **200**, 433–459.

Le Duigou, C., Simonnet, J., Teleñczuk, M.T., Fricker, D., & Miles, R. (2014) Recurrent synapses and circuits in the CA3 region of the hippocampus: An associative network. *Front Cell Neurosci*, **7**, 275.

Le Van Quyen, M., Bragin, A., Staba, R., Crépon, B., Wilson, C.L., & Engel, J. (2008) Cell Type-Specific Firing during Ripple Oscillations in the Hippocampal Formation of Humans. *Journal of Neuroscience*, **28**, 6104–6110.

Leal, S.L. & Yassa, M.A. (2018) Integrating new findings and examining clinical applications of pattern separation. *Nat Neurosci*, **21**, 163–173.

Lentini, C., d'Orange, M., Marichal, N., Trottmann, M.M., Vignoles, R., Foucault, L., Verrier, C., Massera, C., Raineteau, O., Conzelmann, K.K., Rival-Gervier, S., Depaulis, A., Berninger, B., & Heinrich, C. (2021) Reprogramming reactive glia into interneurons reduces chronic seizure activity in a mouse model of mesial temporal lobe epilepsy. *Cell Stem Cell*, **28**, 2104-2121.e10.

Leutgeb, J.K., Leutgeb, S., Moser, M.B., & Moser, E.I. (2007) Pattern separation in the dentate gyrus and CA3 of the hippocampus. *Science (1979)*, **315**, 961–966.

Lewicki, M.S. (1998) A review of methods for spike sorting: the detection and classification of neural action potentials. *Network: Computation in Neural Systems*, **9**, R53.

Lin, Y.C. & Koleske, A.J. (2010) Mechanisms of Synapse and Dendrite Maintenance and Their Disruption in Psychiatric and Neurodegenerative Disorders. *Annu Rev Neurosci*, **33**, 349.

Liu, C.N. & Chambers, W.W. (1958) Intraspinal Sprouting of Dorsal Root Axons: Development of New Collaterals and Preterminals Following Partial Denervation of the Spinal Cord in the Cat. *AMA Arch Neurol Psychiatry*, **79**, 46–61.

Liu, Q., Wu, Y., Wang, H., Jia, F., & Xu, F. (2022) Viral Tools for Neural Circuit Tracing. *Neurosci Bull*, **38**, 1508–1518.

Liu, Z., Li, Y., Zhang, Z.G., Cui, X., Cui, Y., Lu, M., Savant-Bhonsale, S., & Chopp, M. (2010) Bone marrow stromal cells enhance inter-and intracortical axonal connections after ischemic stroke in adult rats. *Journal of Cerebral Blood Flow & Metabolism*, **30**, 1288–1295.

Llinás, R.R. (2003) The contribution of Santiago Ramon y Cajal to functional neuroscience. *Nat Rev Neurosci*, **4**, 77–80.

Lu, P., Wang, Y., Graham, L., McHale, K., Gao, M., Wu, D., Brock, J., Blesch, A., Rosenzweig, E.S., Havton, L.A., Zheng, B., Conner, J.M., Marsala, M., & Tuszynski, M.H. (2012) Long-distance growth and connectivity of neural stem cells after severe spinal cord injury. *Cell*, **150**, 1264–1273.

Lu, P., Woodruff, G., Wang, Y., Graham, L., Hunt, M., Wu, D., Boehle, E., Ahmad, R., Poplawski, G., Brock, J., Goldstein, L.S.B., & Tuszynski, M.H. (2014) Long-Distance Axonal Growth from Human Induced Pluripotent Stem Cells after Spinal Cord Injury. *Neuron*, **83**, 789–796.

Lukacsovich, D., Winterer, J., Que, L., Luo, W., Lukacsovich, T., & Földy, C. (2019) Single-Cell RNA-Seq Reveals Developmental Origins and Ontogenetic Stability of Neurexin Alternative Splicing Profiles. *Cell Rep*, **27**, 3752–3759.

Luo, L., Callaway, E.M., & Svoboda, K. (2018) Genetic Dissection of Neural Circuits: A Decade of Progress. *Neuron*, **98**, 256–281.

Luo, W., Cruz-Ochoa, N.A., Seng, C., Egger, M., Lukacsovich, D., Lukacsovich, T., & Földy, C. (2022) Pcdh11x controls target specification of mossy fiber sprouting. *Front Neurosci*, **16**, 1362.

Luo, W., Egger, M., Domonkos, A., Que, L., Lukacsovich, D., Cruz-Ochoa, N.A., Szőcs, S., Seng, C., Arszovszki, A., Sipos, E., Amrein, I., Winterer, J., Lukacsovich, T., Szabadics, J., Wolfer, D.P., Varga, C., & Földy, C. (2021) Recurrent rewiring of the adult hippocampal mossy fiber system by a single transcriptional regulator, Id2. *Proc Natl Acad Sci U S A*, **118**.

Lüthi, A. & Lüscher, C. (2014) Pathological circuit function underlying addiction and anxiety disorders. *Nat Neurosci*, **17**, 1635–1643.

Maccaferri, G. & Lacaille, J.C. (2003) Interneuron Diversity series: Hippocampal interneuron classifications – making things as simple as possible, not simpler. *Trends Neurosci*, **26**, 564–571.

Madisen, L., Zwingman, T.A., Sunkin, S.M., Oh, S.W., Zariwala, H.A., Gu, H., Ng, L.L., Palmiter, R.D., Hawrylycz, M.J., Jones, A.R., Lein, E.S., & Zeng, H. (2009) A robust and high-throughput Cre reporting and characterization system for the whole mouse brain. *Nat Neurosci*, **13**, 133–140.

Marchionni, I., Oberoi, M., Soltesz, I., & Alexander, A. (2019) Ripple-related firing of identified deep CA1 pyramidal cells in chronic temporal lobe epilepsy in mice. *Epilepsia Open*, **4**, 254–263.

Markakis, E.A. & Gage, F.H. (1999) Adult-Generated Neurons in the Dentate Gyrus Send Axonal Projections to Field CA 3 and Are Surrounded by Synaptic Vesicles. *J. Comp. Neurol*, **406**, 449–460.

Marr, D. (1971) Simple memory: a theory for archicortex. *Philosophical transactions of the Royal Society of London. Series B*, **262**, 23–81.

McCouch, G.P., Austin, G.M., & Liu, C.N. (1958) Sprouting as a cause of spasticity. *J Neurophysiol*, **21**, 205–216.

McHugh, T.J., Jones, M.W., Quinn, J.J., Balthasar, N., Coppari, R., Elmquist, J.K., Lowell, B.B., Fanselow, M.S., Wilson, M.A., & Tonegawa, S. (2007) Dentate gyrus NMDA receptors mediate rapid pattern separation in the hippocampal network. *Science (1979)*, **317**, 94–99.

McNaughton, B.L., Barnes, C.A., Meltzer, J., & Sutherland, R.J. (1989) Hippocampal granule cells are necessary for normal spatial learning but not for spatially-selective pyramidal cell discharge. *Exp Brain Res*, **76**, 485–496.

McTighe, S.M., Mar, A.C., Romberg, C., Bussey, T.J., & Saksida, L.M. (2009) A new touchscreen test of pattern separation: Effect of hippocampal lesions. *Neuroreport*, **20**, 881–885.

Meyer, M.P. & Smith, S.J. (2006) Evidence from In Vivo Imaging That Synaptogenesis Guides the Growth and Branching of Axonal Arbors by Two Distinct Mechanisms.

Migliore, M. & Shepherd, G.M. (2005) An integrated approach to classifying neuronal phenotypes. *Nat Rev Neurosci*, **6**, 810–818.

Missler, M., Südhof, T.C., & Biederer, T. (2012) Synaptic Cell Adhesion. *Cold Spring Harb Perspect Biol*, **4**, a005694.

Mitchison, T. & Kirschner, M. (1988) Cytoskeletal dynamics and nerve growth. *Neuron*, **1**, 761–772.

Mombaerts, P., Wang, F., Dulac, C., Chao, S.K., Nemes, A., Mendelsohn, M., Edmondson, J., & Axel, R. (1996) Visualizing an Olfactory Sensory Map. *Cell*, **87**, 675–686.

Moreland, T. & Poulain, F.E. (2022) To Stick or Not to Stick: The Multiple Roles of Cell Adhesion Molecules in Neural Circuit Assembly. *Front Neurosci*, **16**, 552.

Moser, E.I., Moser, M.B., & McNaughton, B.L. (2017) Spatial representation in the hippocampal formation: a history. *Nat Neurosci*, **20**, 1448–1464.

Naber, P.A., Lopes Da Silva, F.H., & Witter, M.P. (2001) Reciprocal connections between the entorhinal cortex and hippocampal fields CA1 and the subiculum are in register with the projections from CA1 to the subiculum. *Hippocampus*, **11**, 99–104.

Nakashiba, T., Cushman, J.D., Pelkey, K.A., Renaudineau, S., Buhl, D.L., McHugh, T.J., Barrera, V.R., Chittajallu, R., Iwamoto, K.S., McBain, C.J., Fanselow, M.S., & Tonegawa, S. (2012a) Young Dentate Granule Cells Mediate Pattern Separation, whereas Old Granule Cells Facilitate Pattern Completion. *Cell*, **149**, 188–201.

Nakashiba, T., Cushman, J.D., Pelkey, K.A., Renaudineau, S., Buhl, D.L., McHugh, T.J., Barrera, V.R., Chittajallu, R., Iwamoto, K.S., McBain, C.J., Fanselow, M.S., & Tonegawa, S. (2012b) Young dentate granule cells mediate pattern separation, whereas old granule cells facilitate pattern completion. *Cell*, **149**, 188–201.

Nassi, J.J., Cepko, C.L., Born, R.T., & Beier, K.T. (2015) Neuroanatomy goes viral! *Front Neuroanat*, **9**, 80.

Navabpour, S., Kwapis, J.L., & Jarome, T.J. (2020) A neuroscientist's guide to transgenic mice and other genetic tools. *Neurosci Biobehav Rev*, **108**, 732–748.

Niell, C.M., Meyer, M.P., & Smith, S.J. (2004) In vivo imaging of synapse formation on a growing dendritic arbor. *Nat Neurosci*, **7**, 254–260.

Noebels, J.L., Avoli, M., Rogawski, M.A., Olsen, R.W., & Delgado-Escueta, A. V (2012) *Jasper's Basic Mechanisms of the Epilepsies*, 4th Edition. edn, Marine Renewable Energy Guides Series. National Center for Biotechnology Information (US), Bethesda (MD).

Norton, J.D. (2000) ID helix-loop-helix proteins in cell growth, differentiation and tumorigenesis. *J Cell Sci*, **113**, 3897–3905.

O'Keefe, J. & Dostrovsky, J. (1971) The hippocampus as a spatial map. Preliminary evidence from unit activity in the freely-moving rat. *Brain Res*, **34**, 171–175.

Onesto, M.M., Short, C.A., Rempel, S.K., Catlett, T.S., & Gomez, T.M. (2021) Growth Factors as Axon Guidance Molecules: Lessons From in vitro Studies. *Front Neurosci*, **15**, 579.

Osten, P. & Margrie, T.W. (2013) Mapping brain circuitry with a light microscope. *Nat Methods*, **10**, 515–523.

Owji, S. & Shoja, M.M. (2020) The History of Discovery of Adult Neurogenesis. *Clinical Anatomy*, **33**, 41–55.

Pelkey, K.A., Chittajallu, R., Craig, M.T., Tricoire, L., Wester, J.C., & McBain, C.J. (2017) Hippocampal GABAergic Inhibitory Interneurons. *Physiol Rev*, **97**, 1619–1747.

Peng, Z., Zhang, N., Wei, W., Huang, C.S., Cetina, Y., Otis, T.S., & Houser, C.R. (2013) A Reorganized GABAergic Circuit in a Model of Epilepsy: Evidence from Optogenetic Labeling and Stimulation of Somatostatin Interneurons. *Journal of Neuroscience*, **33**, 14392–14405.

Penttonen, M., Kamondi, A., Sik, A., Acsády, L., & Buzsáki, G. (1997) Feed-Forward and Feed-Back Activation of the Dentate Gyrus In Vivo During Dentate Spikes and Sharp Wave Bursts. *Hippocampus*, **7**, 437–450.

Perez, Y., Morin, F., Beaulieu, C., & Lacaille, J.-C. (1996) Axonal Sprouting of CA1 Pyramidal Cells in Hyperexcitable Hippocampal Slices of Kainate-treated Rats. *European Journal of Neuroscience*, **8**, 736–748.

Pernet, V., Joly, S., Jordi, N., Dalkara, D., Guzik-Kornacka, A., Flannery, J.G., & Schwab, M.E. (2013) Misguidance and modulation of axonal regeneration by Stat3 and Rho/ROCK signaling in the transparent optic nerve. *Cell Death Dis*, **4**.

Petsakou, A., Sapsis, T.P., & Blau, J. (2015) Circadian Rhythms in Rho1 Activity Regulate Neuronal Plasticity and Network Hierarchy. *Cell*, **162**, 823–835.

Pilz, G.A., Bottes, S., Betizeau, M., Jörg, D.J., Carta, S., Simons, B.D., Helmchen, F., & Jessberger, S. (2018) Live imaging of neurogenesis in the adult mouse hippocampus. *Science (1979)*, **359**, 658–662.

Pollerberg, G.E., Thelen, K., Theiss, M.O., & Hochlehnert, B.C. (2013) The role of cell adhesion molecules for navigating axons: Density matters. *Mech Dev*, **130**, 359–372.

Polleux, F., Giger, R.J., Ginty, D.D., Kolodkin, A.L., & Ghosh, A. (1998) Patterning of cortical efferent projections by semaphorin-neuropilin interactions. *Science (1979)*, **282**, 1904–1906.

Poulin, J.F., Tasic, B., Hjerling-Leffler, J., Trimarchi, J.M., & Awatramani, R. (2016) Disentangling neural cell diversity using single-cell transcriptomics. *Nat Neurosci*, **19**, 1131–1141.

Purves, D. & Lichtman, J.W. (1980) Elimination of Synapses in the Developing Nervous System. *Science (1979)*, **210**, 153–157.

Qian, H., Kang, X., Hu, J., Zhang, D., Liang, Z., Meng, F., Zhang, X., Xue, Y., Maimon, R., Dowdy, S.F., Devaraj, N.K., Zhou, Z., Mobley, W.C., Cleveland, D.W., & Fu, X.D. (2020) Reversing a model of Parkinson's disease with in situ converted nigral neurons. *Nature*, **582**, 550–556.

Qiao, Q., Ma, L., Li, W., Tsai, J.W., Yang, G., & Gan, W.B. (2016) Long-term stability of axonal boutons in the mouse barrel cortex. *Dev Neurobiol*, **76**, 252–261.

Que, L., Lukacsovich, D., Luo, W., & Földy, C. (2021) Transcriptional and morphological profiling of parvalbumin interneuron subpopulations in the mouse hippocampus. *Nat Commun*, **12**, 1–15.

Que, L., Winterer, J., & Földy, C. (2019) Deep survey of GABAergic interneurons: Emerging insights from gene-isoform transcriptomics. *Front Mol Neurosci*, **12**, 115.

Ramón y Cajal, S. (1888a) Estructura de los centros nerviosos de las aves. *Rev. Trimest. Histol. Norm. Patol*, **2**, 11–16a.

Ramón y Cajal, S. (1888b) Sobre las fibras nerviosas de la capamolecular del cerebelo. *Rev. Trimest. Histol. Norm. Patol.*, **2**, 33–49.

Ramón y Cajal, S. (1890a) A quelle époque apparaissent les expansions des cellules nerveuses de la möelle épinière du poulet?. *Anat Anz*, **21**, 609–613.

Ramón y Cajal, S. (1890b) Sobre la aparición de las expansiones celulares en la médula embrionaria. *Gaceta Sanitaria de Barcelona*, **12**, 413–419.

Ramón y Cajal, S. (1893) La Rétine des vertébrés... *Cellule*, **9**.

Ramón y Cajal, S. (1898) Estructura del kiasma óptico y teoría general de los entrecruzamientos de las vías nerviosas. *Rev. Trim. Micrográfica*, **3**.

Ramón y Cajal, S. (1914) Estudios sobre la degeneración y regeneración del sistema nervioso. *Hijos de Nicolás Moza*,.

Ramón y Cajal, S. (1928) Degeneration and regeneration of the nervous system. *Clarendon Press*,.

Ramón y Cajal, S. (1933) Nêuronismo o reticularismo? Las pruebas objetivas de la unidad anatómica de la celulas nerviosas. *Arch. Neurobiol.*, **13**, 217–291.

Rao, D.D., Vorhies, J.S., Senzer, N., & Nemunaitis, J. (2009) siRNA vs. shRNA: Similarities and differences. *Adv Drug Deliv Rev*, **61**, 746–759.

Raviola, E. & Mazzarello, P. (2011) The diffuse nervous network of Camillo Golgi: Facts and fiction. *Brain Res Rev*, **66**, 75–82.

Ribak, C.E., Seress, L., & Amaral, D.G. (1985) The development, ultrastructure and synaptic connections of the mossy cells of the dentate gyrus. *J Neurocytol*, **14**, 835–857.

Ribeiro, L.F., Verpoort, B., & de Wit, J. (2018) Trafficking mechanisms of synaptogenic cell adhesion molecules. *Mol Cell Neurosci*, **91**, 34–47.

Roy, R., Materi-als, N., Komarneni, S., Parker, J.C., Thomas, G.J., Schmidt, W.G., Huber, C.A., Huber, T.E., Appl Phys, J., Borrelli, N.F., Luong, J.C., Spie, P., Justus, B.L., Tonucci, R.J., Berry, A.D., Aspnes, D.E., Heller, A., Porter, J.D., Diggle, J.W., Downie, T.C., Goulding, C.W., Electrochem Soc, J., Martin, Y., Abraham, D.W., Wickramasinghe, H.K., Phys Lett, A., Stern, J.E., Terris, B.D., Maimin, H.J., Rugar, D., Chalfie, M., Tu, Y., Euskirchen, G., Ward, W.W., & Prasherf, D.C. (1994) Green Fluorescent Protein as a Marker for Gene Expression. *Science (1979)*, **263**, 802–805.

Sahay, A., Scobie, K.N., Hill, A.S., O'Carroll, C.M., Kheirbek, M.A., Burghardt, N.S., Fenton, A.A., Dranovsky, A., & Hen, R. (2011) Increasing adult hippocampal neurogenesis is sufficient to improve pattern separation. *Nature*, **472**, 466–470.

Salin, P., Tseng, G.F., Hoffman, S., Parada, I., & Prince, D.A. (1995) Axonal sprouting in layer V pyramidal neurons of chronically injured cerebral cortex. *Journal of Neuroscience*, **15**, 8234–8245.

Sanes, J.R. (1989) Extracellular matrix molecules thata influence neural development. *Ann. Rev. Neurosci.*, **12**, 516.

Sanes, J.R. & Zipursky, S. (2020) Synaptic Specificity, Recognition Molecules, and Assembly of Neural Circuits. *Cell*, **181**, 536–556.

Sanes, J.R. & Zipursky, S.L. (2010) Design Principles of Insect and Vertebrate Visual Systems. *Neuron*, **66**, 15–36.

Schaffer, K. (1892) Beitrag zur Histologie der Ammonshornformation. *Arch. Mikr. Anat.*, **39**, 611–632.

Scharfman, H.E. (1994) Evidence from simultaneous intracellular recordings in rat hippocampal slices that area CA3 pyramidal cells innervate dentate hilar mossy cells. *J Neurophysiol*, **72**, 2167–2180.

Scharfman, H.E. (2007) The CA3 "Backprojection" to the Dentate Gyrus. *Prog Brain Res*, **163**, 627.

Scharfman, H.E. & Myers, C.E. (2012) Hilar mossy cells of the dentate gyrus: A historical perspective. *Front Neural Circuits*, **6**, 106.

Schauwecker, P.E., Cheng, H.W., Serquinia, R.M.P., Mori, N., & McNeill, T.H. (1995) Lesion-induced sprouting of commissural/associational axons and induction of GAP-43 mRNA in hilar and CA3 pyramidal neurons in the hippocampus are diminished in aged rats. *Journal of Neuroscience*, **15**, 2462–2470.

Scheiffele, P. (2003) Cell-cell signaling during synapse formation in the CNS. *Annu Rev Neurosci*, **26**, 485–508.

Scheiffele, P., Fan, J., Choih, J., Fetter, R., & Serafini, T. (2000) Neuroligin expressed in nonneuronal cells triggers presynaptic development in contacting axons. *Cell*, **101**, 657–669.

Schmidt, H. & Rathjen, F.G. (2010) Signalling mechanisms regulating axonal branching in vivo. *BioEssays*, **32**, 977–985.

Schwab, M.E. (2002) Repairing the injured spinal cord. *Science (1979)*, **295**, 1029–1031.

Schwab, M.E. (2004) Nogo and axon regeneration. *Curr Opin Neurobiol*, **14**, 118–124.

Schwab, M.E. (2010) Functions of Nogo proteins and their receptors in the nervous system. *Nat Rev Neurosci*, **11**, 799–811.

Schwab, M.E., Kapfhammer, J.P., & Bandtlow, C.E. (1993) Inhibitors of Neurite Growth. *Annu. Rev. Neurosci.*, **16**, 565–595.

Seeger, M., Tear, G., Ferres-Marco, D., & Goodman, C.S. (1993) Mutations affecting growth cone guidance in drosophila: Genes necessary for guidance toward or away from the midline. *Neuron*, **10**, 409–426.

Seng, C., Luo, W., & Földy, C. (2022) Circuit formation in the adult brain. *European Journal of Neuroscience*, **56**, 4187–4213.

Sharp, K.G., Yee, K.M., & Steward, O. (2014) A re-assessment of long distance growth and connectivity of neural stem cells after severe spinal cord injury. *Exp Neurol*, **257**, 186–204.

Shen, K. & Bargmann, C.I. (2003) The immunoglobulin superfamily protein SYG-1 determines the location of specific synapses in C. elegans. *Cell*, **112**, 619–630.

Shen, K. & Cowan, C.W. (2010) Guidance Molecules in Synapse Formation and Plasticity. *Cold Spring Harb Perspect Biol*, **2**, 1842–1843.

Shen, K., Fetter, R.D., & Bargmann, C.I. (2004) Synaptic specificity is generated by the synaptic guidepost protein SYG-2 and its receptor, SYG-1. *Cell*, **116**, 869–881.

Sheng, M. & Greenberg, M.E. (1990) The regulation and function of c-fos and other immediate early genes in the nervous system. *Neuron*, **4**, 477–485.

Sherman, D.L. & Brophy, P.J. (2005) Mechanisms of axon ensheathment and myelin growth. *Nat Rev Neurosci*, **6**, 683–690.

Shibata, A., Wright, M. V., David, S., McKerracher, L., Braun, P.E., & Kater, S.B. (1998) Unique Responses of Differentiating Neuronal Growth Cones to Inhibitory Cues Presented by Oligodendrocytes. *J Cell Biol*, **142**, 191.

Shinohara, Y., Hirase, H., Watanabe, M., Itakura, M., Takahashi, M., & Shigemoto, R. (2008) Left-right asymmetry of the hippocampal synapses with differential subunit allocation of glutamate receptors. *Proc Natl Acad Sci U S A*, **105**, 19498–19503.

Shinohara, Y., Hosoya, A., Yahagi, K., Ferecskó, A.S., Yaguchi, K., Sík, A., Itakura, M., Takahashi, M., & Hirase, H. (2012) Hippocampal CA3 and CA2

have distinct bilateral innervation patterns to CA1 in rodents. *European Journal of Neuroscience*, **35**, 702–710.

Shipton, O.A., El-Gaby, M., Apergis-Schoute, J., Deisseroth, K., Bannerman, D.M., Paulsen, O., & Kohl, M.M. (2014) Left-right dissociation of hippocampal memory processes in mice. *Proc Natl Acad Sci U S A*, **111**, 15238–15243.

Shors, T.J., Miesegaes, G., Beylin, A., Zhao, M., Rydel, T., & Gould, E. (2001) Neurogenesis in the adult is involved in the formation of trace memories. *Nature*, **410**, 372–376.

Siddiqui, A.H. & Joseph, S.A. (2005) CA3 axonal sprouting in kainate-induced chronic epilepsy. *Brain Res*, **1066**, 129–146.

Sierra, A., Encinas, J.M., Deudero, J.J.P., Chancey, J.H., Enikolopov, G., Overstreet-Wadiche, L.S., Tsirka, S.E., & Maletic-Savatic, M. (2010) Microglia shape adult hippocampal neurogenesis through apoptosis-coupled phagocytosis. *Cell Stem Cell*, **7**, 483–495.

Smith, B.N. & Dudek, F.E. (2001) Short- and long-term changes in CA1 network excitability after kainate treatment in rats. *J Neurophysiol*, **85**, 1–9.

Somogyi, P. & Klausberger, T. (2005) Defined types of cortical interneurone structure space and spike timing in the hippocampus. *J Physiol*, **562**, 9–26.

Song, B.J., Sharp, S.J., & Rogulja, D. (2021) Daily rewiring of a neural circuit generates a predictive model of environmental light. *Sci Adv*, **7**.

Sperry, R.W. (1963) Chemo affinity in the orderly growth of nerve fiber patterns and connections. *Proc Natl Acad Sci U S A*, **50**, 703.

Squire, L.R. (2009) The Legacy of Patient H.M. for Neuroscience. *Neuron*, **61**, 6.

Squire, L.R., Berg, D., Bloom, F.E., Du Lac, S., Ghosh, A., & Spitzer, N.C. (2012) Fundamental Neuroscience: Fourth Edition. *Fundamental Neuroscience: Fourth Edition*, 1–1127.

Stanfield, B.B. & Trice, J.E. (1988) Evidence that granule cells generated in the dentate gyrus of adult rats extend axonal projections. *Exp Brain Res*, **72**, 399–406.

Steinbeck, J.A., Choi, S.J., Mrejeru, A., Ganat, Y., Deisseroth, K., Sulzer, D., Mosharov, E. V., & Studer, L. (2015) Optogenetics enables functional analysis of human embryonic stem cell-derived grafts in a Parkinson's disease model. *Nat Biotechnol*, **33**, 204–209.

Steinbeck, J.A., Koch, P., Derouiche, A., & Brüstle, O. (2012) Human embryonic stem cell-derived neurons establish region-specific, long-range projections in the adult brain. *Cellular and molecular life sciences*, **69**, 461–470.

Sternson, S.M. (2013) Hypothalamic Survival Circuits: Blueprints for Purposive Behaviors. *Neuron*, **77**, 810–824.

Steward, O. (1992) Lesion-induced synapse reorganization in the hippocampus of cats: Sprouting of entorhinal, commissural/associational, and mossy fiber projections after unilateral entorhinal cortex lesions, with comments on the normal organization of these pathways. *Hippocampus*, **2**, 247–268.

Steward, O. & Scoville, S.A. (1976) Cells of origin of entorhinal cortical afferents to the hippocampus and fascia dentata of the rat. *Journal of Comparative Neurology*, **169**, 347–370.

Stiles, J. & Jernigan, T.L. (2010) The Basics of Brain Development. *Neuropsychol Rev*, **20**, 327.

Stoeckli, E.T. (2018) Understanding axon guidance: are we nearly there yet? *Development*, **145**.

Südhof, T.C. (2017) Synaptic Neurexin Complexes: A Molecular Code for the Logic of Neural Circuits. *Cell*, **171**, 745–769.

Südhof, T.C. (2018) Towards an Understanding of Synapse Formation. *Neuron*, **100**, 276–293.

Südhof, T.C. (2021) The cell biology of synapse formation. *Journal of Cell Biology*, **220**.

Sugino, K., Hempel, C.M., Miller, M.N., Hattox, A.M., Shapiro, P., Wu, C., Huang, Z.J., & Nelson, S.B. (2005) Molecular taxonomy of major neuronal classes in the adult mouse forebrain. *Nat Neurosci*, **9**, 99–107.

Sun, F., Park, K.K., Belin, S., Wang, D., Lu, T., Chen, G., Zhang, K., Yeung, C., Feng, G., Yankner, B.A., & He, Z. (2011) Sustained axon regeneration induced by co-deletion of PTEN and SOCS3. *Nature*, **480**, 372–375.

Sun, G.J., Sailor, K.A., Mahmood, Q.A., Chavali, N., Christian, K.M., Song, H., & Ming, G.L. (2013) Seamless Reconstruction of Intact Adult-Born Neurons by Serial End-Block Imaging Reveals Complex Axonal Guidance and Development in the Adult Hippocampus. *Journal of Neuroscience*, **33**, 11400–11411.

Sun, Y., Chen, X., & Xiao, D. (2007) Tetracycline-inducible Expression Systems: New Strategies and Practices in the Transgenic Mouse Modeling. *Acta Biochim Biophys Sin (Shanghai)*, **39**, 235–246.

Sutula, T., Xiao-Xian, H., Cavazos, J., & Scott, G. (1988) Synaptic reorganization in the hippocampus induced by abnormal functional activity. *Science (1979)*, **239**, 1147–1150.

Swan, A.A., Clutton, J.E., Chary, P.K., Cook, S.G., Liu, G.G., & Drew, M.R. (2014) Characterization of the role of adult neurogenesis in touch-screen discrimination learning. *Hippocampus*, **24**, 1581–1591.

Swanson, L.W. & Cowan, W.M. (1977) An autoradiographic study of the organization of the efferent connections of the hippocampal formation in the rat. *J Comp Neurol*, **172**, 49–84.

Swanson, L.W., Sawchenko, P.E., & Cowan, W.M. (1981) Evidence for collateral projections by neurons in Ammon's horn, the dentate gyrus, and the subiculum: a multiple retrograde labeling study in the rat. *The Journal of Neuroscience*, **1**, 548.

Sytnyk, V., Leshchyns'ka, I., Delling, M., Dityateva, G., Dityatev, A., & Schachner, M. (2002) Neural cell adhesion molecule promotes accumulation of TGN organelles at sites of neuron-to-neuron contacts. *J Cell Biol*, **159**, 649–661.

Tauck, D.L. & Nadler, J. V. (1985) Evidence of functional mossy fiber sprouting in hippocampal formation of kainic acid-treated rats. *Journal of Neuroscience*, **5**, 1016–1022.

Tessier-Lavigne, M. & Goodman, C.S. (1996) The molecular biology of axon guidance. *Science (1979)*, **274**, 1123–1133.

Tessier-Lavigne, M. & Placzek, M. (1991) Target attraction: Are developing axons guided by chemotropism? *Trends Neurosci*, **14**, 303–310.

Tessier-Lavigne, M., Placzek, M., Lumsden, A.G.S., Dodd, J., & Jessell, T.M. (1988) Chemotropic guidance of developing axons in the mammalian central nervous system. *Nature*, **336**, 775–778.

Thompson, L.H., Grealish, S., Kirik, D., & Björklund, A. (2009) Reconstruction of the nigrostriatal dopamine pathway in the adult mouse brain. *Eur J Neurosci*, **30**, 625–638.

Tolman, E.C. (1948) Cognitive maps in rats and men. *Psychol Rev*, **55**, 189–208.

Toni, N., Teng, E.M., Bushong, E.A., Aimone, J.B., Zhao, C., Consiglio, A., Van Praag, H., Martone, M.E., Ellisman, M.H., & Gage, F.H. (2007) Synapse formation on neurons born in the adult hippocampus. *Nat Neurosci*, **10**, 727–734.

Tornero, D., Tsupykov, O., Granmo, M., Rodriguez, C., Grønning-Hansen, M., Thelin, J., Smozhanik, E., Laterza, C., Wattananit, S., Ge, R., Tatarishvili, J., Grealish, S., Brüstle, O., Skibo, G., Parmar, M., Schouenborg, J., Lindvall, O., & Kokaia, Z. (2017) Synaptic inputs from stroke-injured brain to grafted human stem cell-derived neurons activated by sensory stimuli. *Brain*, **140**, 692–706.

Tornero, D., Wattananit, S., Madsen, M.G., Koch, P., Wood, J., Tatarishvili, J., Mine, Y., Ge, R., Monni, E., Devaraju, K., Hevner, R.F., Brüstle, O., Lindvall, O., & Kokaia, Z. (2013) Human induced pluripotent stem cell-derived cortical neurons integrate in stroke-injured cortex and improve functional recovery. *Brain*, **136**, 3561–3577.

Torper, O., Pfisterer, U., Wolf, D.A., Pereira, M., Lau, S., Jakobsson, J., Björklund, A., Grealish, S., & Parmar, M. (2013) Generation of induced neurons via direct conversion in vivo. *Proc Natl Acad Sci U S A*, **110**, 7038–7043.

Trinchero, M.F., Herrero, M., Monzón-Salinas, M.C., & Schinder, A.F. (2019) Experience-dependent structural plasticity of adult-born neurons in the aging hippocampus. *Front Neurosci*, **13**, 739.

Tuszynski, M.H. & Steward, O. (2012) Concepts and methods for the study of axonal regeneration in the CNS. *Neuron*, **74**, 777–791.

Tycko, J., Hess, G.T., Jeng, E.E., Dubreuil, M., & Bassik, M.C. (2017) The expanding CRISPR toolbox. *Nature*, 2017.

Uddin, F., Rudin, C.M., & Sen, T. (2020) CRISPR Gene Therapy: Applications, Limitations, and Implications for the Future. *Front Oncol*, **10**, 1387.

Ueda, H.R., Dodt, H.U., Osten, P., Economo, M.N., Chandrashekar, J., & Keller, P.J. (2020) Whole-Brain Profiling of Cells and Circuits in Mammals by Tissue Clearing and Light-Sheet Microscopy. *Neuron*, **106**, 369–387.

Usoskin, D., Furlan, A., Islam, S., Abdo, H., Lönnerberg, P., Lou, D., Hjerling-Leffler, J., Haeggström, J., Kharchenko, O., Kharchenko, P. V., Linnarsson, S., & Ernfors, P. (2014) Unbiased classification of sensory neuron types by large-scale single-cell RNA sequencing. *Nat Neurosci*, **18**, 145–153.

Van Groen, T. & Wyss, J.M. (1990) Extrinsic projections from area CA1 of the rat hippocampus: Olfactory, cortical, subcortical, and bilateral hippocampal formation projections. *Journal of Comparative Neurology*, **302**, 515–528.

Van Praag, H., Kempermann, G., & Gage, F.H. (1999) Running increases cell proliferation and neurogenesis in the adult mouse dentate gyrus. *Nat Neurosci*, **2**, 266–270.

Van Strien, N.M., Cappaert, N.L.M., & Witter, M.P. (2009) The anatomy of memory: an interactive overview of the parahippocampal–hippocampal network. *Nat Rev Neurosci*, **10**, 272–282.

Verkhratsky, A. & Parpura, V. (2014) History of electrophysiology and the patch clamp. *Methods in Molecular Biology*, **1183**, 1–19.

Verkuijl, S.A. & Rots, M.G. (2019) The influence of eukaryotic chromatin state on CRISPR–Cas9 editing efficiencies. *Curr Opin Biotechnol*, **55**, 68–73.

Voigt, F.F., Kirschenbaum, D., Platonova, E., Pagès, S., Campbell, R.A.A., Kastli, R., Schaettin, M., Egolf, L., van der Bourg, A., Bethge, P., Haenraets, K., Frézel, N., Topilko, T., Perin, P., Hillier, D., Hildebrand, S., Schueth, A., Roebroeck, A., Roska, B., Stoeckli, E.T., Pizzala, R., Renier, N., Zeilhofer, H.U., Karayannis, T., Ziegler, U., Batti, L., Holtmaat, A., Lüscher, C., Aguzzi, A., & Helmchen, F. (2019) The mesoSPIM initiative: open-source light-sheet microscopes for imaging cleared tissue. *Nat Methods*, **16**, 1105–1108.

Wang, C., Chen, X., Lee, H., Deshmukh, S.S., Yoganarasimha, D., Savelli, F., & Knierim, J.J. (2018) Egocentric coding of external items in the lateral entorhinal cortex. *Science (1979)*, **362**, 945–949.

Wang, J. & Zhang, L. (2021) Retrograde axonal transport property of adeno-associated virus and its possible application in future. *Microbes Infect*, **23**, 104829.

Washbourne, P., Dityatev, A., Scheiffele, P., Biederer, T., Weiner, J.A., Christopherson, K.S., & El-Husseini, A. (2004) Cell Adhesion Molecules in Synapse Formation. *The Journal of Neuroscience*, **24**, 9244.

Waxman, S.G. & Bennett, M.V.I. (1972) Relative Conduction Velocities of Small Myelinated and Non-myelinated Fibres in the Central Nervous System. *Nat New Biol*, **238**, 217–219.

Wenzel, H.J., Woolley, C.S., Robbins, C.A., & Schwartzkroin, P.A. (2000) Kainic Acid-Induced Mossy Fiber Sprouting and Synapse Formation in the Dentate Gyrus of Rats. *Hippocampus*, **10**, 244–260.

West, M.J., Gaarskjaer, F.B., & Danscher, G. (1984) The Timm-stained hippocampus of the European hedgehog: A basal mammalian form. *Journal of Comparative Neurology*, **226**, 477–488.

Whoolery, C.W., Yun, S., Reynolds, R.P., Lucero, M.J., Soler, I., Tran, F.H., Ito, N., Redfield, R.L., Richardson, D.R., Shih, H. ying, Rivera, P.D., Chen, B.P.C., Birnbaum, S.G., Stowe, A.M., & Eisch, A.J. (2020) Multi-domain cognitive assessment of male mice shows space radiation is not harmful to high-level cognition and actually improves pattern separation. *Sci Rep*, **10**, 1–15.

Winterer, J., Lukacsovich, D., Que, L., Sartori, A.M., Luo, W., & Földy, C. (2019) Single-cell RNA-Seq characterization of anatomically identified OLM interneurons in different transgenic mouse lines. *European Journal of Neuroscience*, **50**, 3750–3771.

Witter, M.P. (2007a) The perforant path: projections from the entorhinal cortex to the dentate gyrus. *Prog Brain Res*, **163**, 43–61.

Witter, M.P. (2007b) Intrinsic and extrinsic wiring of CA3: Indications for connectional heterogeneity. *Learning & Memory*, **14**, 705–713.

Wolff, S.B. & Ölveczky, B.P. (2018) The promise and perils of causal circuit manipulations. *Curr Opin Neurobiol*, **49**, 84–94.

Xu, X., Holmes, T.C., Luo, M.H., Beier, K.T., Horwitz, G.D., Zhao, F., Zeng, W., Hui, M., Semler, B.L., & Sandri-Goldin, R.M. (2020) Viral vectors for neural circuit mapping and recent advances in trans-synaptic anterograde tracers. *Neuron*, **107**, 1029.

Yamagata, M., Sanes, J.R., & Weiner, J.A. (2003) Synaptic adhesion molecules. *Curr Opin Cell Biol*, **15**, 621–632.

Yamagata, M., Weiner, J.A., & Sanes, J.R. (2002) Sidekicks: Synaptic Adhesion Molecules that Promote Lamina-Specific Connectivity in the Retina. *Cell*, **110**, 649–660.

Yassa, M.A. & Stark, C.E.L. (2011) Pattern separation in the hippocampus. *Trends Neurosci*, **34**, 515.

Yiu, G. & He, Z. (2006) Glial inhibition of CNS axon regeneration. *Nat Rev Neurosci*, **7**, 617–627.

Yizhar, O., Fenno, L.E., Davidson, T.J., Mogri, M., & Deisseroth, K. (2011) Optogenetics in Neural Systems. *Neuron*, **71**, 9–34.

Yu, P., Zhang, Y.P., Shields, L.B.E., Zheng, Y., Hu, X., Hill, R., Howard, R., Gu, Z., Burke, D.A., Whittemore, S.R., Xu, X.M., & Shields, C.B. (2011) Inhibitor of DNA binding 2 promotes sensory axonal growth after SCI. *Exp Neurol*, **231**, 38–44.

Zappone, C.A. & Sloviter, R.S. (2001) Commissurally projecting inhibitory interneurons of the rat hippocampal dentate gyrus: A colocalization study of neuronal markers and the retrograde tracer fluoro-gold. *Journal of Comparative Neurology*, **441**, 324–344.

Zeisel, A., Moz-Manchado, A.B., Codeluppi, S., Lönnerberg, P., Manno, G. La, Juréus, A., Marques, S., Munguba, H., He, L., Betsholtz, C., Rolny, C., Castelo-Branco, G., Hjerling-Leffler, J., & Linnarsson, S. (2015) Cell types in the mouse cortex and hippocampus revealed by single-cell RNA-seq. *Science (1979)*, **347**, 1138–1142.

Zeng, H. & Sanes, J.R. (2017) Neuronal cell-type classification: challenges, opportunities and the path forward. *Nat Rev Neurosci*, **18**, 530–546.

Zhang, C.L., Zou, Y., He, W., Gage, F.H., & Evans, R.M. (2008) A role for adult TLX-positive neural stem cells in learning and behaviour. *Nature*, **451**, 1004–1007.

Zhang, F., Aravanis, A.M., Adamantidis, A., De Lecea, L., & Deisseroth, K. (2007) Circuit-breakers: optical technologies for probing neural signals and systems. *Nat Rev Neurosci*, **8**, 577–581.

Zhang, W., Yamawaki, R., Wen, X., Uhl, J., Diaz, J., Prince, D.A., & Buckmaster, P.S. (2009) Surviving Hilar Somatostatin Interneurons Enlarge, Sprout Axons, and Form New Synapses with Granule Cells in a Mouse Model of Temporal Lobe Epilepsy. *Journal of Neuroscience*, **29**, 14247–14256.

Zhao, C., Teng, E.M., Summers, R.G., Ming, G.L., & Gage, F.H. (2006) Distinct Morphological Stages of Dentate Granule Neuron Maturation in the Adult Mouse Hippocampus. *Journal of Neuroscience*, **26**, 3–11.

Zimmer, J., Sunde, N., & Sørensen, T. (1985) Reorganization and Restoration of Central Nervous Connections after Injury: A Lesion and Transplant Study of the Rat Hippocampus. *Brain plasticity, learning and memory*, 505–518.

Zipursky, S.L. & Sanes, J.R. (2010) Chemoaffinity Revisited: Dscams, Protocadherins, and Neural Circuit Assembly. *Cell*, **143**, 343–353.

Ziv, N.E. & Garner, C.C. (2001) Principles of glutamatergic synapse formation: seeing the forest for the trees. *Curr Opin Neurobiol*, **11**, 536–543.

Acknowledgments

Completing PhD can be incredibly challenging but at the same time rewarding. I need to thank many people, because their support in many different ways was very important throughout my entire journey.

First of all, I would like to thank Prof. Dr. Csaba Földy for giving me the opportunity to work in your lab, and all the advice, support and guidance during the last 4 and a half years. I have learned a great deal from you, your door was always open to discuss new directions and ideas. We have fostered a fruitful collaboration and reached beautiful outcomes. I would also like to express my gratitude to my committee member Prof. em. Dr. Martin E. Schwab and Prof. Dr. Benjamin Grewe. Your guidance, expertise, and insights were invaluable for shaping my thesis. To all of you, thank you for also contributing to my professional development and helping to shape my scientific thinking.

A great team is made of great people. I would like to thank all the past and current members of the Földy lab. Wenshu, I learned a lot from you. You are a wonderful person and colleague. You were there whenever I needed support and guidance, and we pushed each other to obtain fantastic results. I am incredibly grateful to have collaborated with you on so many interesting projects. Charlotte, Natalia, and Lin: beyond your exceptional research abilities, you are genuinely remarkable people! You were always there to help, for good discussions as well as for good laughs. I wish you all the best in your surely bright future. Charlotte, thank you also for all the delicious cakes that you were always bringing to the lab! Soma, Tamas and Rashmit, thank you for your contribution to all the work that we performed and the related discussion. Csaba Varga, thank you for your positive vibes and scientific impact. Your skills are truly remarkable. Also thank you to Gyula and Alice. Although we did not have that much time to spend together since you joined, I embrace our times together and wish you all my best. Special thanks also go to lab neighbors and friends Ali Özgur and George. It was super nice to spend time with you in and out of the institute. I wish all my best to you for your future.

I wish to thank the Wolfer Lab, especially, Irmgard, Sonia and David. You introduced me to the world of behavioral experiments. You were always there to help whenever I needed and patiently answered to all my questions. Thank you for putting so much thought and effort into our project.

Additional special thanks from the heart also go to my family and friends, who helped me to disconnect from the lab world. Fabrizia e Lukas, my parents, and Andrea, my brother, for the person you made me, your continuous support, and believing in me during this time, just as much as throughout my entire life. Also, many thanks for all the cuddles I received every time I was visiting you in Bellinzona or Zürich. Bianca and Olivia, I do not know where to start to express my gratitude to you. You were always there, and even though we lived in different cities in the beginning, I never felt the distance. The days with you start always with a big smile on our face, and I am incredibly excited for our future as a family! Additional thanks to Nadine and Lara. Grazie mille di tutto cuore a tutti voi! È una fortuna avervi!

Many thanks also go to my friends back in Ticino and here Zürich. Especially to Frate, Pietro, Monta, Francezio, NicoBo, Produ, Cico, Wyler, Iris, Dimi, Stra, Jacopin, Borghin, C, ADC, Rocco… and many more. To mention all of you, I would need an extra page. I feel lucky to have you in my life and to call you friends. All the vacations, aperos, events, gatherings, dinners (overrated), espresso, weekends, ski-trips, beers, serate pazze and so on were always amazing and gave me unforgettable memories as well as heavenly energy to pursue my scientific work.

To all of you, thank you! Together we made this journey and experience unforgettable.

MATTEO EGGER

"I have proven my analytical and organizational skills through my education and professional career. My flexible, creative and communicative personality with quick comprehension, help me to adapt to new work environments. I feel comfortable working in teams and independently and I am familiar will all common online communication channels."

INFO

Name	Matteo Egger
Date of Birth	18 | 01 | 1990
Gender	Male
Status	Married
Nationality	Swiss

CONTACT

Phone	+41 78 822 58 01
Mail	matteo.egger @hotmail.com
Address	Max-Bill-Platz 9 8050 Zurich Switzerland

CONNECT

in linkedin.com /matteo-egger

LANGUAGES

ITALIAN (Native)
● ● ● ● ●

GERMAN (good professional proficiency)
● ● ● ● ○

ENGLISH (full professional proficiency)
● ● ● ● ◐

FRENCH (limited working proficiency)
● ● ○ ○ ○

PROFESSIONAL EXPERIENCE

DOCTORAL STUDENT   09/2018 – CURRENTLY
BRAIN RESEARCH INSTITUTE
GROUP OF PROF. DR. CSABA FÖLDY
UNIVERSITY OF ZURICH

- Mechanistic studies on neuronal rewiring events in the adult brain
- Developed, conducted, and published original research projects
- Working in a team in an inter-disciplinary environment
- Learnt and applied diverse molecular and cell biology techniques, including rodents' surgery, tissue preparation, immunohistochemistry, microscopy
- Independently planning experiment sand setting priorities under time pressure
- Communicating research findings through an oral and poster presentations in a clear and persuasive manner, both internally within the research group and externally at conferences (International Society for Extracellular Vesicle (ISEV), Society of Neuroscience (SfN))
- Teaching activities

RESEARCH ASSISTANT   02/2018 – 08/2018
BRAIN RESEARCH INSTITUTE
GROUP OF PROF. DR. CSABA FÖLDY
UNIVERSITY OF ZURICH

- Laboratory of Neural Connectivity
- Implementation of CRISPS-based genome editing strategies

RESEARCH ASSISTANT   02/2016 – 01/2018
BRAIN RESEARCH INSTITUTE
GROUP OF PROF. MARTIN SCHWAB
ETH ZURICH AND UNIVERSITY OF ZURICH

- Collaborating in a research project initiated and led by Mea Holm in the extracellular vesicle field
- Technical expertise includes advanced cell culture, transfection of mammalian cells, exosomes isolation through various methods, immunofluorescence and staining techniques, western blotting, cloning and transmission electron microscopy
- Acquired and expertise responsibility over the use of equipment such as the transmission electron microscope

RESEARCH ASSISTANT   02/2015 – 07/2015
CRPP NEURO-REHAB
GROUP OF PROF. DR. MED. ANDREAS LUFT
UNIVERSITY OF ZURICH

- Collaborating in a research project initiated by Dr. Susan Leemburg focused on the link between the ventral tegmental area (VTA) and the motor cortex
- Technical expertise acquired includes BDA staining, pathway reconstruction, cutting brain tissue with the cryostat, rat motor skill training, protein quantification and analysis

EDUCATION

PHD AT THE FACULTY OF SCIENCE   **2018 – Currently**
NEUROSCIENCE PHD PROGRAM
LIFE SCIENCE ZURICH GRADUATE SCHOOL
UNIVERSITY OF ZURICH

M. SC. IN HEALTH SCIENCE AND TECHNOLOGY   **2015-2017**
MAJOR IN NEUROSCIENCE
ETH ZURICH, SWITZERLAND

B. SC. IN HEALTH SCIENCE AND TECHNOLOGY   **2011-2015**
ETH ZURICH, SWITZERLAND

SELECTED PUBLICATIONS

- Commissural dentate granule cell projections and their rapid formation in the adult brain
  Egger M, Luo W, Cruz-Ochoa N, Lukacsovich D, Varga C, Que L, Maloveczky G, Winterer J, Kaur R, Lukacsovich T, Földy C
  PNAS Nexus (2023), PMID: 37077887

- Pcdh11x controls target specification of mossy fiber sprouting
  Luo W, Cruz-Ochoa NA, Seng C, **Egger M**, Lukacsovich D, Lukacsovich T, Földy C
  Frontiers in Neuroscience (2022), PMID: 888362

- Recurrent rewiring of the adult hippocampal mossy fiber system by a single transcriptional regulator, Id2
  Luo W, **Egger M**, Domonkos A, Que L, Lukacsovich D, Cruz-Ochoa NA, Szőcs S, Seng C, Arszovszki A, Sipos E, Amrein I, Winterer J, Lukacsovich T, Szabadics J, Wolfer DP, Varga C, Földy C
  Proc Natl Acad Sci U S A. (2021) PMID: 34599103

PROFESSIONAL CERTIFICATES

- 2018 – LTK 1 - Introductory Course in Laboratory Animal Science, FELASA category B, University of Zürich, Switerland
  - Currently valid due to yearly continue education courses

- 2017 – Advanced Real PCR - Gene Expression

- 2016 – Good clinical practice 1 and 2

Full list of publications

Holm, M., Rust, R., **Egger, M.**, Weinmann, O., van Rossum, D., Walter, F., Santa-Maria, A.R., Grönnert, L., Maurer, M.A., Kraler, s., Akhmedov, A., Cideciyan, R., Lüscher, T., Deli, M.A., Hermann, I., Schwab, M.E. (2023) Nogo-A is secreted in extracellular vesicles occurs in blood and can influence vascular permeability. *Manuscript in preparation.*

Egger, M., Luo, W., Cruz-Ochoa, N., Lukacsovich, D., Varga, C., Que, L., Maloveczky, G., Winterer, J., Kaur, R., Lukacsovich, T., & Földy, C. (2023) Commissural dentate granule cell projections and their rapid formation in the adult brain. *PNAS Nexus*, **2**.

Luo, W., Cruz-Ochoa, N.A., Seng, C., **Egger, M.**, Lukacsovich, D., Lukacsovich, T., & Földy, C. (2022) Pcdh11x controls target specification of mossy fiber sprouting. *Front Neurosci*, **16**, 1362.

Luo, W., **Egger, M.**, Domonkos, A., Que, L., Lukacsovich, D., Cruz-Ochoa, N.A., Szőcs, S., Seng, C., Arszovszki, A., Sipos, E., Amrein, I., Winterer, J., Lukacsovich, T., Szabadics, J., Wolfer, D.P., Varga, C., & Földy, C. (2021) Recurrent rewiring of the adult hippocampal mossy fiber system by a single transcriptional regulator, Id2. *Proc Natl Acad Sci U S A*, **118**.

Seyedsadr, M.S., Weinmann, O., Amorim, A., Ineichen, B. V., **Egger, M.**, Mirnajafi-Zadeh, J., Becher, B., Javan, M., & Schwab, M.E. (2019) Inactivation of sphingosine-1-phosphate receptor 2 (S1PR2) decreases demyelination and enhances remyelination in animal models of multiple sclerosis. *Neurobiol Dis*, **124**, 189–201.